BUREAU OF RECLAMATION

Directed Outflow Project Technical Report 2

Directed Outflow Project, California
California-Great Basin Region

U.S. Department of the Interior

March 2021

Mission Statements

The Department of the Interior (DOI) conserves and manages the Nation's natural resources and cultural heritage for the benefit and enjoyment of the American people, provides scientific and other information about natural resources and natural hazards to address societal challenges and create opportunities for the American people, and honors the Nation's trust responsibilities or special commitments to American Indians, Alaska Natives, and affiliated island communities to help them prosper.

The mission of the Bureau of Reclamation is to manage, develop, and protect water and related resources in an environmentally and economically sound manner in the interest of the American public.

Directed Outflow Project Technical Report 2

Directed Outflow Project, California
California-Great Basin Region

prepared by

Bureau of Reclamation, Bay-Delta Office
801 I Street, Suite 140, Sacramento, CA 95814

Report Editor and Project Manager
Andrew A. Schultz, Ph.D.; Science Division
U.S. Bureau of Reclamation, Bay-Delta Office
aschultz@usbr.gov

Assistant Editor
Nick G. Bertrand; Science Division
U.S. Bureau of Reclamation, Bay-Delta Office

Administering Office
U.S. Bureau of Reclamation Bay-Delta Office
David Mooney, Ph.D., P.E.; Bay-Delta Office Manager
Mario Manzo, Bay-Delta Deputy Office Manager
Josh Israel, Ph.D.; Bay-Delta Science Division Chief

Chapter Lead Authors*
Bruce G. Hammock
Jason L. Hassrick
Andrew J. Kalmbach
Tomofuri Kurobe
Levi S. Lewis
Marie E. Stillway
Wilson Xieu
*** See individual chapters for full list of coauthors**

Cover Photos: Cover Images: top: Composite image of otoliths by Wilson Xieu, Wildlife, Fish and Conservation Biology, University of California, Davis, Davis, California 95616, USA; middle left: Larval sampling EDSM by USFWS, 850 S. Guild Ave, Suite 105 Lodi, CA 95240; middle right: Delta Smelt dissections by Chelsea Lam, Aquatic Health Program, School of Veterinary Medicine, Department of Anatomy, Physiology, and Cell Biology, University of California, Davis, Davis, California 95616, USA; bottom left: EDSM crew during Kodiak Trawl by USFWS, 850 S. Guild Ave, Suite 105 Lodi, CA 95240; right bottom: Fasting experiment tanks by Bruce Hammock, Fish Conservation and Culture Laboratory, Biological and Agricultural Engineering Department, University of California, Davis, Davis, CA, USA.

Disclaimer

This document does not represent and should not be construed to represent determination, concurrence, or policy of the U.S. Bureau of Reclamation or the U.S. Government.

Any use of trade, product, or firm names is for descriptive purposes only and does not imply endorsement by Reclamation or the U.S. Government.

The public reporting burden for this collection of information is estimated to average 1 hour per response, including the time for reviewing instructions, searching existing data sources, gathering and maintaining the data needed, and completing and reviewing the collection of information. Send comments regarding this burden estimate or any other aspect of this collection of information, including suggestions for reducing the burden, to Department of Defense, Washington Headquarters Services, Directorate for Information Operations and Reports (0704-0188), 1215 Jefferson Davis Highway, Suite 1204, Arlington, VA 22202-4302. Respondents should be aware that notwithstanding any other provision of law, no person shall be subject to any penalty for failing to comply with a collection of information if it does not display a currently valid OMB control number.
PLEASE DO NOT RETURN YOUR FORM TO THE ABOVE ADDRESS.

1. REPORT DATE March, 2021	**2. REPORT TYPE** Research	**3. DATES COVERED** *(From - To)*
4. TITLE AND SUBTITLE Directed Outflow Project: Technical Report 2		**5a. CONTRACT NUMBER** **5b. GRANT NUMBER** **5c. PROGRAM ELEMENT NUMBER**
6. AUTHOR(S) Editor: Andrew A. Schultz Assistant Editor: Nick G. Bertrand Chapter Lead Authors: Bruce G. Hammock, Jason L. Hassrick, Andrew J. Kalmbach, Tomofuri Kurobe, Levi S. Lewis, Marie E. Stillway, Wilson Xieu.		**5d. PROJECT NUMBER** **5e. TASK NUMBER** **5f. WORK UNIT NUMBER**
7. PERFORMING ORGANIZATION NAME(S) AND ADDRESS(ES) Bureau of Reclamation Bay Delta Office 801 I St., Suite 140 Sacramento CA 95814		**8. PERFORMING ORGANIZATION REPORT NUMBER**
9. SPONSORING/MONITORING AGENCY NAME(S) AND ADDRESS(ES) United States Bureau of Reclamation Bay Delta Office 801 I St., Suite 140 Sacramento CA 95814		**10. SPONSOR/MONITOR'S ACRONYM(S)** **11. SPONSOR/MONITOR'S REPORT NUMBER(S)**

12. DISTRIBUTION/AVAILABILITY STATEMENT Available from the National Technical Information Service (NTIS), Operations Division, 5285 Pt. Royal Rd, Springfield VA 22161; and
U.S. Bureau of Reclamation, Bay Delta Office Website: https://www.usbr.gov/mp/bdo/index.html

13. SUPPLEMENTARY NOTE

14. ABSTRACT The U.S. Bureau of Reclamation's Directed Outflow Program (DOP), along with collaborating agencies and non-governmental groups, are continuing efforts to evaluate the hypothesized benefits of outflow/outflow alteration to habitats and species of the Sacramento-San Joaquin Delta and connecting upper estuary (Delta). A particular focus of the DOP is to improve ecological understanding of the critically endangered Delta Smelt (*Hypomesus transpacificus*), a small short-lived osmerid fish endemic to the Delta. The DOP technical report series (Schultz et al. 2019; https://www.usbr.gov/mp/bdo/directed-outflow.html) aims to periodically showcase ongoing DOP-related research studies. Results from DOP-related studies are anticipated to assist decision-making processes and better inform general management actions to benefit Delta habitat conditions and species such as Delta Smelt.

15. SUBJECT TERMS
Directed Outflow Project, Fall X2, Salinity, Delta Smelt, Zooplankton, Contaminants, Growth, Condition, San Francisco Bay, Delta

16. SECURITY CLASSIFICATION OF:			**17. LIMITATION OF ABSTRACT**	**18. NUMBER OF PAGES**	**19a. NAME OF RESPONSIBLE PERSON**
				349	Joshua Israel, Ph.D.
a. REPORT	**b. ABSTRACT**	**a. THIS PAGE**			**19b. TELEPHONE NUMBER** *(Include area code)* 916-414-2405

Table of Contents

Suggested Citation 1
Directed Outflow Project Collaborators 2
Acknowledgments 4
Background and Purpose 5
Chapter 1: The Health and Condition Response of Delta Smelt to Fasting: A Time Series Experiment 9
Abstract 11
Introduction 12
Methods 15
Experimental Endpoints 15
Food Limitation Experiment 16
Ethics Statment 19
Laboratory Fish Processing 19
Comparison to Wild Fish 23
Statistical Analysis 24
Results 26
Water Quality 26
Mortality 27
Condition and Hepatosomatic Indices 27
Nutrition and Growth Indices in Muscle 28
Histology and Immunohistochemistry 28
Oxidative Stress in Liver 30
Comparison to Wild Delta Smelt 31
Discussion 32
Acknowledgments 40
References 41
Tables 47
Figures 50
Supplemental Material 58
Chapter 2: Assessment of Acute Toxcity and Histopathology of Environmental Contaminants in Delta Smelt (*Hypomesus transpacificus*) in Relation to Delta Outflow 61
Abstract 62
Introduction 63
Material and Methods 65
Sampling Design and Water Collections 65
Water Years and Outflow Actions 65
Chemical Analyses 66

Delta Smelt Toxicity Testing....67
Indicators of General Fish Condition....67
Histopathology....67
Results....68
Analytical Chemistry....68
Toxicity Testing and Histopathology....69
Discussion....71
Conclusion....76
Acknowledgments....78
Literature Cited....79
Tables and Figures....84
Supplemental Information....92
Chapter 3: Reproductive Strategy of Delta Smelt *Hypomesus transpacificus* and Impacts of Drought on Reproductive Performance....107
Abstract....109
Introduction....109
Material and Methods....115
Fish Sampling....115
Fish Dissection and Calculation of Somatic Condition Factor and Gonadosomatic Index....115
Water Quality Parameters and Hydrologic Classfication....116
Maturity of Female Delta Smelt....116
Area of Oocytes Measured by Histology....117
Clutch Size....117
Data Analysis....118
Relationship Between Maturity of Female Delta Smelt and Water Quality Parameters....118
Distribution Pattern of Female Delta Smelt During Spring Spawning Season....118
Comparison of Female Delta Smelt Maturity Among 2011-2014 Year Classes During the Spawning Season....119
Comparison of Reproductive Performance of Female Delta Smelt Between Wet and Dry/Drought Years....119
Results....120
Water Quality Parameters and Maturity of Female Delta Smelt....120
Geographical Distribution of Female Delta Smelt During the Spawning Season....121
Comparison of Female Delta Smelt Maturity Among the 2011-2014 Year Classes During the Spawning Season....122
Comparison of Oocyte Areas, Clutch Sizes, Gonadosomatic Index, and Somatic Condition Factor Among 2011-2014 Year Classes....123
Discussion....123
Conclusions....130
Acknowledgements....131

References 131
Supporting Information 139
Figures 141
Chapter 4: Otolith-Based Approaches Indicate Strong Effects of Environmental Variation on the Growth of a Critically Endangered Estuarine Fish 151
Abstract 152
Introduction 153
Materials and Methods 155
Study Site 155
Sample Collection and Processing 156
Otolith Preparation 156
Analysis of Otolith Microstructures 157
Growth Rate 157
Statistical Analyses 158
Intrinsic Models 158
Extrinsic Growth Models 158
Results 159
Intrinsic Growth Model 159
Environmental Attributes 159
Extrinsic Growth Models: 'Environment-Only' Model 160
Extrinsic Growth Models: 'Global-Regional' Model 160
Extrinsic Growth Models: 'Region-specific' Models 161
Discussion 161
Intrinsic Effects 162
Extrinsic Effects: Temperature 162
Extrinsic Effects: Salinity 164
Extrinsic Effects: Clarity 165
Statistical Considerations 165
Management Implications 166
Conclusions 168
Acknowledgements 168
References 168
Tables 176
Figures 181
Supplementary Information 188
Supplement 1: Field Collections of Delta Smelt and Methods Across Surveys 188
Supplement 2: Variation in Growth and Water Quality Among Years and Regions 191
Supplement 3: Environment-Only Model Comparisons 192
Supplement 4: Model Evaluation 195

Chapter 5: Experimental Validation of Otolith-Based Size and Age Reconstructions Across Multiple Life Stages of a Critically Endangered Estuarine Fish 197
Abstract 199
Introduction 200
Materials and Methods 201
Fish Length Measurements 201
Otolith Prepartion 202
Otolith Age and Growth Analyses 202
Accuracy 202
Precision 203
Statistical Analyses 203
Results 204
Somatic and Otolith Growth 204
Accuracy and Precision 204
Effects of Otolith Symmetry, Image Magnification, and Life Stage on Aging Accuracy Among Analysts 205
Discussion 205
Experimental Validation of Otolith-based Metrics 205
Interpretation of Otolith Microsctructures 205
Otolith-Somatic Proportionality 206
Accuracy and Precision of Otolith-based Age Estimates 206
Otolith Symmetry 207
Image Magnification 207
Cultured Versus Wild Fish 208
Conclusions 208
Acknowledgements 208
References 209
List of Tables 212
List of Figures 213
Tables 214
Figures 217
Supplement 1 222
Supplement 2 223
Supplement 3 224
Chapter 6: The Effect of Outflow on Subsidy of a Key Calanoid Copepod Prey Item for Delta Smelt in the San Francisco Estuary 225
Abstract 226
Introdcution 227
Methods 228
Results 231

Discussion 232
Acknowledgements 233
References 234
Tables 237
Figures 238
Chapter 7: How an Estuarine Prey Field Changes with Managed Freshwater Outflow 245
Abstract 246
Introduction 246
Materials and Methods 248
Habitat Sampling 248
Data Analysis 249
Results 250
Discussion 253
Management Implications and Future Directions 255
Acknowledgements 256
Literature Cited 258
Tables 266
Figures 272
Chapter 8: Comparisons of Phytoplankton Community Structure and Nutrient Conditions in the Sacramento River Delta During a Fall Flow Action and Non-Action Period 289
Abstract 290
Introduction 291
Methods 295
Study Area and General Sampling Design Location and Sampling Period 295
Sampling Methods 295
Lab Analysis Methods 296
Statistical Analysis 297
Results 298
Water Flow 298
Nutrient and Water Quality Data 298
Biomass 299
Harmful Algal Blooms 300
Diversity 300
Discussion 302
Dissolved Nutrients 302
Phytoplankton Biomass 303
Phytoplankton Diversity 305
Harmful Algal Blooms 307
Management Implications 308

Acknowledgements 309
References 310
Tables 315
Figures 319

List of Tables

1-1 Sampling time points, details, and effort for each endpoint examined in the study 47

1-2 Mean liver histological results from the experiment. 48

1-3 Comparison of wild Delta Smelt to hatchery Delta Smelt from the Feeding and No Feeding treatments. 49

2-1 Summary of events and test initiation dates across the project. 84

4-1 Total Delta Smelt (N = 459) included in the study by year, region, and subregion (EDSM 2017 "Strata"). 176

4-2 Results of correlation analyses among pairs of the abiotic environmental attributes measured with each sample, including their respective transformations: temperature (cubic), salinity (log10), and Secchi depth (none). 177

4-3 Statistical results of the selected "environment-only" model (Model 18, tsc*) examining variation in age-independent growth rates (Ga) of wild Delta Smelt as the additive and interactive function of the physical environmental attributes measured at capture (t-temperature, s-salinity, c-clarity) ($\chi 2$ = 79.6, df = 15.6, R2 = 0.159, $p < 0.001$). 178

4-4 Statistical results of the "global-regional" GAM examining variation in Ga as a function of the fixed parametric effect of region, additive smooth effects of temperature, salinity, and clarity; both with and without the random effect of year (Model). 179

4-5 Statistical results of separate "region-specific" GAMs examining variation in growth (Ga) as a function of the additive effects of physical environmental attributes (temperature, salinity, and clarity) and the random year effect. 180

5-1 Samples used in the present study. Sample size (N) is shown by age class, along with the mean standard length for the subsample from each age class. 214

5-2 Effects of observer, otolith side, and life stage on aging accuracy. 215

5-3 Effects of observer and image magnification on aging accuracy. 216

6-1 The calculated volume of each box (millions of m^3) at the four modeled X2 scenarios. 237

7-1 Number of samples taken for each habitat in each region during 2017 and 2018. 266

7-2 Kruskal-Wallis Rank Sum test results for water quality variables, total abundance, total biomass, and Shannon's diversity indices for all five regions in the northern San Francisco Estuary during the two years of varying hydrology (shaded). 267

7-3 Kruskal-Wallis Rank Sum test results for taxa abundances (Figure 7) and biomasses (Figure 8) across five regions in the San Francisco Estuary over two years of varying hydrology. 268

7-4 Generalized Additive Model (GAM) model output for relationships between individual zooplankton taxa abundances and biomasses with water quality variables in the San Francisco estuary across two years with varying hydrology. 270

8-1 Mean and standard deviation of water quality parameters over each study season and region. 315

8-2 Model summary for biomass and diversity linear models. 316

8-3 Phytoplankon taxa observed in 2017 and 2018. 317

List of Figures

1-1 Liver histopathology. 50
1-2 Kaplan-Meier survival probability throughout the starvation experiment. 52
1-3 Condition factor (panel A), hepatosomatic index (panel B), RNA to DNA ratio in muscle (Panel C), and triglycerides in muscle (panel D) by day. 53
1-4 Low (Panels A-C) and high (Panels D-F) magnification starvation progression. 54
1-5 Histological indices by day. 56
1-6 Biomarkers of oxidative stress in liver. 57
2-1 Map of study area with delineated strata (technical assistance from Lara Mitchell (USFWS). 85
2-2 Graph of daily mean discharge for USGS site 11313240 Grant Line near Tracy, CA. 85
2-3 Graph of daily mean discharge for USGS site 381142122015801 First Mallard Branch near Fairfield, CA during the 2018 Salinity Gate Flow Action. 86
2-4 Graph of daily mean discharge for USGS site 11453000 Yolo Bypass near Woodland, CA during the 2018 North Delta Flow Action pulse flow. 86
2-5 Graph of daily mean discharge for USGS site 11453000 Yolo Bypass near Woodland, CA during the 2019 North Delta Flow Action pulse flow. 87
2-6 Graph of daily mean discharge for USGS site 11406920 Thermalito Afterbay Release to Feather River near Oroville, CA during the 2019 Fall X2 Action. 87
2-7 Graph of daily mean discharge for USGS site 11446500 American River near Fair Oaks, CA during the 2019 Fall X2 Action. 88
2-8 Graph of daily mean discharge for USGS site 11313240 Grant Line CN near Tracy, CA during the 2019 Fall X2 Action. 88
2-9 A) Severe secondary lamella fusion (F) in 3 gill filaments at low magnification. B) higher magnification showing moderate epithelial cell necrosis (arrows) and aneurysm (ANU) in Delta Smelt exposed to water collected from Cache Slough in a toxicity test initiated on October 27, 2017. 89
2-10 A) Typical regular thin gill lamellae structure of Delta Smelt exposed to FCCL water for 96 hr. B) Severe mucus cell hyperplasia in gill exposed to Cache Slough water for 96 hr. 89
2-11 Severe fatty vacuolation and moderate sinusoidal congestion in the liver of Delta Smelt exposed to water collected from the Sacramento River at Decker Island in a toxicity test initiated on December 8, 2017 (200x magnification). 90
2-12 A) Chloride cell hyperplasia (CCH) and mucus cell proliferation (arrows) in gills. B) Secondary lamellae edema (arrows) and epithelial cell hyperplasia (ECH) in gills. 90
2-13 Mucus cell hyperplasia (black arrows), epithelial cell necrosis (yellow arrows), small aneurysm (ANU), and edema (SLE) in secondary lamella of gill in Delta Smelt exposed for 96 h to water sample from the Sacramento River at Decker Island (200x magnification) on November 8, 2019. 91

2-14 A) Liver of Delta Smelt shows severe lipidosis as indicated by black arrows, exposed to water collected from the Toe Drain (200X magnification). B) Liver of Delta Smelt exposed for 96 h to water collected from Toe Drain, showing severe lipidosis (black arrows) and single cell necrosis (yellow arrows) at 400x magnification, initiated in a toxicity test on September 27, 2019. 91
3-1 Map of Northern California, USA (Panel A) and the sampling stations for long term monitoring survey conducted by the California Department of Fish and Wildlife (Panel B). 141
3-2 Summary of salinity (A), water temperature (B), and turbidity values (C) at each reproductive stage of female Delta Smelt, 2011 – 2014 year classes, and corresponding median absolute deviations (MAD) (D-F). 143
3-3 Maturity and distribution pattern of female Delta Smelt, 2011 (January-April 2012, Panels A-D), 2012 (January-April 2013, Panels E-H), and 2013 year classes (January-April 2014, Panels I-L) 145
3-4 Monthly changes of female Delta Smelt maturity levels for 2011-2014 year classes (Panels A-D). 148
3-5 Comparison of somatic condition factor (A) and reproductive endpoints: area of oocytes (B), clutch size (C), and gonadosomatic index (D), among 2011–2014 year classes. 149
3-6 Comparison of area and location of the mixing zone (salinity 1.0-6.0 ppt) among 2011–2014 (A-D), October. 150
4-1 Map of the "upper" San Francisco Estuary. 181
4-2 Otolith of a 215 day-post-hatch Delta Smelt. 182
4-3 Intrinsic generalized additive models (GAMs) examining the response of log-transformed recent growth rates (G) to age and prior growth rate. 183
4-4 Distribution of environmental conditions from which Delta Smelt were collected. 184
4-5 Results of the "environment-only" GAM examining variation in age-independent growth rates (Ga) of wild Delta Smelt as additive and interactive functions of the physical environmental attributes measured at capture ("environment-only models") 185
4-6 Results of the "global-regional" GAMs examining variation in Ga as a function of the fixed parametric effect of region (A), additive smooth effects of temperature (B), salinity (C), and clarity (D), while including a random year effect. 186
4-7 Results of separate "region-specific" GAMs examining variation in growth (Ga) as a function of the additive smooth effects of physical environmental attributes (temperature, salinity, and clarity) and the random year effect. 187
5-1 Morphological features of Delta Smelt and their otoliths 217
5-2 Somatic and otolith size and growth in Delta Smelt 218
5-3 Aging accuracy across life stages 219
5-4 Aging accuracy and precision among analysts 220
5-5 Effects of otolith side and image magnification on aging accuracy 221

6-1 Map of the northern San Francisco Estuary for X2 scenarios at 67, 74, 81, and 85 km with boundaries (red is seaward, black is landward) of the low-salinity box. 238
6-2 Flow diagram of calculations: Shaded shapes represent calculations made for this paper, whereas copepod development time is unshaded because it involves parameter estimates from Kimmerer et al. (2019); hexagons are three-dimensional simulation models; rectangles are results of calculations based on data and 3-D model output. 239
6-3 Predicted proportion of particles exchanged from source to destination boxes under four X2 conditions based on tidal behavior. 240
6-4 Box plots showing the variability in P. forbesi densities across boxes by life stage (columns), sampling survey (rows). 241
6-5 Proportional subsidies of P. forbesi (Eqn. 2) to the low-salinity zone (LSZ) by X2 scenario based on passive behavior for nauplii, and the tidal migration behavior for copepodites and adults. 242
6-6 Proportional net gain (Eqn. 3) of P. forbesi in the low-salinity zone box (LSZ) by X2 level for each life stage (columns) and sampling survey (rows). 243
6-7 Station-specific estimates of in-situ mortality for P. forbesi as a function of salinity by survey (rows) and life stage (columns). 244
7-1 Sampling locations for each region in the San Francisco Estuary. 272
7-2 Differences in water quality within five regions of the estuary for both years of variable outflow. 273
7-3 Average contribution to dissimilarity between 2017 and 2018 lower trophic community abundance (left) and biomass (right). 275
7-4 Predicted relationships between lower trophic taxa abundance (top) and biomass (bottom) with water quality metrics. 276
7-5 Box plots for total abundance (individuals per m^3), log-transformed total biomass (μg C per m^3), and Shannon's diversity (H') for five regions within the estuary in years with varying hydrology. 278
7-6 *NMD*S ordinations depicting differences in 80 lower trophic taxa abundance across five regions in 2017 (left) and 2018 (right) in the San Francisco Estuary in years with varying hydrology (stress= 0.180). 280
7-7 Mean densities of lower trophic taxa observed during fall of 2017 and 2018 across all regions sampled in the San Francisco Estuary. 282
7-8 Mean biomass of lower trophic taxa observed during fall of 2017 and 2018 across all regions sampled in the San Francisco Estuary. 283
7-9 Box plots for total abundance (individuals per m^3), log-transformed total biomass (μg C per m^3), and Shannon's diversity (H') for habitat in each region across years with varying hydrology. 284
7-10 NMDS ordinations depicting differences in 20 mysid/amphipod taxa abundance (left) and 56 zooplankton taxa abundance (right) in Suisun Bay from 2017 to 2018 (top) and in three habitats (bottom) in the estuary in years with varying low-salinity habitat (stress= 0.175). 286
8-1 Map of regions and locations sampled in the Delta during fall of 2017 and 2018. 319

8-2 Outflow and X2 in the fall of 2017 and 2018. Measurements from DWR dayflow data. 320
8-3 Nutrient concentrations between seasons and study regions in the Delta. Shared letters denote no significant difference observed between regions and years. Outliers are omitted from this plot. 321
8-4 Ratios of dissolved nutrients between years and regions of the Delta, with Dissolved Inorganic Nitrogen to Phosphate (top) and Nitrate to Ammonium (bottom). 322
8-5 Chlorophyll concentrations between years and regions of the Delta. 323
8-6 Explanatory used variables to model chlorophyll concentration, with estimated effects size and 95% confidence intervals. 324
8-7 The predicted effects of selected parameters on phytoplankton biomass as determined by generalized linear modeling. 325
8-8 Proportion of sites with colonial Microcystis observed in each region and year. 326
8-9 Mean abundance of each phytoplankton group by year and region as (A) proportion of the total phytoplankton abundance and (B) scaled to mean chlorophyll-a to highlight the respective contribution of each group to the phytoplankton biomass. 327
8-10 Shannon's index of diversity for phytoplankton samples by region and year. 328
8-11 NMDS ordination of phytoplankton assemblages versus selected environmental variables and year. 329
8-12 NMDS ordination of phytoplankton assemblages versus environmental variables and region. 330
8-13 NMDS ordination of phytoplankton assemblages versus selected environmental variables and habitat. 331

Suggested Citation

Entire Report

Schultz, A.A., editor. 2021. Directed Outflow Project: Technical Report 2. U.S. Bureau of Reclamation, Bay-Delta Office, California-Great Basin Region, Sacramento, CA. March 2021, 349 pp.

Chapter within Report

Hammock B.G., W.F. Ramírez-Duarte, P.A. Triana Garcia, A.A. Schultz, L.I. Avendano, T.C. Hung, J.R. White, Y.T. Bong and S.J. Teh. 2021. The health and condition responses of Delta Smelt to fasting: A time series experiment. Pages 9-60 in A.A. Schultz, editor. Directed Outflow Project: Technical Report 2. U.S. Bureau of Reclamation, Bay-Delta Office, California-Great Basin Region, Sacramento, CA. March 2021, 349 pp.

Directed Outflow Project Collaborators

Andrew Schultz, U.S. Bureau of Reclamation*

April Hennessy, California Department of Fish and Wildlife*

April Smith, ICF

Bruce Hammock, U.C. Davis*

Calvin Lee, ICF*

Catherine Johnston, U.S. Fish and Wildlife Service

Christian Denney, U.C. Davis

Christina Burdi, California Department of Fish and Wildlife*

Colin Brennan, ICF

Daniel Cox, ICF

Darcy Austin, State Water Contractors

Denise Barnard, U.S. Fish and Wildlife Service (currently East Bay Municipal Utility District)*

Ed Gross, Resource Management Associates

Erwin Van Nieuwenhuyse, U.S. Bureau of Reclamation

Feng Zhao, U.C. Davis

Galen Tigan, U.C. Davis

James Hobbs, U.C. Davis (currently California Department of Fish and Wildlife)*

James White, U.C. Davis

Jason Hassrick, ICF*

Jennifer Pierre, State Water Contractors

John Brandon, ICF

Josh Korman, Ecometric

Kristin Arend, U.S. Bureau of Reclamation*

Lauren Damon, California Department of Fish and Wildlife

Lenny Grimaldo, ICF (currently California Department of Water Resources)*

Leonie Avendano, U.C. Davis

Levi Lewis, U.C. Davis*

Lori Smith, U.S. Fish and Wildlife Service

Luke Ellison, U.C. Davis

Malte Willmes, U.C. Davis*

Marie Stillway, U.C. Davis*

Nann Fangue, UC Davis

Nick Bertrand, U.S. Bureau of Reclamation*

Pedro Garcia, U.C. Davis

Rachel Fichman, U.C. Davis

Randy Baxter, California Department of Fish and Wildlife

Randy Dahlgren, U.C. Davis

Shawn Acuña, Metropolitan Water District of Southern California*

Steve Slater, California Department of Fish and Wildlife*

Swee Teh, U.C. Davis*

Tien-Chieh Hung, U.C. Davis

Tomofumi Kurobe U.C. Davis

Troy Stevenson, U.C. Davis

Wilson Ramírez-Duarte, U.C. Davis

Wilson Xieu, U.C. Davis

Wim Kimmerer, San Francisco State University

Yih-Tyng Bong, U.C. Davis

***denotes DOP Investigator Team**

Acknowledgments

The Directed Outflow Project is part of the Interagency Ecological Program (IEP) Annual Work Plan. Early reviews of related study plans were supported by the IEP Flow Alteration Project Work Team and the Collaborative Adaptive Management Team (special thanks to Larry Brown [U.S. Geological Survey]), and U.S. Fish and Wildlife Service (USFWS), California Department of Water Resources (DWR), California Department of Fish and Wildlife (CDFW), and U. S. Bureau of Reclamation (USBR). Permitting for this work was facilitated through CDFW (SC-4086, SC-13523, S-190810003-19127-002 and Memorandum of Understanding issued by CDFW's Delta Habitat Conservation Program and Fisheries Branch) and USWFS (TE-108507, sub-permit FWSLFWO-6.1, 1-1-96-F-1 and 1-1-98-I-1296). This study was supported by contributions from multiple IEP agency field sampling activities of fish and zooplankton (CDFW, USFWS, DOP [USBR]), as well as informed by DWR DAYFLOW. Funding and contractual support was provided by USBR (special thanks to Megan Bryant, Teresa Brown, Christina Munoz, Mouang Phan, Nandini Johnson, Brooke White, Thomas Eckert, John Ridilla, Delyssa Bloxson and Leanne Henderson), DWR, Metropolitan Water District of Southern California (special thanks to Shawn Acuna), State Water Contractors (SWC; special thanks to Jennifer Pierre, Darcy Austin and SWC staff) and State and Federal Contractors Water Agency (special thanks to Laura Valoppi). We acknowledge the support of many people from the Delta community. Further acknowledgement sections are located within each chapter of this report.

Background and Purpose

The U.S. Bureau of Reclamation's (Reclamation) Directed Outflow Program (DOP), along with collaborating agencies and non-governmental groups, are continuing efforts to evaluate the hypothesized benefits of outflow/outflow alteration and improve ecological understanding of the critically endangered Delta Smelt (*Hypomesus transpacificus*), a small short-lived osmerid fish endemic to the Sacramento-San Joaquin Delta and connecting upper estuary (Delta). The DOP technical report series (Schultz et al. 2019; https://www.usbr.gov/mp/bdo/directed-outflow.html) aims to periodically showcase ongoing DOP-related research studies. Each chapter within this report is intended for eventual submittal to a peer-reviewed scientific journal, thus formatting may vary among chapters. Comments at the top of the title page of each chapter will alert the reader of those chapters already published or submitted to a peer-reviewed journal. The following provides additional background information.

In 2008, the U.S. Fish and Wildlife Service (USFWS) issued a Biological Opinion (2008 BiOp; USFWS 2008) on Central Valley Project/State Water Project operations that concluded aspects of those operations jeopardize the continued existence of Delta Smelt and adversely modify the species' critical habitat. Action 4 (Fall X2 Action) of the 2008 BiOp required Delta outflow be maintained at an average X2 (average position of the 2 ppt isohaline from Golden Gate) no greater than 74 km for September and October following wet years and 81 km following above normal years (water-year type [wet, above normal, below normal, dry, critical] is based on measured unimpaired runoff; https://cdec.water.ca.gov/reportapp/javareports?name=WSIHIST). In 2011, Reclamation produced a fall outflow adaptive management plan based on the science underlying the Fall X2 Action and outlining how adaptive management might proceed (Reclamation 2012).

In spring 2016, USFWS requested augmentation of summer outflow from the Sacramento River to benefit the habitat and declining population of Delta Smelt, although the action never occurred. Slightly thereafter the Delta Smelt Resiliency Strategy (DSRS) was finalized in July 2016 (CNRA 2016). The DSRS articulated a suite of actions that could be implemented in the next few years to benefit Delta Smelt based on concepts detailed in Baxter et al. (2015). These actions included augmentation of Delta outflow to push the low salinity zone (0.5-6 ppt) seaward and routing of water through Yolo Bypass Toe Drain to promote food production, to benefit Delta Smelt.

In winter of 2016/2017 Reclamation formed the DOP to assist in evaluating outflow-related hypotheses and predictions (Table 1) using targeted paired biological and physical monitoring. The over-arching hypothesis is summer and fall habitat conditions are improved for juvenile Delta Smelt when X2 moves seaward (USBR 2012; Brown et al. 2014), especially when X2 overlaps the Suisun Bay-Marsh area of the Delta. Predictions are largely based on conceptual models within Baxter et al. (2015) (figures 48 and 49 in particular) and predictions in Brown et al. (2014).

In August of 2016, Reclamation and California Department of Water Resources (DWR) jointly requested a Reinitiation of Consultation on the Coordinated Long-Term Operation of the Central Valley Project (CVP) and State Water Project (SWP). The USFWS accepted the request shortly after and stated therein: "…new information is demonstrating the increasingly imperiled state of the delta smelt and its designated critical habitat, and that emerging science shows the importance of outflows to all life stages of delta smelt and to maintaining the primary constituent elements of designated critical habitat." The new Biological Opinion on operations was finalized in October of 2019 (2019

BiOp; USFWS 2019). The Delta Smelt Summer-Fall Habitat Action (SFHA) and additional measures in Table 2-1 of the 2019 BiOp outlines multiple outflow-related actions geared toward benefitting Delta Smelt habitat and ultimately its population. Such actions include the following:

> *Fall X2: Modify water operations to maintain X2 at 80 km in above normal and wet water years in September and October. Maintain low salinity habitat in Suisun Marsh and Grizzly Bay when water temperatures are suitable. Manage the low salinity zone to overlap with turbid water and available food supplies. Establish contiguous low salinity habitat from Cache Slough Complex to the Suisun Marsh.*
>
> *Suisun Marsh Salinity Control Gate: The freshening of Montezuma Slough through gate operations could provide additional low salinity habitat for Delta Smelt to forage, spawn and rear.*
>
> *Suisun Marsh and Roaring River Distribution System Food Subsidies Study: Add fish food to Suisun Marsh through coordinating managed wetland flood and drain operations in Suisun Marsh, Roaring River Distribution System food production, and reoperation of the Suisun Marsh Salinity Control Gates.*
>
> *North Delta Food Subsidies/Colusa Basin Drain Study: Augment flow in the Yolo Bypass in July and/or September by closing Knights Landing Outfall Gates and routing water from Colusa Basin into Yolo Bypass to promote fish food production.*
>
> *Sacramento River Deepwater Ship Channel Food Study: Repair or replace the West Sacramento lock system to hydraulically reconnect the ship channel with the mainstem of the Sacramento River. The ship channel has the potential to flush food production into the north Delta for Delta Smelt.*

While much has been learned regarding the impacts of environmental conditions on Delta Smelt habitat, some uncertainty remains as to how outflow-related actions, such as those listed above, may affect certain habitat factors and the species' response. We anticipate results from DOP-related studies will assist decision-making processes regarding the SFHA and better inform general management actions to benefit the wild Delta Smelt population, including augmentation of the population through supplementation using cultured fish.

Literature Cited

Baxter, R., Brown, L.R., Castillo, G., Conrad, L., Culberson, S.D., Dekar, M.P., Dekar, M., Feyrer, F., Hunt, T., Jones, K. and Kirsch, J. 2015. An updated conceptual model of Delta Smelt biology: our evolving understanding of an estuarine fish (No. 90). Interagency Ecological Program, California Department of Water Resources.

Brown, L.R., Baxter, R., Castillo, G., Conrad, L., Culberson, S., Erickson, G., Feyrer, F., Fong, S., Gehrts, K., Grimaldo, L. and Herbold, B. 2014. Synthesis of studies in the fall low-salinity zone of the San Francisco Estuary, September–December 2011. US Geological Survey Scientific Investigations Report, 5041, p.136.

California Natural Resources Agency (CNRA). 2016. Delta Smelt resiliency strategy. CNRA, Sacramento, California. Available: http://resources.ca.gov/docs/Delta-Smelt-ResiliencyStrategy-FINAL070816.pdf. (May 2019).

Schultz, A. A., editor. 2019. Directed Outflow Project: Technical Report 1. U.S. Bureau of Reclamation, Bay-Delta Office, Mid-Pacific Region, Sacramento, CA. November 2019, 318 pp.

United States Bureau of Reclamation (USBR). 2012. Adaptive management of fall outflow for delta smelt protection and water supply reliability [Internet]. Revised milestone draft dated 28 June 2012. Sacramento (CA): U.S. Bureau of Reclamation; 99 pp. Available from: https://www.waterboards.ca.gov/waterrights/water_issues/programs/bay_delta/docs/cmnt081712/dfg/cdfgusbr2012.pdf

United States Fish and Wildlife Service (USFWS). 2008. Formal Endangered Species Act consultation on the proposed coordinated operations of the Central Valley Project (CVP) and State Water Project (SWP): U.S. Fish and Wildlife Service, Sacramento, CA.

United States Fish and Wildlife Service (USFWS). 2019. Biological Opinion for the Reinitiation of Consultation on the Coordinated Operations of the Central Valley Project and State Water Project. U.S. Fish and Wildlife Service, Sacramento, CA.

Table 1. Qualitative predictions regarding the effect of X2 (location of 2 ppt salinity isohaline) in or near the Suisun Bay/Marsh area during summer and fall compared to other regions, and within this area during summer and Fall X2 Action periods.

Dynamic Abiotic Habitat Components	**X2 in/near Suisun Region During Summer or Fall Compared to Other Regions and Within Suisun Region During Summer or Fall X2 Action Periods (in parentheses)**	**Chapters within the DOP Technical Report 2 with Related Data**
Low Salinity Habitat Area	Higher (Increases)	
Habitat Complexity	Higher (Increases)	
Hydrodynamic Complexity	Higher (Increases)	
Water Temperature	Lower (Decreases)	
Turbidity	Higher (Increases)	
Contaminants*	Lower (Decreases)	2
Dynamic Biotic Habitat Components		
Delta Smelt Prey Density and Biomass	Higher (Increases)	6, 7
Phytoplankton Density and Biomass	Higher (Increases)	8
Harmful Algal Constituents/Cyanotoxins	Lower (Decreases)	
Impact of Non-Native Competitors	Lower	
Impact of Non-Native Predators	Lower	
Delta Smelt Responses		
Occupancy/Residence	Greater (Increases)	
Health	Greater (Increases)	1,2
Growth	Higher (Increases)	4, 5
Survival	Higher (Increases)	
Prey Quality, Foraging Success	Better (Increases)	6, 7
Fecundity	Higher	3
Population Range/Distribution	Broader, Less Constricted	4
Life History Diversity	Greater, More Even Spread	4

Chapter 1: The Health and Condition Responses of Delta Smelt to Fasting: A Time Series Experiment

Published September 24, 2020

Hammock, B.G., Ramírez-Duarte, W.F., Triana Garcia, P.A., Schultz, A.A., Avendano, L.I., Hung, T.C., White, J.R., Bong, Y.T. and Teh, S.J., 2020. The health and condition responses of Delta Smelt to fasting: A time series experiment. *PloS one*, *15*(9), p.e0239358.

The health and condition responses of Delta Smelt to fasting: A time series experiment

Authors: Bruce G. Hammock*[,1], Wilson F. Ramírez-Duarte*[,1,2], Pedro Alejandro Triana Garcia[1,2], Andrew A. Schultz[3], Leonie I. Avendano[1], Tien-Chieh Hung[4], James R. White[5], Yih-Tyng Bong[1], Swee J. Teh[1]

[1]Aquatic Health Program, School of Veterinary Medicine, Department of Anatomy, Physiology, and Cell Biology, University of California, Davis, California 95616, USA

[2]Grupo de Investigación en Sanidad de Organismos Acuáticos, Instituto de Acuicultura de los Llanos, Universidad de los Llanos, Villavicencio, Meta, Colombia

[3]Science Division, U.S. Bureau of Reclamation Bay-Delta Office, Sacramento, CA, USA

[4]Fish Conservation and Culture Laboratory, Biological and Agricultural Engineering Department, University of California, Davis, Davis, CA, USA

[5]California Department of Fish and Wildlife, Stockton, CA, USA

Corresponding author: brucehammock@gmail.com

*Authors contributed equally

Abstract

There is an extensive literature establishing, validating, and quantifying a wide range of responses of fishes to fasting. Our study complements this work by comparing fed and unfed treatments of hatchery-raised Delta Smelt (*Hypomesus transpacificus*)—an imperiled fish that is endemic to the San Francisco Estuary and its tributaries in California, USA—across a diverse suite of endpoints over a two-month time series. The experiment was conducted at 15.9 °C, and individuals were sampled at 12 time points as starvation became increasingly severe. We found that hepatosomatic index and condition factor were relatively sensitive to starvation, becoming significantly depressed at Day 4 and 7, respectively. Histological analysis of liver showed elevated cytoplasmic inclusion bodies at Day 7, followed by increased glycogen depletion, single cell necrosis, and hydropic vacuolar degeneration at Day 14, 21, and 28, respectively. Of four antioxidants measured, glutathione decreased at Day 4, superoxide dismutase increased at Day 14, catalase increased at Day 56, and glutathione peroxidase was not affected by starvation. The net result was a ~2-fold increase in lipid peroxidation (malondialdehyde) in fasted fish that was highly inconsistent through time. RNA to DNA ratio and triglycerides in muscle were relatively insensitive to starvation, only consistently decreasing with fasting after mortality began increasing in the 'No Feeding' treatment, at Day 21. Together, these results suggest that Delta Smelt mobilize hepatic energy stores far more rapidly than lipids in muscle when subjected to fasting, leading to rapid atrophy of liver and the development of cytoplasmic inclusion bodies—possibly autophagosomes—in hepatocytes.

Keywords: atrophy, autophagy, fish, hepatosomatic index, oxidative stress, starvation

Introduction

A major consequence of anthropogenic global change is the disruption of aquatic food webs. Moderate nutrient increases, for example, can stimulate primary productivity, leading to elevated fishery production [1]. Higher levels of nutrients may lead to excess primary productivity, hypoxia, and fish kills (e.g., Gulf of Mexico, Mediterranean Sea, Black Sea; [1]). Invasive species can be particularly disruptive to aquatic food webs, with effects ranging from prey field shifts to trophic cascades (e.g., [2, 3]). Given the preponderance of ectotherms, aquatic food webs are also highly vulnerable to climate change [4, 5][6]. As the climate warms, the oxygen and feeding requirements of ectotherms increases, even as dissolved oxygen decreases [6, 7]. These changes can also interact. For instance, high temperatures and nutrients can trigger blooms of the invasive cyanobacteria *Microcystis* spp. When *Microcystis* spp. cells lyse, communities are exposed to microcystin, a potent hepatotoxin that bioaccumulates in aquatic organisms [8-12]. Thus, given the global alterations of aquatic food webs, understanding how aquatic organisms respond is key.

Commonly used tools for identifying altered food web linkages are metrics of nutritional status in fish. These metrics often include Fulton's condition factor, hepatosomatic index, RNA to DNA ratio in muscle, triglyceride concentration in muscle, and liver glycogen. Condition factor reflects nutritional status because body mass responds more quickly to food limitation than body length (e.g., [13]). Similarly, hepatosomatic index is responsive to food limitation because liver weight declines more rapidly than body weight as hepatic energy stores are rapidly mobilized (i.e, glycogen, lipid, and protein; [14-16]). The ratio of RNA to DNA in muscle is an

indicator of recent growth, and therefore fasting, because RNA concentration in cells correlates with protein synthesis, whereas DNA concentration remains constant (e.g., [17, 18]). Triglycerides, the main long-term energy substrate in fishes, are also widely used, and tend to reflect longer-term responses to food limitation [19, 20]. However, the speed and extent to which these metrics respond to changes in diet depend on the study organism, experimental conditions, and reproductive stage [21]. For example, while liver glycogen depletion typically declines rapidly in response to food limitation (e.g., [15, 22]), Nagai and Ikeda [23] reported no decrease in liver glycogen in carp (*Cyprinus carpio*) following 22 days of fasting, Sockeye Salmon migrate 1000 km with no decrease in liver glycogen, and hepatic lipid and glycogen were mobilized simultaneously during early fasting in Atlantic Cod [21, 24, 25]. Thus, species specific laboratory validation is helpful for interpreting biomarkers of nutritional stress.

Given that the liver is highly sensitive to starvation, its condition is especially important for understanding nutritional stress in fishes. Histology studies indicate that the initial sensitivity of liver weight to fasting is due to a rapid atrophy of hepatocytes as energy sources are consumed (e.g., [16, 26, 27]), rather than because of a decline in the number of hepatocytes [28]. For example, Fernández-Díaz et al. [29] noted several alterations in the liver of *Solea senegalensis* larvae fed inert diet, including a decline in hepatocyte size, the loss of lipid vacuoles, and an increase in basophilia, possibly related to reduced protein synthesis. At later stages of fasting (i.e., starvation), hepatocyte loss occurs via several interrelated cell death mechanisms, including necrosis and apoptosis [30].

Another potential hepatic response to starvation is oxidative damage, which occurs when the production of reactive oxygen species overcomes antioxidant defense mechanisms [31]. The liver is the main organ for metabolic control, plays a key role in production of reactive oxygen

species, and is therefore vulnerable to oxidative damage [32]. Major antioxidant enzymes include superoxide dismutase, catalase, and glutathione peroxidase [33], while glutathione is the main non-enzymatic antioxidant [34]. Glutathione is the co-substrate for glutathione peroxidase and glutathione S-transferase and is the most abundant low molecular weight thiol synthesized by cells [34]. One of the major mechanisms of cellular injury due to oxidative damage is lipid peroxidation, typically indicated by elevated levels of the lipid peroxidation product malondialdehyde [35]. However, the oxidative stress response to fasting in fish livers is difficult to predict. On one hand, food is necessary for the acquisition and production of antioxidants, so fasting might be expected to increase oxidative stress [36]. On the other hand, metabolic demand of fishes declines rapidly with food deprivation [16, 37], which reduces the production of free radicals as the rate of mitochondrial respiration declines [38]. Studies to date suggest that glutathione and antioxidant enzymes in the livers of fishes are reduced by starvation, leading to oxidative stress [32, 33, 39].

Here, we conducted a time series experiment comparing the sensitivities of a wide range of biomarkers along a gradient of mild to severe starvation. We define sensitivity as the length of time (a proxy for severity of starvation) before a statistically significant difference was detected, with earlier detection considered more sensitive. We conducted the study on hatchery-raised Delta Smelt (*Hypomesus transpacificus*), a species listed as threatened and endangered at the federal and state levels, respectively [40]. Delta Smelt is endemic to the Sacramento and San Joaquin River Delta and San Francisco Estuary (SFE), an ecosystem that exhibits chronically low pelagic productivity [41-43]. There is a history of biomarker and stomach fullness work on Delta Smelt collected from the field, which provides evidence of contaminant and food limitation stress in the species [44, 45]. However, the nutritional biomarkers have not been empirically

validated in Delta Smelt, causing difficulties both in understanding the sensitivities of biomarkers to nutritional stress, and distinguishing between liver abnormalities caused by poor nutrition or contaminants, another known stressor in the SFE [46-48]. This study will therefore improve interpretation of health and condition data collected from wild Delta Smelt, informing conservation and restoration efforts. Key features of the study are that we 1) sampled up to 12 time points (depending on the biomarker), particularly early in the experiment, and 2) quantified a wide range of endpoints, including condition and hepatosomatic indices, biochemical, immunohistochemical, and histological biomarkers of nutritional stress, as well as daily mortality. These study features allowed us to compare the sensitivities of the biomarkers, gain a more mechanistic understanding of the progression of starvation in Delta Smelt and fish more generally, and to associate specific liver abnormalities with poor nutrition. Finally, we compared the starved and fed hatchery-origin experimental Delta Smelt to wild Delta Smelt in terms of the nutritional metrics examined in both groups.

Methods

Experimental endpoints

We examined six indices in the fasting experiment that we also measured on wild Delta Smelt. Fulton's condition factor, hepatosomatic index, RNA to DNA ratio in muscle, and triglyceride concentration in muscle were measured at 12 time points (Table 1). Liver lesion score (a summation of liver lesions scored histologically), and liver glycogen depletion (also scored histologically) were assessed at 10 time points (Table 1). The liver histopathology scoring and lesions are described in detail in Teh et al. [49]. As a summation of the severity scores of liver

lesions, liver lesion score provided a general indication of liver condition (higher scores indicate worse condition, [44, 49]; individual lesions in Table 2). The responses of the disaggregated lesions are also provided (Table 2). We expected liver lesion score to increase as starvation progressed as specific lesions were triggered and exacerbated by starvation. For example, we expected single cell necrosis or apoptosis to occur as hepatocytes starved, and then macrophages to aggregate around the dead cells [50].

We included ten additional endpoints that we do not routinely measure on wild fish (Table 1). Mortality was recorded daily. Hepatocyte area was measured at six time points, hepatocyte nucleus area at ten time points, and apoptosis at four time points (Table 1). These endpoints were included to understand whether livers of fasting fish decline in size due to atrophy of hepatocytes, loss of cells via apoptosis or necrosis, or some combination of these processes. Glutathione and lipid peroxidation (indicated by malondialdehyde) were both measured in liver at 12 time points. The enzymatic antioxidants superoxide dismutase, catalase, and glutathione peroxidase, as well as protein concentration, were measured in liver at five time points. Measurement of the oxidative stress endpoints allowed us to evaluate the impact of starvation on antioxidants, cell/tissue damage and the potential implications for fish health [31]. We expected starvation to deplete the concentration of total glutathione, tipping the balance toward a prooxidant state, enhancing hepatic lipid peroxidation. Decisions on how many time-points to sample and whether to pool tissue were based on maximizing use of the limited quantity of tissue available, feasibility (hepatocyte area, explained below) and cost, to a lesser extent.

Food limitation experiment

We conducted the fasting experiment at the Fish Conservation and Culture Laboratory (FCCL), near Byron, CA, USA [51]. The FCCL raises Delta Smelt in bead-filtered, UV-treated, recirculated, and temperature-controlled water pumped from the Sacramento-San Joaquin Delta. A two-week acclimation period began on Sept 24, 2018 when 800 Delta Smelt (143 days post-hatch) were moved from two holding tanks into eight experimental tanks in black '5-gallon' buckets, at a density of 100 fish tank^{-1} (Fig S1). At the time of sampling, mean fork length and body weight was 45.7 mm (SD = 6.4) and 0.54 g (SD = 0.27), respectively. Sub-adults were used in the experiment to both minimize the influence of reproduction on liver condition of female fish (glycogen depletion, [49]), while also providing sufficient tissue for each endpoint. The fish were in the buckets for no more than five min during transfer to the tanks. Tanks were roughly cylindrical, black, and plastic (Fig S1). Tank depth was 60 cm, wetted depth was 47 cm, diameter was 100 cm, and the working volume was 290 L. The fish in all eight tanks were fed to satiation throughout the acclimation period (i.e., aiming for a food to feces ratio of 0.25 on the bottom of the tanks), using the same feed on which they were cultured (Bio-vita Crum #1). Feedings occurred five times during the day (at ~06:45, 08:00, 10:00, 12:00, and 14:00). The tank bottoms were cleaned with a siphon three days per week, and this effort was maintained for all tanks throughout the experiment. We installed 5-µm filters on the inputs to each tank to ensure that no food particles entered the tanks other than during feedings ('10 inch by 2.5-inch sediment filters', iSpring Water Systems, LLC, Alpharetta, Georgia; Fig S1). The handful of mortalities that occurred during the two-week acclimation period were replaced with fish from the same cohort so that the density was exactly 100 fish tank^{-1} at the start of the experiment.

The experiment had two treatments called 'Feeding' (i.e., control) and 'No Feeding,' which were randomly assigned to the eight tanks (four tanks per treatment). We continued

feeding the Feeding treatment according to the regime described above. The final feeding for the No Feeding treatment occurred on Oct 8 at 08:00 (Day 0), and no further food was provided for the remainder of the eight-week experiment. Fish were sampled from ~10:30-12:30 at Day 0, 1, 2, 4, 7, 14, 21, 28, 35, 42, 49, and 56. At all but the final time point, four fish per tank were removed from the tanks with an aquarium net, gently shaken to remove water, wrapped in aluminum foil, and flash-frozen in liquid nitrogen [52]. At the final time point, one of the No Feeding tanks had only two fish remaining, which were both flash-frozen (all other tanks had at least 4 fish remaining). In addition to the flash-frozen samples, an additional fish from each tank was sampled, anesthetized in an ice-water bath, and placed in 10% buffered formalin for fixation and subsequent histology at a subset of the time points (Day 0, 4, 7, 14, 21, 28, 35, 42, 49, and 56).

Individual fish were not tagged, so initial measurements of length and weight were not made. While these measurements would have improved the sensitivity of condition factor and hepatosomatic index by accounting for inter-individual variation, they would have stressed the fish, and Delta Smelt is an unusually sensitive species [53]. In addition, we wanted the results to mimic the sensitivity of our long-term study on Delta Smelt in the wild, in which repeated measurements on the same individual cannot be made.

Water temperature was measured hourly throughout the experiment (HOBO Water Temp Pro v2, Onset). Ammonia, nitrite, and nitrate levels were measured using Hach testing kits every 3-4 days (Loveland, CO). Dissolved oxygen, pH, and salinity were also measured every 3-4 days, using a handheld YSI-85 m (YSI Incorporated, Yellow Springs, OH, USA). Mortalities were recorded and removed daily (only live sampled fish were measured for biomarkers).

Ethics statement

This study was approved by the University of California, Davis Institutional Animal Care and Use Committee and followed the experimental protocol for Animal Care and Use protocol #19872. The predefined humane endpoint was swimming activity, with our protocol stipulating that the experiment would be terminated when overall differences in swimming activity between the treatments were observed during daily monitoring. Fish in both treatments remained active throughout the experiment, so this criterion was not met. Mortality was not a planned outcome, but mortalities were recorded as part of standard protocol at the hatchery, so the data were included post-hoc. Occasional fish that appeared to be under duress in either treatment were not euthanized because it was difficult to predict whether such small, delicate fish would recover. Delta Smelt exhibit high mortality rates even under optimal conditions [51]. All staff obtained animal care and use training from UC Davis.

Laboratory fish processing

The 382 flash-frozen Delta Smelt sampled during the experiment were dissected at UC Davis following a slightly modified version of the methods of Teh et al. [52]. Briefly, each fish was removed from liquid nitrogen, photographed, weighed on an analytical balance (±0.01 mg), and measured for fork length. Each fish was dissected as it thawed over 5-10 min. Dorsal muscle tissue was excised, weighed on an analytical balance (±0.1 mg), frozen in liquid nitrogen, and then stored at -80 °C until processing for RNA to DNA ratio and triglycerides. The livers were removed from each fish, weighed, pooled in a 1.5-mL tube (4 livers per tube), placed in liquid nitrogen, and stored at -80 °C for oxidative stress analysis (glutathione, superoxide dismutase,

catalase, glutathione peroxidase, and malondialdehyde). Three fish were excluded because they had livers that were too small to be excised.

Fulton's condition factor and hepatosomatic index were calculated as follows: condition factor = $(W_B / FL^3) \times 100$ and hepatosomatic index = $(W_L / W_B) \times 100$, where W_B is the body weight (mg), FL is the fork length (mm) and W_L is the liver weight in mg [54].

Triglyceride concentration was measured in the frozen dorsal muscle samples using an adipogenesis assay kit (Catalog #K610- 100, Biovision, CA, USA), as per the manufacturer's instructions, and standardized to protein concentration using the method of Lowry et al. [55]. Samples were analyzed using a microplate reader (Tecan Infinite M200, Männedorf, Switzerland). Triglyceride concentration is reported in µmol of triglyceride per mg of protein.

RNA to DNA ratio in dorsal skeletal muscle was measured using the ethidium bromide fluorometric technique reported by Caldarone et al. [56].

Activities of catalase, superoxide dismutase, and glutathione peroxidase as well as lipid peroxidation by the thiobarbituric acid reactive substance (TBARS) assay were assessed in pools of 4 livers per tank-time point combination as described in Ramírez-Duarte et al. [57] with some modifications. Livers were homogenized by grinding at 4 °C in 50 mM potassium phosphate buffer (pH 7.4) containing 1 mM EDTA, 1 mM phenylmethanesulfonyl fluoride, 1% peroxidase free Triton X-100 and 1 mM dithiothreitol using a liver weight:buffer volume ratio of 1:20. Raw homogenate was used to assess lipid peroxidation following the method described by Ohkawa et al. [58] with some modifications and reported as malondialdehyde in nmol/g wet tissue. Homogenates were centrifuged at 10,000 × g for 20 min at 4 °C and the resulting supernatant was stored at -80 °C until analysis. Superoxide dismutase activity was determined by measuring the combined effects of EDTA, manganese ions and mercaptoethanol on the rate of NADH

oxidation according to Paoletti et al. [59]. Briefly, a final volume of 200 µL of reaction cocktail containing 0.05 mM potassium phosphate buffer, 0.25 mM NADH, 3.5 mM EDTA, 1.75 mM $MnSO_4$, 4 mM mercaptoethanol, and 5 µL of supernatant was prepared and absorbance at 340 nm was measured for 20 min at 25 °C. Superoxide dismutase activity is reported as Units/mg protein in the supernatant, where one unit is equal to 50% inhibition of NADH oxidation of the blank. The catalase assay was performed as described by Fernández-Díaz et al. [29] by following the reduction in absorbance of hydrogen peroxide at 240 nm in 96-well plates. Catalase activity was reported as Units/min/mg protein. Glutathione peroxidase activity was assessed by recording the oxidation of NADPH at 340 nm according to the method of Flohé and Günzler [60] and reported as Units/min/mg protein. A microplate reader (Tecan Infinite M200, Männedorf, Switzerland) was used to measure changes in absorbance. Protein concentration in the supernatant was measured following Lowry et al. [55] using the DC protein assay kit (Bio-Rad Laboratories, Hercules, CA, USA) and reported as mg/mg wet tissue. Concentration of total glutathione was measured as described in Ramírez-Duarte et al. [57] and reported as nmol/mg wet tissue.

The fish that were fixed directly in formalin were used for histological analysis (Day 0, 4, 7, 14, 21, 28, 35, 42, 49, and 56). Four transverse sections along the length of each fish were made using a razor blade (~4 mm thickness). Sections were taken immediately behind the opercular cavity, between the opercular cavity and the dorsal fin, just anterior to the dorsal fin, and just posterior to the dorsal fin. The four transverse sections were processed for histology and stained either with eosin and hematoxylin for histopathological assessment or periodic acid-Schiff (PAS) for glycogen depletion assessment following Teh et al. [61].

Using a compound microscope, the liver slides were scored for seven characteristics: glycogen depletion, hydropic vacuolar degeneration, single cell necrosis, macrophage aggregate, inflammation, cytoplasmic inclusion bodies, and lipidosis. Hydropic vacuolar degeneration is typified by a single large, hydropic-appearing vacuole, with smooth edges that nearly fills affected cells, with occasional unknown material within the vacuole [62]. The other histologic endpoints are described in Teh et al. [49]. Each endpoint was scored on an ordinal scale of 0-3, where 0 = absent/minimal, 1 = mild, 2 = moderate, and 3 = severe. Thus, the higher the score the more damaged or glycogen depleted the liver. The scores for each lesion (all but glycogen depletion) were summed to produce a composite score indicative of the overall condition of the liver (i.e., 'lesion score'; [44, 49]). Liver glycogen depletion was analyzed separately because it is not a lesion, and it typically responds within days to one week in response to food deprivation, whereas we expected the other endpoints to respond more slowly [15, 22, 63]. The liver was also screened for parasites, bacterial infection, preneoplastic foci and neoplasms, but these alterations were not observed.

To measure hepatocyte and nucleus area, photographs were taken of the liver sections on each histology slide. Identical settings and magnification were used for each photo (400×). The hepatocytes and nuclei (usually 10 of each, but as few as 6) were manually outlined using the program ImageJ and the area was calculated [64]. Hepatocytes and nuclei were selected for measurement that 1) could be clearly differentiated from one-another, and 2) had a visible nucleus (for hepatocyte area measurements) or nucleolus (for nuclei area measurements), indicating that a significant proportion of the cell or nucleus volume was sectioned (Figs 1E, F). To prevent bias, we began measuring hepatocytes and nuclei in the upper left-hand corner of each photo and proceeded back and forth, ultimately toward the lower right corner of the photo.

Along this 'backward S' pattern we measured every hepatocyte or nuclei that met both criteria until 10 measurements were collected for each endpoint or the end of the slide was reached. Hepatocyte area was not measured after Day 28 because it became too difficult to differentiate hepatocytes in the No Feeding treatment. Nuclei area was measured for all time points.

Using the formalin-fixed fish, liver tissue from the No Feeding treatment at Day 0, 21, 42, and 56 was prepared for immunohistochemical detection of apoptosis. Liver tissue from two fed fish was used as a control (Day 0 and 49). Tissues for immunohistochemistry were sectioned (3 µm) and adhered to Superfrost®Plus Microscope Slides (Fisher Scientific, Pittsburgh, PA, USA). Copper-exposed olfactory tissue from Delta Smelt was used as positive control and normal horse serum was substituted for the primary antibody as a no primary antibody control. After deparaffinization and rehydration, heat-induced epitope retrieval was performed in citrate buffer (pH 6) at 95-98 ºC for 10 min in a microwave (800W). Endogenous peroxidase activity was blocked using 3% H_2O_2 in methanol for 15 min followed by non-specific blocking with 10% normal horse serum for 15 min. Anti-cleaved caspase-3 polyclonal antibodies (Cat# G7481, Promega, Madison, WI, USA) at 1:2000 dilution were applied to the sections overnight at 4 ºC and subsequently incubated with HRP-conjugated secondary antibodies for 30 min at room temperature. Finally, antigen-antibody complexes were visualized with chromogen for 1 min. Sections were counterstained with Meyer's hematoxylin for 15 sec and mounted with Krystalon™ mounting media (MilliporeSigma, Burlington, MA, USA)

Comparison to wild fish

Our lab has received wild Delta Smelt collected during California Department of Fish and Wildlife and United States Fish and Wildlife trawls in 2011 and 2017, respectively. During the trawls, wild Delta Smelt were frozen in liquid nitrogen on agency boats and sent to our lab where we measured a range of indices (e.g., [44, 49, 52, 65]. The livers were scored histologically as described above. We note that while the preservation method between the experimental and wild fish was identical for condition, hepatosomatic and biochemical indices (i.e., flash freezing in liquid nitrogen), this was not the case for liver lesion score and glycogen depletion. For the wild fish, histology was performed on flash-frozen tissue, while histology was performed on tissue preserved in phosphate buffered formalin for the hatchery fish. Therefore, the results may not be perfectly comparable, although Teh et al. [52] reported no noteworthy differences between Delta Smelt liver tissue that was flash-frozen or fixed in phosphate buffered formalin. The present study includes data from wild Delta Smelt collected from Aug 2011 through Sep 2018.

Statistical analysis

A Kaplan-Meier survival analysis [66] was conducted to compare the mortality rates between the two treatments (Feeding [n= 400] and No Feeding [n= 400]). A log rank (Mantel-Cox) test was run to determine if there were differences in the survival distribution between the two treatments. Time to significance was determined by assessing overlap of the 95% confidence intervals of the survival curves for both treatments. The analysis was run in R.

Condition factor, hepatosomatic index, RNA to DNA ratio, and triglycerides were each analyzed using identical factorial ANOVAs. These analyses had 32 fish per time point, 16 in each treatment (except for the final time point, which had 14 fish in the No Feeding treatment). ‘Tank’ was included as a random effect to account for the repeated samples taken from the same

experimental unit [67]. Fixed effects included 'day' (as a discrete variable), 'treatment' (Feeding or No Feeding), and a 'day' by 'treatment' interaction. The interaction was included to account for any treatment specific changes in each endpoint as the experiment progressed from Day 0 to 56. Significant interactions between 'day' and 'treatment' were followed by 'test slices' at each time point to test for differences between the Feeding and No Feeding treatments (i.e., planned linear contrasts; [67]).

Glutathione, superoxide dismutase, catalase, glutathione peroxidase, protein, lipid peroxidation, malondialdehyde, hepatocyte area, and nucleus area were analyzed with nearly identical ANOVAs to the ones described above. For glutathione, superoxide dismutase, catalase, glutathione peroxidase, protein, malondialdehyde, and lipid peroxidation, the differences were that sample size was smaller because the four livers from each tank-time point combination were physically pooled during dissections, so 'tank' was not included in the analysis due to the pooling (n = 8 for each time point, 4 samples per treatment). In addition, malondialdehyde was $\log_{10}$-transformed because its variance increased with its mean. For superoxide dismutase, catalase, glutathione peroxidase and protein, there were fewer time points (Day 0, 7, 14, 21, and 56). For hepatocyte and nucleus area, the differences were that there were eight fish per time point in each analysis, one fish per tank-time point combination (i.e., the subset of fish that were preserved initially in buffered formalin, not flash-frozen). In addition, 'fish' was included as a random effect because multiple hepatocytes were measured per fish. For hepatocyte area, only Day 0, 4, 7, 14, 21, and 28 were included. Planned linear contrasts were applied following either significant interactions between 'treatment' and 'day' or a significant effect of 'treatment.' For all ANOVAs, consistency with their assumptions was confirmed with residual plots.

As non-parametric endpoints, glycogen depletion and liver lesion score were analyzed with Wilcoxon Rank Sum tests between the two treatments across all time points. All ANOVAs and the Wilcoxon tests were run at an alpha of 0.05 using JMP Pro 14.

Our final analysis compared wild Delta Smelt to the hatchery-reared Delta Smelt used in our experiment. We calculated means and standard deviations of variables that were measured on both the wild and experimental fish, including condition factor, hepatosomatic index, liver lesion score, liver glycogen depletion, RNA to DNA ratio, and triglycerides in muscle. For the experimental fish, means were calculated from Day 21-56, a period for which we know starvation was severe because both hepatocyte necrosis and mortality began to increase in the No Feeding treatment 3 weeks into the experiment (Table 2, Fig 2). We excluded all fish in the wild fish dataset that were outside the body weight range of the experimental fish to improve comparability (0.085 to 1.474 g). Sample sizes for each metric are in Table 3. All relevant data are within the Appendix S1.

Results

Water quality

Mean water temperature during the experiment was 15.9 °C (SD = 0.47), dissolved oxygen was 9.9 mg L^{-1} (SD = 0.3), salinity was 0.3 (SD = 0.04), pH was 7.7 (SD = 0.1), total ammonia nitrogen was 0.0 mg L^{-1} (SD = 0.03), nitrate was 1.5 mg L^{-1} (SD = 0.65), and nitrite was 0.0 mg L^{-1} (SD = 0.01).

Mortality

The mortality rate was similar between the two treatments until ~Day 21, when mortality began to increase in the No Feeding treatment (Fig 2). The survival distributions for the two treatments (Feeding and No Feeding) were statistically different ($X^2_1 = 21.3$, $P < 0.001$). Based on the overlap of the 95% confidence intervals, the difference in survival between the treatments became significant at Day 32 (Fig 2). Fish in the No Feeding treatment had a median time to mortality of 44 days, 95% CI [39.0, 49.0], while survival in the Feeding treatment did not decline below 50% during the experiment. A similar percentage of censored cases was present in the Feeding (75.3%) and No Feeding (62.0%) treatments (censored cases are individuals for which survival cannot be determined, such as individuals which survived until the experiment was terminated, or sampled fish). The number of live fish remaining in the tanks at Day 56 ranged from 17-23 in the Feeding treatment and 2-8 in the No Feeding treatment.

Condition and hepatosomatic indices

Condition factor declined with an increase in the fasting period (ANOVA, day × treatment, $F_{11, 352.3} = 8.2572$, $P <0.0001$), with the No Feeding treatment becoming significantly different from the Feeding treatment at Day 7 (planned linear contrast, $P = 0.0023$; Fig 3A). The fish in the Feeding treatment had a mean condition factor that was 1.16-fold higher than the No Feeding treatment at Day 7. The difference increased to 1.42-fold by Day 56.

Hepatosomatic index also declined with increased fasting (ANOVA, day × treatment, $F_{11, 349.2} = 5.0831$, $P < 0.0001$), with the No Feeding treatment becoming marginally significantly

different from the Feeding treatment at Day 2 (planned linear contrast, P = 0.0579), and significantly different at Day 4 (planned linear contrast, P = 0.0421). At Day 4, the Feeding treatment had a hepatosomatic index that was 1.34-fold higher than the No Feeding treatment. This difference increased to 2.31-fold by Day 56 (Fig 3B). The decline in hepatosomatic index in the No Feeding treatment plateaued after roughly Day 21 at ~0.75, indicating that livers were no longer decreasing as a proportion of body weight.

Nutrition and growth indices in muscle

RNA to DNA ratio declined in the No Feeding treatment as the experiment progressed (ANOVA, day × treatment, $F_{11, 349.2} = 2.5505$, P = 0.0041; Fig 3C). The difference between the treatments first became significant at Day 28 (planned linear contrast, P = 0.0029), when the Feeding treatment had an RNA to DNA ratio that was 1.4-fold higher than the No Feeding treatment. By Day 56 that difference had increased to 1.7-fold.

Triglyceride in muscle also declined in the No Feeding treatment as the experiment progressed (ANOVA, day × treatment, $F_{11, 350} = 2.1156$, P = 0.0187; Fig 3D). According to the planned linear contrasts, the difference between the treatments first became significant at Day 14 (P = 0.0308), with the Feeding treatment having triglyceride concentrations that were 1.35-fold higher than the No Feeding treatment. However, it was not until Day 49 that the differences became consistently significant (i.e., linear contrasts at Day 21, 28, 35, and 42 were not significant; Fig 3D).

Histology and immunohistochemistry

100% of the fish in both the Feeding and No Feeding treatments had food in their stomachs at Day 0 (8 of 8). Averaged over the rest of the time points, 90% and 10% of the fish in the Feeding and No Feeding treatments had food in their stomachs, respectively (e.g., Figs 4A, B). The occasional stomach contents in the No Feeding treatment appeared to be fish tissue, presumably eaten from mortalities before they were removed each day.

A significant difference was detected between the two treatments at Day 14 for both glycogen depletion (Wilcoxon Rank Sum test, Chi Square = 4.3974, DF = 1, P = 0.0360; Fig 5A) and liver lesion score (Wilcoxon Rank Sum test, Chi Square = 6.1370, DF = 1, P = 0.0132; Fig 5B). The most prevalent lesions in the No Feeding treatment were cytoplasmic inclusion body (CIB), single cell necrosis (SCN), and hydropic vacuolar degeneration (HVD). CIB was characterized by the presence of rimmed vesicles and unknown inclusion bodies in the cytoplasm of hepatocytes (Figs 1A, 1B). Higher incidences of CIB were observed from Day 7-21 (Table 2). SCN is characterized by cells having eosinophilic cytoplasm with pyknosis and karyorrhexis. Higher incidences of SCN began in the No Feeding treatment at Day 21 and lasted through Day 56 (i.e., the rest of the experiment; Fig 4E). Higher incidences of HVD began at Day 28 in the No Feeding treatment and lasted through the end of the experiment (Day 56; Table 2, Fig 4E). Gross liver atrophy was increasingly common in the No Feeding treatment as the experiment progressed (Fig 4C).

Hepatocyte area declined as the experiment progressed in the No Feeding treatment (ANOVA, day × treatment, $F_{5, 28.9} = 4.0483$, P = 0.0066), with hepatocyte area becoming significantly lower in the No Feeding treatment at Day 7 (planned linear contrast, P = 0.0145; Fig 5C). At Day 7, the hepatocytes had areas that were 1.45-fold larger in the Feeding treatment. By Day 28, the last time point during which hepatocytes could be differentiated reliably in the

No Feeding treatment, the hepatocytes in the Feeding treatment were 2.01-fold larger than in the No Feeding treatment (Figs 5C, 1E, 1F).

In addition to the decline in hepatocyte area, the hepatocyte nuclei became increasingly pyknotic as fasting progressed (Figs 1F, 4E, 4F). This observation is supported by the nucleus area measurements, which declined in the No Feeding treatment during the experiment (ANOVA, day × treatment, $F_{9, 54} = 3.7586$, $P = 0.0010$; Fig 5D). The difference between the treatments was marginally significant at Day 4 and 7 ($P = 0.0532$ and 0.0560, respectively), and highly significant by Day 14 ($P < 0.0001$; Fig 5D). Nucleus area at Day 14 was 1.72-fold higher in the fed treatment.

Apoptotic cells were not detected in the liver at any of the time points examined in the No Feeding treatment (Day 0 [control], 21, 42, or 56; Fig S2).

Oxidative stress in liver

Protein in liver was significantly reduced by starvation (ANOVA, treatment, $F_{1, 29} = 28.5707$, $P < 0.0001$; Fig 6A). Although a day by treatment interaction was not detected (ANOVA, $F_{4, 29} = 2.2552$, $P = 0.0875$), we observed a progressive decrease in liver protein in the No Feeding treatment over time, with the difference becoming significant at Day 14 (planned linear contrast, $P = 0.0068$; Fig 6A). Liver protein was 1.3-fold higher in the Feeding treatment at Day 14, and reached 1.5-fold higher than the No Feeding treatment by Day 56 of the experiment.

Glutathione declined as starvation progressed (ANOVA, day × treatment, $F_{11, 72} = 2.7175$, $P < 0.0055$; Fig 6B). The difference between the two treatments first became significant at Day 4 (planned linear contrast, $P = 0.0121$), at which glutathione was 1.32-fold higher in the No Feeding treatment. At Day 56 the difference was 1.80-fold.

Superoxide dismutase was significantly elevated in the No Feeding treatment (ANOVA, treatment, $F_{1, 25} = 15.3918$, $P = 0.0005$), but a significant day by treatment interaction was not observed (ANOVA, day × treatment, $F_{4, 29} = 1.0910$, $P = 0.3794$). A difference between the treatments was first detected at Day 14 (planned linear contrast, $P = 0.0228$), when superoxide dismutase activity was 1.51-fold higher in the No Feeding treatment (Fig 6C). This difference increased to 1.58-fold by Day 56.

Catalase activity increased as the experiment progressed in the No Feeding treatment (ANOVA, day × treatment, $F_{4, 29} = 4.5641$, $P = 0.0056$), becoming significantly different at Day 56 (planned linear contrast, $P = 0.0002$; Fig 6D).

Glutathione peroxidase was not affected by starvation (ANOVA, treatment, $F_{1, 25} = 0.2614$, $P = 0.6136$; day × treatment, $F_{4, 25} = 0.4625$, $P = 0.7625$; Fig 6E).

Malondialdehyde was affected by starvation (ANOVA, treatment, $F_{1, 71} = 7.1018$, $P = 0.0095$), but the day by treatment interaction was insignificant (ANOVA, $F_{11, 71} = 0.9367$, $P = 0.5111$; Fig 6F). Malondialdehyde in the No Feeding treatment was 2.1-fold higher than in the Feeding treatment, averaged across all time points. While malondialdehyde became significantly different at Day 2 between the treatments (planned linear contrast, $P = 0.0255$), the difference was highly inconsistent over time (Fig 6F).

Comparison to wild Delta Smelt

The wild fish were not consistently in better or worse nutritional condition compared to the experimental fish. In terms of hepatosomatic index, liver lesion score, and liver glycogen depletion, the means of the wild fish fell between the means of the fed and starved treatments

(Table 3), suggesting possible nutritional stress in the wild fish. Hepatosomatic index appeared to be especially depressed in the wild fish, with very similar scores to severely starved hatchery fish. In contrast, condition factor was higher in the wild fish than even the fish in the Feeding treatment (Table 3). RNA to DNA ratio was similar between the wild fish and fed fish, and wild fish had triglycerides in muscle that were considerably higher than the fed fish. In terms of liver lesion score, wild fish had livers that were in somewhat worse condition than the fed hatchery fish, but were in far better condition than the starved fish (Table 3). In summary, the wild fish outperformed the fish in the Feeding treatment in terms of three endpoints (condition factor, RNA to DNA ratio, and triglycerides), and underperformed the Feeding treatment fish in terms of the other three (hepatosomatic index, liver lesion score, and glycogen depletion; Table 3).

Discussion

In this study, we compared the sensitivities of an array of endpoints to increasingly severe starvation in Delta Smelt. The experiment was run at a temperature typical of fall and spring habitat of the species (15.9 °C), more than ten degrees below its critical thermal maximum [40, 68, 69]. Because we ran the experiment on an ectotherm, the indices would presumably have responded more quickly if the experiment was run at a higher temperature, and less quickly if it was run at a lower temperature (e.g., [6, 22]). While there are many studies examining the responses of hatchery fish to fasting, two aspects of our study set it apart. First, a wide range of endpoints were examined, including condition, hepatosomatic, biochemical, histological, and immunohistochemical indices (Tables 1 and 2). Second, 12 time points were sampled over the two-month experiment, including multiple time points during the first week. This experimental

design allowed us to compare the sensitivities of a wide range of indices to fasting, and to draw conclusions integrated across several disparate responses.

Hepatosomatic index was one of the most sensitive biomarkers measured in our study, responding significantly to fasting at Day 4 (Fig 3B). The rapid decline in hepatosomatic index indicates that the liver lost weight more quickly than extrahepatic tissue, leading to a decline in the liver's proportion of total body weight. Hepatosomatic index is well known to decline with food limitation, occurring as hepatic metabolic reserves are consumed (i.e., glycogen, lipid, and protein), and water used to maintain osmolarity is lost [14, 15, 22, 39, 70]. Surprisingly, we did not observe an increase in liver glycogen depletion until Day 14, whereas liver glycogen typically declines within hours or days of fasting (e.g., [22, 39, 71, 72]). It is possible that the declining size of the hepatocytes made the density of glycogen appear constant on the slides during the first two weeks of the experiment, even as total liver glycogen declined (Figs 1E, 1F). A biochemical assessment of hepatic glycogen in starved Delta Smelt would therefore be necessary to confirm that liver glycogen in Delta Smelt is indeed slow to respond to starvation (e.g., [72]), precluded here due to limitation of available liver tissue.

One goal of our study was to differentiate between hepatocyte death and atrophy as mechanisms driving the rapid decline in liver weight (i.e., 4 days, Fig 3B). While a high number of apoptotic cells were present in the positive control, they were not detected in the livers of the fish from the No Feeding treatment, even after 56 days of fasting (Fig S2). As in our experiment, Baumgarner et al. [28] detected a decline in hepatosomatic index but not apoptosis in the livers of Rainbow Trout starved for 28 days. Necrosis was detected in the No Feeding treatment, but not until the fish had been fasted for 21 days (Table 2). Thus, we found no evidence that the initial decline in hepatosomatic index was due to a decline in the number of hepatocytes.

However, there was strong evidence of hepatocyte atrophy, first in terms of hepatocyte area, followed by hepatocyte nuclei area (Figs 1F, 5C, 5D). While hepatocyte area responded more slowly to fasting (7 days) than hepatosomatic index (4 days), hepatosomatic index likely had more power because it had four times the sample size (32 vs 8 fish per time point). Our interpretation is therefore that the livers lost mass largely due to hepatocyte atrophy, at least until necrosis began, at Day 21 (Table 2). This interpretation is largely in line with previous studies that show declines in hepatocyte size as starvation progresses [16, 26, 27], although Peragón et al. [14] detected a loss of DNA in the livers of starved fish, which the authors interpreted as evidence of cell loss. However, the loss of DNA occurred after 70 days of fasting at 15.0 °C [14], well after necrosis became elevated in our experiment at a similar temperature (15.9 °C).

Although we found that hepatosomatic index is relatively sensitive to starvation in Delta Smelt, it should not be used in isolation. In mature females, vitellogenin is produced in the liver, increasing the weight of the organ (e.g., [73]). The endpoint can also be affected by contaminants (e.g., [74, 75]), known stressors in the SFE (e.g., [46, 76, 77]). In addition, hepatosomatic index is unlikely to be as sensitive as stomach fullness, which reflects daily foraging success in Delta Smelt (e.g., [44, 78]). A suite of laboratory-validated biomarkers is therefore recommended.

The liver histology results revealed a clear progression of pathologies as starvation increased in severity. Cytoplasmic inclusion bodies, which we suspect were autophagosomes, were the first abnormality detected histologically, becoming elevated in the No Feeding treatment at Day 7 (Table 2; [79]). Autophagy is a ubiquitous, highly conserved, protective mechanism that allows cells to maintain homeostasis during exposure to a variety of stressors, including starvation, infections, and contaminants [80-82]. During autophagy, long-lived proteins and organelles are packed inside vesicles within the cytoplasm. These vesicles then fuse

their outer membranes with lysosomes to form an autophagosome, which digests the enclosed material, providing nutrition [81]. Autophagy can begin 1-14 days after fasting begins, depending on the taxon (e.g., nematode: [83], fish [autophagy gene expression]: [84], mice: [85]). This timing is consistent with the appearance of cytoplasmic inclusion bodies in our experiment (Day 4-7). Starting at Day 21, the cytoplasmic inclusion bodies largely disappeared, and single cell necrosis, hydropic vacuolar degeneration, and mortality all became elevated above background levels (Table 2, Fig 2). We suggest that after 21 days of starvation, the role of autophagy as a mechanism to extend cell survival was impaired or no longer functional, leading to a failure of homeostatic mechanisms (i.e., ATP depletion and calcium homeostasis failure), necrosis, and mortality (Table 2, Fig 2). The liver protein data are also consistent with this interpretation, because liver protein became significantly depressed following the appearance of cytoplasmic inclusion bodies (Fig 6A). However, additional work is needed to confirm that the hepatic cytoplasmic inclusion bodies are autophagosomes (e.g., electron microscopy, [86]).

Another goal of our study was to distinguish liver abnormalities caused by starvation from other causes, because Delta Smelt are exposed to a variety of stressors in the SFE ([42, 87]). In Hammock et al. [44], we reported elevated lipidosis and inflammation in livers of juvenile Delta Smelt collected from Cache Slough, common responses of fish to contaminants (e.g., [76, 88, 89]). In the present study, liver lipidosis and inflammation were largely absent, even in severely starved fish. Instead, the major lesions were cytoplasmic inclusion bodies, followed by cell necrosis and hydropic vacuolar degeneration (Table 2). Thus, although the starved fish had unhealthy livers, like wild fish collected from Cache Slough, the specific lesions were quite distinct. Moreover, other lines of evidence support the hypothesis that the livers of Delta Smelt collected from Cache Slough were damaged by contaminants rather than nutritional

stress, including: 1) both zooplankton abundance and stomach fullness are relatively high in freshwater in summer [44, 45], 2) Delta Smelt collected from Cache Slough exhibited robust condition relative to fish collected from other regions [44], 3) contaminants have occurred in relatively high concentrations in the region [47], and 4) acute toxicity has been repeatedly detected in the region [46, 48, 77]. In addition, parasites and bacterial infections are unlikely causes of lesions because they are rare in the wild Delta Smelt population ([90], S. Teh *personal observation*), as well as the hatchery Delta Smelt. Thus, the present results strengthen the association between contaminants and liver alterations previously observed in Delta Smelt collected from Cache Slough [44], and will help disentangle liver damage caused by contaminants from nutritional stress in future studies.

RNA to DNA ratio and triglycerides in muscle were relatively insensitive to starvation, responding significantly at Day 28 and 14, respectively (Figs 3C, 3D). The RNA to DNA result was surprising given that the endpoint generally responds rapidly to changes in feeding rate. In one review, Buckley et al. [18] reported that RNA to DNA ratio responds to food limitation in as little as 1-3 days in a variety of young fishes. More recently, Duguid et al. [91] detected a decrease in RNA to DNA ratio within 6 days after a reduction in feeding in juvenile Atlantic Salmon. While triglycerides in muscle responded more quickly than RNA to DNA ratio, the difference between the Feeding and No Feeding treatments was small and inconsistent during the remaining six weeks of the experiment (Fig 3D). Thus, neither RNA to DNA ratio or triglycerides in muscle consistently responded to starvation before mortality rate became elevated (Fig 2). This presents a problem for detecting food limitation using these metrics in the wild, particularly if sample size is low, because Delta Smelt may experience lethal levels of nutritional stress before a response in either metric is detectable. One possible solution would be

to quantify RNA to DNA ratio and triglycerides in liver tissue, which was highly sensitive to starvation in other ways (Figs 1, 4, and 5). In Zebrafish for example, Lu et al. [72] recently detected a decline in triglycerides in liver after 3 days of fasting, at 28 °C.

One difficulty associated with measuring multiple endpoints on wild fish is that they can disagree, complicating interpretation. Hammock et al. [44] reported significantly depressed stomach fullness, condition factor, RNA to DNA ratio, and hepatosomatic index in Suisun Bay, a region that has exhibited a crash in primary and secondary productivity (e.g., [2, 92, 93]). However, the biomarker data were not entirely consistent with the paper's conclusion of nutritional stress in the region, because triglyceride concentration in muscle, 10-day otolith increment, and glycogen depletion were not significantly depressed in Suisun Bay [44]. Our rationale was that 10-day otolith increment and triglycerides in muscle might have been homogenized by movement of individuals among regions before they could respond to the environmental conditions of the region, whereas biomarkers that respond more quickly to environmental conditions, like stomach fullness, may better reflect conditions where an individual was collected [17, 18, 44]. However, the lack of a response in glycogen depletion weakened this interpretation because it generally responds rapidly to food limitation (e.g., [15, 22]). The current study therefore helps reconcile this inconsistency, demonstrating that glycogen depletion, at least when estimated histologically (as was the case in Hammock et al.[44]), is relatively slow to respond to food limitation in Delta Smelt. Thus, our experimental results strengthen the conclusion of summertime nutritional stress for Delta Smelt in Suisun Bay [44].

Of the four antioxidants measured, one decreased (glutathione), two increased (superoxide dismutase and catalase), and one was not affected by starvation (glutathione peroxidase; Fig 6). The net result was a roughly two-fold increase in levels of lipid peroxidation

in the No Feeding treatment that was highly inconsistent through time (Fig 6F). This contrasts with other fish species which show more consistent starvation-induced oxidative stress responses due to inadequate neutralization of reactive oxygen species [32, 33, 39, 94]. Our interpretation is that the increase in activities of catalase and superoxide dismutase could not compensate for the decreased concentration of glutathione, leading to an overall increase in lipid peroxidation in the starved fish. Another contributing factor to pro-oxidant effects of starvation may have been the loss of food-derived antioxidants such as vitamins C and E [94]. Given the evidence for both food limitation [41-43, 45]) and contaminants [46-48, 76, 77] in its habitat, Delta Smelt in the wild may be vulnerable to oxidative damage caused by contaminants, especially xenobiotic electrophiles detoxified by glutathione (e.g., organophosphates, such as chlorpyrifos or polycyclic aromatic hydrocarbons). Future work could explore the potential interaction between starvation and xenobiotics that are detoxified by glutathione-dependent mechanisms.

The comparison of nutritional condition between fed, starved, and wild Delta Smelt was inconclusive. On one hand, hepatosomatic index and glycogen depletion of the wild fish were very similar to the severely starved experimental fish, suggestive of nutritional stress in wild Delta Smelt (Table 3). On the other hand, condition factor, RNA to DNA ratio, and triglycerides were higher in wild fish than even the control fish, suggesting the opposite (Table 3). This result is unsurprising given that stark differences between hatchery and wild fish, especially in terms of diet and environmental conditions, are known to make comparisons difficult [21]. We note that although triglycerides in muscle were higher in the wild fish, there was far more adipose tissue present in the abdomen of the control hatchery fish (S. Teh, *personal observation*), which is typical of hatchery fishes [95]. Therefore, triglyceride in muscle appears to be a poor indicator of lipid reserves in Delta Smelt. Overall, we consider the relative sensitivities and mechanisms of

the responses to fasting as more applicable to the wild population than the values of the biomarkers themselves.

In conclusion, despite extensive work on other fishes, species-specific validation of biomarkers is necessary. In Delta Smelt, hepatosomatic index was highly sensitive to starvation, condition factor was somewhat sensitive, and RNA to DNA ratio in muscle, triglycerides in muscle, and glycogen depletion in liver (estimated histologically) were relatively insensitive. The initial decline in hepatosomatic index was most likely due to hepatocyte atrophy, rather than apoptosis or necrosis. In terms of liver histology, starved fish first exhibited cytoplasmic inclusion bodies, followed by glycogen depletion, necrosis, and hydropic vacuolar degeneration. Importantly, we detected no inflammation or lipidosis associated with starvation, in contrast to wild fish collected from Cache Slough [44]. Starvation induced a mixed response in hepatic antioxidants, resulting in lipid peroxidation. Glutathione in particular was rapidly lost as starvation progressed, suggesting that Delta Smelt under nutritional stress may become vulnerable to electrophilic contaminants. While some biomarkers were more sensitive to starvation than others, a range of endpoints are still recommended for use in wild fish exposed to multiple stressors. These could include not only a variety of biomarkers on the focal species, but also environmental data, such as toxicity, analytical chemistry, and prey abundance. Overall, our results strengthened the conclusions of Hammock et al. [44] of regionally specific stressors.

Acknowledgments

We are grateful to Galen Tigan and Luke Ellison for assistance running the experiment at the Fish Conservation and Culture Laboratory, and to California Department of Fish and Wildlife and the U.S. Fish and Wildlife Service for providing the wild Delta Smelt. We also thank Ching Teh, Adam Chorazyczewski, and other members of the Aquatic Health Program for their assistance and expertise processing the experimental fish, and Stuart Meyers for the use of his photomicroscope. Comments from several reviewers greatly improved the manuscript. Funding for this study was provided by U.S. Bureau of Reclamation R17AC00129. The views expressed are those of the authors and do not represent the official opinion of any employer, institution or government agency. The authors have no conflict of interest to declare.

References

1. Rabalais NN. Nitrogen in aquatic ecosystems. AMBIO: A Journal of the Human Environment. 2002;31(2):102-13.
2. Alpine AE, Cloern JE. Trophic interactions and direct physical effects control phytoplankton biomass and production in an estuary. Limnology and Oceanography. 1992;37(5):946-55.
3. Ricciardi A, Neves RJ, Rasmussen JB. Impending extinctions of North American freshwater mussels (Unionoida) following the zebra mussel (*Dreissena polymorpha*) invasion. Journal of Animal Ecology. 1998;67(4):613-9.
4. Pörtner HO, Farrell AP. Physiology and climate change. Science. 2008;322(5902):690-2.
5. Isaak DJ, Rieman BE. Stream isotherm shifts from climate change and implications for distributions of ectothermic organisms. Global Change Biology. 2013;19(3):742-51.
6. Brown JH, Gillooly JF, Allen AP, Savage VM, West GB. Toward a metabolic theory of ecology. Ecology. 2004;85(7):1771-89.
7. Deutsch C, Ferrel A, Seibel B, Pörtner H-O, Huey RB. Climate change tightens a metabolic constraint on marine habitats. Science. 2015;348(6239):1132-5.
8. Williams DE, Craig M, Dawe SC, Kent ML, Holmes CF, Andersen RJ. Evidence for a covalently bound form of microcystin-LR in salmon liver and dungeness crab larvae. Chemical Research in Toxicology. 1997;10(4):463-9.
9. Davis TW, Berry DL, Boyer GL, Gobler CJ. The effects of temperature and nutrients on the growth and dynamics of toxic and non-toxic strains of Microcystis during cyanobacteria blooms. Harmful algae. 2009;8(5):715-25.
10. Lehman P, Teh SJ, Boyer G, Nobriga M, Bass E, Hogle C. Initial impacts of Microcystis aeruginosa blooms on the aquatic food web in the San Francisco Estuary. Hydrobiologia. 2010;637(1):229-48.
11. Lehman P, Kurobe T, Lesmeister S, Baxa D, Tung A, Teh SJ. Impacts of the 2014 severe drought on the Microcystis bloom in San Francisco Estuary. Harmful Algae. 2017;63:94-108.
12. Cazenave J, Wunderlin DA, de los Ángeles Bistoni M, Amé MV, Krause E, Pflugmacher S, et al. Uptake, tissue distribution and accumulation of microcystin-RR in Corydoras paleatus, Jenynsia multidentata and Odontesthes bonariensis: a field and laboratory study. Aquatic Toxicology. 2005;75(2):178-90.
13. Hards AR, Gray MA, Noël SC, Cunjak RA. Utility of Condition Indices as Predictors of Lipid Content in Slimy Sculpin (Cottus cognatus). Diversity. 2019;11(5):71.
14. Peragón J, Barroso JB, García-Salguero L, Aranda F, De La Higuera M, Lupiáñez JA. Selective changes in the protein-turnover rates and nature of growth induced in trout liver by long-term starvation followed by re-feeding. Molecular and cellular biochemistry. 1999;201(1-2):1-10.
15. De Pedro N, Delgado M, Gancedo B, Alonso-Bedate M. Changes in glucose, glycogen, thyroid activity and hypothalamic catecholamines in tench by starvation and refeeding. Journal of Comparative Physiology B. 2003;173(6):475-81.
16. Zeng L-Q, Li F-J, Li X-M, Cao Z-D, Fu S-J, Zhang Y-G. The effects of starvation on digestive tract function and structure in juvenile southern catfish (Silurus meridionalis Chen). Comparative Biochemistry and Physiology Part A: Molecular & Integrative Physiology. 2012;162(3):200-11.
17. Buckley L. RNA-DNA ratio: an index of larval fish growth in the sea. Marine Biology. 1984;80(3):291-8.
18. Buckley L, Caldarone E, Ong T-L. RNA–DNA ratio and other nucleic acid-based indicators for growth and condition of marine fishes. Hydrobiologia. 1999;401:265-77.

19. Håkanson J, Coombs S, Ré P. Lipid and elemental composition of sprat (Sprattus sprattus) larvae at mixed and stratified sites in the German Bight of the North Sea. ICES Journal of Marine Science: Journal du Conseil. 1994;51(2):147-54.
20. Lochmann SE, Maillet GL, Frank KT, Taggart CT. Lipid class composition as a measure of nutritional condition in individual larval Atlantic cod (Gadus morhua). Canadian Journal of Fisheries and Aquatic Sciences. 1995;52(6):1294-306.
21. Navarro I, Gutiérrez J. Fasting and starvation. Biochemistry and molecular biology of fishes. 4: Elsevier; 1995. p. 393-434.
22. Mehner T, Wieser W. Energetics and metabolic correlates of starvation in juvenile perch (Perca fluviatilis). Journal of fish biology. 1994;45(2):325-33.
23. NAGAI M, IKEDA S. Carbohydrate metabolism in fish. 1. Effects of starvation and dietary composition on the blood glucose level and the hepatopancreatic glycogen and lipid contents in carp. Bulletin of the Japanese Society of Scientific Fisheries. 1971;37(5):404-9.
24. French CJ, Hochachka PW, Mommsen TP. Metabolic organization of liver during spawning migration of sockeye salmon. American Journal of Physiology-Regulatory, Integrative and Comparative Physiology. 1983;245(6):R827-R30.
25. Black D, Love RM. The sequential mobilisation and restoration of energy reserves in tissues of Atlantic cod during starvation and refeeding. Journal of Comparative Physiology B. 1986;156(4):469-79.
26. Hur JW, Jo JH, Park I-S. Effects of long-term starvation on hepatocyte ultrastructure of olive flounder Paralichthys olivaceus. Ichthyological Research. 2006;53(3):306-10.
27. Li S, Li J, Zhao Y, Zhang Q, Wang Q. Nutrient sensing signaling integrates nutrient metabolism and intestinal immunity in grass carp, Ctenopharyngodon idellus after prolonged starvation. Fish & shellfish immunology. 2017;71:50-7.
28. Baumgarner BL, Riley CP, Sepulveda MS, Brown PB, Meyer JL, Adamec J. Increased expression of GAPDH protein is not indicative of nitrosative stress or apoptosis in liver of starved rainbow trout (Oncorhynchus mykiss). Fish physiology and biochemistry. 2012;38(2):319-27.
29. Fernández-Díaz C, Kopecka J, Cañavate JP, Sarasquete C, Solé M. Variations on development and stress defences in Solea senegalensis larvae fed on live and microencapsulated diets. Aquaculture. 2006;251(2-4):573-84.
30. Mariño G, Niso-Santano M, Baehrecke EH, Kroemer G. Self-consumption: the interplay of autophagy and apoptosis. Nature Reviews Molecular cell biology. 2014;15(2):81-94.
31. Monserrat J, Letts RE, Ferreira JLR, Ventura-Lima J, Amado LL, Rocha AM, et al. Biomarkers of oxidative stress: benefits and drawbacks for their application in biomonitoring of aquatic environments. Oxidative stress in aquatic ecosystems. 2011:317-26.
32. Morales AE, Pérez-Jiménez A, Hidalgo MC, Abellán E, Cardenete G. Oxidative stress and antioxidant defenses after prolonged starvation in Dentex dentex liver. Comparative Biochemistry and Physiology Part C: Toxicology & Pharmacology. 2004;139(1-3):153-61.
33. Furné M, García-Gallego M, Hidalgo M, Morales A, Domezain A, Domezain J, et al. Oxidative stress parameters during starvation and refeeding periods in Adriatic sturgeon (Acipenser naccarii) and rainbow trout (Oncorhynchus mykiss). Aquaculture Nutrition. 2009;15(6):587-95.
34. Forman HJ, Zhang H, Rinna A. Glutathione: overview of its protective roles, measurement, and biosynthesis. Molecular aspects of medicine. 2009;30(1-2):1-12.
35. Lesser MP. Oxidative stress in tropical marine ecosystems. Oxidative stress in aquatic ecosystems. 2011:7-19.
36. Birnie-Gauvin K, Costantini D, Cooke SJ, Willmore WG. A comparative and evolutionary approach to oxidative stress in fish: a review. Fish and Fisheries. 2017;18(5):928-42.

37. García-Esquivel Z, Bricelj VM, Felbeck H. Metabolic depression and whole-body response to enforced starvation by Crassostrea gigas postlarvae. Comparative Biochemistry and Physiology Part A: Molecular & Integrative Physiology. 2002;133(1):63-77.
38. Lambert AJ, Brand MD. Reactive oxygen species production by mitochondria. Mitochondrial DNA: Springer; 2009. p. 165-81.
39. Rossi A, Cazenave J, Bacchetta C, Campana M, Parma MJ. Physiological and metabolic adjustments of Hoplosternum littorale (Teleostei, Callichthyidae) during starvation. Ecological Indicators. 2015;56:161-70.
40. Bennett WA. Critical assessment of the delta smelt population in the San Francisco Estuary, California. San Francisco Estuary and Watershed Science. 2005;3(2).
41. Feyrer F, Herbold B, Matern SA, Moyle PB. Dietary shifts in a stressed fish assemblage: consequences of a bivalve invasion in the San Francisco Estuary. Environmental Biology of Fishes. 2003;67(3):277-88.
42. Sommer T, Armor C, Baxter R, Breuer R, Brown L, Chotkowski M, et al. The collapse of pelagic fishes in the upper San Francisco Estuary. Fisheries. 2007;32(6):270-7.
43. Hamilton SA, Murphy DD. Analysis of Limiting Factors Across the Life Cycle of Delta Smelt (Hypomesus transpacificus). Environmental management. 2018:1-18.
44. Hammock BG, Hobbs, J.A., Slater, S.B., Acuña, S, Teh S.J. Contaminant and food limitation stress in an endangered estuarine fish. Science of the Total Environment. 2015;532:316-26. doi: 10.1016/j.scitotenv.2015.06.018.
45. Hammock BG, Slater SB, Baxter RD, Fangue NA, Cocherell D, Hennessy A, et al. Foraging and metabolic consequences of semi-anadromy for an endangered estuarine fish. PLOS ONE. 2017;12(3):e0173497.
46. Werner I, Deanovic LA, Connor V, de Vlaming V, Bailey HC, Hinton DE. Insecticide-caused toxicity to Ceriodaphnia dubia (CLADOCERA) in the Sacramento–San Joaquin River delta, California, USA. Environmental Toxicology and Chemistry. 2000;19(1):215-27.
47. Kuivila KM, Moon GE, editors. Potential exposure of larval and juvenile delta smelt to dissolved pesticides in the Sacramento-San Joaquin Delta, California. American Fisheries Society Symposium; 2004: American Fisheries Society.
48. Weston DP, Moschet C, Young TM. Chemical and Toxicological Effects on Cache Slough after Storm-Driven Contaminant Inputs. San Francisco Estuary and Watershed Science. 2019;17:3.
49. Teh SJ, Schultz AA, Duarte WR, Acuña S, Barnard DM, Baxter RD, et al. Histopathological assessment of seven year-classes of Delta Smelt. Science of The Total Environment. 2020:138333.
50. Kumar V, Abbas AK, Fausto N, Aster JC. Robbins and Cotran pathologic basis of disease, professional edition e-book: Elsevier health sciences; 2014.
51. Lindberg JC, Tigan G, Ellison L, Rettinghouse T, Nagel MM, Fisch KM. Aquaculture methods for a genetically managed population of endangered Delta Smelt. North American Journal of Aquaculture. 2013;75(2):186-96.
52. Teh SJ, Baxa DV, Hammock BG, Gandhi SA, Kurobe T. A novel and versatile flash-freezing approach for evaluating the health of Delta Smelt. Aquatic Toxicology. 2016;170:152-61.
53. Moyle PB, Brown LR, Durand JR, Hobbs JA. Delta smelt: life history and decline of a once-abundant species in the San Francisco Estuary. San Francisco Estuary and Watershed Science. 2016;14(2).
54. Ricker WE. Computation and interpretation of biological statistics of fish populations. Fish Research Board Canada. 1975;191:1-382.
55. Lowry OH, Rosebrough NJ, Farr AL, Randall RJ. Protein measurement with the Folin phenol reagent. The Journal of Biological Chemistry. 1951;193(1):265-75.

56. Caldarone EM, Wagner M, St Onge-Burns J, Buckley LJ. Protocol and guide for estimating nucleic acids in larval fish using a fluorescence microplate reader. Northeast Fisheries Science Center Reference Document. 2001;1(11):1-22.
57. Ramírez-Duarte WF, Jin J, Kurobe T, Teh SJ. Effects of prolonged exposure to low pH on enzymatic and non-enzymatic antioxidants in Japanese Medaka (Oryzias latipes). Science of The Total Environment. 2016;568:26-32.
58. Ohkawa H, Ohishi N, Yagi K. Assay for lipid peroxides in animal tissues by thiobarbituric acid reaction. Analytical biochemistry. 1979;95(2):351-8.
59. Paoletti F, Mocali A, Aldinucci D. Superoxide-driven NAD (P) H oxidation induced by EDTA-manganese complex and mercaptoethanol. Chemico-biological interactions. 1990;76(1):3-18.
60. Flohe L, Günzler WA. [12] Assays of glutathione peroxidase. Methods in enzymology. 105: Elsevier; 1984. p. 114-20.
61. Teh S, Adams S, Hinton D. Histopathologic biomarkers of anthropogenic stress in resident redbreast sunfish (Lepomis auritus) and largemouth bass (Micropterus salmoides lacèpède) from contaminant impacted sites. Aquatic Toxicology. 1997;37:51-70.
62. Stehr C, Johnson LL, Myers MS. Hydropic vacuolation in the liver of three species of fish from the US West Coast: lesion description and risk assessment associated with contaminant exposure. Diseases of aquatic organisms. 1998;32(2):119-35.
63. Li H, Xu W, Jin J, Yang Y, Zhu X, Han D, et al. Effects of starvation on glucose and lipid metabolism in gibel carp (Carassius auratus gibelio var. CAS III). Aquaculture. 2018;496:166-75.
64. Schneider CA, Rasband WS, Eliceiri KW. NIH Image to ImageJ: 25 years of image analysis. Nature methods. 2012;9(7):671-5.
65. Hammock BG, Hartman R, Slater SB, Hennessy A, Teh SJ. Tidal Wetlands Associated with Foraging Success of Delta Smelt. Estuaries and Coasts. 2019;42:857-67. doi: 10.1007/s12237-019-00521-5.
66. Kaplan EL, Meier P. Nonparametric estimation from incomplete observations. Journal of the American statistical association. 1958;53(282):457-81.
67. Sall J, Lehman A, Creighton L. JMP start statistics: a guide to statistics and data analysis using JMP2007.
68. Moyle PB, Herbold B, Stevens DE, Miller LW. Life history and status of delta smelt in the Sacramento-San Joaquin Estuary, California. Transactions of the American Fisheries Society. 1992;121(1):67-77.
69. Komoroske L, Connon R, Lindberg J, Cheng B, Castillo G, Hasenbein M, et al. Ontogeny influences sensitivity to climate change stressors in an endangered fish. Conservation Physiology. 2014;2(1):cou008.
70. Cahill Jr GF. Starvation in man. New England Journal of Medicine. 1970;282(12):668-75.
71. Boujard T, Leatherland J. Circadian pattern of hepatosomatic index, liver glycogen and lipid content, plasma non-esterified fatty acid, glucose, T3, T4, growth hormone and cortisol concentrations in Oncorhynchus mykiss held under different photoperiod regimes and fed using demand-feeders. Fish Physiology and Biochemistry. 1992;10(2):111-22.
72. Lu DL, Ma Q, Wang J, Li LY, Han SL, Limbu SM, et al. Fasting enhances cold resistance in fish through stimulating lipid catabolism and autophagy. The Journal of physiology. 2019;597(6):1585-603.
73. Nicolas J-M. Vitellogenesis in fish and the effects of polycyclic aromatic hydrocarbon contaminants. Aquatic toxicology. 1999;45(2-3):77-90.
74. Pereira J, Mercaldo-Allen R, Kuropat C, Luedke D, Sennefelder G. Effect of cadmium accumulation on serum vitellogenin levels and hepatosomatic and gonadosomatic indices of winter flounder (Pleuronectes americanus). Archives of Environmental Contamination and Toxicology. 1993;24(4):427-31.

75. Deng S-X, Tian L-X, Liu F-J, Jin S-J, Liang G-Y, Yang H-J, et al. Toxic effects and residue of aflatoxin B1 in tilapia (Oreochromis niloticus× O. aureus) during long-term dietary exposure. Aquaculture. 2010;307(3-4):233-40.
76. Greenfield BK, Teh SJ, Ross JR, Hunt J, Zhang G, Davis JA, et al. Contaminant concentrations and histopathological effects in Sacramento splittail (Pogonichthys macrolepidotus). Archives of environmental contamination and toxicology. 2008;55(2):270-81.
77. Weston DP, Asbell AM, Lesmeister SA, Teh SJ, Lydy MJ. Urban and agricultural pesticide inputs to a critical habitat for the threatened delta smelt (Hypomesus transpacificus). Environmental Toxicology and Chemistry. 2014;33(4):920-9.
78. Hobbs J, Bennett W, Burton J. Assessing nursery habitat quality for native smelts (Osmeridae) in the low-salinity zone of the San Francisco estuary. Journal of Fish Biology. 2006;69(3):907-22.
79. Xia X, Wang X, Qin W, Jiang J, Cheng L. Emerging regulatory mechanisms and functions of autophagy in fish. Aquaculture. 2019:734212.
80. Moore MN, Koehler A, Lowe D, Viarengo A. Chapter Thirty-Three Lysosomes and Autophagy in Aquatic Animals. Methods in Enzymology. 2008;451:581-620.
81. Yabu T, Imamura S, Mizusawa N, Touhata K, Yamashita M. Induction of autophagy by amino acid starvation in fish cells. Marine biotechnology. 2012;14(4):491-501.
82. Chiarelli R, Martino C, Agnello M, Bosco L, Roccheri MC. Autophagy as a defense strategy against stress: focus on Paracentrotus lividus sea urchin embryos exposed to cadmium. Cell Stress and Chaperones. 2016;21(1):19-27.
83. Kang C, You Y-j, Avery L. Dual roles of autophagy in the survival of Caenorhabditis elegans during starvation. Genes & development. 2007;21(17):2161-71.
84. Seiliez I, Gutierrez J, Salmerón C, Skiba-Cassy S, Chauvin C, Dias K, et al. An in vivo and in vitro assessment of autophagy-related gene expression in muscle of rainbow trout (Oncorhynchus mykiss). Comparative Biochemistry and Physiology Part B: Biochemistry and Molecular Biology. 2010;157(3):258-66.
85. Mizushima N, Komatsu M. Autophagy: renovation of cells and tissues. Cell. 2011;147(4):728-41.
86. Eskelinen E-L, Reggiori F, Baba M, Kovács AL, Seglen PO. Seeing is believing: the impact of electron microscopy on autophagy research. Autophagy. 2011;7(9):935-56.
87. Feyrer F, Newman K, Nobriga M, Sommer T. Modeling the effects of future outflow on the abiotic habitat of an imperiled estuarine fish. Estuaries and Coasts. 2011;34(1):120-8.
88. Agamy E. Histopathological liver alterations in juvenile rabbit fish (Siganus canaliculatus) exposed to light Arabian crude oil, dispersed oil and dispersant. Ecotoxicology and Environmental Safety. 2012;75:171-9.
89. Wolf JC, Wolfe MJ. A brief overview of nonneoplastic hepatic toxicity in fish. Toxicologic Pathology. 2005;33(1):75-85.
90. Foott JS, Bigelow J. Pathogen survey, gill Na-K-ATPase activity, and leukocyte profile of adult Delta Smelt. California Fish and Game. 2010;96(4):223-31.
91. Duguid WD, Iwanicki TW, Journey ML, Noel AL, Beckman BR, Juanes F. Assessing Indices of Growth for Field Studies of Juvenile Salmon: An Experiment and Synthesis. Marine and Coastal Fisheries. 2018;10(2):204-23.
92. Kimmerer WJ, Gartside E, Orsi JJ. Predation by an introduced clam as the likely cause of substantial declines in zooplankton of San Francisco Bay. Marine Ecology Progress Series Oldendorf. 1994;113(1):81-93.
93. Sobczak WV, Cloern JE, Jassby AD, Müller-Solger AB. Bioavailability of organic matter in a highly disturbed estuary: The role of detrital and algal resources. Proceedings of the National Academy of Sciences. 2002;99(12):8101-5.

94. Morales AE, Pérez-Jiménez A, Furné M, Guderley H. Starvation, energetics, and antioxidant defenses. Oxidative stress in aquatic ecosystems. 2011:281-94.
95. Houlihan D, Boujard T, Jobling M. Food intake in fish: John Wiley & Sons; 2008.

Table 1. Sampling time points, details, and effort for each endpoint examined in the study. Preservation is the initial method used to preserve the fish, 'n' refers the number of fish per time-point (i.e., for condition factor 16 fish were used from each treatment), and 'Wild' refers to whether the endpoint was also measured on wild fish.

Endpoint	Method	Tissue	Time points (days)	n	Pres	Wild
CF	M/Grav	Fish	0, 1, 2, 4, 7, 14, 21, 28, 35, 42, 49, 56	32	LN	Yes
HSI	Grav	Liver/fish	0, 1, 2, 4, 7, 14, 21, 28, 35, 42, 49, 56	32	LN	Yes
RNA/DNA	Biochem	Muscle	0, 1, 2, 4, 7, 14, 21, 28, 35, 42, 49, 56	32	LN	Yes
TAG	Biochem	Muscle	0, 1, 2, 4, 7, 14, 21, 28, 35, 42, 49, 56	32	LN	Yes
LS	Histo	Liver	0, 4, 7, 14, 21, 28, 35, 42, 49, 56	8	Form	Yes
GD	Histo	Liver	0, 4, 7, 14, 21, 28, 35, 42, 49, 56	8	Form	Yes
HA	Histo	Liver	0, 4, 7, 14, 24, 28	8	Form	No
HNA	Histo	Liver	0, 4, 7, 14, 21, 28, 35, 42, 49, 56	8	Form	No
Apoptosis	IH	Liver	0, 24, 42, 56	1	Form	No
Glutathione	Biochem	Liver	0, 1, 2, 4, 7, 14, 21, 28, 35, 42, 49, 56	8	LN	No
Malon	Biochem	Liver	0, 1, 2, 4, 7, 14, 21, 28, 35, 42, 49, 56	8	LN	No
SOD	Biochem	Liver	0, 7, 14, 21, 56	8	LN	No
Catalase	Biochem	Liver	0, 7, 14, 21, 56	8	LN	No
Glut P	Biochem	Liver	0, 7, 14, 21, 56	8	LN	No
Protein	Biochem	Liver	0, 7, 14, 21, 56	8	LN	No
Mortality	Count	Fish	Daily	NA	NA	No

Abbreviations: CF: condition factor, HSI: hepatosomatic index, TAG: triglycerides, LS: lesion score, GD: glycogen depletion, HA: hepatocyte area, HNA: hepatocyte nucleus area, Malon: malondialdehyde, SOD: Superoxide dismutase, Glut P: Glutathione peroxidase IH: immunohistochemistry, M: morphometric, Grav: gravimetric, Histo: histological, Pres: Preservative, LN: liquid nitrogen, Form: formalin

	GD		HVD		SCN		MA		INF		CIB		LIP	
Day	F	NF	F	NF	F	NF	F	NF	F	NF	F	NF	F	NF
0	1.3	0.5			0.25					0.25				
4	0.8	0.7			0.25	0.67						0.33		
7	1	1			0.5						0.25	0.75		
14	1	2.5				0.5		0.75				0.75		
21	0.5	2				1			0.25	0.25		0.75		
28	0.5	1		0.5				0.25		0.25	0.25			
35		2.5		0.75		0.75				0.25		0.25	0.25	
42	0.5	2.8		0.75		2.25		0.5					0.25	
49	1	2.8		1.25		0.75	0.25	0.5					0.25	
56		1.5		1		1.25		0.25		0.25				

Table 2. Mean liver histological results from the experiment. F is Feeding, No F is No Feeding. GD is glycogen depletion, HVD is hydropic vacuolar degeneration, SCN is single cell necrosis, MA is macrophage aggregate, INF is inflammation, CIB is cytoplasmic inclusion body, and LIP is lipidosis. 0 = absent/minimal, 1 = mild, 2 = moderate, and 3 = severe. Note that fields with mean scores of 0.0 were left blank.

Table 3. Comparison of wild Delta Smelt to hatchery Delta Smelt from the Feeding and No Feeding treatments. For the hatchery fish, means were calculated across Day 21-56 (i.e., 21 days is the point where starvation induced mortality was first apparent, Fig 2). CF is condition factor, HSI is hepatosomatic index, Liver LS is liver lesion score, and Liver GD is liver glycogen depletion (higher scores indicate worse condition for Liver LS and GD).

	Feeding			No Feeding			Wild		
Biomarker	Mean	SD	n	Mean	SD	n	Mean	SD	n
CF	0.553	0.082	96	0.418	0.074	94	0.696	0.086	967
HSI	1.67	0.607	96	0.723	0.239	93	0.793	0.287	854
Liver LS	0.25	0.532	24	2.29	1.83	24	0.380	0.915	526
Liver GD	0.417	0.717	24	2.083	0.974	24	1.854	0.993	526
RNA/DNA	1.89	0.600	96	1.35	0.45	94	1.984	0.828	665
Triglycerides	0.175	0.043	96	0.133	0.043	94	0.294	0.191	356

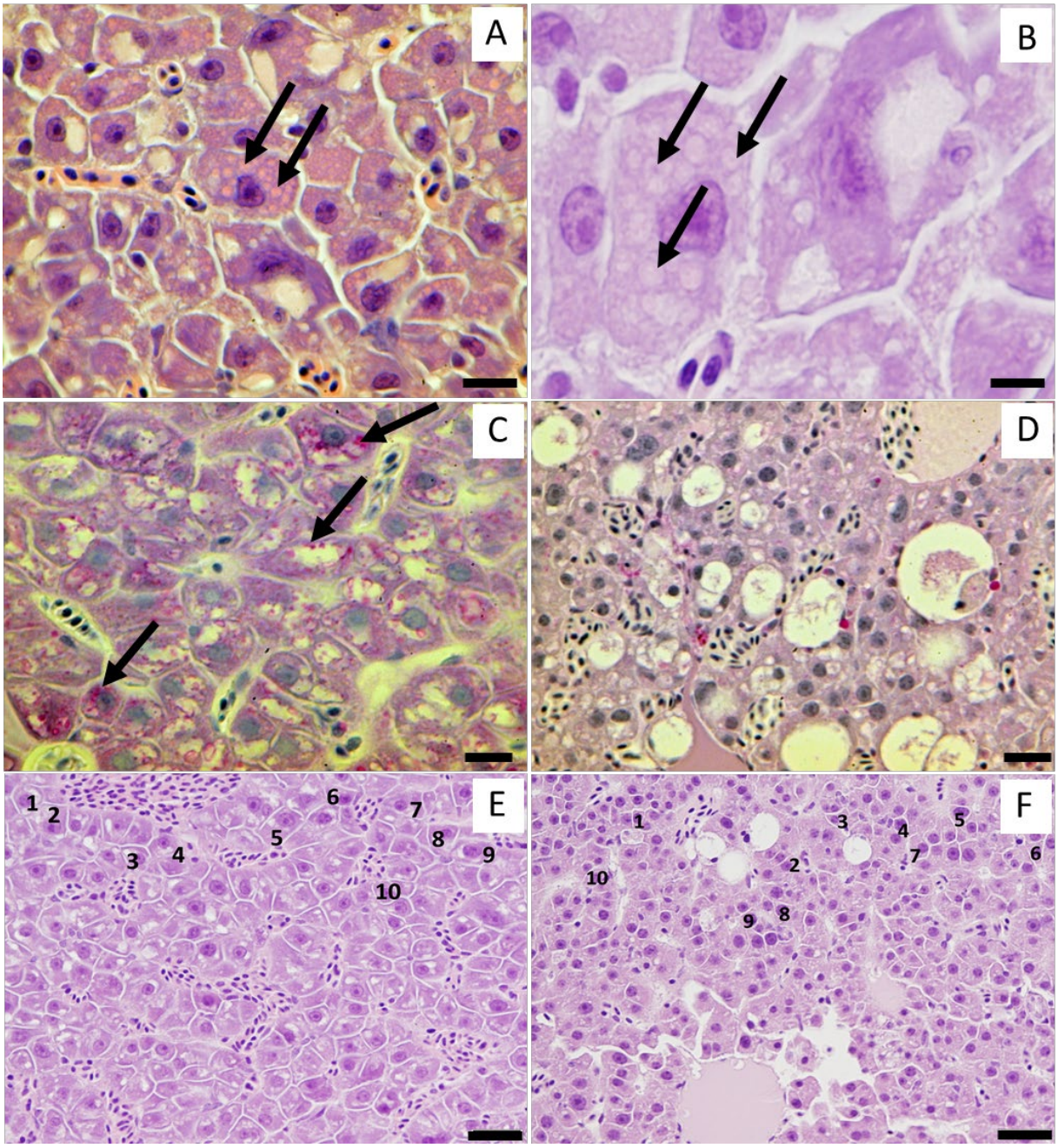

Fig 1. Liver histopathology. Panel A: Liver of Delta Smelt from the No Feeding treatment at Day 4. Arrows indicate eosinophilic cytoplasmic inclusion bodies, possibly autophagosomes. Panel B: Liver of Delta Smelt from the No Feeding treatment at Day 7, cytoplasmic inclusion bodies (indicated by arrows) at higher magnification. Note possible double membranes. Panel C: Liver of Delta Smelt from the Feeding treatment, PAS stain. Arrows indicate glycogen granules

in the cytoplasm of hepatocytes that are stained magenta (compare to panel D). Panel D: Liver from Delta Smelt from the No Feeding treatment at Day 21, PAS stain. No magenta glycogen granules observed in cytoplasm of hepatocytes (compare to panel C). Panel E: Liver of Delta Smelt from the Feeding treatment, H&E stain; the numbered hepatocytes were used to measure hepatocyte area. Panel F: Liver of Delta Smelt at Day 21 from the No Feeding treatment, H&E stain. Note atrophied hepatocytes (compare to Panel E). For both the Feeding and No Feeding treatments, hepatocytes were selected for area measurement based on three criteria: 1) well demarcated cell membranes, 2) presence of nucleolus in the nucleus, and 3) cells were along a 'backward S' path moving from the top-left corner to the bottom-right corner of each photo (Panels E and F). Scale bars = 20 µm (Panel A), 8 µm (Panel B), 15 µm (Panels C and D), 20 µm (Panels E and F).

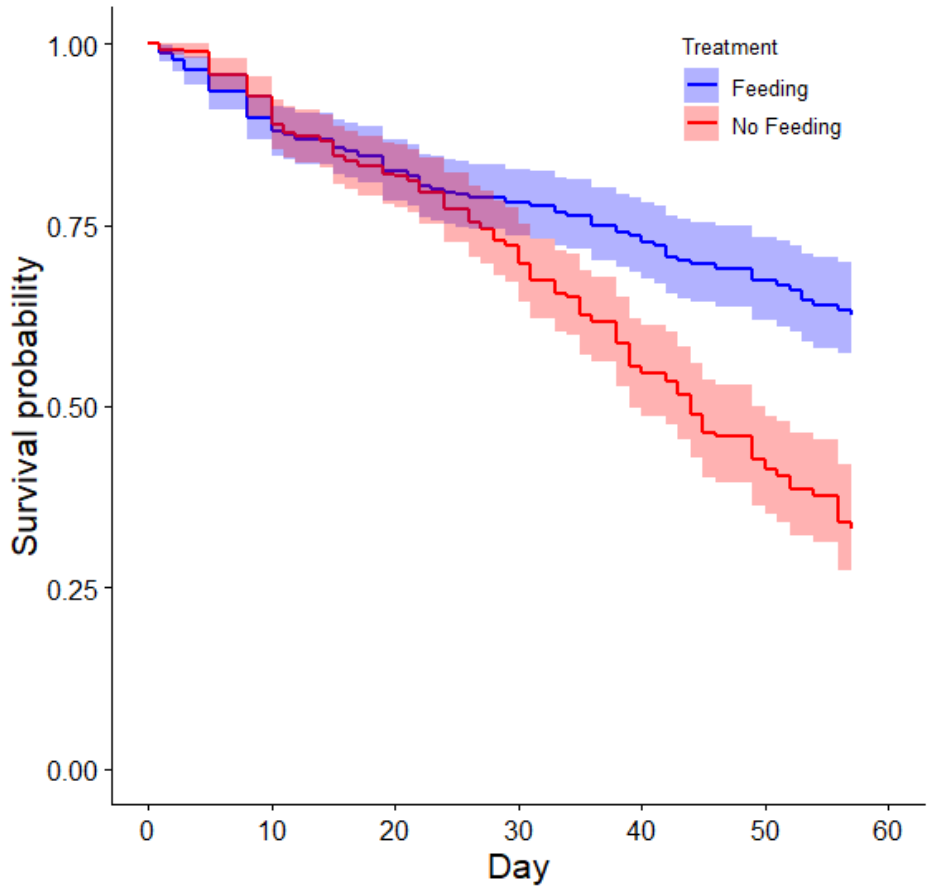

Fig 2. Kaplan-Meier survival probability throughout the starvation experiment. The blue line shows the Feeding treatment (control) and the red (lower) line shows the same for the No Feeding treatment. Shaded areas are 95% confidence intervals. We note that Delta Smelt is an extraordinarily delicate species [51, 53], so the mortality rate in the Feeding treatment was not atypical.

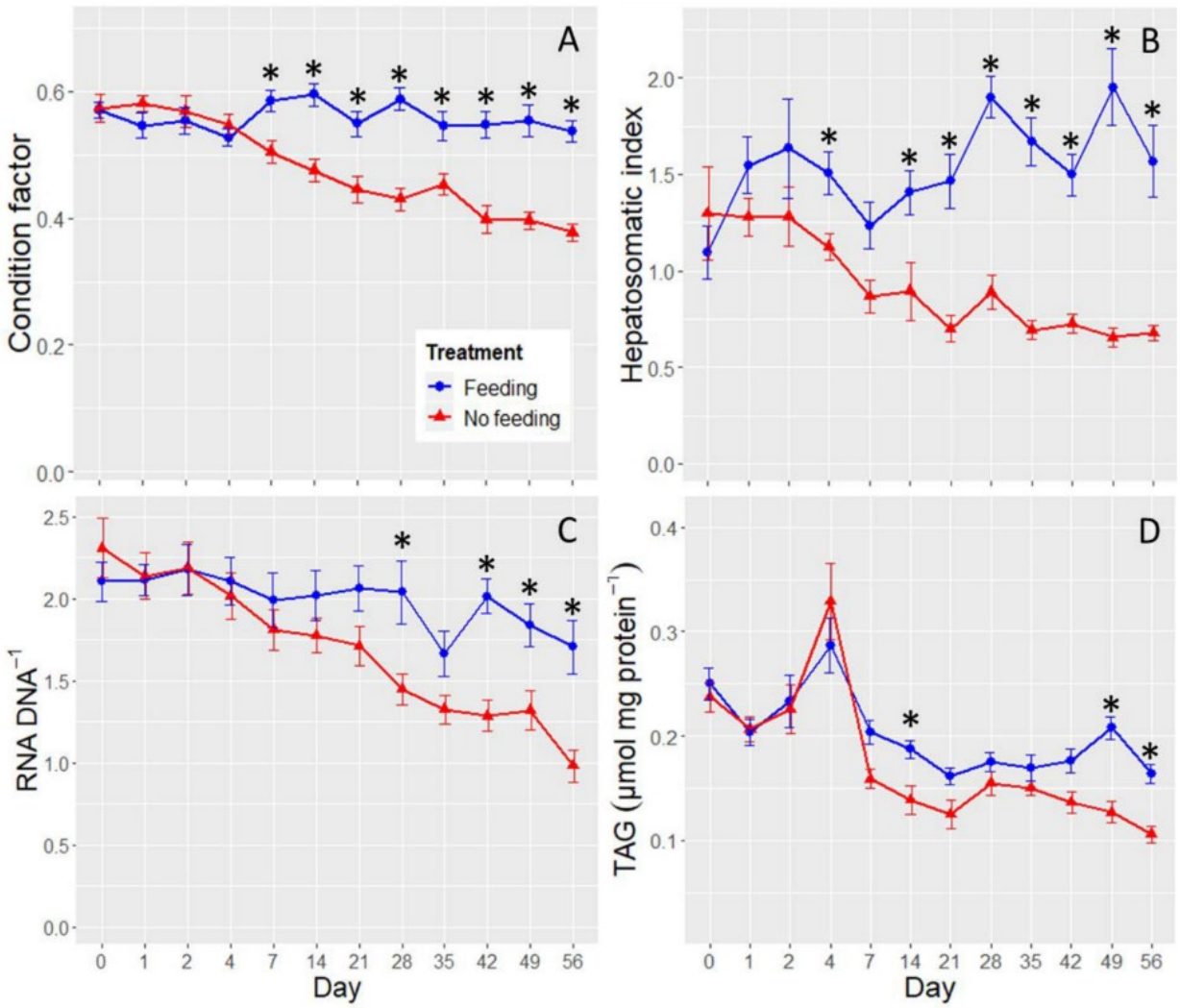

Fig 3. Condition factor (panel A), hepatosomatic index (panel B), RNA to DNA ratio in muscle (Panel C), and triglycerides in muscle (panel D) by day. The Feeding treatment is shown by blue circles and the No Feeding treatment by red triangles. The stars denote the time points at which significant differences were detected between the two treatments. The error bars are ±SE. The x-axis is not to scale.

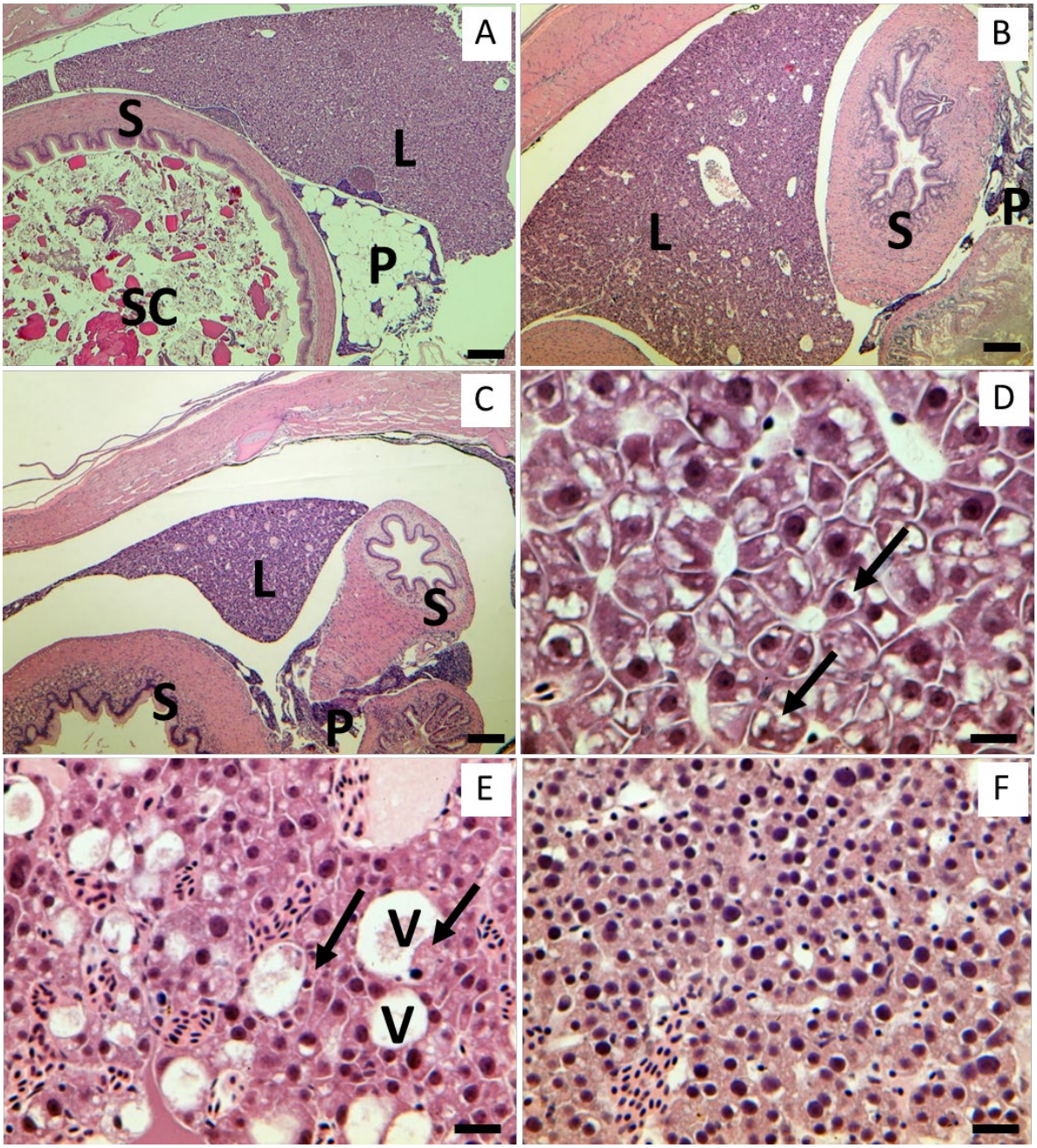

Fig 4. Low (Panels A-C) and high (Panels D-F) magnification starvation progression. Panel A: Delta Smelt transverse section from the Feeding treatment (control), Panel B: Delta Smelt transverse section at Day 21 from the No Feeding treatment, Panel C: Delta Smelt transverse section at Day 49 from the No Feeding treatment. S: stomach, L: liver, SC: stomach contents, P: pancreas. Note atrophy of liver, stomach and pancreas as fasting period lengthens, and empty

stomach in panels B and C. Panel D: Liver of Delta Smelt from the Feeding treatment. Arrows indicate glycogen in the cytoplasm of hepatocytes. Panel E: Liver of Delta Smelt at Day 21 from the No Feeding treatment, hydropic vacuolar degeneration (V) with eosinophilic fibrillary material, likely remnants of hepatocytes. Arrows indicate necrotic hepatocytes. Panel F: Liver of Delta Smelt at Day 49 in the No Feeding treatment. Note severely atrophied hepatocytes, loss of cell-to-cell border, basophilia, and crowded nuclei. All panels H&E stained. Scale bars = 150 µm (Panels A, B and C), 15 µm (Panels D, E and F).

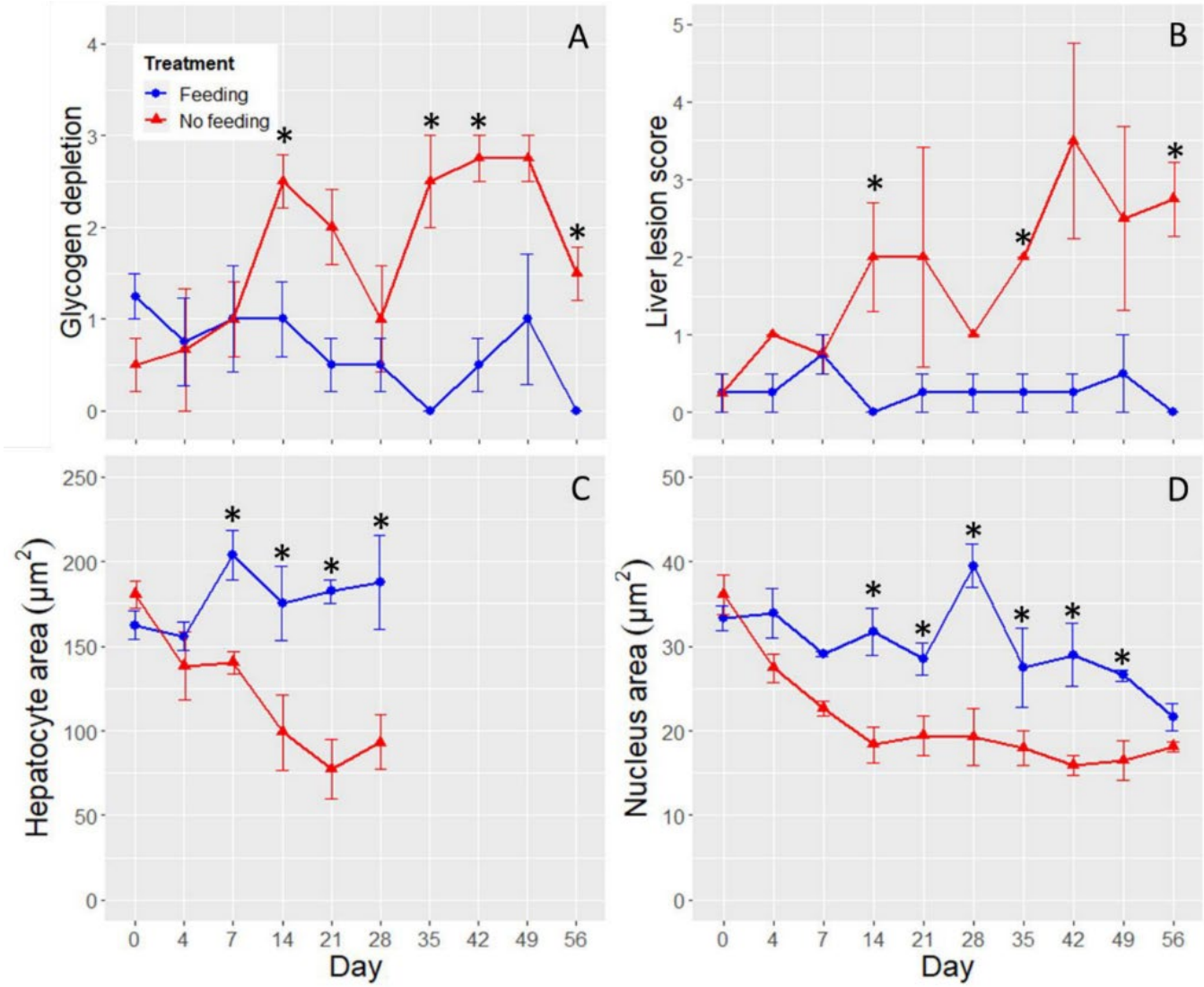

Fig 5. Histological indices by day. Panel A is glycogen depletion, panel B is liver lesion score, panel C is hepatocyte area, and panel D is nucleus area for the Feeding treatment (blue circles) and the No Feeding treatment (red triangles). The stars denote the time points at which significant differences were detected between the two treatments. The error bars are ±SE and the x-axis is not to scale.

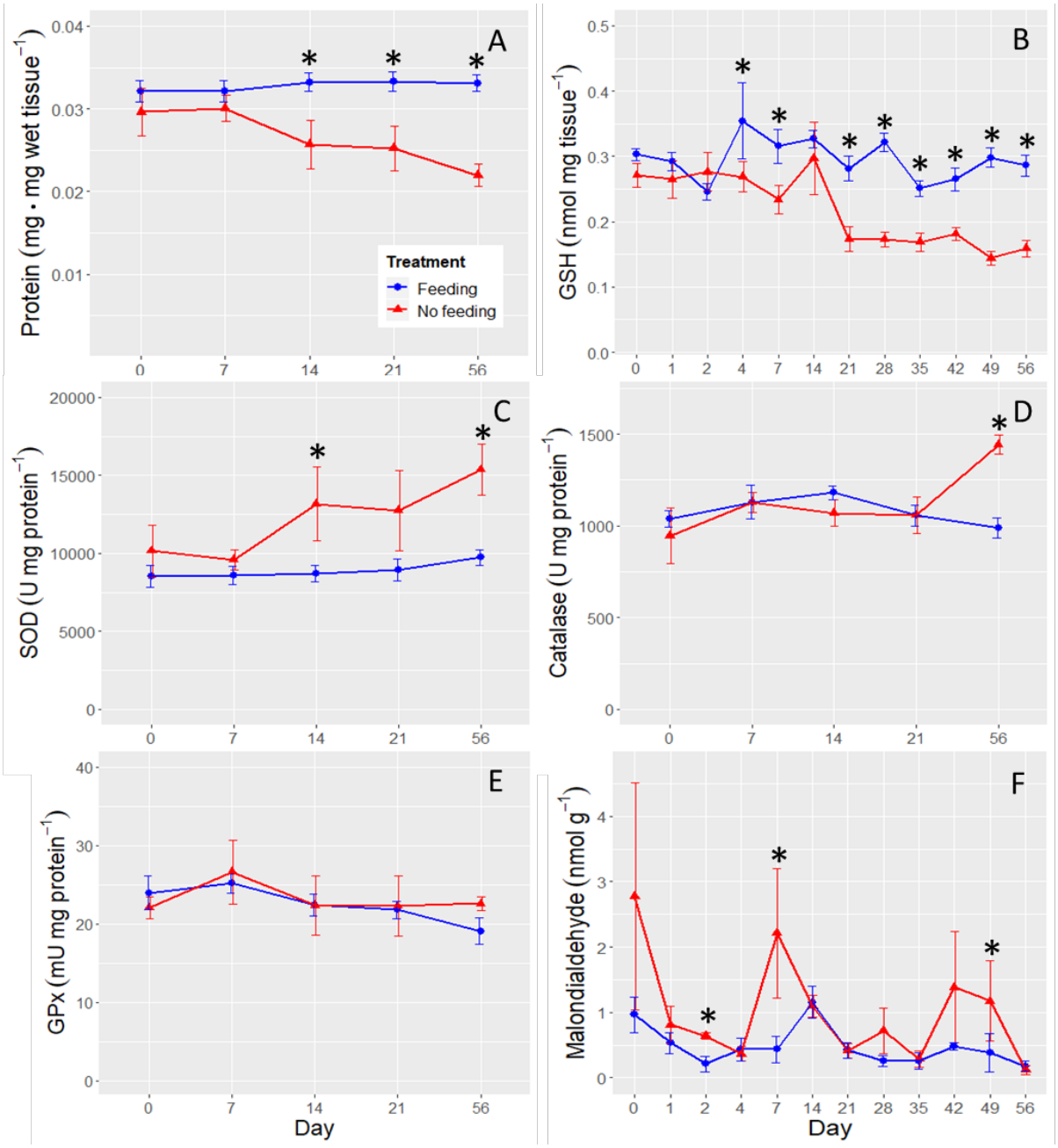

Fig 6. Biomarkers of oxidative stress in liver. Panel A is liver protein concentration, panel B is Glutathione, panel C is superoxide dismutase, panel D is catalase, panel E is glutathione peroxidase, and panel F is malondialdehyde. The stars denote the time points at which significant differences were detected between the two treatments. The x-axis is not to scale and the error bars are ±SE.

Supplemental Material

Fig. S1 Tanks used in the starvation experiment. Each tank was equipped with a 5 µm filter on the input to ensure that no particles of food reached the No feeding tanks. Each tank also has black shade-cloth to minimize light. The treatments were randomly assigned to each tank (4 tanks for each treatment).

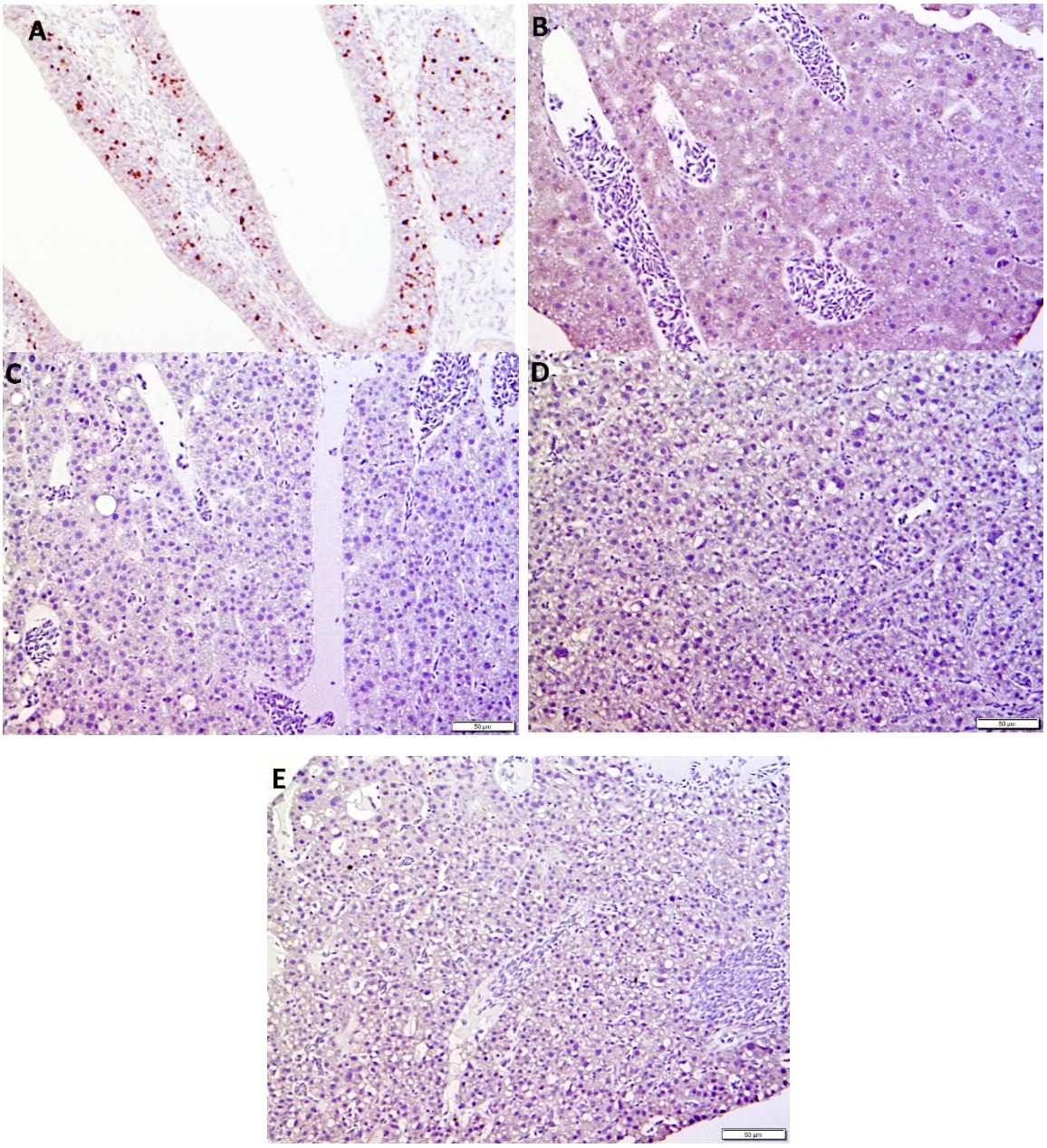
A
B
C
D
E

Fig. S2 Panel A: Anti-Caspase 3 Immunohistochemistry of olfactory epithelium from copper-exposed Delta Smelt used as a positive control. Multiple caspase 3 positive apoptotic cells are demonstrated (red-brown staining). Panels B, C, D and E: Anti-Caspase 3 immunohistochemistry of liver from the 0 day time-point (control, panel B) and fish starved for 21 days (panel C), 42 days (panel D), and 56 days (panel E). Magnification 200×

Chapter 2: Assessment of Acute Toxcity and Histopathology of Environmental Contaminants in Delta Smelt (*Hypomesus transpacificus*) in Relation to Delta Outflow

ASSESSMENT OF ACUTE TOXICITY AND HISTOPATHOLOGY OF ENVIRONMENTAL CONTAMINANTS IN DELTA SMELT (*HYPOMESUS TRANSPACIFICUS*) IN RELATION TO DELTA OUTFLOW

Marie E. Stillway[1], Shawn Acuńa[2], Tien-Chieh Hung[3], Andrew A. Schultz[4], Swee J. Teh[1].

1. School of Veterinary Medicine, Department of Anatomy, Physiology, and Cell Biology, Aquatic Health Program Laboratory, 1028 Veterinary Medicine Drive, University of California, Davis, California 95616, USA
2. Metropolitan Water District of Southern California, 1121 L Street, Suite 900, Sacramento 95814, USA
3. Department of Biological and Agricultural Engineering, One Shields Avenue, University of California, Davis, California 95616, USA
4. Science Division, U.S. Bureau of Reclamation Bay-Delta Office, 801 I Street, Suite 140, Sacramento, CA 95814, USA

Abstract

As a component of the Directed Outflow Project, we evaluated the hypothesized benefits of increased water outflow as well as site specific effects on the survival and health of Delta Smelt (*Hypomesus transpacificus*) through water collections, analytical chemistry, and in-lab toxicity tests on cultured Delta Smelt. We evaluated fish health and condition factor through histopathologic biomarkers in sub-adult Delta Smelt across three different years: Fall 2017, Summer and Fall 2018, and Fall 2019. Managed flows were conducted in each year with 2017 consisting of reservoir releases down the Sacramento River, agricultural return water through the Yolo Bypass in 2018, and 2019 had both increased reservoir releases and increased flow through the Yolo Bypass. Our data show that these managed flow actions do have the potential to provide benefit to Delta Smelt health and condition; however, these benefits are not consistent. Delta Smelt exhibited significantly negative responses in the gills when exposed to water collected in 2017, especially in Exposures 1 and 3, spanning the Fall X2 Action. These lesions were particularly severe in fish exposed to Cache Slough, Toe Drain, and Montezuma Slough. Thus, the Fall X2 Action was unlikely to provide benefits to Delta Smelt health and condition at those times. In 2018, the Suisun Marsh Salinity Gate Flow Action did have the potential to provide benefits to Delta Smelt, as many negative effects were observed prior to the start of this action. We did observe significant lesions in Delta Smelt during Summer Exposure 4, which coincided with the start of the North Delta Flow Action, and these lesions were prevalent in fish exposed to Cache Slough and the two Sacramento River sites. The lack of significant gill lesions observed during the fall of 2018 indicate that aside from the first flush pulse, the North Delta Flow Action likely provided benefits to Delta Smelt during this time. In comparison, the North Delta Flow Action in 2019 was unlikely to provide benefits to Delta Smelt during the times we tested. We observed significant negative effects to the liver of fish, especially to Delta Smelt exposed to Cache Slough and Toe Drain waters associated with the end of the pulse flow. Although agricultural tail-water was used as the source of the North Delta augmented flow pulses in both years, we saw a higher prevalence and variety of pesticides present in 2019 when compared to 2018. This difference may be due to the source of the pulse flow, as 2019 was sourced from a combination of locations rather than the one used in 2018, the types and amounts of chemicals present,

or the time of year when the water was released, collected, and tested. Significant gill lesions were categorized mostly as severe and were frequently observed in the Decker Island site in 2019, but mainly absent in fish exposed to other regions of the Delta, indicating that in general, flows used to maintain Fall X2 in 2019 were potentially beneficial to Delta Smelt. Histologic analyses from our study and others continue to suggest contaminant effects on Delta Smelt in Cache Slough, the Toe Drain, and the Sacramento River at Isleton and Decker Island. These areas may be considered as regions of concern with respect to contaminant detection frequency and deleterious histopathological effects to Delta Smelt.

Introduction

The Suisun Bay and adjacent Sacramento-San Joaquin Delta (Bay-Delta), California, USA, is part of the largest estuary on the west coast, the San Francisco Estuary, and is a highly complex altered estuarine system, rife with anthropogenic changes that followed with the increase of urban and agricultural development. The Bay-Delta is home to the Delta Smelt (*Hypomesus transpacificus*), which is listed as threatened by the United States Fish and Wildlife Service due to its sustained low population numbers since 1993 (MAST 2015; Jin et al. 2018). In 2010, Delta Smelt were upgraded to endangered status in California. Currently, the Delta Smelt population is so imperiled that the year 2020 marks the third consecutive year where zero Delta Smelt were found in the California Department of Fish and Wildlife's Fall Midwater Trawl Survey (CDFW 2020). The Delta Smelt is a semi-anadromous fish which can live up to two years, is endemic to the Bay-Delta, and has both resident and migratory life histories (Moyle et al. 2016, 2018).

Delta Smelt distribution in the Bay-Delta varies according to life stage, with younger fish rearing in the Low Salinity Zone (LSZ; 0.5-6 PSU) and later moving upstream to freshwater areas in the Delta for spawning purposes (MAST 2015; Moyle et al. 2018). Freshwater flow is thought to have a considerable impact on Delta Smelt physical habitat (Jassby et al. 1995; Feyrer et al. 2007; Feyrer et al. 2011; Bever et al. 2016) and conceptual models developed by the Interagency Ecological Program suggest that managed flows may potentially improve Delta Smelt habitat conditions (MAST 2015). Water use in California is controversial and at times, contentious. Large amounts of freshwater are pumped from the Bay-Delta to southern California as drinking water and to irrigated agriculture within much of the Central Valley, with restrictions on pumping and exports based, not exclusively, on drought conditions and the California Endangered Species Act. The Delta Smelt is often at the heart of California's water debate due to its listed status and its use as an indicator for the overall environmental health of the Bay-Delta. To date, much of water use management has been aimed at water exports by the Central Valley (CVP) and State Water (SWP) Projects, and management of salinity intrusion into the Delta (MAST 2015). A combination of managed flows and tidal influences within the Bay-Delta results in movement of the LSZ location throughout the year.

The isohaline position of the LSZ is commonly referred to as "X2" and is measured in distance (km) from the Golden Gate bridge, typically representing the center of the LSZ (Jassby et al. 1995; Kimmerer et al. 2013). The size and location of the LSZ are considered key factors in Delta Smelt rearing habitat and have been instrumental in determining flow management. Fall Low Salinity Habitat (FLaSH) conceptual models indicate that habitat conditions are more favorable for Delta Smelt when the fall X2 is

approximately 74 km or less, and unfavorable when X2 is about 84 km or greater (Reclamation 2011, 2012). A lower X2 value is associated with an increase in available low salinity habitat, whereas a higher X2 value leaves less favorable habitat available to Delta Smelt (MAST 2015).

Water use management in the Bay-Delta consists of, among other things, mandated freshwater flows during various times in the year, especially during winter-spring and in the fall (Sommer et al. 2020). These mandates include the US Fish and Wildlife Service (USFWS) 2008 Biological Opinion Fall X2 Action (USFWS 2008), which requires the U.S. Bureau of Reclamation (USBR) and the California Department of Water Resources (CDWR) to manage exports to ensure that the monthly average location of Fall X2 meets target locations based on wet (74 km) or above normal water years (81 km; CSD 2018). The North Delta Flow Action from the Delta Smelt Resiliency Strategy developed in 2016 includes augmentation of Delta outflow through the Yolo Bypass to increase downstream food availability, and other actions that require localized control of river flow dynamics (CNRA 2016), such as the purchase of an additional 250,000 acre-feet of water for outflow augmentations in 2017 and 2018 (MAST 2015). The goals of these actions are to push the LSZ westward, which is thought to improve the overlap of the LSZ and the turbid, cooler environment of Suisun Bay, while also increasing high quality Delta Smelt habitat and food availability (MAST 2015; CNRA 2017).

High quality Delta Smelt habitat requires high quality freshwater flows. Freshwater flows that are impaired by contaminants can be harmful to Delta Smelt, resulting in decreased growth, biomass, and fecundity (Hammock et al. 2015; Kurobe et al. 2016; Jin et al. 2018), which can then lead to decreases in survival and overall abundance. It has been well demonstrated that the Sacramento-San Joaquin Delta is polluted from numerous anthropogenic sources such as industrial, urban, and agricultural contaminants (Thompson et al. 2007; Smalling et al. 2013; Orlando et al. 2014; Jabush et al 2018; De Parsia et al 2018; 2019). Land use within the Bay-Delta is mostly irrigated agriculture with some urban, the majority of which reside in the surrounding outer areas. Field, pasture, and sub-irrigated pasture crops make up the majority of the north Delta agriculture that is mixed with native vegetation as well as tidal marshes and deep open water (CDFW 2015). Urban discharges flow downstream from municipal waste water treatment plans, notably from Sacramento and Vacaville, as well as non-treated storm runoff. California's Mediterranean climate with dry hot summers and wet winters results in transport of pesticides and other contaminant loads during winter and spring storm events. Irrigated agriculture in the area discharges tail-water in timed pulse flows in the dry summer months, whereas urban effluents are typically continuous throughout the year. Pesticide use and timing often influences transport dynamics (Orlando et al. 2013), with compounds with outdoor applications being mainly storm-driven as they are washed into surrounding aquatic systems, and those used indoor being more continuous through municipal wastewater treatment plants (Weston et al. 2019).

Increasing outflow has long been suggested as an action to improve the habitat for Delta Smelt but the relationship between Delta Smelt abundance and outflow have been mixed (CSD 2018). Contaminants may be confounding the hypothesized relationship between outflow and abundance; therefore, we evaluated the effects of flow actions on the growth, health, and condition vital rates of Delta Smelt as part of the Directed Outflow Project. While not a mandated Action, we also evaluated the Suisun Marsh Salinity Gate Flow Action in 2018. Cultured Delta Smelt were used in short-term in-lab toxicity tests

conducted with water samples collected from various locations in the Bay-Delta, to evaluate the Fall X2 and the North Delta Flow Action managed pulse flows through the Yolo Bypass. Delta Smelt health and condition was evaluated using histopathology biomarkers. Chemical analyses were included to determine the presence of contaminants in the collected water and to investigate their potential effects on Delta Smelt.

Materials and Methods

Sampling design and water collections

Water collections took place every two weeks from October to December in 2017, July to November in 2018, and through September to November 2019. We used fixed sampling sites in each of five sub-strata of the Enhanced Delta Smelt Monitoring Program (Figure 1) and included the following sites: 1) Toe Drain, 2) Cache Slough [Cache], 3) Sacramento River at Isleton [Isleton], 4) Sacramento River at Decker Island [Decker Island], 5) Montezuma Slough [Montezuma], and 6) Grizzly Bay. Sites were chosen to strategically cover areas of the Bay-Delta based on prior distribution of Delta Smelt as well as delta- and region-wide hydrology. At the start of the project in 2017, Lindsey Slough was collected for Exposure 1 but replaced with the Toe Drain by Exposure 2. There were only four test exposures in the Summer 2018 event due to a broken boat which precluded us from collecting samples during the second week of August (Table 1).

The use of fixed sampling locations was chosen in order to make spatial and temporal comparisons over the course of multiple project years. Up to 80L of ambient water was collected from each site for use in Delta Smelt toxicity tests. Samples were collected via bilge pump as sub-surface grabs, in four 20L plastic (LDPE) cubitainers (I-CHEM, Fisher Scientific). Plastic cubitainers were selected as sample collection containers to avoid using large glass containers on the boats due to breakage and safety concerns. Additional sub-samples were collected in 1L glass amber bottles (I-CHEM, Fisher Scientific) and 1L plastic (HDPE) bottles (I-CHEM, Fisher Scientific) for water quality measurements and chemical analyses.

Water years and outflow actions

<u>2017</u>

The 2017 water year was classified as a wet water year, which resulted in a Fall X2 Action. There was no North Delta Flow Action during this year. At the request of USBR, the 2017 Fall X2 Action was amended by USFWS for USBR to manage flows resulting in an X2 location for an above average water year (81 km) rather than a wet water year (74 km). The location of X2 was 74 km in September and 80 km in October, resulting in a two-month average of 77 km (Reclamation 2019). There were no changes to CVP upstream storage or releases, other than differences in South Delta exports in October (Reclamation 2019; Figure 2). The Fall X2 Action coincided with Delta Smelt Exposures 1 and 2. Hydrographs of American and Sacramento River flows are provided as supplemental information (Figures S1-S3, Supplemental Information).

<u>2018</u>

The 2018 water year was classified as a below average water year and as such, there was no Fall X2 Action. In August there was the Salinity Gate Flow Action, where the Suisun Marsh Salinity Control Gates

were used for a managed freshwater flow pulse into Suisun Marsh. This Action directed approximately 196 x 10^6 m^3 of low salinity water into Suisun Marsh between August 2 and September 7 (Figure 3; Sommer et al. 2020). This pulse flow coincided with Delta Smelt Summer Exposures 3 and 4. Hydrographs of American and Sacramento River flows are provided as supplemental information (Figures S4-S6, Supplemental Information).

In conjunction with the Salinity Gate Flow Action, the North Delta Flow Action through the Yolo Bypass occurred for four weeks between August 25 and September 19. This outflow pulse was comprised of agricultural tail-water from Colusa Basin Drain, with peak mean flows in the Toe Drain reaching 600 ft^3/sec (Orlando et al. 2020; Figure 4), which coincided with Delta Smelt Summer Exposure 4 and Fall Exposure 1.

<u>2019</u>

The 2019 water year was classified as a higher than average water year, triggering a Fall X2 Action and a North Delta Flow Action pulse flow through the Yolo Bypass. The North Delta Flow Action pulse flow was comprised of agricultural return water sourced from a combination of Colusa Basin Drain, Ridge Cut, and Yolo Bypass slough inputs, and was timed with the rice harvest period (J. Frantzich, written communication) between August 25 and September 20. Peak mean flows in the Toe Drain reached approximately 800 ft^3/sec, which coincided with Delta Smelt Fall Exposure 1 and to a degree Exposure 2 (Figure 5). Hydrographs of American and Sacramento River flows are provided as supplemental information (Figures S7-S8, Supplemental Information).

Based on the results from the 2017 Fall X2 Action amendment, USBR proposed an augmented CVP Fall X2 location of no more eastward than 80 km for September and October of 2019, in conjunction with CDWR operations of the SWP (Reclamation 2019). This amendment was not granted by the USFWS due to non-compliance with the California Endangered Species Act, and in response, USBR and CDWR made operational changes with extra water releases from Shasta, Oroville, Folsom and New Melones Reservoirs. There was reduced Delta inflow due to a reduction of releases from Folsom reservoir on September 25 and 26, 2019. Oroville releases were increased by 2,000 cfs to compensate (Figure 6). Folsom releases were increased on September 30 (Figure 7), and in conjunction with a 50% reduction of South Delta Exports (Figure 8) on September 28 and 29, the location of X2 was 74 km by the end of September. The Fall X2 Action for this year coincided with all Delta Smelt Exposures.

Chemical analyses

Chemical analyses varied slightly across project years. For 2017, water samples collected for organic/inorganic analyses were delivered to the Young lab at UC Davis, Department of Civil and Environmental Engineering, for each event during the project period. Analyses included Gas Chromatography Quadrupole Time-Of-Flight Mass Screening (GC-QTOF-MS) and Liquid Chromatography Quadrupole Time-of-Flight Mass Screening (LC-QTOF-MS) for targeted and non-target suspect analyses (NTA). Non-target contaminants analysis, focusing on non-polar- and polar-organic compounds and pyrethroids used standardized LC and GC HRMS techniques. Upon receipt, 1L water samples were divided into two extractions, polar and non-polar Electrospray Ionization positive and negative ion modes (ESI+ and ESI-) for analyses, following methods outlined in Moschet et al. (2017). Two additional

sub-samples (one whole water for total, one filtered for dissolved) were delivered to the California Animal Health and Food Safety Laboratory at UC Davis for trace metals analysis. Inorganics (metals) analysis samples were analyzed via Elan 9000 ICP-MS methods for: silver, arsenic, cadmium, copper, manganese, nickel, lead, zinc, aluminum, selenium, chromium, and mercury. For 2018, chemical analyses consisted of ESI-targeted analyses, together with an extract-and-hold, to follow up with non-target analyses if significant toxicity was observed. There were no metals analyses included for this project year. In 2019, samples were analyzed for target Negative Chemical Ionization (NCI), ESI+, and metals, all of which were conducted by the Tom Young Lab at UC Davis following the aforementioned methods.

Delta Smelt toxicity testing

Sub-adult Delta Smelt were obtained from and tested at the UC Davis Fish Conservation and Culture Laboratory (FCCL; Byron, CA) to minimize transport and acclimation stressors to the fish. Toxicity tests were 96-hours in duration, using a static water system with temperature control. Experimental replicates consisted of 20L black plastic buckets with lids (Encore Plastics, Lowe's). Lids were loosely placed on top of the replicate buckets to block out light but allowing room for constant aeration of the replicates. Tests in 2017 and 2019 consisted of four replicates with 8L of sample per replicate and five fish each, for a total of 20 fish per treatment. In 2018, experimental replicates were reduced from four to three, with five fish each for a total of 15 smelt per treatment, due to a lack of Delta Smelt available for toxicity testing during this project year.

Ambient water from the California Aqueduct, used for routine fish culturing practices after basic water treatment processes including solids removal and UV disinfection, was used as the primary control. A secondary, "High Salinity" control was included, adjusted with Instant Ocean® to match the site with the highest salinity (Grizzly Bay), in order to elucidate salinity stressors on Delta Smelt, if present. Test replicates were kept in a temperature-controlled water bath maintained at 16 ± 2°C. Water quality parameters (pH: 7.45-8.02, dissolved oxygen: 11.46-15.56 mg/L, specific conductance: 200.4-279.6 µS/cm, hardness: 60-70 mg/L as $CaCO_3$, alkalinity: 48-60 mg/L as $CaCO_3$) were in range for all experiments. Mortality and abnormal swimming behavior were visually monitored once daily by fish culture staff, including the removal of dead fish if observed. At the end of the 96-hours exposure, surviving fish were euthanized with an overdose of tricaine methane sulfonate, flash-frozen in liquid nitrogen and preserved according to procedures outlined in Teh et al. (2016) for histopathological analyses.

Indicators of general fish condition

Gross measurement and weights were used to determine condition factor (CF) and hepatosomatic Index (HSI) in fish (Goede 1989; Schmitt et al. 1999; Schmitt and Dethloff 2000). CF is a measure of "plumpness" and was defined as: body weight in grams x 100 / length in cm^3. HSI is the liver to body weight ratio (100 x liver weight/body weight).

Histopathology

Histopathology was performed on gill and liver tissues of Delta Smelt. Tissues were fixed in 10% neutral buffered formalin and were processed according to Teh at al. (1997). Briefly, tissues were embedded in paraffin, sectioned at 3-µm thickness and stained with hematoxylin and eosin. Liver and gill lesions were evaluated using the criteria as described in Teh et al. (2020). Lesions were scored semi-quantitatively based on a scale of 0-3, where 0 = not present, 1 = mild, 2 = moderate, and 3 = severe. To assess the overall health condition of liver and gill, a histopathological index was developed by averaging the sum of the lesion scores in each organ. The average summed lesion score represents the degree of damage to the liver and gill, with higher scores indicating a higher degree of damage. Statistical comparisons were made on average summed lesion scores of liver and gill within individual project years with a Kruskal-Wallis Rank Sum test, followed by pairwise comparisons using a Wilcoxon Rank Sum test with continuity corrections. Significance was set with an alpha level of 0.05. Summed lesion scores for the liver do not include glycogen depletion, as it is not considered a lesion and is more indicative of a nutrition metric (Hammock et al. 2015).

Results

Analytical chemistry

Fall 2017

In 2017 chemical analyses consisted of Target ESI+ and ESI-, NCI, and NTA as well as trace metals. For the targeted analyses, only the pesticide fipronil and its degradates were detected consistently across the 2017 project year: fipronil, fipronil-desulfinyl, fipronil-sulfide, and fipronil-sulfone. These compounds were detected in 99% of the samples in all of the collection dates (fipronil-sulfone was <LOQ in Grizzly Bay in Exposure 1). Fipronil-desulfinyl amide was detected twice (Decker Island in Exposure 4 and Montezuma in Exposure 5). These detections ranged from 0.05 to 0.54 nanogram per liter (ng/L; Table S1, Supplemental Information). The only other two compounds detected were the pesticide chlorpyrifos (four times: Isleton in Exposure 3; Toe Drain, Cache, and Decker Island in Exposure 4) with concentrations ranging from 0.11 to 0.23 ng/L, and fungicide azoxystrobin (once: Isleton in Exposure 4) at 4.73 ng/L. For trace metals, total and dissolved barium was detected in all sites across all events, with some instances of total/dissolved manganese, as well as total iron and one instance of dissolved nickel.

Summer and Fall 2018

In 2018, given the lack of quantifiable detections observed in the previous project year, we reduced the analytical chemistry portion to just the targeted NCI analyses, as 99.5% of detected analytes from the previous project year were captured by this method. We opted for an “extract and hold”, where all samples were extracted, and then held for non-target analysis if toxicity was observed. As in the prior year, consistently detected analytes in 2018 included fipronil and its degradates. Fipronil-desulfinyl was detected in every sample in 2018, ranging from 0.1 to 0.7 ng/L. In the Summer events, 30.6 ng/L of bifenthrin and 0.7 ng/L of fipronil-sulfone were detected in Isleton during Summer Exposure 1. There were four detections of chlorpyrifos: 21.8 ng/L at Cache in Summer Exposure 1; 2.9 ng/L in the Toe Drain and 3.4 ng/L in Isleton in Summer Exposure 3, and 3.4 ng/L at Decker Island in Summer Exposure 4. In the Fall events, the parent fipronil was detected in the Toe Drain during Fall Exposure 2 at 6.5 ng/L, and fipronil-sulfone was detected at 1.7 ng/L (Table S2, Supplemental Information). Non-target analyses were not conducted because of the high survival in all fish during this project period. Metals were not measured for 2018 due to lab oversight.

Fall 2019

In 2019, we included both NCI, target ESI+, and trace metals. Unlike previous years, there were only three detections of fipronil-desulfinyl (Cache, Montezuma, and Grizzly Bay at 0.20, 0.35 and 0.29 ng/L, respectively) and one fipronil-sulfone (Montezuma at 0.23 ng/L), all of which were the only NCI detections across the 2019 study period and occurred during Exposure 1. Herbicides and fungicides were the most prevalently detected chemical classes during this study year. The fungicide azoxystrobin was detected in 100% of all samples across all events, with the highest concentration of 1,601 ng/L detected in the Toe Drain during Exposure 1. The insecticide DEET (N,N-diethyl-*m*-toluamide) was detected all but three times across the study period, with a maximum concentration of 33 ng/L in Exposure 3 at Cache. A variety of metals were detected in each sample at each site throughout the study period (Table S3, Supplemental Information).

Exposure 1, initiated on September 13, 2019, had the largest variety of contaminants detected, especially in the Toe Drain, including DEET, chlorantraniprole, azoxystrobin, methoxfenozide, metolachlor, and thiobencarb. Metolachlor and chlorantraniprole were also detected in Cache in Exposures 1 and 2. Methoxfenozide was detected in Decker Island during Exposure 2. For trace metals analysis, manganese and aluminum were the most frequently detected compounds and had the highest concentrations. Manganese was detected 34 times in 2019 in every sample in every event, with a highest concentration of 136 µg/L in Montezuma during Exposure 5. Aluminum was detected 30 times across 2019, with the highest concentrations in Exposure 4 at Grizzly Bay (1,365 µg/L) and in Exposure 1 in the Toe Drain (995 µg/L). The remaining metals detections were considerably lower in comparison, with arsenic being detected 16 times, 15 µg/L the highest concentration detected in Exposure 5 at Grizzly Bay; copper was detected 11 times with 82 µg/L as the highest detection in Exposure 5 at Grizzly Bay; zinc (6 detections, with 928 µg/L detected in Exposure 4 at Isleton), and nickel, with five detections and a highest concentration of 8 µg/L in Exposure 4 at Grizzly Bay. Grizzly Bay in Exposure 4 had the highest number of metals detections, which included aluminum, manganese, nickel, copper, zinc, and arsenic.

Toxicity testing and histopathology

No acute toxicity was observed in Delta Smelt exposed to water from the six sampling locations, nor were there any statistically significant differences in condition factor observed in any of the exposure treatments in 2017, 2018, and 2019 (data not presented). Significant effects were observed in the biomarkers evaluated.

Fall 2017

Histopathologic biomarkers analyzed revealed significant changes when compared to the control, especially in the gills (Kruskal-Wallis X^2: 34.049, df: 8, $P<0.0001$). Ambient sites eliciting notably higher average summed gill lesion scores in fish include Grizzly Bay ($P<0.0001$), Decker Island ($P<0.0001$), Cache ($P<0.0001$), and Toe Drain ($P<0.0001$). Significant lesions such as chloride cell hyperplasia (CCH) and mucus cell hyperplasia (MCH) were the most frequently observed gill lesions in fish, especially during Exposures 1 and 3. These lesions were observed in fish exposed to Cache (88% and 26%, respectively; Figure 9), Toe Drain (21% and 38%, respectively), and Montezuma (63% and 20%, respectively). Fish

exposed to Cache generally had more severe lesions (Figure 10) including three of six fish with severe mucus cell hyperplasia in Exposure 3 (MCH; Figure 10B) as well as one fish with severe gill aneurysm or telangiectasia in Exposure 2 (ANU; Figure 10C). One fish exposed to water from Decker Island had moderate gill aneurysm in Exposure 5.

Glycogen depletion (GD) and lipidosis (LIP) were observed in most Delta Smelt livers throughout 2017. Moderate and severe GD were more prevalent in fish exposed to water collected from Grizzly Bay (50%) and the High Salinity Control (83%) in Exposure 1, indicating potential salinity effects. Moderate and severe LIP were more prevalent in fish exposed to water collected from Cache (38%), Grizzly Bay (75%), Montezuma (75%), and the High Salinity Control (50%) in Exposure 1 when compared to the primary control. Severe lipidosis was more prevalent in Delta Smelt exposed to water collected from Montezuma (50%) and Decker Island (63%) in Exposure 5, including one fish with severe lipidosis and moderate sinusoidal congestion (Figure 11). As the prevalence of glycogen depletion and lipidosis were observed in the majority of Delta Smelt in 2017, there were no statistically significant differences in average summed lesion score across sites (Kruskal-Wallis X^2: 12.758, df: 8, P= 0.1204).

Summer and Fall 2018

In the summer, Delta Smelt had a higher prevalence and severity of gill lesions when exposed to water collected at Cache in Summer Exposures 1, 2, and 4; Decker Island in Summer Exposure 1; Isleton in Summer Exposures 1, 2, and 4; and Montezuma in Summer Exposure 2 (Kruskal-Wallis X^2: 28.66, df: 7; P=0.00017). Moderate chloride cell hyperplasia (CCH) was observed in all fish and moderate to severe secondary lamella dilation or edema (SLE) was present in 40% of fish exposed to Cache in Exposures 1 (Figure 12) and 4 (80% CCH); fish exposed to Decker Island exhibited a range of significant lesions such as CCH (83%), epithelial cell hyperplasia (ECH; 17%), and SLE (17%) in Summer Exposure 1. Delta Smelt exposed to water collected from Isleton during Summer Exposures 1, 2, and 4 had a variety of significant gill lesions such as CCH (50%, 33%, 100%, respectively), MCH (17% Exposure 2) and ECH (33% Exposure 2). In the liver, moderate to severe glycogen depletion was observed in many of the fish tested in the summer (Kruskal-Wallis X^2: 9.8698, df: 7, P=0.1961). In the fall there were intermittent observations of moderate CCH in the gills of fish exposed to ambient waters, however these results were not significant (Kruskal-Wallis X^2: 4.5575, df: 7, P=0.7138). We did not observe any significant liver lesions in Delta Smelt in the fall. (Kruskal-Wallis X^2: 4.6452, df: 7, P=0.7032).

Fall 2019

In 2019, Delta Smelt exposed to Decker Island had the highest frequency of gill lesions, where no less than 25% of fish exhibited these gill lesions in any given toxicity exposure (Kruskal-Wallis X^2: 26.697, df: 7, P=0.00038). Lesions such as mucus cell hyperplasia and epithelial cell hyperplasia were prevalent most notably in Exposures 1, 2, 3, and 5 (Figure 13). Twenty-five percent of Delta Smelt each exposed to Grizzly Bay and Isleton exhibited mucus cell hyperplasia and epithelial cell hyperplasia in Exposure 2. Mild chloride cell hyperplasia in the gills was observed in all fish in all events across the 2019 study period.

Significant lesions in the liver were observed across sites (Kruskal-Wallis X^2: 18.653, df: 7, P=0.009348). Delta Smelt exposed to water collected from Cache (P=0.0021) and the Toe Drain (P=0.0401; Figure 14)

had significantly higher average summed liver lesion scores compared to the control. Fish exposed to Cache had a higher average summed liver lesion score compared to Grizzly Bay (P=0.0404), Montezuma (P=0.0235), and the High Salinity Control (P=0.0021). Moderate to severe glycogen depletion in the liver was observed in fish exposed to the Toe Drain (50% and 25%, respectively in Exposures 1 and 2; Figure 14), Cache (75% and 50%, respectively in Exposures 1 and 2), Isleton (25% in each of Exposures 1 and 2), and Grizzly Bay (50% in Exposure 4). In Exposure 5 Delta Smelt at all sites demonstrated mild glycogen depletion. Moderate to severe lipidosis was observed in 25% fish exposed to the Toe Drain, Cache, and Decker Island, respectively, in Exposure 1.

Discussion

Exposure to contaminants can have negative effects on various aquatic organisms at the concentrations detected in the Delta (Hasenbein et al. 2014; Weston and Lydy 2014; Hammock et al. 2015). Our toxicity testing results indicate that individual contaminants present in Bay-Delta water during the time periods and areas we sampled were in concentrations unlikely to cause direct mortality or a reduction in the general health condition of fish. However, synergistic and/or additive interactions can cause sub-lethal toxic effects to tissue, and physiological processes can occur in organisms exposed to low concentrations of contaminants (Fong et al. 2016).

Histopathological lesions are considered nonspecific responses to stress and are characteristic of fish exposed to different kinds of water contamination (Mallat 1985; Bernet et al. 1999). There are various environmental factors that can cause histopathological changes in fish gills and in the liver. In general, these changes are related to the presence of toxic chemical stressors in the environment. For example, increased hepatocellular lipidosis or vacuolation is more commonly associated with over-nutrition or toxicity (Wolf and Wolfe, 2005). Gill aneurysm and epithelial cell necrosis, which was observed in our study, are usually but not specifically attributed to metal contamination (Mallatt, 1985). Our histopathology results from the current study showed the occurrence of 1) aneurysm, epithelial cell necrosis, mucus and chloride cell hyperplasia, and secondary lamella fusion and edema in gill; and 2) glycogen depletion, hepatocellular necrosis, and lipidosis in liver.

In 2017, fipronil and its metabolites were detected in greater than 99% of samples collected, with concentrations ranging between 0.05 and 0.54 ng/L. Chlorpyrifos was the second-most frequent contaminant detected in 2017, specifically in sites located within the north Delta, including the Toe Drain, Cache Slough, and both Sacramento River sites. Chlorpyrifos concentrations ranged between 0.11 and 0.23 ng/L and detections coincided with the Fall X2 Action. Fipronil is a broad-spectrum insecticide used for pest control on animals and structures (Fong et al. 2016). Fipronil breaks down into the byproducts fipronil-sulfide, fipronil-sulfone, and fipronil-desulfinyl, which are more toxic to aquatic organisms than the parent compound (US EPA 1996, 1998; Weston and Lydy, 2014). Topical flea products such as those that have fipronil as an active ingredient, are applied to pets and enter municipal wastewater typically through pet bathing, either from home or commercial grooming facilities (Sutton et al. 2019). It is probable that was the source of the continued fipronil + metabolite detections we observed during 2017, likely combined with untreated wash-off of fipronil from structures (Sutton et al. 2019). Chlorpyrifos is an organophosphorus pesticide, which has been banned from residential use since

the early 2000s, although is still used by professionals and in agriculture, which results in detections in California water bodies (Orlando et al. 2014). We detected chlorpyrifos in the Cache Slough and Yolo Bypass region as well as both Sacramento River sites; the surrounding agriculture near these sites is the likely culprit for contamination source. We also had one detection of the fungicide azoxystrobin at the Isleton site during Exposure 4, initiated November 24, 2017. This fungicide is used on rice and processing tomatoes (Orlando et al. 2020), which aligns with the time of year when it was detected, again likely sourced from the surrounding agriculture.

We observed significant and severe lesions such as chloride cell hyperplasia and mucus cell hyperplasia in Delta Smelt exposed to Bay-Delta outflow waters in the 2017 project year. These gill lesions were especially prevalent in smelt exposed to water collected in Cache during Exposures 1 and 3, which were initiated on October 13, 2017 and November 10, 2017. Glycogen depletion and lipidosis in the liver were observed in most smelt exposed to ambient water collected throughout 2017; however it is likely that the glycogen depletion and lipidosis observed in the Grizzly Bay fish were due to salinity effects, as the fish in the corresponding High Salinity Control exhibited similar responses, particularly in Exposures 1, 3, and 5. These toxicity exposures occurred during the Fall X2 Action, the results of which may be representative of the Bay-Delta water quality of this Action. This year's Action did not require any changes to upstream storage or water releases and the Flow Action was met through the reduction of South Delta exports (Reclamation 2019). Thus, water quality during this time is indicative of the summer flow regimes of a wet water year, as well as the agricultural practices during this time in surrounding areas. Overall for 2017, we observed higher severity and prevalence of significant lesions in the majority of Delta Smelt tested when compared to the control, particularly affecting the gills in fish exposed to Cache Slough, Toe Drain, Decker Island, and Montezuma. The significant differences in lesions observed in Delta Smelt indicate toxicity at these sites; thus, it would appear that Bay-Delta outflow water was less likely to provide benefits to Delta Smelt in the fall of 2017.

Chemical detections in 2018 were similar to those observed in 2017. The byproduct fipronil-desulfinyl was detected in 99% of samples collected during the 2018 project year. Fipronil-desulfinyl concentrations ranged between 0.1 and 0.7 ng/L for both the summer and fall project periods. High frequency detections of fipronil metabolites indicate continuous municipal effluent discharges. We saw multiple detections of chlorpyrifos in the summer, with 21.8 ng/L detected in Cache in Summer Exposure 1, initiated on July 12, 2018. Other chlorpyrifos detections ranged from 2.9-3.4 ng/L and were detected in the Toe Drain in Summer Exposure 3 initiated August 8, 2018, Isleton in Summer Exposure 3, and in Decker Island in Summer Exposure 4, initiated September 6, 2018. These concentrations are higher than those observed in 2017. In addition, we detected 30.6 ng/L of bifenthrin and 0.7 ng/L fipronil-sulfone in Isleton during Summer Exposure 1. We detected fipronil at 6.5 ng/L and fipronil-sulfone at 1.7 ng/L at the Toe Drain in Fall Exposure 2, initiated on October 4, 2018.

There were two managed flow actions in 2018 which spanned between August and September. The first was the Suisun Marsh Salinity Control Gate Flow Action, which took place between August 2 and September 7, the goal of which was to improve summer habitat conditions for Delta Smelt in Suisun Marsh (Sommer et al. 2020). The pumping of low salinity water through the salinity gates, when sourced from the Sacramento River, can cause saltwater intrusion into Suisun Bay; therefore, this flow action

coincided with additional flows from upstream reservoirs (Sommer et al. 2020). The second managed action was the North Delta Managed Flow Action, which took place from August 26 to September 19, 2018. The North Delta Flow Action was aimed to support the Delta food web in downstream areas with a pulse flow through the Yolo Bypass, an area known to have a high plankton richness (MAST 2015). This pulse flow was comprised of agricultural tail-water from Colusa Basin Drain (Orlando et al. 2020). The Salinity Gate Flow Action coincided with Delta Smelt Summer Exposures 3 and 4, whereas the North Delta Managed Flow Action coincided with Delta Smelt Summer Exposure 4 and Fall Exposures 1 and 2.

Delta Smelt exhibited a higher prevalence and severity of gill lesions when exposed to Cache and Isleton in Summer Exposures 1, 2 and 4. Exposures 1 and 2 occurred prior to the start of the Suisun Marsh Salinity Gate Flow Action, however the end of that Flow Action did coincide with Summer Exposure 4. Fish exposed to Decker Island exhibited significant lesions during Summer Exposure 1 and Montezuma affected fish during Exposure 2. The detection of 30.6 ng/L bifenthrin in the Isleton site and the 21.8 ng/L concentration of chlorpyrifos in the Cache site in the July 13 Summer Exposure 1 indicate pesticides were likely sourced from the surrounding agriculture, as both insecticides are used on alfalfa and corn, two crops which are present in the directly surrounding agricultural areas located near these sites (CDFW 2015). Delta Smelt exposed to water collected from Cache during the summer had significantly higher average summed gill lesion scores, indicating continued toxicity at this site, as has been suggested in prior research studies (Hammock et al. 2015, Teh et al. 2020). Delta Smelt exposed to water collected in the Fall of 2018 did not have any significant lesions in the gills, other than two fish exposed to Isleton during the Fall Exposure 4. Glycogen depletion was observed in the liver in the majority of fish used in the fall of 2018, making it difficult to see significant differences, indicating that Delta Smelt used in the fall exposures may have been affected by stressors other than the collected ambient water.

It would appear that the Suisun Marsh Salinity Gate Flow Action was likely to provide benefits to Delta Smelt, as the majority of significant gill lesions that were present in fish were observed in July prior to the start of the Flow Action. Delta Smelt exposed to water collected from Grizzly Bay had the lowest summed lesion scores during the summer, and although not statistically significant, it indicates that the Suisun Marsh Salinity Gate Flow Action was likely beneficial to Delta Smelt, at least in terms of water quality of the managed flow in the Grizzly Bay area. Significant and severe lesions observed in Delta Smelt gills were those exposed to water collected prior to the managed flow actions and indicate early summer toxicity, likely due to typical agricultural practices during that time in combination with a below average water year. However, we did observe instances of chloride cell hyperplasia in fish exposed to Isleton as well as in Cache during Summer Exposure 4, which did coincide with the tail end of the Suisun Marsh Flow Action and the beginning of the North Delta Managed Flow Action. The general lack of significant gill lesions during the Fall Exposures, including those outside of the Yolo Bypass flow action footprint, indicate a potential benefit of Sacramento River flows in conjunction with the North Delta Flow Action in 2018.

Chemical detections in 2019 differ greatly when compared to the prior two project years. Notably absent were the ubiquitous detections of fipronil and/or its metabolites, with only three detections in 2019, both in Exposure 1 initiated on September 13, 2019, in Montezuma and Grizzly Bay. It is unclear

why there was such a distinct difference in these detections, as it is assumed that municipal wastewater discharges still continued uninterrupted during this time and we did see continuous pesticide transport loads via wastewater effluent with the frequent detections of DEET, an insecticide used topically on people and which is embedded in pest-resistant clothing. Instead, azoxystrobin was detected in 100% of the samples collected, and the insecticide DEET was detected in 95% of all samples collected in 2019. Exposure 1 had the highest number of chemicals detected as well as some of the highest concentrations when compared to the previous project years. In the Toe Drain, azoxystrobin was detected at 1,601 ng/L, along with methoxyfenozide (166 ng/L), thiobencarb (113 ng/L), aluminum (99 µg/L), manganese (94 µg/L), and chlorantraniprole (33 ng/L), with metolachlor (9 ng/L) and DEET (6 ng/L). Cache had azoxystrobin detected at 381 ng/L, DEET at 13 ng/L, and metolachlor at 19 ng/L. Decker Island had 168 ng/L of azoxystrobin and 8 ng/L of DEET.

2019 was an above average water year with North Delta Flow and Fall X2 Actions. The North Delta Flow Action took place between August 25 to September 20, was comprised of agricultural return water sourced from a combination of Colusa Basin Drain, Ridge Cut, and Yolo Bypass slough inputs, and was timed with the rice harvest period (J. Frantzich, written communication). The Fall X2 Action took place in September and October, and included a combination of reduced South Delta exports and increased upstream reservoir releases. The North Delta Flow Action pulse coincided with Delta Smelt Exposure 1 and 2, where we observed a variety of contaminants detected in the Toe Drain and Cache. Of the chemicals detected in Exposure 1, azoxystrobin, methoxyfenozide, and thiobencarb are largely used on rice crops (Orlando et al. 2020), which aligns with the source and type of water used for the North Delta Flow Action pulse flow, as well as the agricultural land use of the Yolo Bypass and surrounding areas (CDFW 2015; Orlando et al. 2020). The Fall X2 Action coincided with all Delta Smelt Exposures conducted in 2019.

It would appear that the North Delta Flow Action negatively impacted Delta Smelt exposed to water collected from the Toe Drain and Cache in Exposure 1 and 2. We observed a high prevalence and severity of glycogen depletion and lipidosis in the liver of Delta Smelt exposed to the Toe Drain, and fish also exhibited moderate to severe lipidosis when exposed to Cache, the results of which were statistically significant. Noteworthy was the complete absence of liver lesions in the Primary and High Salinity Control Delta Smelt, and almost no lesions were observed in Delta Smelt exposed to Montezuma.

In comparison, gill lesions such as mucus cell hyperplasia, secondary lamellar fusion, and lamellar aneurysms, were mostly severe and observed frequently in the Decker Island site in 2019. Mild to moderate mucus secretion is considered a protective response to contaminant exposure, but severe mucus secretion and aneurysm can impede respiration resulting in fish death due to hypoxia (Matey et al. 2011). Thus, the presence of these gill lesions could indicate metals, pesticide, and mixed contaminants exposure in this region (Hammock et al. 2015). At this time, it is unclear why the Decker Island site had such a negative effect on Delta Smelt gills, as chemical analyses do not reveal any smoking guns in terms of contaminant type or concentration aside from the presence of DEET and azoxystrobin in every sample in 2019, but those concentrations were in the low ng/L range. It is possible that there was a different kind of contaminant or stressor present in the Decker Island site during the

fall of 2019 that was not included in our chemical monitoring. This would indicate that in general, flows used to maintain Fall X2 in 2019 were potentially beneficial to Delta Smelt.

There is little information available in the literature regarding the specific chemicals or concentrations detected in this study and their toxicity to fish, and there are virtually none on Delta Smelt in particular. Ardeshir et al. (2018) exposed the Caspian kutum fish (*Rutilus frisii kutum*) to three intraperitoneal doses of fipronil (65, 130, and 200 mg/kg) and found liver damage such as glycogen depletion, hypertrophy, and sinusoid dilation. Degenerative fatty vacuolization increased significantly in the highest concentration after 14 days and significant gill damage such as fusion, hypertrophy, and hyperplasia were also observed between the treatment groups and the control (Ardeshir et al. 2018). These concentrations and exposure routes are different than what was observed in our study, yet demonstrate that the concentrations of fipronil and the degradates we observed in 2017 and 2018 were unlikely to cause significant negative effects on Delta Smelt. Devi and Mishra (2013) exposed the teleost fish *Channa punctatus* to sub-lethal concentrations of chlorpyrifos, including 1.46 µg/L and 0.538 µg/L (1/3rd and 1/10th the 24h LC50, respectively) for 3- and 7-days, which caused moderate to severe changes in the gills and livers. Various lesions in the gills included epithelial cell hyperplasia and lamellar aneurism, and vacuolar degeneration was observed in the liver (Devi and Mishra 2013). Chlorpyrifos was detected multiple times in this study in 2017 and 2018 at concentrations well below those that Devi and Mishra examined. Cao et al. (2018) exposed both larval and adult zebrafish (*Danio rerio*) to three concentrations of azoxystrobin (5 µg/L, 10 µg/L and 200 µg/L) during an 8-day exposure, with fish observed on Day 4 and on Day 8. There were no negative effects observed on the larval or adult zebrafish at 10 µg/L. These doses are higher than what we detected in the environment during our study periods, but may be indicative of the potential harm that can be caused through extended exposure or exposure during storm events, which may have higher contaminant loads.

The concentrations of metals we detected during this study were generally in the microgram-per-liter range, whereas pesticides and herbicides detected in the Delta outflow waters we sampled were in the picogram- to nanogram-per liter range, which is typical for the Bay-Delta during the times of year we sampled (Orlando et al. 2013; DeParsia 2018; DeParsia 2019; Orlando et al. 2020). At no point during this study did we capture a storm event, which would have had an impact on pesticide transport dynamics and concentrations. Contaminants associated with indoor and structural pest control (e.g., fipronil and metabolites; DEET) followed continuous municipal wastewater effluent discharge patterns, whereas those used in agriculture (chlorpyrifos, bifenthrin) were detected discreetly throughout the study period, the timing of which mirrored the agricultural practices for the particular time of year and area collected (CDFW 2015; Sutton et al. 2019; Weston et al. 2019; Orlando et al. 2020). Detected concentrations matched the discharge dynamics, with continuous discharging having lower, consistent concentrations over time, and discreet discharges having fewer, but higher concentrations (Weston et al. 2019). The exception to this is the fungicide azoxystrobin, which had consistent detections across 2019. USEPA Aquatic Life Benchmarks for some of the contaminants we detected, such as fipronil (2.2 µg/L), fipronil-desulfinyl (0.59 µg/L), chlorpyrifos (0.57 µg/L), DEET (37,500 µg/L) and azoxystrobin (147 µg/L) are much higher than the concentrations detected in our study (USEPA 2019). The concentrations of contaminants present in Delta outflow waters were unlikely to be the sole cause of the observed sub-lethal effects in the Delta Smelt we examined.

It is important to consider that although the individual chemical concentrations seen in this study are far below those considered to cause significant acute or chronic effects, exposure to contaminant mixtures have shown numerous adverse effects on aquatic organisms at concentrations below the no observable effect concentration (NOEC) for the individual chemical in question (Carvalho et al. 2014; Cedergreen 2014; in Fong et al. 2016). We therefore cannot rule out the possibility of potentially additive and/or synergistic mixture effects which could be responsible for the sub-lethal effects observed in this study. Moreover, these chemical concentrations may be low enough to not significantly harm Delta Smelt directly, but they are in a range that would negatively affect lower trophic levels, especially those important to the food web and Delta Smelt in particular (Hasenbein et al. 2014, Weston et al. 2019). Thus, the presence and concentrations of the chemicals detected in this study should not be ruled out as having the potential to affect Delta Smelt health and abundance in the wild.

Conclusion

Our data demonstrate that managed flow actions do have the potential to provide benefit to Delta Smelt health and condition; however, these benefits are not consistent. While the results of these managed flow actions on Delta Smelt habitat and food availability are outside the scope of this paper, in terms of water quality of these managed flows, contaminants were observed in low concentrations that by themselves, are unlikely to cause deleterious effects on Delta Smelt health and condition, but they were often ubiquitous in the waters we collected. It is important to note, however, that although these concentrations are below aquatic life benchmarks and may not acutely affect Delta Smelt, the chemical concentrations we observed are likely at levels of concern for lower food web species (Hasenbien et al. 2014; Fong et al. 2016; Weston et al. 2019) which can have indirect negative effects on Delta Smelt health and abundance, and should not be overlooked.

Delta Smelt exhibited significant negative responses in the gills when exposed to water collected in 2017, especially in Exposures 1 and 3, spanning the Fall X2 Action. These lesions were particularly severe in fish exposed to Cache Slough, Toe Drain, and Montezuma Slough. Thus, the Fall X2 Action was unlikely to provide benefits to Delta Smelt health and condition at those times. In 2018, the Suisun Marsh Salinity Gate Flow Action did have the potential to provide benefits to Delta Smelt, as many negative effects were observed prior to the start of this action. We did observe significant lesions in Delta Smelt during Summer Exposure 4, which coincided with the start of the North Delta Flow Action, and these lesions were prevalent in fish exposed to Cache Slough and the two Sacramento River sites. The lack of significant gill lesions observed during the fall of 2018 indicate that aside from the first flush pulse, the North Delta Flow Action likely provided benefits to Delta Smelt during this time. In comparison, the North Delta Flow Action in 2019 was unlikely to provide benefits to Delta Smelt during the times we tested. We observed significant negative effects in the liver of fish during this time, especially to Delta Smelt exposed to Cache Slough and Toe Drain waters associated with the end of the pulse flow. This may be due to the type of contaminants detected in the augmented pulse water, which was mainly associated with rice crops (Orlando et al. 2020), and coincide with the increase in histopathological lesions that were observed in Delta Smelt. Although agricultural tail-water was used as the source of the North Delta augmented flow pulses in both years, we saw a higher prevalence and variety of pesticides present in 2019 when compared to 2018. This difference may be due to the source of the pulse flow, as

2019 was sourced from a combination of locations rather than the one used in 2018, the types and amounts of chemicals present, or the time of year when the water was released, collected, and tested. Significant gill lesions were mostly severe and observed frequently in the Decker Island site in 2019, but mainly absent in fish exposed to other regions of the Delta, indicating that in general, flows used to maintain Fall X2 in 2019 were potentially beneficial to Delta Smelt. Histologic analyses from our study and others (e.g., Hammock et al. 2015, Teh et al. 2020), continue to suggest contaminant effects on Delta Smelt in Cache Slough, the Toe Drain, and the Sacramento River at Isleton and Decker Island. These areas may be considered as regions of concern with respect to contaminant detection frequency and deleterious histopathological effects to Delta Smelt.

Chapter 2: Assessment of Acute Toxcity and Histopathology of Environmental Contaminants in Delta Smelt (*Hypomesus transpacificus*) in Relation to Delta Outflow

Acknowledgements

Funding for this study was provided by the State and Federal Contractors Water Agency, Contract No. 18-10 and the State Water Contractors, Contract No. 20-07, and the United States Bureau of Reclamation (USBR) contract No. R19AC00025 in conjunction with the Metropolitan Water District of Southern California, as part of the larger Directed Outflow Project. Delta Smelt and testing facilities were provided by the UC Davis Fish Conservation and Culture Laboratory, and the authors would like to thank Luke Ellison, Troy Stevenson, Matt Rooney, Taylor Diamond, Daniel Carr and James Krause for their assistance with the toxicity tests, as well as Ching Teh, Franklin Tran, Khiet Huynh, Pedro Alejandro Triana Garcia, and Bruce Hammock for fish necropsy and tissue processing. We are grateful for water collections provided by the field staff of ICF. The authors also want to acknowledge Luann Wong and Thomas Young for their expertise with analytical chemistry. We thank Elissa Buttermore and Nick Bertrand (USBR) for helpful reviews of the manuscript. This study was approved by the Institutional Animal Care and Use Committee (IACUC), University of California, Davis, and followed the experimental protocol for Animal Care and Use protocol #19872. The authors declare no conflicts of interest. The views expressed are those of the authors and do not represent the official opinion of any employer, institution or government agency.

Literature Cited

Ardeshir RA, Zolgharnein H, Movahedinia A, Salamat N, Zabihi E. (2018). CYP1A gene expression as a basic factor for fipronil toxicity in Caspian kutum fish. *Toxicology Reports*. 113-124. https://doi.org/10.1016/j.toxrep.2017.12.014.

Bernet D, Schmidt H, Meier W, Burkhardt-Holm P, Wahli T. (1999). Histopathology in fish: proposal for a protocol to assess aquatic pollution. *J. Fish. Diseases*. 22: 25-34.

Bever, A., M. MacWilliams, B. Herbold, L. Brown, and F. Feyrer. (2016). Linking hydrodynamic complexity to Delta Smelt Hypomesus transpacificus distribution in the San Francisco Estuary, USA. *San Francisco Estuary and Watershed Science.* 14(1).

California Department of Fish and Wildlife (CDFW). (2015). Land Use – Sacramento San Joaquin Delta – 2015 Land IQ (ds2791). https://apps.wildlife.ca.gov/bios/?al=ds2791. Website accessed 21 January 2021.

California Department of Fish and Wildlife (CDFW). (2020). Fall Midwater Trawl Monthly Abundance Indices. https://www.dfg.ca.gov/delta/data/fmwt/indices.asp. Visited January 20, 2021.

California Natural Resources Agency (CNRA). (2017). Delta Smelt Resiliency Strategy Progress Report. June 2017. Department of Water Resources – 1235. https://www.waterboards.ca.gov/waterrights/water_issues/programs/bay_delta/california_waterfix/exhibits/docs/petitioners_exhibit/dwr/part2_rebuttal/dwr_1235.pdf. Accessed 1 July 2020.

Castillo, GC. (2019). Modeling the Influence of Outflow and Community Structure on an Endangered Fish Population in the Upper San Francisco Estuary. *Water*. 11: 1162. DOI: 10.3390/w11061162.

Cao F, Zhu L, Li H, Yu S, Wang C, Qiu L. (2016). Reproductive toxicity of azoxystrobin to adult zebrafish (*Danio rerio*). *Environ. Pollut*. 219: 1109-1121. http://dx.doi.org/10.1016/j.envpol.2016.09.015

Cao F, Wu P, Huang L, Li H, Qian L, Pang S, Qiu L. (2018). Short-term developmental effects and potential mechanisms of azoxystrobin in larval and adult zebrafish (*Danio rerio*). *Aquat. Toxicol*. 198: 129-140. https://doi.org/10.1016/j.aquatox.2018.02.023.

Carvalho RN, Arukew A, Ait-Aissa S, Bado-Niles A, Balzamo S, Baun A. (2014). Mixtures of chemical pollutants at European legislation safety concentrations: how safe are they? *Toxicol. Sci.* 141: 218-33. DOI: http://toxsci.oxfordjournals.org/content/ early/2014/06/23/toxsci.kfu118.short.

Cedergreen N. (2014). Quantifying synergy: a systematic review of mixture toxicity studies within environmental toxicology. *PLoS ONE*. DOI:http://dx.doi.org/10.1371%2Fjournal.pone.0096580.

Coalition for a Sustainable Delta (CSD). (2018). Reconsidering the Fall X2 Action Using the Best Available Scientific Information. Technical Report prepared by the Coalition for a Sustainable Delta for the Bureau of Reclamation and US Fish and Wildlife Service. Document no. 56760612.v1. December, 2018.

Delta Science Program. (2020). Delta Smelt Conditions Report (2002-present). Delta Science Program. March 16, 2020. Accessed online 29 June 2020. https://sbashevkin.github.io/Delta-Smelt-conditions-report/.

De Parsia, M., Orlando, J. L., McWayne, M. M., & Hladik, M. L. (2018). Pesticide inputs to the Sacramento–San Joaquin Delta, 2015–16: Results from the Delta Regional Monitoring Program (No. 1089). US Geological Survey.

De Parsia, M., Woodward, E. E., Orlando, J. L., & Hladik, M. L. (2019*).* Pesticide Mixtures in the Sacramento–San Joaquin Delta, 2016–17: Results from Year 2 of the Delta Regional Monitoring Program (No. 1120). US Geological Survey.

Devi Y and Mishra A. (2013). Histopathological Alterations in Gill and Liver Anatomy of Fresh Water, Air Breathing Fish *Channa Punctatus* after Pesticide Hilban (Chlorpyrifos) Treatment. *Adv. Biores*. 4(2): 57-62.

Feyrer, F., M. L. Nobriga, and T. R. Sommer. (2007). Multidecadal trends for three declining fish species: habitat patterns and mechanisms in the San Francisco Estuary, California, USA. *Can. J. Fish. Aqua. Sci.* 64:723–734.

Feyrer, F., K. Newman, M. Nobriga, and T. Sommer. (2011). Modeling the effects of future outflow on the abiotic habitat of an imperiled estuarine fish. *Estuaries and Coasts.* 34(1):120–128.

Fong, S, Louie S, Werner I, Davis J, Connon RE. (2016). Contaminant Effects on California Bay-Delta Species and Human Health. *San Francisco Estuary and Watershed Science*. 14(4).

Ghisi N de C, Ramsdorf WA, Ferraro MVM, de Almeida MIM, Riberio CA de O, Cestari MM. (2011). Evaluation of genotoxicity in *Rhmadia quelen* (Pices, Siluriformes) after sub-chronic contamination with Fipronil. *Envron. Monit. Assess*. 180: 589-599. DOI 10.1007/s10661-010-1807-7.

Hammock BG, Hobbs JA, Slater SB, Acuña S, Teh SJ. (2015). Contaminant and food limitation stress in an endangered estuarine fish. *Sci. Tot. Environ.* 532: 316-326.

Hasenbein M, Werner I, Deanovic LA, Geist J, Fritsch EB, Javidmehr A. (2014). Transcriptomic profiling permits the identification of pollutant sources and effects in ambient water samples. *Sci. Tot. Environ*. 468-469:688-98. DOI: http://dx.doi.org/10.1016/j.scitotenv.2013.08.081.

Jabusch, T., Trowbridge, P., Heberger, M., Orlando, J., De Parsia, M., & Stillway, M. (2018). Delta Regional Monitoring Program Annual Monitoring Report for Fiscal Year 2015–16: Pesticides and Toxicity. Richmond, CA: Aquatic Science Center. http://www. sfei. org/documents/delta-pesticides-2016.

Jassby AD, Kimmerer WJ, Monismith SG, Armor C, Cloern JE, Powel TM, Schubel JR, Vendlinski TJ. (1995). Isohaline Position as a Habitat Indicator for Estuarine Populations. *Ecological Applications*. 5(1): 272-289. https://doi.org/10.2307/1942069.

Kimmerer WJ, MacWilliams ML, Gross ES. (2013). Variation of Fish Habitat and Extent of the Low Salinity Zone with Freshwater Flow in the San Francisco Estuary. *San Francisco Estuary and Water Science*. 11(4). https://doi.org/10.15447/sfews.2013v11iss4art1.

Kuivila KM, Moon GE. (2004). Potential exposure of larval and juvenile delta smelt to dissolved pesticides in the Sacramento–San Joaquin Delta, California. American Fisheries Society Symposium. *American Fisheries Society*, pp. 229–242.

Kurobe T, Park MO, Javidmehr A, Teh FC, Acuna SC, Corbin CJ, Conley AJ, Bennett WA, Teh SJ. (2016). Assessing oocyte development and maturation in the threatened Delta Smelt, Hypomesus transpacificus. *Environ Biol Fish*. 99:423-432. DOI 10.1007/s10641-016-0483-z.

Mallatt JM. (1985). Fill Gill Structural Changes Inducted by Toxicants and Other Irritants: A Statistical Review. *Can. J. Fish. Aqua. Sci*. 42(4): 630-648. DOI: 10.1139/f85-083.

MAST, I. (2015). An updated conceptual model of Delta Smelt biology: our evolving understanding of an estuarine fish. Technical Report 90. DWR-1089. Interagency Ecology Program for the San Francisco Bay/Delta Estuary. *Management, Analysis, and Synthesis Team*. January 2015.

Matey V, Iftikar FI, De Boeck G, Scott GR, Slowman KA, Almeida-Val VMF, Val AL, Wood CM. (2011). Gill morphology and acute hypoxia: responses of mitochondria-rich, pavement, and mucous cells in the Amazonian Oscar (*Astronotus ocellatus*) and the rainbow trout (*Oncorhynchus mykiss*), two species with very different approaches to the osmo-respiratory compromise. *Can. J. Zool*. 89: 307-324. DOI:10.1139/Z11-002.

Moschet, C.; Lew, B.M.; Hasenbein, S.; Anumol, T.; Young, T.M. (2017). LC- and GC-QTOF-MS as Complementary Tools for a Comprehensive Micropollutant Analysis in Aquatic Systems. *Environmental Science and Technology.* 51: 1553-1561.

Moyle PB, Hobbs, JA, Durand JR. 2018. Delta Smelt and Water Politics in California. (2018). *Fisheries*. 43(1): 42-60.

Orlando, J.L., McWayne, M., Sanders, C., and Hladik, M. (2013). Dissolved pesticide concentrations in the Sacramento-San Joaquin Delta and Grizzly Bay, California, 2011–12: U.S. Geological Survey Data Series 779, 24 p.

Orlando JL, McWayne M, Sanders C, Hladik M. (2014). Dissolved pesticide concentrations entering the Sacramento-San Joaquin Delta from the Sacramento and San Joaquin Rivers, California, 2012-13. U.S. Geological Survey Data Series 876, 28p.

Orlando JL, DeParsia M, Sanders C, Hladik M, Frantzich J. (2020). Pesticide Concentrations Associated with Augmented Flow Pulses in the Yolo Bypass and Cache Slough Complex, California. 2020-1076. Open-file Report. Water Availability and Use Science Program. United States Geological Survey, Sacramento, CA. ISSN 2331-1258 (online); https://doi.org/ 10.3133/ ofr20201076.

Pal S, Kokushi E, Koyama J, Uno S, Ghosh AR. (2012). Histopathological alterations in gill, liver and kidney of common carp exposed to chlorpyrifos. *J. Environ. Sci. and Health. Part B*. 47: 180-195. DOI: 10.1080/03601234.2012.632285

Slanionova A, Modra H, Hostovsky M, Sisperova E, Blahova J, Matejova I, Vicenova M, Faldyna M, Zelnickova L, Tichy F, Svobodova Z. (2014). Effects of Subchronic Exposure to N,N-Diethyl-*m*-toluamide on Selected Biomarkers in Common Carp (*Cyprinus carpio* L.). *BioMed Res. Int.* http://dx.doi.org/10.1155/2014/828515.

Smalling KL, Kuivila KM, Orlando JL, Phillips BM, Anderson BS, Siegler K, Hunt JW, Hamilton M. (2013). Environmental fate of fungicides and other current-use pesticides in a central California estuary. *Marine Pollut. Bull*. 73: 144-153.

Sommer T, Hartman R, Koller M, Koohafkan M, Conrad JL, MacWilliams M, Bever A, Burdi C, Hennessy A, Beakes M. (2020). Evaluation of a large-scale flow manipulation to the upper San Francisco Estuary: Response of habitat conditions for an endangered native fish. *PLoS ONE*. 15(10): e0234673. https://doi.org/10.1371/journal.pone.0234673.

Sutton R, Xie Y, Moran KD, Teerlink J. (2019). Occurrence and Sources of Pesticide to Urban Wastewater and the Environment. In Goh et al. Pesticides in Surface Water: Monitoring, Modeling, Risk Assessment, and Management. ACS Symposium Series; American Chemical Society. Washington DC. 2019.

Teh SJ, Baxa DV, Hammock BG, Gandhi SA, Kurobe T. (2016). A novel and versatile flash–freezing approach for evaluating the health of Delta Smelt. *Aquat. Toxicol.* 170:152–161.

Teh SJ, Schultz AA, Duarte WR, Acuña S, Barnard DM, Baxter D, Garcia PAT, Hammock BG. (2020). Histopathological assessment of seven year-classes of Delta Smelt. *Sci. Tot. Environ*. 726, p. 138333. ISSN: 0048-9697; DOI: 10.1016/j.scitotenv.2020.138333.

Thompson B, Adelsbach T, Brown C, Hunt J, Kuwabara J, Neale J, Ohlendorf H, Schwarzbach S, Spies R, Taberski K. (2007). Biological effects of anthropogenic contaminants in the San Francisco Estuary. *Environ. Research*. 105: 156-174.

U.S. Bureau of Reclamation (Reclamation). (2011). Adaptive management of fall outflow for delta smelt protection and water supply reliability. U.S. Bureau of Reclamation, Sacramento, CA. Available at: http://www.usbr.gov/mp/BayDeltaOffice/docs/Adaptive%20Management%20of%20Fall%20Outflow%20for%20Delta%20Smelt%20Protection%20and%20Water%20Supply%20Reliability.pdf.

U.S. Bureau of Reclamation (Reclamation). (2012). Adaptive management of fall outflow for delta smelt protection and water supply reliability. U.S. Bureau of Reclamation, Sacramento, CA. Available at: http://deltacouncil.ca.gov/sites/default/files/documents/files/Revised_Fall_X2_Adaptive_MgmtPlan_EVN_06_29_2012_final.pdf.

U.S. Bureau of Reclamation (Reclamation). (2019). Delta Smelt Fall Habitat Action in 2019. Finding of No New Significant Impact. US Department of the Interior, Bureau of Reclamation, Interior Region 10 – California Great Basin. September 2019.

United States Environmental Protection Agency. (1996). Office of prevention, pesticides and toxic substances. New pesticide fact sheet. EPA-737-F-96–005, Washington, D.C. http://www.epa.gov/EPA-PEST/1996/June/day-12/Factsheet.pdf. Accessed 28 August 2009.

United States Environmental Protection Agency. (1998). Fipronil for use on rice (Regent®, Icon®), and pets (Frontline®). HED risk assessment. Office of prevention, pesticide and toxic substances. Washington, D.C. pps. 19-22.

United States Environmental Protection Agency. (2019). Aquatic Life Benchmarks and Ecological Risk Assessments for Registered Pesticides. https://www.epa.gov/pesticide-science-and-assessing-

pesticide-risks/aquatic-life-benchmarks-and-ecological-risk. Office of prevention, pesticide and toxic substances. March, 2019 update. Accessed 29 June 2020.

U.S. Fish and Wildlife Service (USFWS). (2008). Formal Endangered Species Act Consultation on the Proposed Coordinated Operations of the Central Valley Project (CVP) and State Water Project (SWP). United States Fish and Wildlife Service, Sacramento, CA.

Werner I, Deanovic LA, Connor V, de Vlaming V, Bailey HC, Hinton DE. (2000). Insecticide-caused toxicity to Ceriodaphnia dubia (CLADOCERA) in the Sacramento–San Joaquin River delta, California, USA. *Environ. Toxicol. Chem.* 19, 215–227.

Weston DP and Lydy MJ. (2014). Toxicity of the Insecticide Fipronil and Its Degradates to Benthic Macroinvertebrates of Urban Streams. *Env. Sci. Technol*. 48: 1290-1297. DOI: http://dx.doi.org/10.1021/es4045874.

Weston DP, Asbell AM, Lesmeister SA, Teh SJ, Lydy MJ. (2014). Urban and agricultural pesticide inputs to a critical habitat for the threatened delta smelt (*Hypomesus transpacificus*). *Environ. Toxicol*. Chem. 33, 920–929.

Weston DP, Moschet C, Young TM, Johanif N, Poynton HC, Major KM, Connon RE, Hasenbein S. (2019). Chemical and Toxicological Effects on Cache Slough after Storm-Driven Contaminant Inputs. *San Francisco Estuary and Watershed Science*. DOI: 10.15447/sfews.2019v17iss3art3.

Wolf JC, Wolfe MJ. (2005). A brief overview of nonneoplastic hepatic toxicity in fish. *Toxicol. Pathol*. 33, 75–85.

Zenobio JE, Sanchez BC, Archuleta LC, Sepulveda MS. (2013). Effects of triclocarban, N,N-diethyl-meta-toluamide, and a mixture of pharmaceuticals and personal care products on fathead minnows (*Pimephales promelas*). *Environ. Toxicol. Chem*. DOI: 10.1002/etc.2511.

Chapter 2: Assessment of Acute Toxcity and Histopathology of Environmental Contaminants in Delta Smelt (*Hypomesus transpacificus*) in Relation to Delta Outflow

Tables and Figures

Table 1. Summary of events and test initiation dates across the project

Project Year	Test Exposure	Flow Action	Test Initiation Date
2017 Fall	1	Fall X2	October 13, 2017
	2	Fall X2	October 27, 2017
	3	Fall X2	November 10, 2017
	4	Fall X2	November 24, 2017
	5		December 8, 2017
2018 Summer	1		July 12, 2018
	2		July 27, 2018
	3	Salinity Gate	August 8, 2018
	4	Salinity Gate, North Delta	September 6, 2018
2018 Fall	1	North Delta	September 20, 2018
	2		October 4, 2018
	3		October 19, 2018
	4		October 26, 2018
	5		November 16, 2018
2019	1	North Delta, Fall X2	September 13, 2019
	2	North Delta, Fall X2	September 27, 2019
	3	Fall X2	October 11, 2019
	4	Fall X2	October 25, 2019
	5	Fall X2	November 8, 2019

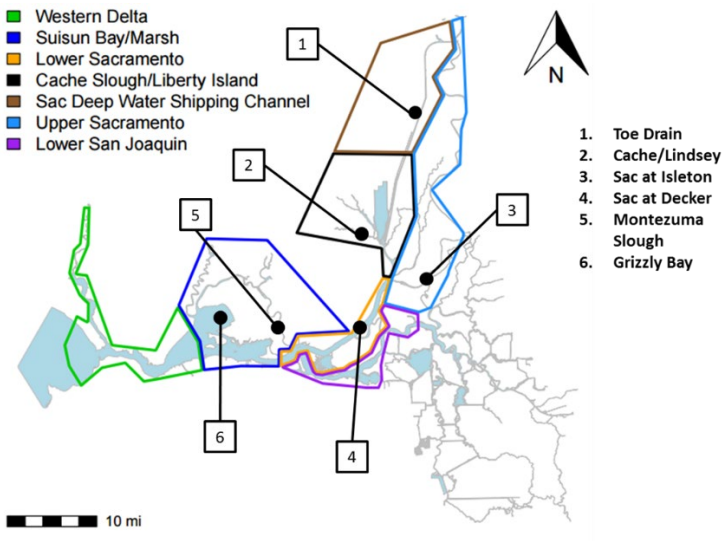

Figure 1. Map of study area with delineated strata (technical assistance from Lara Mitchell (USFWS).

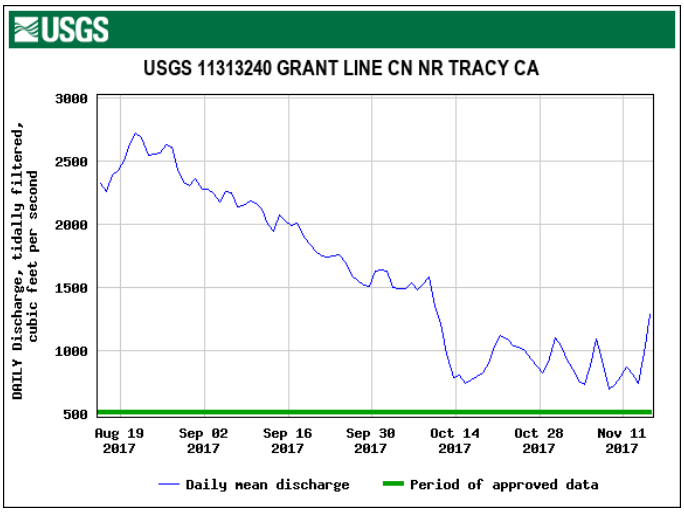

Figure 2. Graph of daily mean discharge for USGS site 11313240 Grant Line near Tracy, CA. Graph depicts reduced South Delta exports in October 2017 related to the Fall X2 Action. Graph generated using USGS Surface-Water Daily Data for the Nation, https://nwis.waterdata.usgs.gov/nwis/dv?.

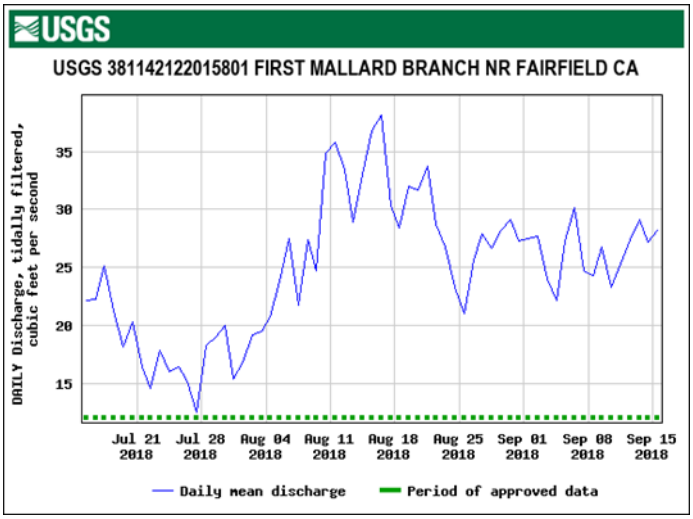

Figure 3. Graph of daily mean discharge for USGS site 381142122015801 First Mallard Branch near Fairfield, CA during the 2018 Salinity Gate Flow Action. Graph generated using USGS Surface-Water Daily Data for the Nation, https://nwis.waterdata.usgs.gov/nwis/dv?.

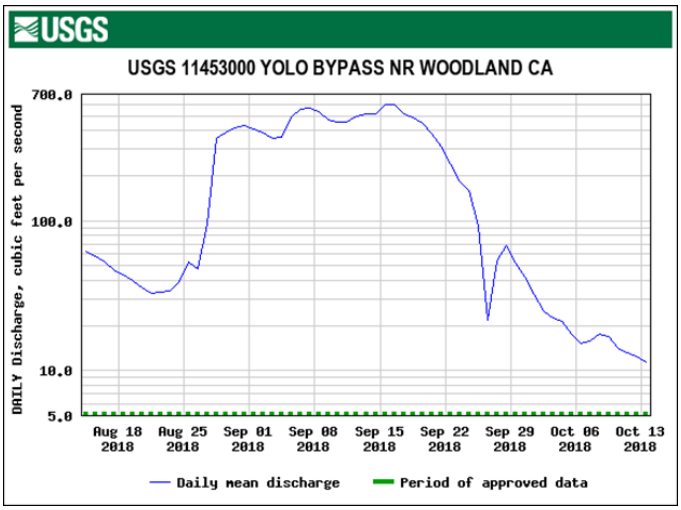

Figure 4. Graph of daily mean discharge for USGS site 11453000 Yolo Bypass near Woodland, CA during the 2018 North Delta Flow Action pulse flow. Graph generated using USGS Surface-Water Daily Data for the Nation, https://nwis.waterdata.usgs.gov/nwis/dv?.

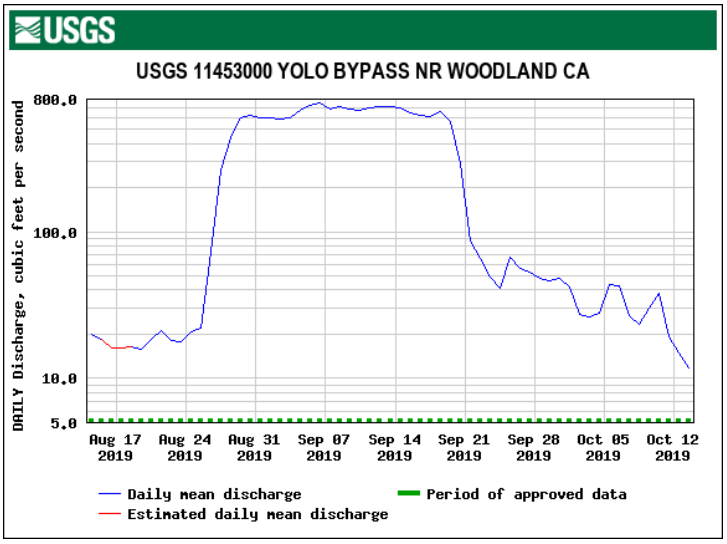

Figure 5. Graph of daily mean discharge for USGS site 11453000 Yolo Bypass near Woodland, CA during the 2019 North Delta Flow Action pulse flow. Graph generated using USGS Surface-Water Daily Data for the Nation, https://nwis.waterdata.usgs.gov/nwis/dv?.

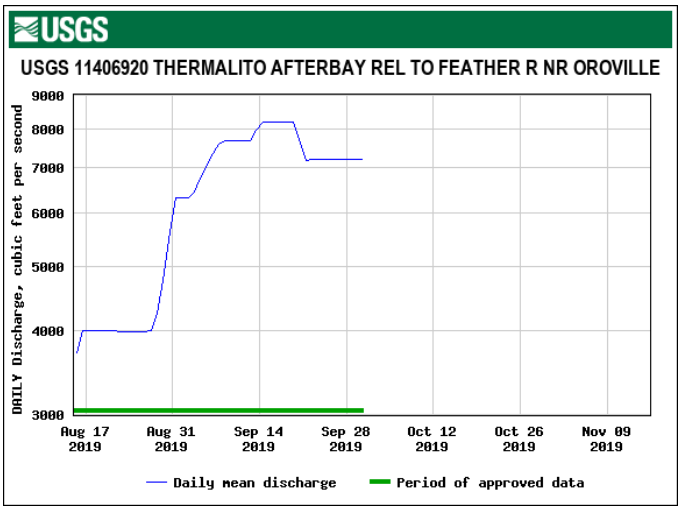

Figure 6. Graph of daily mean discharge for USGS site 11406920 Thermalito Afterbay Release to Feather River near Oroville, CA during the 2019 Fall X2 Action. Graph depicts increased releases from Oroville Reservoir on September 25 and 26, 2019. Graph generated using USGS Surface-Water Daily Data for the Nation, https://nwis.waterdata.usgs.gov/nwis/dv?.

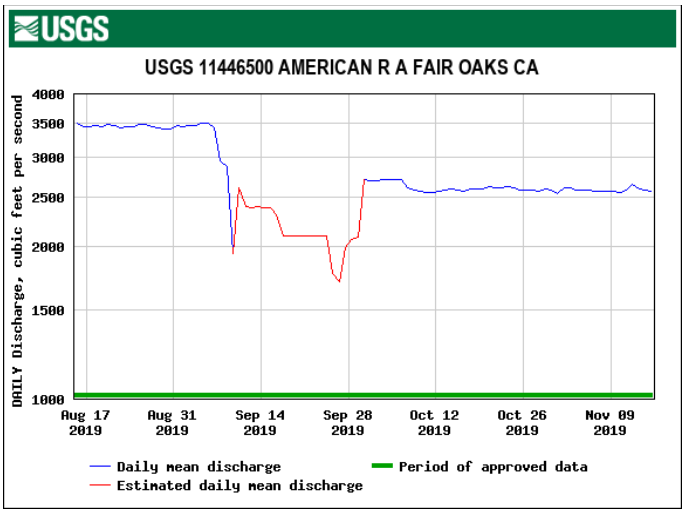

Figure 7. Graph of daily mean discharge for USGS site 11446500 American River near Fair Oaks, CA during the 2019 Fall X2 Action. Graph depicts reduced releases from Folsom Reservoir on September 25 and 26, and increased releases on September 30, 2019. Graph generated using USGS Surface-Water Daily Data for the Nation, https://nwis.waterdata.usgs.gov/nwis/dv?.

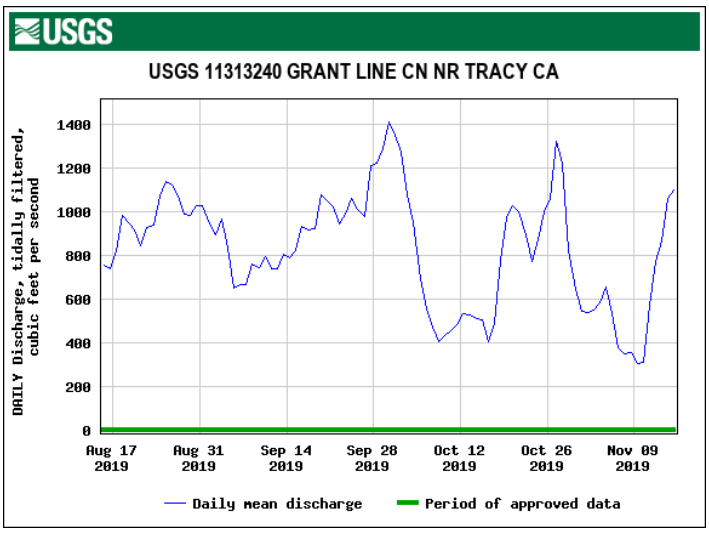

Figure 8. Graph of daily mean discharge for USGS site 11313240 Grant Line CN near Tracy, CA during the 2019 Fall X2 Action. Graph depicts reduced exports from the South Delta on September 28 and 29, 2019. Graph generated using USGS Surface-Water Daily Data for the Nation, https://nwis.waterdata.usgs.gov/nwis/dv?.

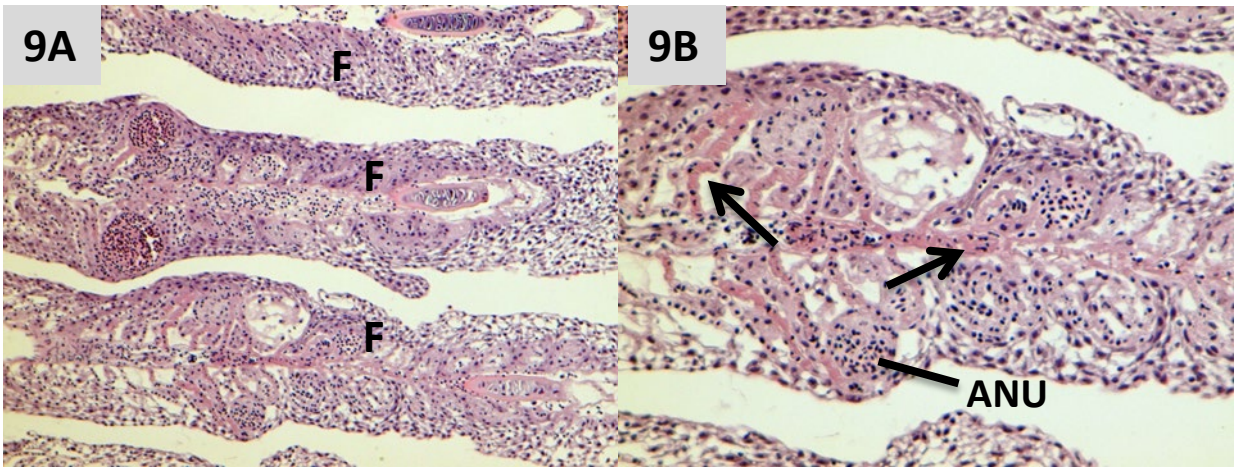

Figure 9. A) Severe secondary lamella fusion (F) in 3 gill filaments at low magnification. B) higher magnification showing moderate epithelial cell necrosis (arrows) and aneurysm (ANU) in Delta Smelt exposed to water collected from Cache Slough in a toxicity test initiated on October 27, 2017.

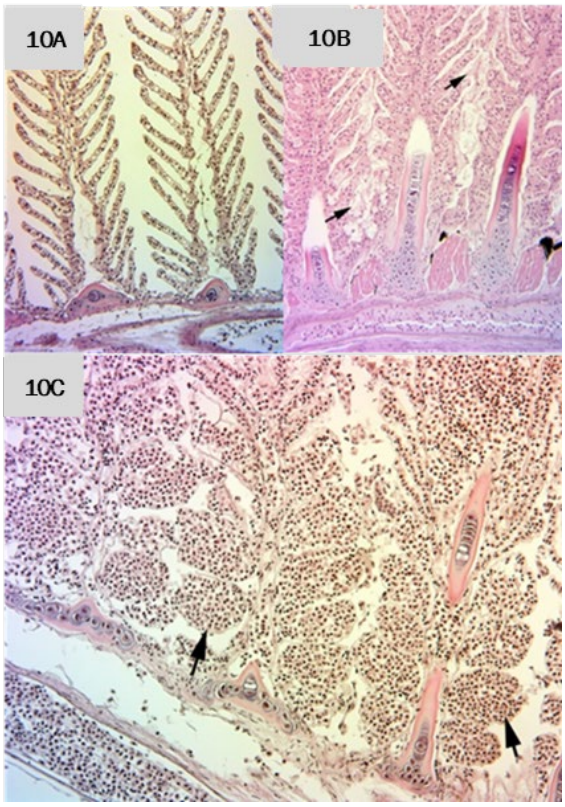

Figure 10. A) Typical regular thin gill lamellae structure of Delta Smelt exposed to FCCL water for 96 hr. B) Severe mucus cell hyperplasia in gill exposed to Cache Slough water for 96 hr. Arrows point to mucus discharges filling the space of primary and secondary lamellae. C) Severe gill aneurysm or telangiectasia (arrows) in Delta Smelt exposed to water from Cache Slough in a toxicity test initiated on November 10, 2017.

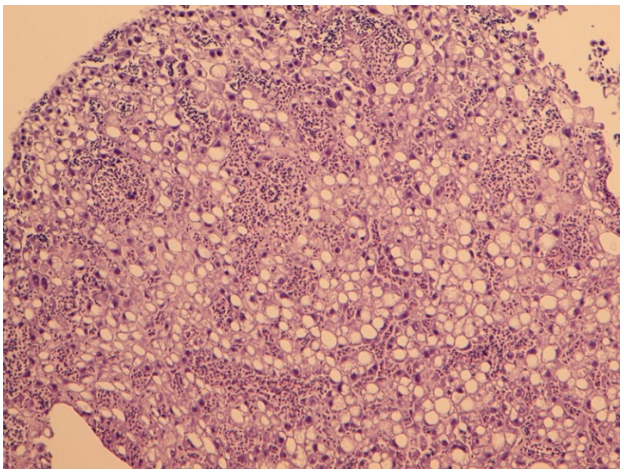

Figure 11. Severe fatty vacuolation and moderate sinusoidal congestion in the liver of Delta Smelt exposed to water collected from the Sacramento River at Decker Island in a toxicity test initiated on December 8, 2017 (200x magnification).

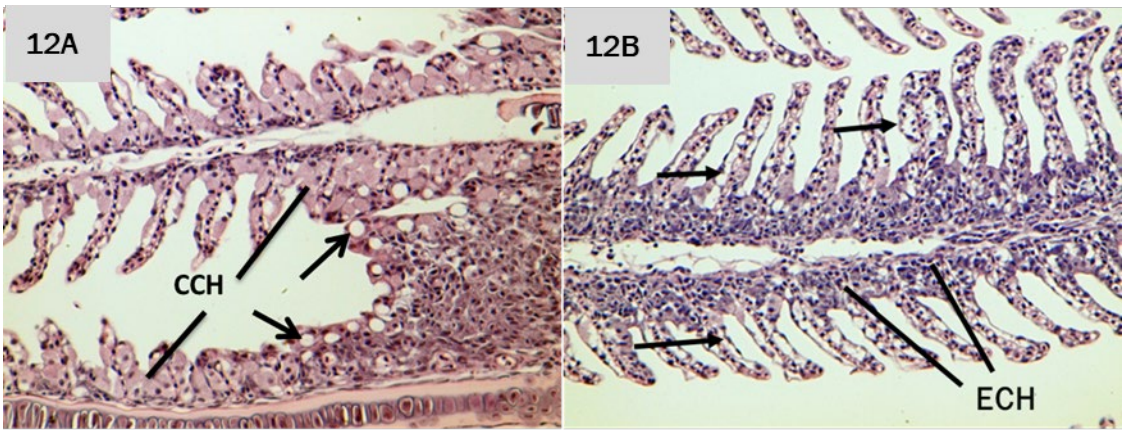

Figure 12. A) Chloride cell hyperplasia (CCH) and mucus cell proliferation (arrows) in gills. B) Secondary lamellae edema (arrows) and epithelial cell hyperplasia (ECH) in gills. Gills are from Delta Smelt exposed to water collected from Cache Slough in a toxicity test initiated on July 12, 2018 (Summer Exposure 1; 200x magnification).

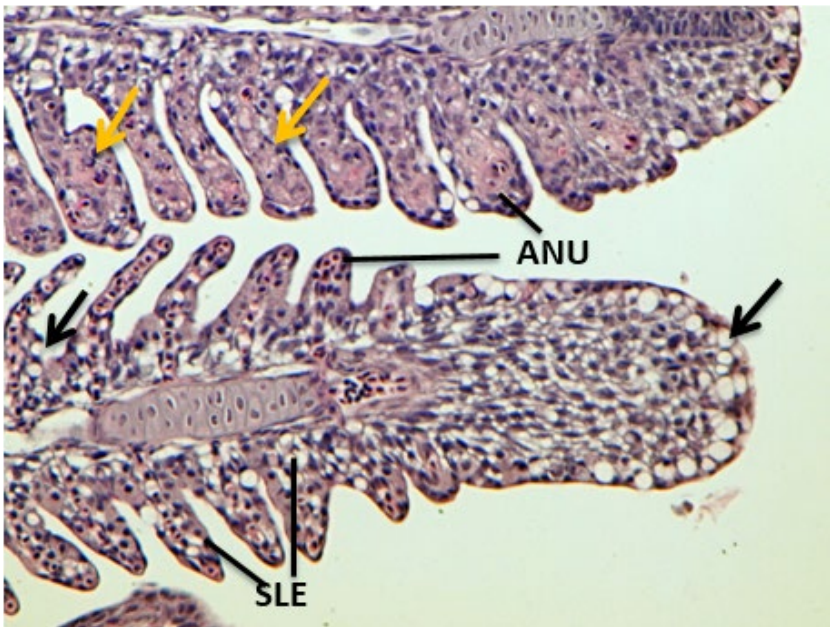

Figure 13. Mucus cell hyperplasia (black arrows), epithelial cell necrosis (yellow arrows), small aneurysm (ANU), and edema (SLE) in secondary lamella of gill in Delta Smelt exposed for 96 h to water sample from the Sacramento River at Decker Island (200x magnification) on November 8, 2019.

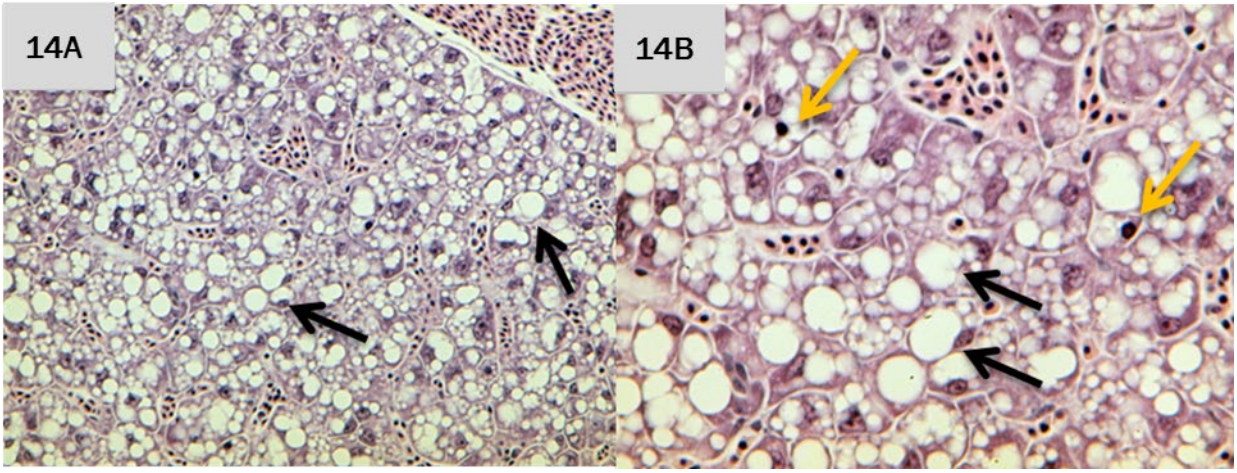

Figure 14. A) Liver of Delta Smelt shows severe lipidosis as indicated by black arrows, exposed to water collected from the Toe Drain (200X magnification). B) Liver of Delta Smelt exposed for 96 h to water collected from Toe Drain, showing severe lipidosis (black arrows) and single cell necrosis (yellow arrows) at 400x magnification, initiated in a toxicity test on September 27, 2019.

Chapter 2: Assessment of Acute Toxcity and Histopathology of Environmental Contaminants in Delta Smelt (*Hypomesus transpacificus*) in Relation to Delta Outflow

Supplemental Information

Table S1. Summary of contaminants detected across the 2017 study period.

Site	Exposure	Analyte	Result (ng/L)
Toe Drain	1	-	-
	2	Fipronil-desulfinyl	0.1
		Fipronil-sulfide	0.05
		Fipronil	0.14
		Fipronil-sulfone	0.1
		Chlorpyrifos	0.11
		Total Barium	24,000
		Dissolved Barium	25,000
	3	Fipronil-desulfinyl	0.11
		Fipronil-sulfide	0.05
		Fipronil	0.12
		Fipronil-sulfone	0.11
		Total Barium	24,000
		Dissolved Barium	24,000
	4	Fipronil-desulfinyl	0.12
		Fipronil-sulfide	0.06
		Fipronil	0.17
		Fipronil-sulfone	0.12
		Chlorpyrifos	0.11
		Total Barium	27,000
		Dissolved Barium	27,000
	5	Fipronil-desulfinyl	0.11
		Fipronil-sulfide	0.06
		Fipronil	0.16
		Fipronil-sulfone	0.16
		Total Barium	35,000
		Dissolved Barium	31,000
		Total Iron	310,000
		Total Manganese	13,000
Lindsey Slough	1	Fipronil-desulfinyl	0.09
		Fipronil-sulfide	0.06
		Fipronil	0.15
		Fipronil-sulfone	0.12
		Total Barium	21,000
		Dissolved Barium	23,000
Cache Slough at Steamboat Slough	1	Fipronil-desulfinyl	0.08
		Fipronil-sulfide	0.05
		Fipronil	0.19
		Fipronil-sulfone	0.15
		Total Barium	18,000
		Dissolved Barium	18,000
	2	Fipronil-desulfinyl	0.1
		Fipronil-sulfide	0.06

Site	Exposure	Analyte	Result (ng/L)
		Fipronil	0.23
		Fipronil-sulfone	0.13
		Chlorpyrifos	0.23
		Total Barium	21,000
		Dissolved Barium	23,000
	3	Fipronil-desulfinyl	0.1
		Fipronil-sulfide	0.06
		Fipronil	0.23
		Fipronil-sulfone	0.14
		Total Barium	24,000
		Dissolved Barium	24,000
	4	Fipronil-desulfinyl	0.13
		Fipronil-sulfide	0.06
		Fipronil	0.41
		Fipronil-sulfone	0.26
		Chlorpyrifos	0.11
		Total Barium	27,000
		Dissolved Barium	28,000
	5	Fipronil-desulfinyl	0.1
		Fipronil-sulfide	0.07
		Fipronil	0.25
		Fipronil-sulfone	0.26
		Total Barium	30,000
		Dissolved Barium	30,000
		Total Iron	72,000
		Dissolved Nickel	10,000
Sacramento River at Isleton	1	-	-
	2	Fipronil-desulfinyl	0.07
		Fipronil-sulfide	0.05
		Fipronil	0.23
		Fipronil-sulfone	0.18
		Total Barium	16,000
		Dissolved Barium	18,000
	3	Fipronil-desulfinyl	0.07
		Fipronil-sulfide	0.05
		Fipronil	0.31
		Fipronil-sulfone	0.16
		Chlorpyrifos	0.11
		Total Barium	21,000
		Dissolved Barium	21,000
	4	Fipronil-desulfinyl	0.09
		Fipronil-sulfide	0.06
		Fipronil	0.49
		Fipronil-sulfone	0.28
		Azoxystrobin	4.73
		Total Barium	24,000
		Dissolved Barium	27,000

Site	Exposure	Analyte	Result (ng/L)
		Total Iron	92,000
		Dissolved Iron	13,000
	5	Fipronil-desulfinyl	0.07
		Fipronil-sulfide	0.06
		Fipronil	0.28
		Fipronil-sulfone	0.23
		Total Barium	28,000
		Dissolved Barium	25,000
		Total Iron	100,000
Sacramento River at Decker Island	1	-	-
	2	Fipronil-desulfinyl	0.11
		Fipronil-sulfide	0.06
		Fipronil	0.24
		Fipronil-sulfone	0.17
		Total Barium	18,000
		Dissolved Barium	20,000
	3	Fipronil-desulfinyl	0.09
		Fipronil-sulfide	0.05
		Fipronil	0.23
		Fipronil-sulfone	0.15
		Total Barium	20,000
		Dissolved Barium	22,000
	4	Fipronil-desulfinyl	0.14
		Fipronil-sulfide	0.07
		Fipronil	0.64
		Fipronil-sulfone	0.4
		Fipronil-desulfinyl amide	0.1
		Chlorpyrifos	0.12
		Total Barium	24,000
		Dissolved Barium	25,000
		Total Iron	12,000
	5	Fipronil-desulfinyl	0.09
		Fipronil-sulfide	0.06
		Fipronil	0.23
		Fipronil-sulfone	0.24
		Total Barium	27,000
		Dissolved Barium	28,000
		Total Iron	86,000
Montezuma Slough	1	Fipronil-desulfinyl	0.09
		Fipronil-sulfide	0.05
		Fipronil	0.14
		Fipronil-sulfone	0.11
		Fipronil-desulfinyl amide	0.06
		Total Barium	42,000
		Dissolved Barium	34,000
	2	Fipronil-desulfinyl	0.09
		Fipronil-sulfide	0.06

Site	Exposure	Analyte	Result (ng/L)
		Fipronil	0.18
		Fipronil-sulfone	0.13
		Fipronil-desulfinyl amide	0.05
		Total Barium	33,000
		Dissolved Barium	33,000
		Total Manganese	14,000
		Dissolved Manganese	12,000
	3	Fipronil-desulfinyl	0.1
		Fipronil-sulfide	0.06
		Fipronil	0.16
		Fipronil-sulfone	0.17
		Total Barium	38,000
		Dissolved Barium	38,000
	4	Fipronil-desulfinyl	0.12
		Fipronil-sulfide	0.06
		Fipronil	0.29
		Fipronil-sulfone	0.16
		Total Barium	40,000
		Dissolved Barium	41,000
		Total Iron	84,000
		Total Manganese	58,000
		Dissolved Manganese	40,000
	5	Fipronil-desulfinyl	0.11
		Fipronil-sulfide	0.06
		Fipronil	0.32
		Fipronil-sulfone	0.22
		Fipronil-desulfinyl amide	0.06
		Total Barium	40,000
		Dissolved Barium	41,000
Grizzly Bay	1	Fipronil-desulfinyl	0.1
		Fipronil-sulfide	0.05
		Fipronil	0.13
		Total Barium	34,000
		Dissolved Barium	34,000
		Total Iron	82,000
		Total Manganese	11,000
	2	-	-
	3	Fipronil-desulfinyl	0.1
		Fipronil-sulfide	0.05
		Fipronil	0.15
		Fipronil-sulfone	0.1
		Total Barium	42,000
		Dissolved Barium	41,000
		Total Iron	82,000
		Total Manganese	11,000
	4	Fipronil-desulfinyl	0.12
		Fipronil-sulfide	0.06

Site	Exposure	Analyte	Result (ng/L)
		Fipronil	0.2
		Fipronil-sulfone	0.13
		Total Barium	38,000
		Dissolved Barium	39,000
	5	Fipronil-desulfinyl	0.12
		Fipronil-sulfide	0.06
		Fipronil	0.21
		Fipronil-sulfone	0.14
		Fipronil-desulfinyl amide	0.06
		Total Barium	40,000
		Dissolved Barium	40,000
		Total Manganese	22,000
		Dissolved Manganese	11,000

Table S2. Summary of contaminants detected across the 2018 study period.

Site	Exposure	Analyte	Result (ng/L)
Toe Drain	1	Fipronil-desulfinyl	0.2
	2	Fipronil-desulfinyl	0.4
		Fipronil-sulfone	1.7
		Fipronil	6.5
	3	Fipronil-desulfinyl	0.3
	4	Fipronil-desulfinyl	0.3
	5	Fipronil-desulfinyl	0.3
Cache Slough	1	Fipronil-desulfinyl	0.2
	2	Fipronil-desulfinyl	0.2
	3	Fipronil-desulfinyl	0.3
	4	Fipronil-desulfinyl	0.3
	5	Fipronil-desulfinyl	0.3
Sacramento River at Isleton	3	Fipronil-desulfinyl	0.1
	4	Fipronil-desulfinyl	0.3
	5	Fipronil-desulfinyl	0.2
Sacramento River at Decker Island	1	Fipronil-desulfinyl	0.1
	2	Fipronil-desulfinyl	0.1
	3	Fipronil-desulfinyl	0.3
	4	Fipronil-desulfinyl	0.3
	5	Fipronil-desulfinyl	0.4
Montezuma Slough	1	Fipronil-desulfinyl	0.3
	2	Fipronil-desulfinyl	0.3
	3	Fipronil-desulfinyl	0.4
	4	Fipronil-desulfinyl	0.4
	5	Fipronil-desulfinyl	0.5
Grizzly Bay	1	Fipronil-desulfinyl	0.3
	2	Fipronil-desulfinyl	0.4
	3	Fipronil-desulfinyl	0.3
	4	Fipronil-desulfinyl	0.4
	5	Fipronil-desulfinyl	0.4

Table S3. Summary of contaminants detected across the 2019 study period.

Site	Exposure	Analyte	Result (ng/L)
Toe Drain	1	DEET	6
		Chlorantraniprole	33
		Azoxystrobin	1601
		Methoxyfenozide	166
		Metolachlor	9
		Thiobencarb	113
		Aluminum	995,000
		Manganese	94,000
		Nickel	10,000
		Arsenic	4,000
	2	DEET	9
		Chlorantraniprole	23
		Azoxystrobin	635
		Methoxyfenozide	65
		Aluminum	464,000
		Manganese	53,000
		Nickel	6,000
		Arsenic	4,000
	3	DEET	12
		Azoxystrobin	231
		Diuron	21
		Aluminum	518,000
		Manganese	45,000
		Arsenic	4,000
	4	Azoxystrobin	110
		Aluminum	609,000
		Manganese	50,000
		Nickel	5,000
		Arsenic	3,000
	5	DEET	6
		Azoxystrobin	21
		Aluminum	250,000
		Manganese	27,000
Cache Slough	1	DEET	13
		Azoxystrobin	381
		Metolachlor	19
		Fipronil-desulfinyl	0.20
		Manganese	12,000
		Arsenic	3,000
	2	DEET	7
		Chlorantraniprole	7
		Azoxystrobin	186
		Methoxyfenozide	34
		Aluminum	11,000
		Manganese	23,000

Site	Exposure	Analyte	Result (ng/L)
		Arsenic	3,000
	3	DEET	33
		Azoxystrobin	234
		Aluminum	60,000
		Manganese	30,000
		Arsenic	3,000
	4	Azoxystrobin	36
		Aluminum	22,000
		Manganese	26,000
	5	DEET	6
		Azoxystrobin	7
		Aluminum	49,000
		Manganese	16,000
Sacramento River at Isleton	1	DEET	7
		Azoxystrobin	63
		Aluminum	352,000
		Manganese	31,000
	2	DEET	6
		Azoxystrobin	39
		Aluminum	69,000
		Manganese	6,000
	3	DEET	10
		Azoxystrobin	10
		Aluminum	58,000
		Manganese	8,000
	4	DEET	6
		Azoxystrobin	3
		Aluminum	43,000
		Manganese	10,000
		Zinc	928,000
	5	DEET	5
		Azoxystrobin	5
		Aluminum	39,000
		Manganese	5,000
Sacramento River at Decker Island	1	DEET	8
		Azoxystrobin	168
		Aluminum	27,000
		Manganese	6,000
	2	DEET	4
		Azoxystrobin	74
		Methoxyfenozide	25
		Aluminum	29,000
		Manganese	5,000
	3	DEET	14
		Azoxystrobin	53
		Aluminum	106,000
		Manganese	8,000

Site	Exposure	Analyte	Result (ng/L)
		Copper	6,000
	4	DEET	9
		Azoxystrobin	16
		Aluminum	194,000
		Manganese	24,000
	5	DEET	12
		Azoxystrobin	15
		Aluminum	88,000
		Manganese	6,000
Montezuma Slough	1	DEET	20
		Azoxystrobin	94
		Fipronil-desulfinyl	0.35
		Fipronil-sulfone	0.23
		Aluminum	191,000
		Manganese	33,000
	2	DEET	7
		Azoxystrobin	98
		Methoxyfenozide	23
		Aluminum	234,000
		Manganese	42,000
		Arsenic	3,000
		Copper	15,000
		Zinc	12,000
	3	DEET	10
		Azoxystrobin	62
		Aluminum	824,000
		Manganese	58,000
		Arsenic	3,000
		Copper	7,000
	4	Azoxystrobin	6
		Aluminum	404,000
		Manganese	136,000
		Nickel	6,000
		Arsenic	5,000
		Copper	8,000
		Zinc	11,000
	5	DEET	8
		Azoxystrobin	22
		Aluminum	404,000
		Manganese	136,000
		Arsenic	5,000
		Copper	7,000
		Zinc	11,000
Grizzly Bay	1	DEET	14
		Azoxystrobin	73
		Fipronil-desulfinyl	0.29
		Aluminum	332,000

Site	Exposure	Analyte	Result (ng/L)
		Manganese	43,000
		Arsenic	6,000
		Copper	9,000
	2	DEET	11
		Azoxystrobin	95
		Methoxyfenozide	23
		Aluminum	210,000
		Manganese	25,000
		Arsenic	11,000
		Copper	18,000
		Zinc	11,000
	3	DEET	8
		Azoxystrobin	43
		Aluminum	727,000
		Manganese	42,000
	4	DEET	13
		Azoxystrobin	60
		Aluminum	1,365,000
		Manganese	102,000
		Copper	16,000
		Zinc	11,000
	5	DEET	5
		Azoxystrobin	28
		Aluminum	111,000
		Manganese	11,000
		Arsenic	15,000
		Copper	82,000

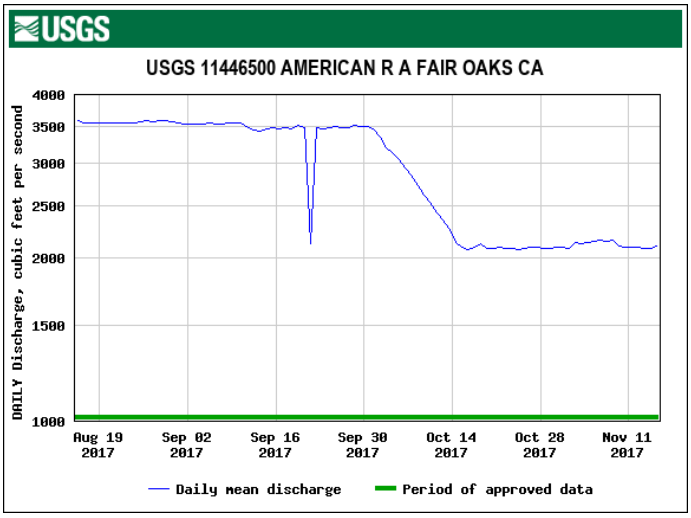

Figure S1. Hydrograph of 2017 reservoir flows at USGS site 11446500 American River at Fair Oaks, CA. Graph depicts American River flows during 2017 Fall X2. Graph generated using USGS Surface-Water Daily Data for the Nation, https://nwis.waterdata.usgs.gov/nwis/dv?.

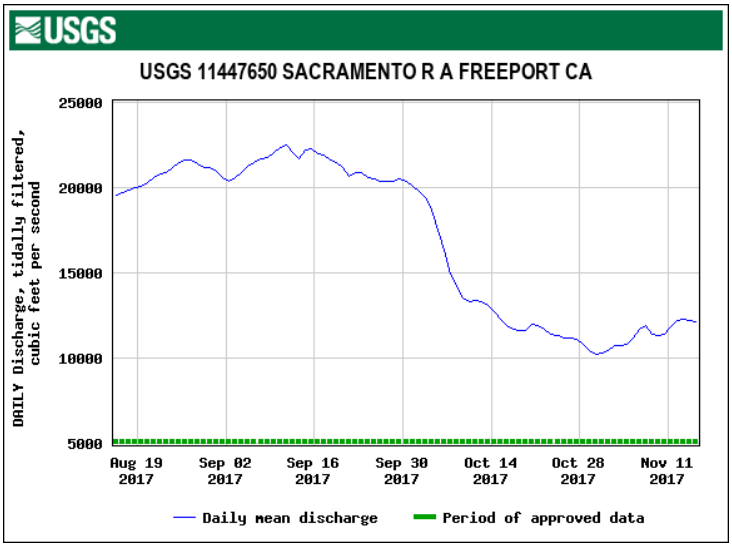

Figure S2. Hydrograph of 2017 river flows at USGS site 11447650 Sacramento River at Freeport, CA. Graph depicts Sacramento River flows during 2017 Fall X2. Graph generated using USGS Surface-Water Daily Data for the Nation, https://nwis.waterdata.usgs.gov/nwis/dv?.

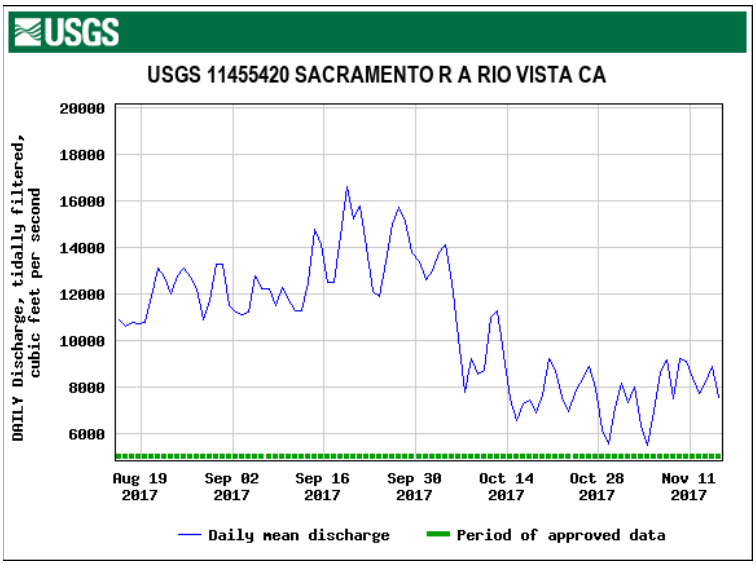

Figure S3. Hydrograph of 2017 river flows at USGS site 11455420 Sacramento River at Rio Vista, CA. Graph depicts Sacramento River flows during 2017 Fall X2. Graph generated using USGS Surface-Water Daily Data for the Nation, https://nwis.waterdata.usgs.gov/nwis/dv?.

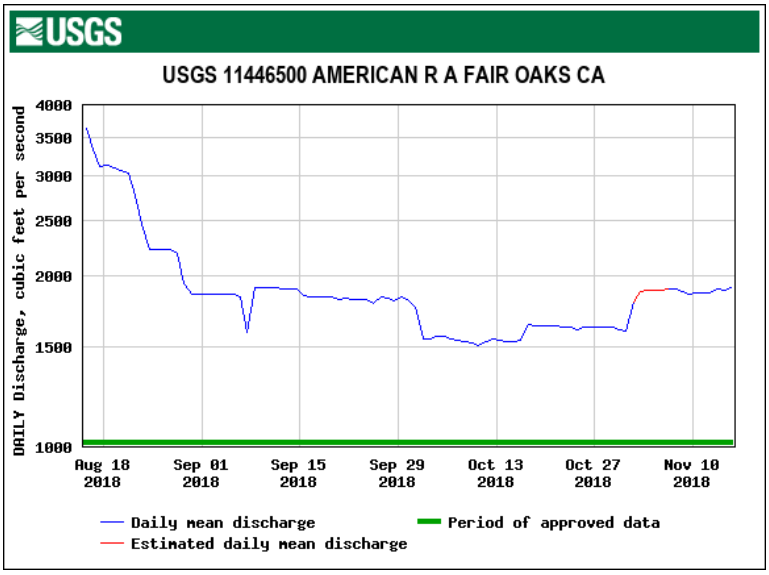

Figure S4. Hydrograph of 2018 river flows at USGS site 11446500 American River at Fair Oaks, CA. Graph depicts American River flows spanning the 2018 North Delta Flow and Fall X2 Actions. Graph generated using USGS Surface-Water Daily Data for the Nation, https://nwis.waterdata.usgs.gov/nwis/dv?.

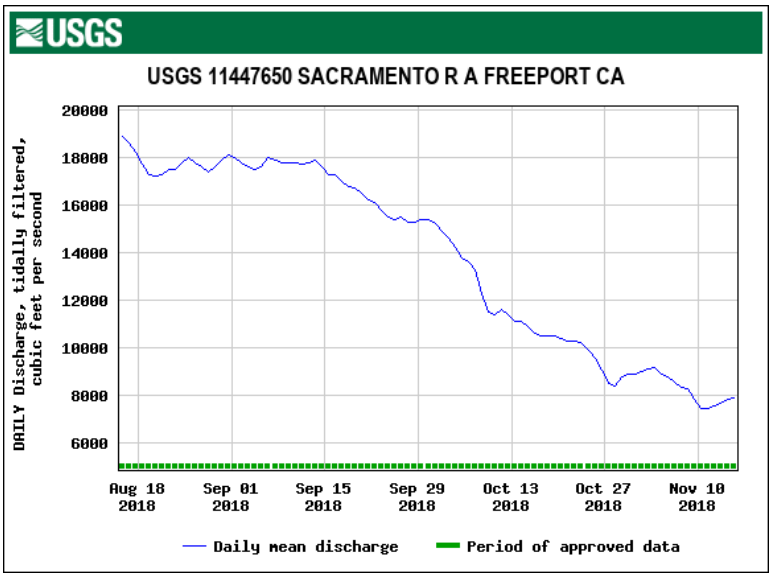

Figure S5. Hydrograph of 2018 river flows at USGS site 11447650 Sacramento River at Freeport, CA. Graph depicts Sacramento River flows spanning the 2018 North Delta Flow and Fall X2 Actions. Graph generated using USGS Surface-Water Daily Data for the Nation, https://nwis.waterdata.usgs.gov/nwis/dv?.

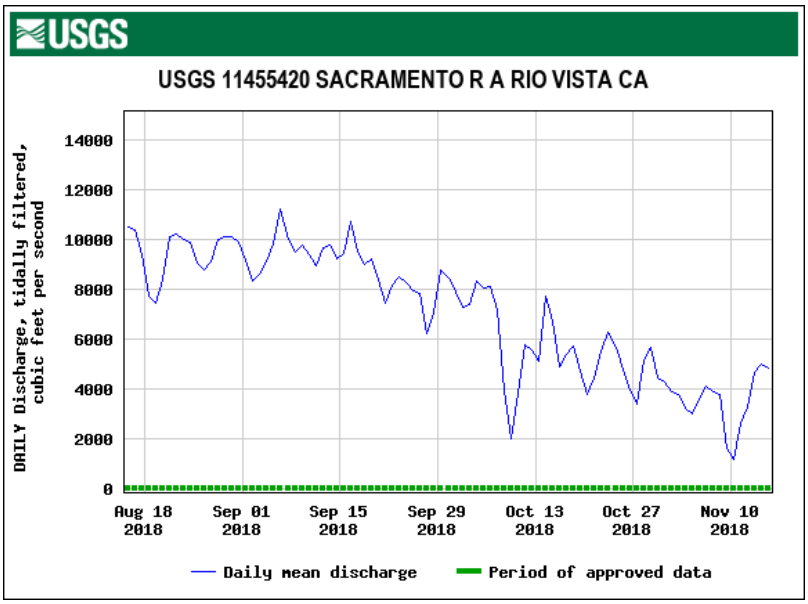

Figure S6. Hydrograph of 2018 river flows at USGS site 11455420 Sacramento River at Rio Vista, CA. Graph depicts Sacramento River flows spanning the 2018 North Delta Flow and Fall X2 Actions. Graph generated using USGS Surface-Water Daily Data for the Nation, https://nwis.waterdata.usgs.gov/nwis/dv?.

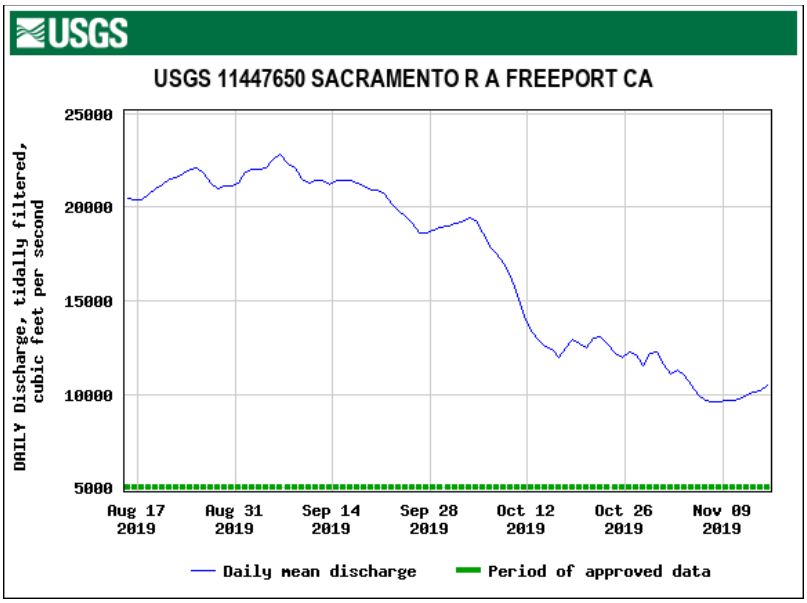

Figure S7. Hydrograph of 2019 river flows at USGS site 11447650 Sacramento River at Freeport, CA. Graph depicts Sacramento River flows spanning the 2019 North Delta Flow and Fall X2 Actions. Graph generated using USGS Surface-Water Daily Data for the Nation, https://nwis.waterdata.usgs.gov/nwis/dv?.

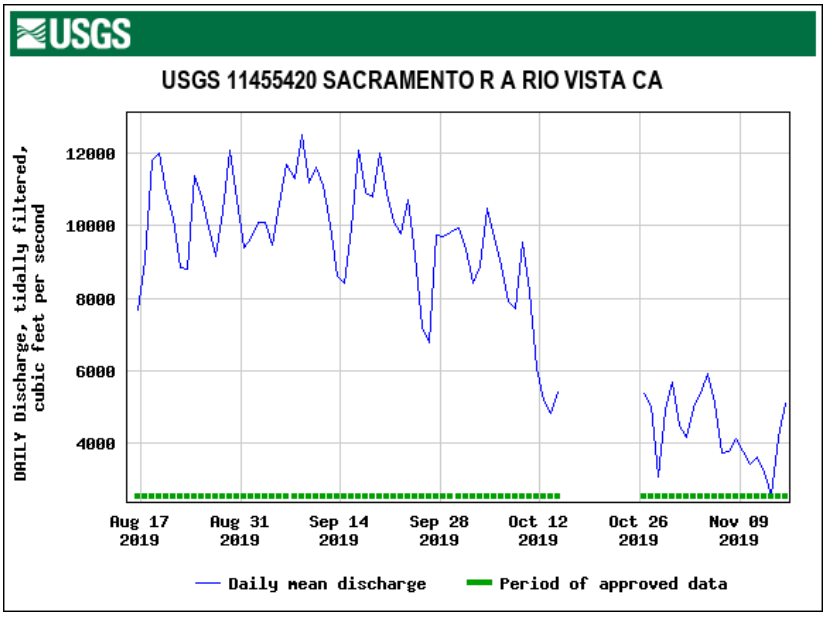

Figure S8. Hydrograph of 2019 river flows at USGS site 11455420 Sacramento River at Rio Vista, CA. Graph depicts Sacramento River flows spanning the 2019 North Delta Flow and Fall X2 Actions. Graph generated using USGS Surface-Water Daily Data for the Nation, https://nwis.waterdata.usgs.gov/nwis/dv?.

This page intentionally left blank

Chapter 3: Reproductive Strategy of Delta Smelt *Hypomesus transpacificus* and Impacts of Drought on Reproductive Performance

Reproductive strategy of Delta Smelt *Hypomesus transpacificus* and impacts of drought on reproductive performance

Tomofumi Kurobe[1*], Bruce G. Hammock[1], Lauren J. Damon[2], Randall D. Baxter[2], Tien-Chieh Hung[3], Alireza Javidmehr[1], Shawn Acuña[4], Erwin Van Nieuwenhuyse[5], Andrew A. Schultz[5], Swee J. Teh[1]

[1] Department of Anatomy, Physiology, and Cell Biology, School of Veterinary Medicine, University of California Davis, Davis, California, United States of America,
[2] California Department of Fish and Wildlife, Stockton, California, United States of America
[3] Department of Biological and Agricultural Engineering, University of California, Davis, Davis, California, United States of America
[4] Metropolitan Water District of Southern California, Sacramento, California, United States of America
[5] Science Division, U.S. Bureau of Reclamation Bay-Delta Office, Sacramento, CA, United States of America

Corresponding author

E-mail: tkurobe@ucdavis.edu (TK)

Abstract

Understanding reproductive biology and performance of fish is essential to formulate effective conservation and management programs. In this study we report reproductive strategies of female Delta Smelt *Hypomesus transpacificus*, an endangered fish species in the State of California, the United States, focusing on (1) better understanding their distribution pattern during the winter and spring spawning season at very fine scale and (2) assessing impacts of a recent, severe drought on their reproductive performance. Salinity seemed to better explain the distribution pattern of Delta Smelt at subadult and adult stages compared with water temperature or turbidity. Although there are some freshwater locations where mature Delta Smelt can be frequently found during the spawning season, Delta Smelt appeared to be widespread in the area where salinity was below 1.0 during the spawning season and fish at the final maturation stage (Stage 5: hydration) were found in the Cache Slough Complex as well as other locations such as sites near the confluence of the Sacramento and San Joaquin rivers. Therefore, Delta Smelt could theoretically spawn in any freshwater location, with more specific spawning requirements (e.g., substrate type and depth) still unknown. Delta Smelt, which experienced dry and drought conditions (the 2013 and 2014 year classes), showed smaller oocytes, and lower clutch size and gonadosomatic index compared with the fish caught in a wet year (2011 year class), suggesting reproductive performance was negatively affected by environmental conditions during the drought.

Introduction

Fish species are facing extinction all over the world. Two of the major causes in the decline of fish populations are overfishing and habitat destruction caused by anthropogenic activities (Hutchings and Reynolds, 2004; Burkhead, 2012). In populations declining due to habitat destruction, habitat protection and restoration are tools for successful fish population recovery. For example, the removal of dams improved fish passages, created wetlands as more natural flow regimes were restored (e.g., seasonal flooding), and subsequently increased diversity of fish species (Iversen et al., 1993; Shuman, 1995; Bednarek, 2001). However, in most cases, habitat restoration and protection are challenging as they often require reconciliation with anthropogenic activities.

In Northern California, USA, the fresh water entering the Sacramento and San Joaquin River Delta (hereafter the Delta), upstream from the San Francisco Estuary (SFE), is mainly supplied by rainstorms in winter, snowmelt from the Sierra Nevada mountains in early summer, and water withheld in reservoirs from both these sources in late summer and fall, providing habitat for resident fishes (Fig 1A). Fresh water from the Delta is also exported to the Central Valley and Southern California to irrigate millions of hectares and for use by municipalities. The freshwater exports from the Delta affect the availability of freshwater habitats and influence the location of the low salinity mixing zone in the SFE in which saltwater and freshwater create brackish-water habitat (Moyle et al., 1992; Feyrer et al., 2011).

The population sizes of pelagic fish species relying on freshwater and brackish-water habitats in the SFE-Delta have been declining since at least 1980 (Finstad and Baxter, 2016). The causes of the fish population declines are still unknown because there are numerous ecological issues in the SFE-Delta, such as habitat destruction by levee construction, changes in physical water parameters due to the water exports, invasive organisms (e.g., clams), low phytoplankton

and zooplankton abundances, blooms of harmful algae, and contaminants released from urbanized areas and agricultural lands (Bennett, 2005; Feyrer et al., 2007; Thompson et al., 2007 and 2010; Hammock et al., 2019). It is plausible to think that a combination of these ecological issues is contributing to the decline of fish populations. Adding to these long-term changes was a severe drought from 2012-2015, which peaked in severity during 2014 and 2015. Precipitation was far below the average and air temperature was historically high, resulting in reduced freshwater inflow (i.e., precipitation/snow melt entering the SFE-Delta), saltwater intrusion, and elevated water temperatures in Northern California (Work et al., 2017; Lehman et al., 2020).

Reduced freshwater flow to the SFE may be one of the main factors that negatively affects fitness and performance of endemic fish species. Bennett (2005) discussed possible relationships between abundance of Delta Smelt and salinity in the Suisun Bay/Marsh (Fig 1B). Later, Jassby et al. (1995) and Feyrer et al. (2011) reported that the amount of freshwater inputs and location of the low salinity mixing zone influences the biotic resources for fishes, particularly the abundance and distribution of prey items such as copepods and mysids. In addition, Hammock et al. (2019) reported that water exports and the invasion of the clam *Potamocorbula amurensis* largely explain the current low concentrations of chlorophyll *a* in the SFE.

Delta Smelt (*Hypomesus transpacificus*) is endemic to the SFE-Delta and is federally listed as a threatened species (US Fish and Wildlife Service, 1993). It is an annual, multi-spawning fish species belonging to the family Osmeridae. Juvenile and sub-adult stage of fish can be found in summer and fall, respectively, and spawning occurs in spring (Bennett, 2005; Moyle et al., 2016). Delta Smelt has three major life-history phenotypes: freshwater resident, brackish-water resident, and semi-anadromous fish (Bush, 2017; Hobbs et al., 2019). The

relative abundance of each life history phenotype varied inter-annually with the migratory phenotype being most common in every year, but not always dominant, and the brackish-water resident the least common. In 2011, the majority of Delta Smelt (81%) were semi-anadromous, with fish rearing in the low salinity mixing zone (salinity 1 to 6), and migrating back to freshwater regions during spawning season (Hobbs et al., 2019). Delta Smelt are thought to initiate an annual spawning migration that appears to begin immediately following the 'first flush', the arrival of turbid water from land runoff mobilized by the first major winter rainstorm (Sommer et al., 2011; Bennett and Burau, 2015).

There are several papers regarding migration and distribution of Delta Smelt during the spawning season in the SFE-Delta. For example, Sommer et al. (2011) reported spawning migration of Delta Smelt to upstream regions such as the Cache Slough Complex with emphasis on migration rates and timing of maturation (Fig 1). Similarly, seasonal distribution patterns of Delta Smelt by life stage was thoroughly studied by Murphy and Hamilton (2013) and the authors reported that relative densities of Delta Smelt in Suisun Bay and the confluence region diminished while high densities were found in Montezuma and Cache Slough Complex during the spawning season. Bennett and Burau (2015) concluded that Delta Smelt exploit tidal action to migrate to upstream spawning habitat in the northern Delta (e.g., Cache Slough Complex). Furthermore, Hammock et al. (2017) studied the causes and consequences of migration from the viewpoint of foraging and food availability in the SFE-Delta, reporting increased stomach fullness in brackish-water regions during fall, winter, and spring compared to freshwater regions. However there still are unknowns, such as environmental factor(s) that affect regional to finer scale distribution and behavior of Delta Smelt during the spawning season. One possibility is turbidity as described previously by other researchers (Sommer et al., 2011; Bennett and Burau,

2015). Delta Smelt distributions are closely associated with turbid water so that turbidity is thought to be a cue for the migration of Delta Smelt (Feyrer et al., 2007; Nobriga et al., 2008; Sommer et al., 2011). In addition, it is unclear whether there are particular spawning grounds or Delta Smelt spawn at any locations where water quality parameters are suitable for mature fish.

Another unknown is whether a severe, recent drought in California from 2013-2015 impacted reproductive performance of Delta Smelt. Damon et al. (2016) predicated that Delta Smelt had lower annual fecundity (i.e., total number of eggs released per female per year) due to the shortened spawning window during the drought, however reproductive data at higher resolutions are still missing. In previous study, Feyrer et al. (2011) forecasted that reduced freshwater flow, particularly due to drought, can decrease the abundance of Delta Smelt via changes in the location of the low salinity mixing zone where the majority of semi-anadromous Delta Smelt occur as juveniles/sub-adults. Droughts associated with climate change are predicted to increase in frequency, duration, and intensity (Christensen et al., 2007; Trenberth et al., 2003). Given the relationships among freshwater flow, fish distribution, and habitat availability and accessibility, it is crucial to assess the impact of recent drought on Delta Smelt at the highest resolution.

In addition, elevated water temperature associated with the drought was another concern on the health of Delta Smelt (Damon et al., 2016; Jeffries et al., 2016; Davis et al., 2019). Fishes are ectotherms and many species, especially ones in temperate zone, evolved to cope with seasonal changes in water temperatures for their reproduction (Roy et al., 2018). Water temperature can affect various reproductive processes of fishes, such as gamete development and maturation (Pankhurst and Munday, 2011), therefore it was very likely that the elevated water temperature during the drought in California had effects on Delta Smelt reproduction.

Chapter 3: Reproductive Strategy of Delta Smelt *Hypomesus transpacificus* and Impacts of Drought on Reproductive Performance

The main objectives of this study are to improve understanding of the reproductive strategy of female Delta Smelt and to assess the impact of drought on their reproduction by investigating fish distribution and a suite of reproductive endpoints. We focused on female fish because their reproductive performance is more directly associated with recruitment success than males in fishes (Subbey et al., 2014). We formulated our hypotheses as follows: (1) female Delta Smelt migrate to particular locations for spawning so that mature female fish can be frequently found in particular locations throughout the spawning season and (2) reproductive performance of individual female fish declined during the drought.

To examine the hypotheses, we analyzed female Delta Smelt collected across the SFE-Delta via long term monitoring surveys conducted by the California Department of Fish and Wildlife (CDFW), collected from winter 2011 to spring 2015. To obtain high resolution sexual maturity data, ovaries of Delta Smelt were staged by histological examination (Kurobe et al., 2016). We first investigated relationships between water quality parameters (i.e., salinity, water temperature, and turbidity) and maturity of female Delta Smelt. We further examined the distribution of female Delta Smelt at each stage during the spawning season for each year. To assess the impact of drought on reproductive performance of female Delta Smelt, we compared reproductive metrics of mature fish at late vitellogenic stage: oocyte areas, clutch size, and gonadosomatic index, across four years representing a wide range in water year types. Together, the three reproductive metrics represent reproductive fitness of each individual, including egg quality (oocyte area), number of eggs that individual female fish produce per spawning event (clutch size), and the mass of ovary relative to body weight (gonadosomatic index). Finally, the timing of maturation between wet and dry/drought years was also compared among different year classes.

Materials and methods

Fish sampling

Delta Smelt were collected during a long-term survey conducted by the CDFW: Spring Kodiak Trawl for collecting adult fish (January through April or May) (Souza, 2002ab; Honey et al., 2004; Damon, 2015). In this study, only intact fish that were not dissected in the field were used for the analyses. The sampling stations for the Spring Kodiak Trawl are shown in Fig 1B. Female Delta Smelt collected from 2011 (n = 300), 2012 (n = 125), 2013 (n = 174), and 2014 year classes (n = 74) were used for the analyses. Year-classes were defined by hatch year. For example, fully matured fish in spring 2012 were considered the 2011 year class. Delta Smelt are generally annual fish and second year fish are rarely observed (Damon et al., 2016).

In the field, Delta Smelt were individually wrapped in aluminum foil with an identification number, and then flash-frozen in liquid nitrogen immediately after collection on sampling boats. Liquid nitrogen dewars containing fish samples were then brought back to the Aquatic Health Program, University of California, Davis, and Delta Smelt were stored in liquid nitrogen until dissection (Kurobe et al., 2016; Teh et al., 2016).

Fish dissection and calculation of somatic condition factor and gonadosomatic index

Individual Delta Smelt were removed from liquid nitrogen and fork length and body weight were measured while the fish were still frozen. The ovaries were excised once the fish were partly defrosted. The ovaries were weighed and partitioned into two portions by a scalpel;

one portion (~60%) was fixed in 10% phosphate-buffered formalin for histology and the remainder (~40%) was stored at −80°C for clutch size estimation. Somatic condition factor (K_s) and gonadosomatic index (GSI) were calculated by the formulas $K_s = (W_t - W_g) / L_f^3 \times 100$, where: W_t = total weight (g); W_g = gonadal weight (g); L_f: fork length (cm) and $GSI = (W_g / W_t) \times 100$ (Shankar et al., 2007; Kurobe et al., 2016).

Water quality parameters and hydrologic classification

Physical water quality parameters including water temperature, turbidity, conductivity, and Secchi depth were measured from the boats (Honey et al., 2004). The identification number on the aluminum foil was used to associate individuals with catch location, date, and water quality.

Hydrologic classifications of water years were obtained from the California Data Exchange Center, California Department of Water Resources (http://cdec.water.ca.gov/reportapp/javareports?name=WSIHIST). Based on the Sacramento Valley Index, 2011 was a wet year, followed by a below normal year (2012), a dry year (2013), and a critically dry year (2014).

Maturity of female Delta Smelt

Histological examination was used for staging maturity of female Delta Smelt based on physiological changes in ovaries (Kurobe et al., 2016). Briefly, ovaries fixed in 10% phosphate-buffered formalin were embedded in paraffin blocks and sectioned to a thickness of 3 μm using a microtome. Each section was mounted on a glass microscope slide and stained with hematoxylin and eosin solution (Kurobe et al., 2016; Teh et al., 2016). Based on the histological

characterization of ovaries (i.e., majority of the most advanced oocytes in ovaries), fish were categorized into six major stages: immature stage (Stage 1 and 2), cortical alveolus stage (Stage 3), vitellogenic stage (Stage 4), final maturation stage (hydration stage, Stage 5), and post-spawner (Stage 6) (Kurobe et al., 2016). Maturity at Stage 3 and 4 were further divided into three sub-stages (Early, Middle, and Late) based on the abundance of cortical alveoli in Stage 3 oocytes and egg yolk bodies in Stage 4 oocytes.

Area of oocytes measured by histology

The cross-sectional areas of oocytes (mm^2) were obtained using histological images of ovaries. The average oocyte size and standard deviation were obtained based on measurements from a minimum of 10 oocytes randomly selected from each ovary (Kurobe et al., 2016). Delta Smelt is a multiple spawner and immature oocytes can be found in their ovaries even during spawning season (Damon et al., 2016; Kurobe et al., 2016). Therefore, only oocytes at the most advanced stage within each ovary were used for measuring oocyte area. To ensure that oocytes sectioned roughly in half were measured, only the oocytes with a visible nucleus transection were chosen for measurement. ImageJ software ver. 1.8.0_112 was used for the image analysis (Schneider et al., 2012).

Clutch size

A portion of the ovary was used for estimating clutch size. Oocytes were dispersed and counted in 1× phosphate-buffered saline using a dissecting microscope, and clutch size (C) was calculated using this equation: $C = O \times (W_{intact} / W_{portion})$, where C is the clutch size, O is the

count of oocytes in the ovary, W_{intact} is the weight of the intact ovary, and $W_{portion}$ is the weight of the portion of the ovary used for counting oocytes.

Data analysis

Relationships between maturity of female Delta Smelt and water quality parameters

To investigate relationships between maturity of female Delta Smelt and water quality parameters (salinity, water temperature, and turbidity), boxplots were made using the water quality data at stations where female Delta Smelt were collected. Additional bar graphs were made to depict median absolute deviation of water quality parameters at each maturity stage.

Distribution pattern of female Delta Smelt during spring spawning season

To examine our first hypothesis (i.e., female Delta Smelt migrate to particular locations for spawning so that mature female fish can be frequently found in particular locations throughout the spawning season), we visualized spatiotemporal distribution patterns of female Delta Smelt in the 2011-2014 year classes at major maturity level. Fish catch data were visualized by bubble map charts using Microsoft® PowerPoint for Mac (ver. 16.16.17) with a base map downloaded from the United States Geological Survey website (https://www.usgs.gov/products/maps/overview).

In addition, historical data from the CDFW Spring Kodiak Trawl Survey were obtained from the CDFW website to assess spatiotemporal distribution patterns of female Delta Smelt for periods when the fish species was more abundant (CDFW Spring Kodiak Trawl: http://www.dfg.ca.gov/delta/projects.asp?ProjectID=SKT). Two objectives of the CDFW Spring Kodiak Trawl Survey are to determine the distribution and relative abundance of adult Delta

Smelt in the SFE-Delta and to monitor their gonadal maturation on a monthly basis to determine when and where spawning is likely to occur or is occurring (Damon, 2015). In the CDFW Spring Kodiak Trawl Survey, maturity of female Delta Smelt were classified into six stages by gross examination of their ovaries: developing stages (Stage 1 and 2), near-ripe (Stage 3), ripe (Stage 4), atretic (Stage 5), and post spawn (Stage 6) (Damon et al., 2016).

Comparison of female Delta Smelt maturity among the 2011-2014 year classes during the spawning season

Maturity of female fish were scored by histological examination as describe above (Section "Maturity of female Delta Smelt"). Stacked bar graphs showing the relative abundances of each maturity level were made using the R package ggplot2 ver. 3.2.1 (Wickham, 2016; R Core Team, 2020).

Comparison of reproductive performance of female Delta Smelt between wet and dry/drought years

To test our second hypothesis that reproductive performance of female Delta Smelt was lower during the dry and drought years, we performed one-way ANOVAs to compare area of oocytes, clutch size, gonadosomatic index, and somatic condition factor among 2011-2014 year classes (Wickham, 2016; R core team, 2020). ANOVA was chosen since the datasets are normally distributed (Shapiro-Wilk Test $P > 0.05$). Homogeneity of variance was assessed by Levine's Test. When necessary, the data were $\log_{10}$-transformed to meet the homogeneity of variance assumption. A *post-hoc* Tukey Test was performed when statistically significant differences were detected by ANOVA. The analyses were performed only for fish at Stage 4 Late since the fish at this stage have mature oocytes and are about to spawn, and therefore better represent reproductive performance of spawning females compared with earlier stages (Kurobe

et al., 2016). We did not include fish at Stage 5 because fish at this stage are rare (comprise <1% of adult female Delta Smelt in this study), and may have been actively spawning at capture, affecting clutch size and GSI.

We also analyzed dynamic changes of water temperature that a majority of Delta Smelt in the 2011-2014 year classes were likely experiencing in the wild (January 1st, 2011 through March 31st 2015). The water temperature data collected at time of capture, along with other water quality parameters were downloaded from the CDFW FTP server (ftp://ftp.wildlife.ca.gov/). Water quality data from three different surveys, 20mm Survey (March-July), Fall Midwater Trawl Survey (September-December), and Spring Kodiak Trawl Survey (January-April) were first pooled together (Honey et al., 2004), and then a subset of the data was prepared based on two criteria: regions and salinity range. Only the water temperature data in the four regions, (1) Suisun Marsh/Bay and Montezuma Slough, (2) Confluence of the Sacramento and San Joaquin rivers, (3) Sacramento River, and (4) Cache Slough Complex, were used for the analysis. Data from other regions such as San Joaquin River were not included, nor was data from high salinity stations (salinity >6.0).

Results

Water quality parameters and maturity of female Delta Smelt

The pooled data from the 2011-2014 year classes showed unique relationships between maturity of female Delta Smelt and water quality parameters. The median salinity values decreased as female Delta Smelt matured (Fig 2A). At the early cortical alveolus stages (Stage 3 Early and Middle, grouped), approximately 78% of fish were found at a wide range of salinities (salinity < 6.0). In contrast, Delta Smelt at Stage 3 Late and later stages were collected at lower

salinities as their maturity level advanced. Approximately 77% of fully matured fish (Stage 4 Late and 5) and post-spawners (Stage 6) were found in fresh water (salinity <0.5). The median values of water temperature and turbidity increased as fish reproductively matured, with the exception of the Stage 2 fish which occurred in relatively warmer water (Fig 2B&C). Fish at Stage 5 showed the highest median turbidity of 33 NTU (25 and 75 percentiles are 23 and 39 NTU, respectively).

The comparison of variabilities in salinity and turbidity across reproductive stages revealed a contrast; in salinity, the variabilities gradually decreased as Delta Smelt maturity level advanced while such clear trend was not observed in water temperature or turbidity (Fig 2E&F). We chose salinity for further investigation at a finer scale because salinity better explained the distribution pattern of mature Delta Smelt than water temperature or turbidity in our initial analysis (Fig 2).

Geographical distribution of female Delta Smelt during the spawning season

The data from the 2011 – 2014 year classes suggested that a majority of mature female Delta Smelt were found in freshwater habitat at salinities below 1.0 after spawning migration and there were some locations where mature fish were frequently found during the spawning season such as Cache Slough Complex and Suisun Marsh/Montezuma Slough, however there was plasticity in the distribution of Delta Smelt, as fish appeared to be widespread in the area where salinity was below 1.0 during the spawning season. In January 2014, sub-adult female Delta Smelt in the 2013 year class exhibited a wide geographical distribution ranging from a freshwater area (the Cache Slough Complex) to a brackish-water area (Suisun

Marsh/Montezuma Slough) where salinity was approximately 6.0 (Fig 3I). This pattern changed in March 2014 when most females were Stage 4; the majority of fish were found in the Cache Slough Complex and Suisun Marsh/Montezuma Slough and a few collected in the Sacramento River where the salinity was below 1.0 (Fig 3K). By the following month, fish were collected mostly in the Cache Slough Complex, with only a few fish found in other freshwater areas (Fig 3L). A similar progression of distribution was observed in the 2011 year class (Fig 3D), as well as historically, particularly in 2001 through 2003 year classes (S3 Fig). However, the historical data showed a much wider distribution in April and/or May throughout the SFE-Delta at salinities below 1.0. The data for the 2014 year class can be found in S2 Fig.

Comparison of female Delta Smelt maturity among the 2011-2014 year classes during the spawning season

A prominent difference is apparent between 2011 and other year-classes; female Delta Smelt in the 2013 and 2014 year classes matured earlier than in 2011 (Fig 4). In the 2013 and 2014 year classes, Delta Smelt at Stage 4 (Early, Middle, and Late) were dominant in February, accounting for over 90% of the females. In contrast, only 62% of the fish collected in February, 2011 were Stage 4.

We found over 15% of fish at Stage 3 Late in March and April in the 2012 year class (Fig 4B). Those fish were very likely to be post-spawners although there were no signs of spawning such as presence of post-ovulatory follicles in the histological sections. Stage 3 is characterized by the presence of cortical alveoli, which can be found in early winter. In addition, the mean fork length of the Stage 3 Late fish collected in March and April (77.0 mm) was significantly longer than the same stage of fish collected in January (67.7 mm) ($t_{[24]} = 4.79$, $P < 0.001$) and was

similar to the one at Stage 6 fish (post spawners, mean fork length: 76.1 mm) collected in March and April in the 2012 year class ($t_{[23]} = 0.42$, $P = 0.68$).

Comparison of oocyte areas, clutch size, gonadosomatic index, and somatic condition factor among 2011-2014 year classes

The comparison of oocyte areas revealed that the 2012 and 2013 year classes had significantly smaller oocytes than the 2011 year class at Stage 4 Late (Fig 5B; ANOVA, $F_{[3, 112]} = 10.4$, $P < 0.001$). Clutch size was lower in 2013 and 2014 year classes than 2011 year class, however the difference between 2011 and 2014 year classes was not significant (Fig 5C, ANOVA, $F_{[3, 144]} = 7.3$, $P < 0.0005$). A similar trend was observed in gonadosomatic index; the 2013 and 2014 year classes had significantly lower values of gonadosomatic index than the 2011 and 2012 year classes (Fig 5D, ANOVA, $F_{[3, 144]} = 7.2$, $P < 0.001$). In contrast, significant differences were not observed among the 2011 through 2014 year classes in somatic condition factor (Fig 5A, ANOVA, $F_{[3, 144]} = 1.5$, $P > 0.05$).

Discussion

Understanding the reproductive biology of imperiled fishes is one of the key elements in effective conservation and restoration of fish populations. Several previous studies reported migration, seasonal distribution patterns, and timing of spawning of Delta Smelt (Moyle et al., 1992; Bennett, 2005; Sommer et al., 2011; Bennett and Burau, 2015; Hobbs et al., 2019). However, field-based data for environmental factors that affect distribution of Delta Smelt during the spawning season at regional to finer scale levels is still limited. In addition, the exact

spawning ground of Delta Smelt is still unknown; it is unclear whether Delta Smelt spawn at any locations where water quality parameters are suitable for them or there are particular regions for their spawning. Furthermore, little is known about how drought condition affects the reproductive performance of Delta Smelt.

Migration of Delta Smelt to brackish-water regions at early life stages is believed to improve foraging success. Hammock et al. (2017) reported that Delta Smelt collected from the brackish-water area in fall through spring showed higher stomach fullness than those from the freshwater areas during the same period, while the opposite was true in summer. Data from other smelts also support the hypothesis that smelts migrate to brackish-water or saltwater environments for foraging and growth. For example, migratory populations of European Smelt (*Osmerus eperlanus*) were larger than those from non-migratory freshwater residential populations (Maitland and Lyle, 1996). Similarly, anadromous or migratory Wakasagi (*H. nipponensis*) were larger than freshwater populations (Katayama et al., 2001). These findings can explain the migration of Delta Smelt to brackish regions, however, it is still unclear why smelts migrate back to freshwater regions to spawn. Given that mature Delta Smelt (Stage 4 Late and 5) were predominantly found in freshwater regions, it is plausible to think that spawning in turbid freshwater environments is somehow beneficial. Hammock et al. (2017) discussed the possibility that Delta Smelt spawn in freshwater regions to provide hatchlings and young fish better access to high summertime densities of mesozooplankton species. In other anadromous fishes, spawning in freshwater environments is thought to reduce predation risks (Brönmark et al., 2013). Arctic Charr and Brown Trout showed five to eight times higher daily mortality rates at sea than freshwater environment (Jensen et al., 2019). Another possibility is that spawning in freshwater regions reduces salinity stress, which can affect fertilization, yolk sac sorption, early

embryogenesis, and larval growth (Bœuf and Payan, 2001, Fuda et al., 2007). For example, elevated salinity decreased growth rate of Chinook Salmon and Rainbow Trout at larval and juvenile stages (Enayatmehr and Jamili, 2013). In addition, turbid water in the freshwater environment due to winter rainstorms may be important for survival of early life stages of Delta Smelt. Hasenbein et al. (2016) reported that larval Delta Smelt showed better survival and higher feeding rates in moderate turbidities (25-80 Nephelometric Turbidity Units). To culture Delta Smelt, turbidity is increased in larval- and late larval-stage by addition of phytoplankton because Delta Smelt at these life stages fail to feed in clear water (Lindberg et al., 2013, Tigan et al., 2020). Turbidity may help reduce predation risk as well. For example, Humpback Chub (*Gila cypha*) cultured in turbid water significantly reduced predation by Rainbow Trout and Brown Trout when cultured in turbid water as low as 25 Formazin Nephelometric Units (Ward et al., 2016).

The environmental driver(s) that trigger the onset of migration of Delta Smelt are still unknown, however it's very likely that changes in physical and/or physicochemical parameters due to winter rainstorm events are associated (Sommer et al., 2011; Bennett and Burau, 2015). Given the data from our study showing that (1) median salinity values gradually decreased as fish matured, (2) matured female Delta Smelt at Stage 4 Late, 5 and 6 (post spawners) were predominantly found in areas where salinity was less than 0.5 with very low variability, and (3) such clear trends were not observed in water temperature or turbidity, salinity could better explain distribution of Delta Smelt (Fig 2). This suggests that Delta Smelt may use freshwater influxes or its correlates, possibly associated with winter rainstorms, as a cue for their spawning migration. Fresh water is not the immediate cue for the migration of the closely related species, Wakasagi, because spawning migration was observed even in an entirely freshwater

environment, from a lake to adjacent inflowing rivers (Okazaki et al., 2011). In Wakasagi, eggs were also found in sites at approximately 10 m depth, nearby underwater springs (Kiryu et al., 1978). Nevertheless, turbidity seems to be still critically important for survival of early life stages of Delta Smelt, especially for foraging success as described above.

Otolith geochemistry has shown that semi-anadromous Delta Smelt migrate to freshwater regions for spawning (e.g., Cache Slough Complex; Hobbs et al., 2019), however, spawning habitats and their distribution pattern after spawning migration, are still largely unknown. The data obtained in this study partly fill the knowledge gap. The distribution pattern observed in the 2013 and other year classes such as 2001-2003 cohorts suggests that spawning habitat is likely to occur where salinity is below 1.0 (Fig 3, S3 Figs). In April 2012 and March 2013, fully matured fish at Stage 5 as well as Stage 4 Late and 6 (post spawners) were found along the Sacramento River and sites near the confluence of the Sacramento and San Joaquin River (Fig 3). Stage 5 is characterized as the final maturation stage and hydration takes place in oocytes (Kurobe et al., 2016). Given that only a very small percentage of fish at Stage 5 were found in the four years of the study, retention time of the oocytes at Stage 5 is likely to be very short. The short retention time of hydration stage seems to be common in fishes. For example, in Anchovy and Sea Trout, the final maturation (hydration) and spawning can be completed within 24 hours (Hunter and Macewicz, 1985; Brown-Peterson et al., 1988). Although the exact retention time of Delta Smelt and other species in the family Osmeridae at Stage 5 is still unknown, Delta Smelt at the stage can be an indicator of spawning areas assuming the retention time is very short like other fish species. Given that the predicted upstream migration rates of Delta Smelt are 1.8-6.3 km per day (Sommer et al., 2011), it is unlikely that the Delta Smelt at Stage 5 found at the site near the confluence of the Sacrament and San Joaquin rivers in April 2012 swam over 38 km of the

distance and reached particular upstream freshwater locations such as Cache Slough Complex within the short retention time (Fig 3G).

The reproductive performance of fully matured Delta Smelt was relatively poor in the 2013 and 2014 year classes (which experienced dry and drought conditions) compared with the 2011 year class (which experienced a wet year) as indicated by smaller oocytes, lower clutch size, and lower gonadosomatic index (Fig 5). The cause of the poor reproductive performance in the 2013 and 2014 year classes is still unclear, however it could be influenced by poor food availability during the sub-adult stage. The low salinity mixing zone (salinity between 1.0-6.0) was located at the confluence of the rivers in October 2013 and 2014 (Fig 6C and D). In contrast, the low salinity mixing zone included the Suisun Marsh and Montezuma Slough in October 2011, the region that is relatively rich in tidal wetlands (Fig 6A; Hammock et al., 2019). Given that (1) the majority of Delta Smelt including both migratory and non-migratory populations (i.e., freshwater and brackish water residents) are distributed in regions where salinity is below 6 (Fig 2A; Hobbs et al., 2019) and (2) wetlands are associated with improved foraging success of Delta Smelt (Hammock et al., 2015 and 2019; Teh et al., 2020), Delta Smelt in 2011 year class might have been getting benefits from increased access to tidal marsh lands, both in the Suisun Marsh/Montezuma Slough and at the confluence of the rivers in fall 2011, while fish in the 2013 and 2014 year classes had access to only the wetlands at the at the confluence of the rivers (Bennett, 2005; Feyrer et al., 2007 and 2011).

Another possibility is that elevated water temperature during the dry and drought years lowered available surplus energy used for reproduction. Ectotherms dedicate more energy to respiration at warmer temperatures so that an increase in temperature results in higher metabolic rates, and subsequently an increase in the energy requirements (Ficke et al., 2007). This can

exacerbate nutritional stress in food limited aquatic ecosystems such as the SFE-Delta (Hammock et al., 2017). The mean water temperatures in the 2014 drought year was approximately 2.6ºC higher than 2011 throughout the year with maximum water temperature 23.1ºC recorded in July 2014 (S4 Fig). Previous studies reported that Delta Smelt exhibited sub-lethal physiological effects (increase in metabolic rates measured by changes in oxygen consumption) at 20ºC (Jeffries et al., 2016). Komoroske et al (2014) reported that critical thermal maximum, which is defined as the upper temperature at which fish lose the ability to escape conditions that will ultimately lead to death, of adult Delta Smelt was 27-28 ºC with continuous feeding. However, it is unknown how Delta Smelt would respond to sub-lethal but potentially stressful temperatures under food-limited conditions. Currently there are only a few publications reporting impacts of elevated water temperature and food limitation on fish reproduction. Donelson et al. (2010) reported that coral reef Damselfish (*Acanthochromis polyacanthus*) failed to reproduce when cultured at higher water temperatures with lower quantity food. In addition, the same authors reported that eggs produced were smaller at warmer water temperatures compared to those at the optimum temperatures. It is very likely that responses to the multiple stressors (i.e., warmer water temperature and food limitation) can vary among different fish species, therefore further analyses are warranted to better understand the impacts of elevated water temperature on metabolic demand and subsequently on growth and reproduction of Delta Smelt under food limited conditions. Whatever the cause of the poor reproductive indices during the drought, Delta Smelt reached historical lows as the drought peaked in 2015-16 (Teh et al., 2020; Malinich et al., 2020).

It is noteworthy that no difference was detected in somatic condition factor among the 2011-2014 year classes while significant differences were observed in the reproductive endpoints

(Fig 5). This can be explained by energy allocation over reproduction and somatic growth, more specifically, Delta Smelt may use energy preferentially for their somatic growth and survival, and then use 'surplus energy' for gonadal development. Strategies of energy allocation for reproduction can vary depending on fish species, however it can be largely classified into two types: 'capital breeders' and 'income breeders'. Capital breeders show cessation or reduction in feeding activity during spawning season and use stored energy for reproduction while income breeders continue feeding throughout the spawning season and use energy from food intake for their survival and reproduction (Silva et al. 2019). Sockeye Salmon (*Oncorhynchus nerka*) is a typical capital breeder and, ceases feeding during spawning season and uses reserved energy for reproduction. In contrast, income breeders prioritize their survival over spawning (Su et al., 2020). Income breeders are often observed in multiple spawners such as Medaka (*Oryzias latipes*) and Rare Minnow (*Gobiocypris rarus*). When mature Rare Minnow are starved, late maturing oocytes start to degrade and are absorbed by fish body (Su et al., 2020). Therefore food availability at adult stage is critically important for income breeders for their reproduction. Although Delta Smelt is a multiple spawner as indicated by the presence of immature oocytes in the gonad of fully mature females by histology, Delta Smelt could be a capital breeder since (1) reduction in feeding activity was observed prior to and during the spawning season in the wild and at a fish culture facility (Hung et al., 2014; Hammock et al., 2017) and (2) atrophic oocytes are rarely found in late maturing oocytes in wild fish by histology (Personal observation). Further investigation is needed since the reduction in feeding activity during the spawning season may be because of other causes such as food availability in the wild or abiotic factors such as lower water temperatures. However, if Delta Smelt is a capital breeder, accessibility to

abundant prey items during pre-spawning season at subadult stage (fall and early winter) would be critically important to increase 'surplus energy' which can be used for gonadal development.

Warmer water temperature during the drought might have affected timing of maturation. Delta Smelt in the 2013 and 2014 year classes matured earlier compared with the 2011 year class, with a prominent difference in February (Fig 4). A possible explanation of the earlier maturation during the drought is the warmer water temperature in January, when the fish in the 2013 and 2014 year classes experienced approximately 1.0ºC higher water temperature than the 2011 year class (S4 Fig). As Damon et al. (2016) reported previously, elevated water temperature expedited the spawning season (shifting it earlier). The early maturation may provide a longer spawning window which could result in higher spawning frequency assuming that energy is not limiting, however it is unlikely under the current food-limited conditions during the summer and fall (Slater and Baxter, 2014; Hammock et al., 2017).

Conclusions

In this study we report on (1) the distribution pattern of female Delta Smelt during the winter and spring spawning season and (2) the impacts of severe drought on their reproductive performance. Salinity seemed to better explain the distribution pattern of Delta Smelt at subadult and adult stages compared with water temperature or turbidity. Although there are some freshwater locations where mature Delta Smelt can be frequently found during the spawning season (e.g., Cache Slough Complex and Suisun Marsh/Montezuma Slough), Delta Smelt appeared to be widespread in the area where salinity is below 1.0 during the spawning season. Therefore, Delta Smelt could theoretically spawn in any freshwater location, with more specific spawning requirements (e.g., substrate type and depth) still unknown. Delta Smelt, which

experienced dry and drought conditions (2013 and 2014 year classes), had smaller oocytes and lower clutch size and gonadosomatic index than the fish caught in a wet year (2011 year class), suggesting reproductive performance was negatively affected by environmental conditions during the drought.

Acknowledgments

We are grateful to Ching Teh, Chris Perry and other members at the Aquatic Health Program, UC Davis, for dissecting and processing fish for obtaining the data used in this study. The authors also thank Nicholas Bertrand at the United States Bureau of Reclamation for reviewing the manuscript and staff members at the California Department of Fish and Wildlife for field sampling and for management of historical data. The views expressed are those of the authors and do not represent the official opinion of any employer, institution or government agency.

References

Bednarek AT. Undamming rivers: a review of the ecological impacts of dam removal. Environ Manage. 2001;27:803-814. doi: 10.1007/s002670010189.

Bennett WA. Critical assessment of the Delta Smelt population in the San Francisco Estuary, California. San Francisco Estuary and Watershed Science 2005;3(2). doi: 10.15447/sfews.2005v3iss2art1.

Bennett WA, Burau JR. Riders on the storm: selective tidal movements facilitate the spawning migration of threatened Delta Smelt in the San Francisco Estuary. Estuaries Coast. 2015;38:826-835. doi: 10.1007/s12237-014-9877-3.

Bœuf G, Payan P. How should salinity influence fish growth? Comp Biochem Physiol C. 2001;130:411-423.

Brönmark C, Hulthén K, Nilsson PA, Skov C, Hansson LA, Brodersen J, et al. There and back again: migration in freshwater fishes. Can J Zool. 2013;91:1–13. doi: 10.1139/cjz-2012-0277.

Brown-Peterson NJ, Thomas P, Arnold CR. Reproductive biology of the spotted seatrout, Cynoscion nebulous, in south Texas. US Fish Bull. 1988;86:373–388.

Burkhead NM. Extinction rates in Norther American freshwater fishes. BioSci. 2012;62:798-808.

Bush EE. Migratory life histories and early growth of the endangered estuarine Delta Smelt (Hypomesus transpacificus). M.Sci. Thesis, The University of California, Davis. 2017 Available from doi: 10.13140/RG.2.2.19204.42888.

Christensen JH, Hewitson B, Busuioc A, Chen A, Gao X, Held I, et al. Regional Climate Projections IPCC, 2007: Climate Change 2007: the physical science basis. contribution of Working Group I to the Fourth Assessment Report of the Intergovernmental Panel on Climate Change. Vol. 11. 2007, Cambridge University Press, Cambridge, U.K., pp. 847-940.

Damon L. 2014 Spring Kodiak Trawl Survey. IEP Newsletter. 2015;28(3):8-11.

Damon LJ, Slater SB, Baxter RD, Fujimura RW. Fecundity and reproductive potential of wild female delta smelt in the upper San Francisco Estuary, California. Calif Fish Game. 2016;102:188-210.

Davis BE, Cocherell DE, Sommer T, Baxter RD, Hung TC, Todgham AE, et al. Sensitivities of an endemic, endangered California smelt and two non-native fishes to serial increases in temperature and salinity: implications

for shifting community structure with climate change. Conserv Physiol. 2019;7:coy076. doi: 10.1093/conphys/coy076.

Donelson JM, Munday PL, McCormick MI, Pankhurst NW, Pankhurst PM. Effects of elevated water temperature and food availability on the reproductive performance of a coral reef fish. Mar Ecol Prog Ser. 2010;401:233-243.

Enayatmehr M, Jamili S. Effects of salinity on growth, hormonal and enzymatic status in fish: a review. Int J Sci Res. 2013;4:805-813.

Feyrer F, Newman K, Nobriga M, Sommer T. Modeling the effects of future outflow on the abiotic habitat of an imperiled estuarine fish. Estuaries Coast. 2011;34:120-128.

Feyrer F, Nobriga ML, Sommer TR. Multidecadal trends for three declining fish species: habitat patterns and mechanisms in the San Francisco Estuary, California, USA. Can J Fish Aquat Sci. 2007;64:723-734.

Ficke AD, Myrick CA, Hansen LJ. Potential impacts of global climate change on freshwater fisheries. Rev Fish Biol Fish. 2007;17:581–613. doi: 10.1007/s11160-007-9059-5.

Finstad S, Baxter RD. 2015 status and trends report for pelagic fishes of the upper San Francisco Estuary. IEP Newsletter. 2016;29:12-27.

Fuda KM, Smith BM, Lesser MP, Legare BJ, Breig HR, Stack RB, et al. The effects of environmental factors on rainbow smelt Osmerus mordax embryos and larvae. J Fish Biol. 2007;71:539–549.

Hammock BG, Hartman R, Slater SB, Hennesy A, Teh SJ. Tidal wetlands associated with foraging success of Delta Smelt. Estuaries Coast. 2019;42:857–867. doi: 10.1007/s12237-019-00521-5.

Hammock BG, Hobbs JA, Slater SB, Acuña S, Teh SJ. Contaminant and food limitation stress in an endangered estuarine fish. Sci Total Environ. 2015;532;316–326. doi: 10.1016/j.scitotenv.2015.06.018.

Hammock BG, Slater SB, Baxter RD, Fangue NA, Cocherell D, Hennessy A, et al. Foraging and metabolic consequences of semi-anadromy for an endangered estuarine fish. PLoS One. 2017;12: e0173497.

Hasenbein M, Fangue NA, Geist J, Komoroske LM, Truong J, McPherson R, et al. Assessments at multiple levels of biological organization allow for an integrative determination of physiological tolerances to turbidity in an endangered fish species. Conserv Physiol. 2016;4:cow004. doi: 10.1093/conphys/cow004.

Hobbs JA, Lewis LS, Willmes M, Denney C, Bush E. Complex life histories discovered in a critically endangered fish. Sci Rep. 2019;9:16772. doi: 10.1038/s41598-019-52273-8.

Honey K, Baxter R, Hymanson Z, Sommer T, Gingras M, Cadrett P. IEP long-term fish monitoring program element review: State of California, the Resources Agency, Department of Water Resources, Interagency Ecological Program. 2004.

Hung T, Eder KJ, Javidmehr A, Loge FJ. Decline in feeding activity of female cultured Delta Smelt prior to spawning, N Am J Aquac. 2014;76:159-163.

Hunter JR, Macewicz BJ. Measurement of spawning frequency in multiple spawning fishes. NOAA Tech Rep. 1985;36:79–94.

Hutchings JA, Reynolds JD. Marine fish population collapses: Consequences for recovery and extinction risk. BioSci. 2004;54:297-309.

Iversen TM, Kronvang B, Madsen BL, Markmann P, Nielsen MB. Re-establishment of Danish streams: Restoration and maintenance measures. Aquat Conserv. 1993;3:73–92.

Jassby AD, Kimmerer WJ, Monismith SG, Armor C, Cloern JE, Powell TM, et al. Isohaline position as a habitat indicator for estuarine populations. Ecol Appl. 1995;5:272-289.

Jeffries KM, Connon RE, Davis BE, Komoroske LM, Britton MT, Sommer T, et al. Effects of high temperatures on threatened estuarine fishes during periods of extreme drought. J Exp Biol. 2016;219:1705-1716. doi: 10.1242/jeb.134528.

Jensen AJ, Finstad B, Fiske P. The cost of anadromy: marine and freshwater mortality rates in anadromous Arctic char and brown trout in the Arctic region of Norway. Can J Fish Aquat Sci. 2019;76:2408–2417. doi: 10.1139/cjfas-2018-0428.

Kahle D, Wickham H. ggmap: Spatial Visualization with ggplot2. The R Journal, 5(1), 144-161. URL http://journal.r-project.org/archive/2013-1/kahle-wickham.pdf

Katayama S. Spawning grounds and reproductive traits of anadromous and resident pond smelt, Hypomesus nipponensis, in Lake Ogawara, Japan. Fish Sci. 2001;67:401-407.

Kiryu T, Haga M, Takahashi K. Investigation on spawning behavior of Wakasagi Hypomesus nipponensis in Lake Kawaguchi, Part I. Yamanashi Prefecture Aquaculture Research Center Technical Report. 1978;5:49-59. https://agriknowledge.affrc.go.jp/RN/2010844339.pdf

Komoroske LM, Connon RE, Lindberg J, Cheng BS, Castillo G, Hasenbein M, et al. Ontogeny influences sensitivity to climate change stressors in an endangered fish. Conserv Physiol. 2014;2:cou008. doi: 10.1093/conphys/cou008.

Kurobe T, Park MO, Javidmehr A, Teh FC, Acuña SC, Corbin CJ, et al. Assessing oocyte development and maturation in the threatened Delta Smelt, Hypomesus transpacificus. Environ Biol Fishes. 2016;99:423–432. doi: 10.1007/s10641-016-0483-z.

Lehman PW, Kurobe T, Teh SJ. Impact of extreme wet and dry years on the persistence of Microcystis harmful algal blooms in San Francisco Estuary. Quat Int. 2020. doi: 10.1016/j.quaint.2019.12.003.

Lindberg JC, Tigan G, Ellison L, Rettinghouse T, Nagel MM, Fisch KM. Aquaculture methods for a genetically managed population of endangered Delta Smelt. N Am J Aquac. 2013;75:186–196. doi: 10.1080/15222055.2012.751942.

Maitland P, Lyle A. The smelt Osmerus eperlanus in Scotland. Freshwat. 1996;6:57-68.

Malinich TD, White J, Campbell E, Graham C, Chorazyczewski A, Tempel T, et al. 2019 status and trends report for pelagic fishes of the upper San Francisco Estuary. IEP Newsletter. 2020;39(1).

Moyle PB, Herbold B, Stevens DE, Miller LW. Life history and status of Delta Smelt in the Sacramento-San Joaquin Estuary, California. Trans Am Fish Soc. 1992;121:67-77.

Moyle PB, Brown LR, Durand JR, Hobbs JA. Delta Smelt: Life history and decline of a once-abundant species in the San Francisco Estuary. San Francisco Estuary and Watershed Science. 2016;14:2. doi: 10.15447/sfews.2016v14iss2art6.

Murphy DD, Hamilton SA. Eastward migration or marshward dispersal: exercising survey data to elicit an understanding of seasonal movement of Delta Smelt. San Francisco Estuary and Watershed Science. 2013;11(3). doi: 10.15447/sfews.2013v11iss3art12.

Nobriga ML, Sommer TR, Feyrer F, Fleming K. Long-term trends in summertime habitat suitability for Delta Smelt (*Hypomesus transpacificus*). San Francisco Estuary and Watershed Science. 2008;6(1). doi: 10.15447/sfews.2008v6iss1art1.

Okazaki T, Miura M, Oohama H. Spawning behavior of Wakasagi in inflowing rivers of Lake Kawaguchiko. Report of Yamanashi Prefectural Fisheries Technology Center. 2011;35:44-59. https://www.pref.yamanashi.jp/suisan-gjt/documents/jiho38_p44-59.pdf

Pankhurst NW, Munday PL. Effects of climate change on fish reproduction and early life history stages. Mar Freshw Res. 2011;62,1015–1026.

R Core Team. R: A language and environment for statistical computing. R Foundation for Statistical Computing, Vienna, Austria. 2020 https://www.R-project.org/.

Roy K, Majumder S, Mandal DK. Seasonal variation on fish reproduction: A review. Int J Sci Res Rev. 2018;7:452-466.

Schneider CA, Rasband WS, Eliceiri KW. NIH Image to ImageJ: 25 years of image analysis. Nat Methods. 2012;9:671-675. doi: 10.1038/nmeth.2089.

Shankar DS, Sudarashan S, Kulkarni RS. Role of cortisol on condition factor in the female freshwater fish, Notopterus notopterus during four reproductive phases. J Environ Biol. 2007;28:275-8.

Shuman JR. Environmental considerations for assessing dam removal alternatives for river restoration. Regulated Rivers: Research and Management. 1995;11:249–261. doi: 10.1002/rrr.3450110302.

Silva JPC, Costa MR, Araújo FG. Energy acquisition and allocation to the gonadal development of Cynoscion leiachus (Perciformes, Sciaenidae) in a tropical Brazilian bay. Mar Biol Res. 2019;15:170-180. doi: 10.1080/17451000.2019.1610777.

Slater SB, Baxter RD. Diet, prey selection, and body condition of age-0 Delta Smelt, Hypomesus transpacificus, in the Upper San Francisco Estuary. San Francisco Estuary and Watershed Science, 2014;12(3).

Sommer T, Mejia F, Nobriga M, Feyrer F, Grimaldo L. The spawning migration of Delta Smelt in the upper San Francisco Estuary. San Francisco Estuary and Watershed Science. 2011; 9(2). doi: 10.15447/sfews.2014v9iss2art2.

Souza K. Townet Survey and Fall Midwater Trawl Survey. IEP Newsletter 2002a;15(2):21–24.

Souza K. Revision of California Department of Fish and Game's Spring Midwater Trawl and Results of the 2002 Spring Kodiak Trawl. IEP Newsletter. 2002b;15(3):44-47.

Su L, Luo S, Qiu N, Xiong X, Wang J. The reproductive strategy of the Rare Minnow (Gobiocypris rarus) in response to starvation stress. Zool Stud 2020;59:1. doi: 10.6620/ZS.2020.59-01.

Subbey S, Devine JA, Schaarschmidt U, Nash RDM. Modelling and forecasting stock – recruitment: current and future perspectives. ICES J Mar Sci. 2014;71;2307–2322. doi: 10.1093/icesjms/fsu148.

Teh SJ, Baxa DV, Hammock BG, Gandhi SA, Kurobe T. A novel and versatile flash-freezing approach for evaluating the health of Delta Smelt. Aquat Toxicol. 2016;170:152–161.

Teh SJ, Schultz AA, Duarte WR, Acuña S, Barnard DM, Baxter RD, et al. Histopathological assessment of seven year-classes of Delta Smelt. Sci Total Environ. 2020 Jul 15;726:138333. doi: 10.1016/j.scitotenv.2020.138333.

Thompson B, Adelsbach T, Brown C, Hunt J, Kuwabara J, Neale J, et al. Biological effects of anthropogenic contaminants in the San Francisco Estuary. Environ Res. 2007;105:156-174.

Thomson JR, Kimmerer WJ, Brown LR, Newman KB, MacNally R, Bennett WA, et al. Bayesian change point analysis of abundance trends for pelagic fishes in the upper San Francisco Estuary. Ecol Appl. 2010;20:1431-1448.

Tigan G, Mulvaney M, Ellison L, Schultz A, Hung T. Effects of light and turbidity on feeding, growth, and survival of larval Delta Smelt (*Hypomesus transpacificus*, Actinopterygii, Osmeridae). Hydrobiologia. 2020;847:2883–2894. doi: 10.1007/s10750-020-04280-4.

Trenberth KE, Dai A, Rasmussen RM, Parsons DB. The changing character of precipitation. Bull Am Meteorol Soc. 2003;84,1205-1217.

US Fish and Wildlife Service. Endangered and threatened wildlife and plants; determination of threatened status for the delta smelt. 1993;58:12854-12864.

Ward DL, Morton-Starner R, Vaage B. Effects of turbidity on predation vulnerability of juvenile humpback chub to rainbow trout and brown trout. J Fish Wildlife Manag. 2016;7, pp.205-212.

Wickham H. ggplot2: Elegant graphics for data analysis. Springer-Verlag New York. 2016 ISBN 978-3-319-24277-4, https://ggplot2.tidyverse.org.

Work PA, Downing-Kunz MA, Livsey D. Record-high specific conductance and water temperature in San Francisco Bay during water year 2015. U.S. Geological Survey Open-File Report 2017–1022, 4 p., doi: 10.3133/ofr20171022.

Supporting information

Please contact Tomo Kurobe for the supporting materials (tkurobe@ucdavis.edu)

S1 Fig. Turbidity at each reproductive stage of female Delta Smelt collected in the Fish Health Study, 2011 – 2014 year classes including extreme values observed (>150 NTU). Maturity of female fish was scored based on the gonadal histological features (Kurobe et al., 2016). The numbers above the top hinges indicate sample size for each reproductive stage.

S2 Fig. Maturity and distribution pattern of female Delta Smelt for the 2014 year class.

S3 Fig. Maturity and distribution pattern of female Delta Smelt for 2001-2010 year classes. The data were obtained from the California Department of Fish and Wildlife website (https://www.wildlife.ca.gov/Conservation/Delta/Spring-Kodiak-Trawl). The blue and red lines indicate salinity boundary for 1.0 and 6.0 ppt, respectively.

S4 Fig. Comparison of water temperatures that Delta Smelt (2011-2014 year classes) likely experienced in the wild, from spring for larvae (April-June), summer for juveniles (June-September), fall for subadults (September-December), and winter for adults (January-April). The water temperature data were obtained from the California Department of Fish and Wildlife FTP server (ftp://ftp.wildlife.ca.gov/; 20mm Survey, Fall Midwater Trawl Survey, and Spring Kodiak Trawl Survey). The August data are not available. Mean water temperatures of the four regions (Suisun Marsh and Montezuma Slough, Confluence of the Sacramento and San Joaquin rivers, Sacramento River, and Cache Slough Complex) are depicted for each month. Stations with salinity higher than 6 are not included. The error bars indicate standard deviation.

(A)

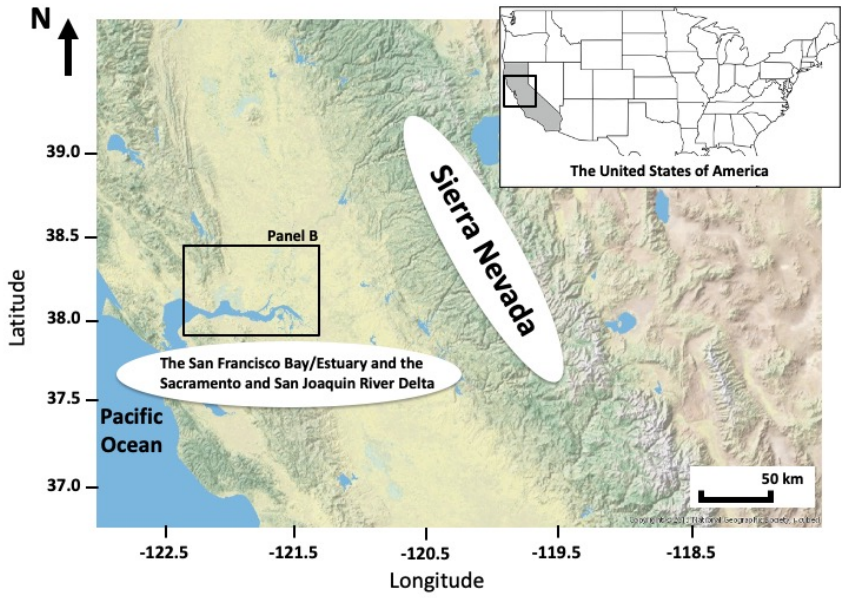
N
The United States of America
Sierra Nevada
Panel B
The San Francisco Bay/Estuary and the Sacramento and San Joaquin River Delta
Pacific Ocean
50 km
39.0
38.5
38.0
37.5
37.0
Latitude
-122.5
-121.5
-120.5
-119.5
-118.5
Longitude

(B)

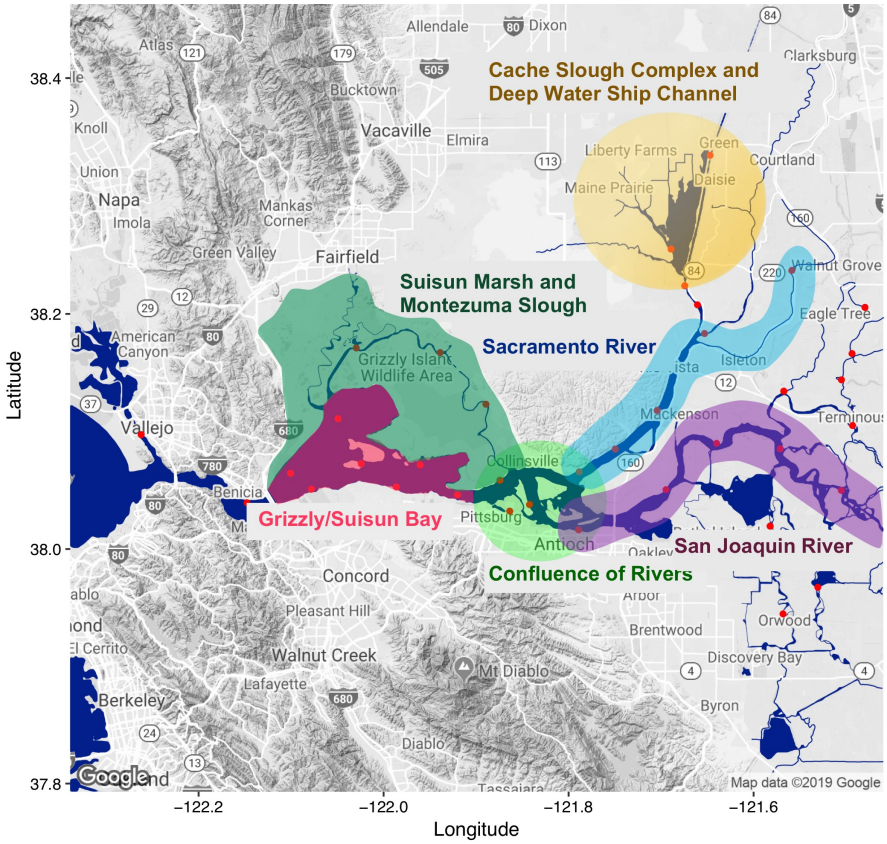
Cache Slough Complex and Deep Water Ship Channel
Suisun Marsh and Montezuma Slough
Sacramento River
Grizzly/Suisun Bay
San Joaquin River
Confluence of Rivers
Allendale
Dixon
Clarksburg
Bucktown
Vacaville
Elmira
Liberty Farms
Green
Courtland
Daisie
Maine Prairie
Napa
Imola
Mankas Corner
Green Valley
Fairfield
Walnut Grove
Eagle Tree
American Canyon
Grizzly Island Wildlife Area
Isleton
Vallejo
Collinsville
Benicia
Pittsburg
Antioch
Concord
Pleasant Hill
Brentwood
Walnut Creek
Mt Diablo
Discovery Bay
Lafayette
Berkeley
Byron
Diablo
Map data ©2019 Google
38.4
38.2
38.0
37.8
Latitude
−122.2
−122.0
−121.8
−121.6
Longitude

Fig 1. Map of Northern California, USA (Panel A) and the sampling stations for long term monitoring survey conducted by the California Department of Fish and Wildlife (Panel B). The sampling stations for the Spring Kodiak Trawl are depicted by red points in Panel B. The base map for Panel A was downloaded from the U.S. Geological Survey (https://viewer.nationalmap.gov/advanced-viewer/viewer/index.html?extent=-13809717.9302%2C4505236.7823%2C-13369746.3954%2C4697552.3454%2C102100). Panel B was created using the R package 'ggmap' using basemaps downloaded from Google LLC (Kahle and Wickham 2013).

A)

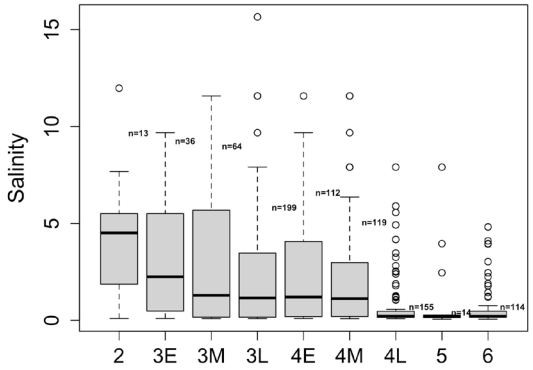
Salinity
0
5
10
15
n=13
n=36
n=64
n=199
n=112
n=119
n=155
n=14
n=114
2
3E
3M
3L
4E
4M
4L
5
6

B)

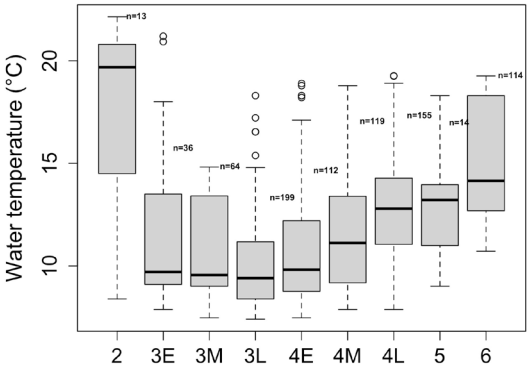
Water temperature (°C)
10
15
20
n=13
n=36
n=64
n=199
n=112
n=119
n=155
n=114
2
3E
3M
3L
4E
4M
4L
5
6

C)

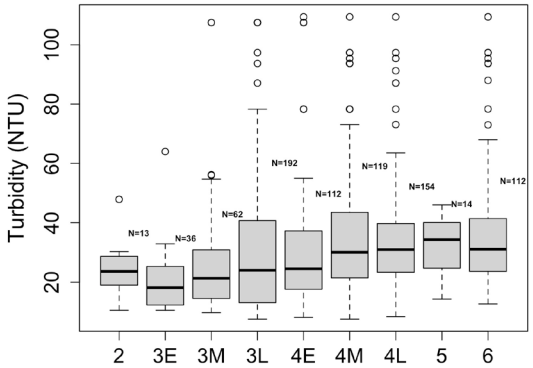
Turbidity (NTU)
20
40
60
80
100
N=13
N=36
N=62
N=192
N=112
N=119
N=154
N=14
N=112
2
3E
3M
3L
4E
4M
4L
5
6

D)

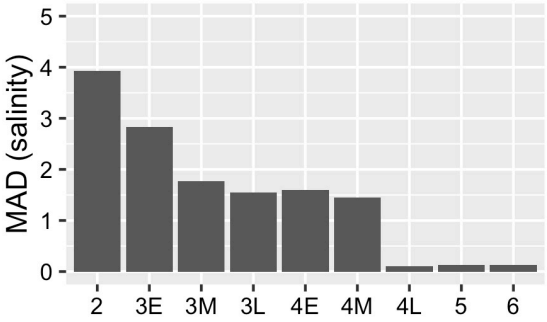
MAD (salinity)
0
1
2
3
4
5
2
3E
3M
3L
4E
4M
4L
5
6

E)

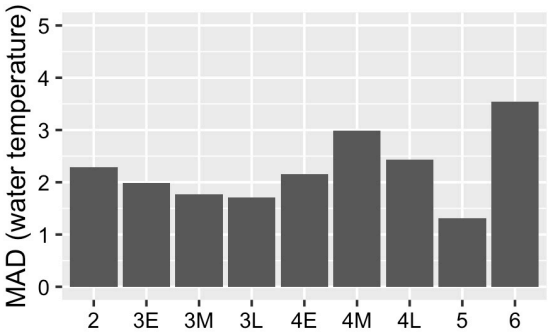
MAD (water temperature)
0
1
2
3
4
5
2
3E
3M
3L
4E
4M
4L
5
6

F)

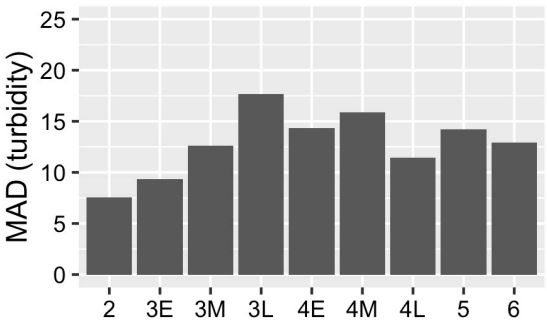

Fig 2. Summary of salinity (A), water temperature (B), and turbidity values (C) at each reproductive stage of female Delta Smelt, 2011 – 2014 year classes, and corresponding median absolute deviations (MAD) (D-F). Maturity of female fish was scored based on the gonadal histological features, Stage 1&2: immature stages, Stage 3: cortical alveolus stage, Stage 4: vitellogenic stage, Stage 5: final maturation stage (hydration), and Stage 6: post spawners (Kurobe et al. 2016). In the boxplots (Panels A-C), the numbers above the top hinges indicate sample size for each reproductive stage. For the ease of data presentation, fish with extreme turbidity values (>150 NTU) are not included in Panel C. The original figure including those fish with extreme turbidity values can be found in S1 Fig.

A) Jan 2012

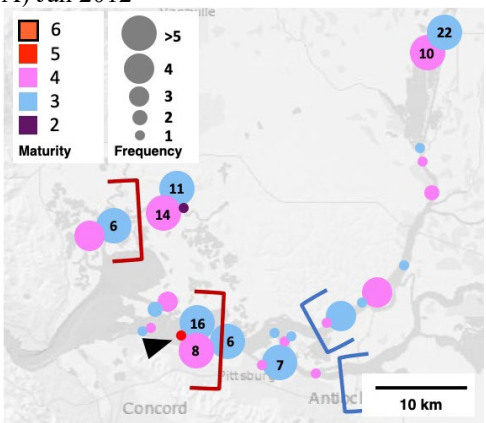

B) Feb 2012

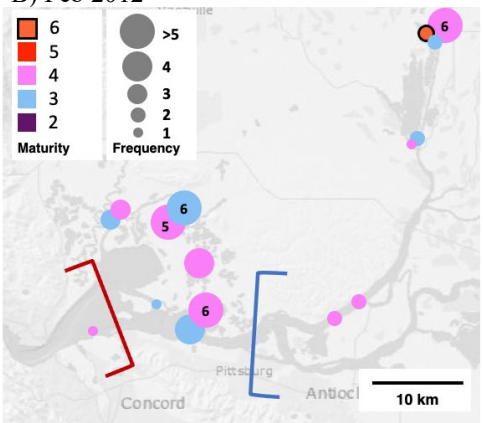

C) Mar 2012

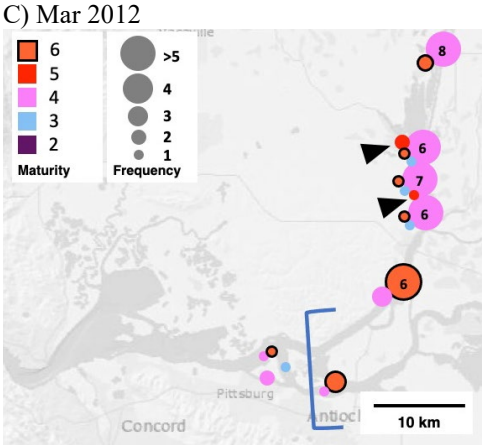

D) Apr 2012

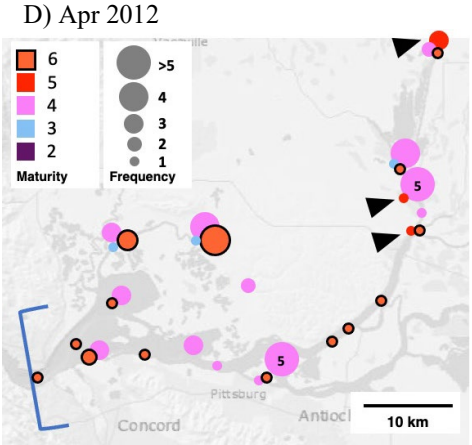

E) January 2013

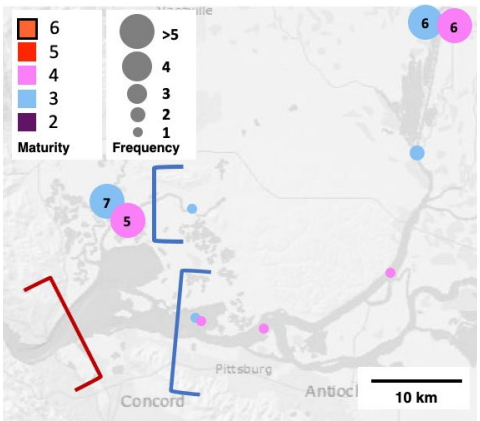

F) February 2013

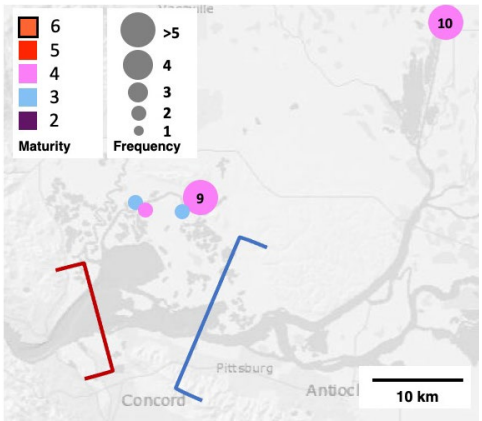

G) March 2013

H) April 2013

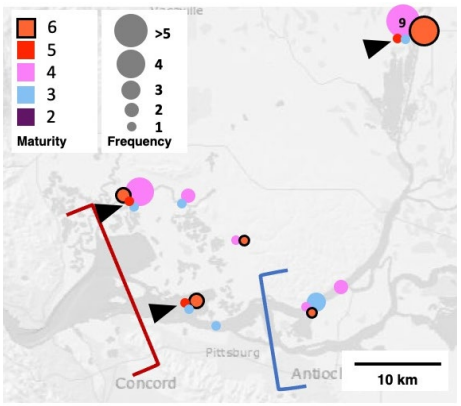

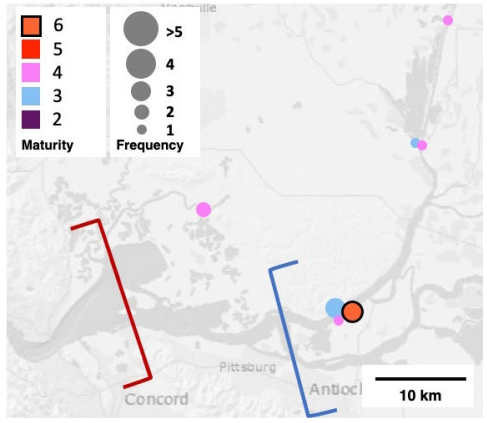

I) January 2014

J) February 2014

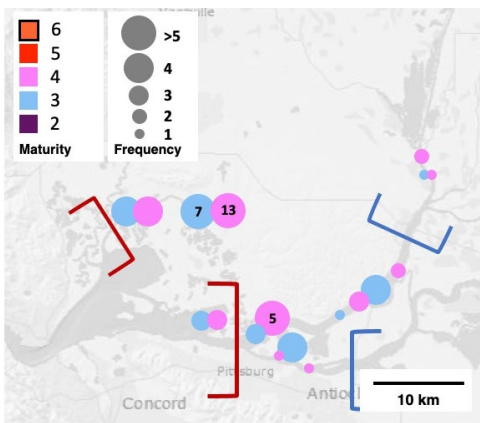

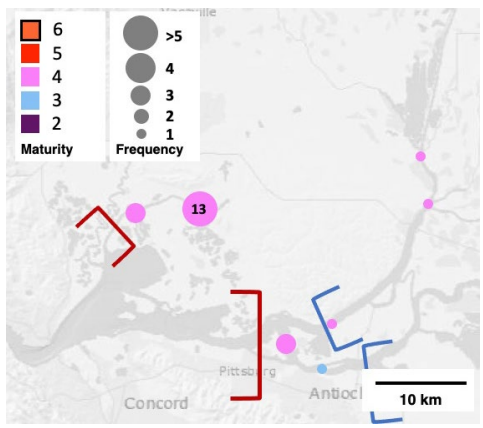

K) March 2014

L) April 2014

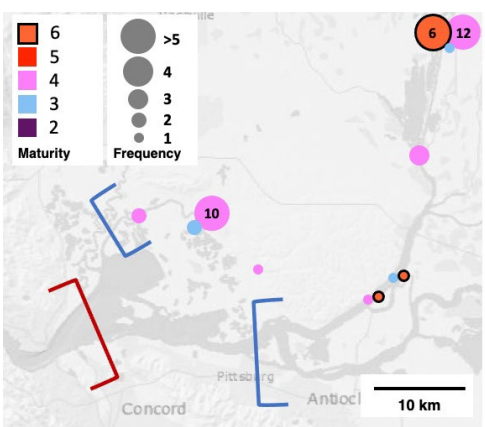

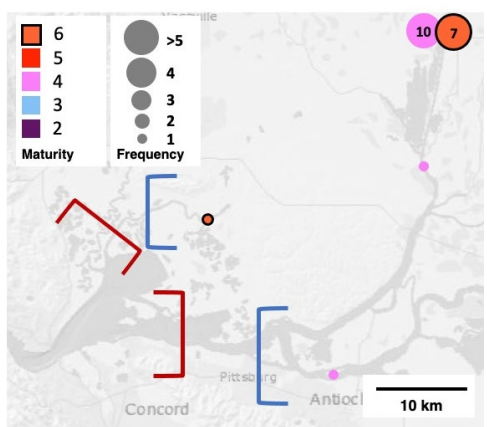

Fig 3. Maturity and distribution pattern of female Delta Smelt, 2011 (January-April 2012, Panels A-D), 2012 (January-April 2013, Panels E-H), and 2013 year classes (January-April 2014, Panels I-L). Fish at Stage 5

(hydration stage) are indicated by arrow heads. The blue and red brackets indicate salinity boundary for 1.0 and 6.0 ppt, respectively. The field sampling was not performed in the Grizzly/Suisun Bay in March 2012 (Panel C).

A) 2011 year class B) 2012 year class

C) 2013 year class D) 2014 year class

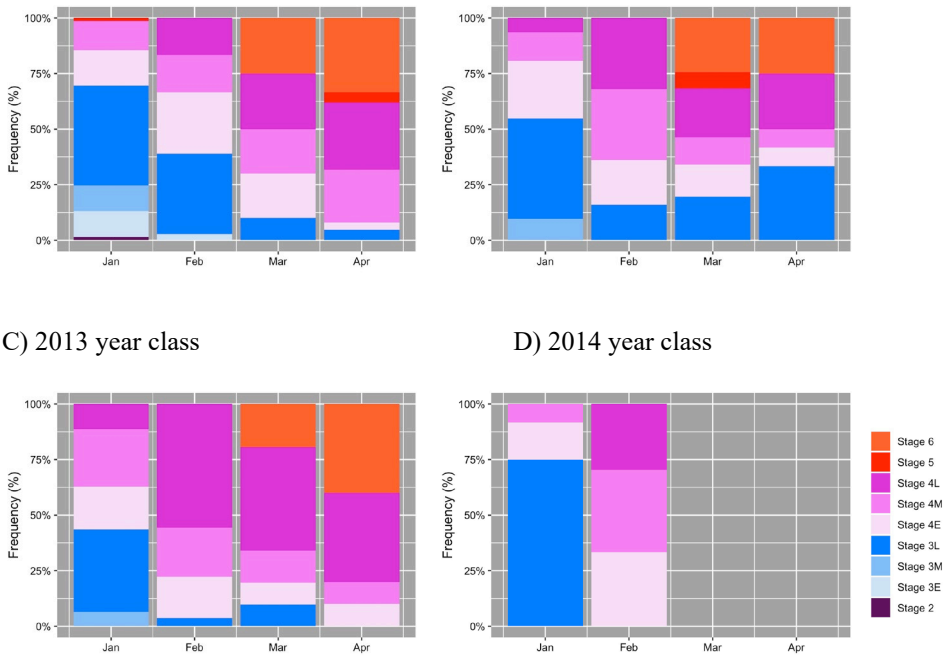

Fig 4. Monthly changes of female Delta Smelt maturity levels for 2011-2014 year classes (Panels A-D). Months with extremely low catches (n < 5) are not depicted in the figure (i.e., March and April in the 2014 year class; Panel D).

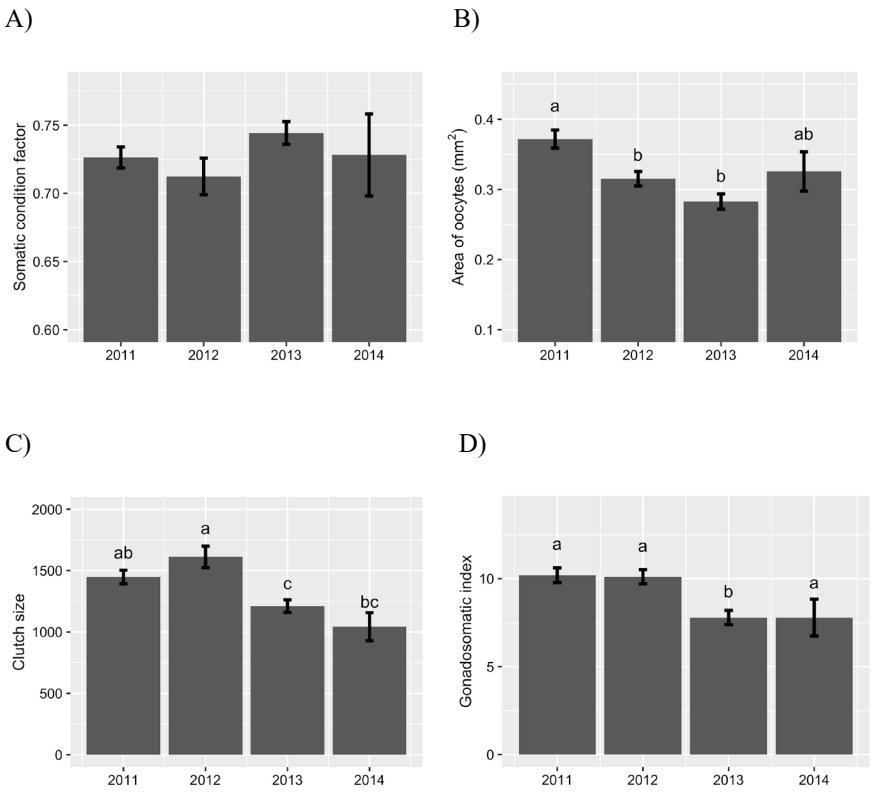

Fig 5. Comparison of somatic condition factor (A) and reproductive endpoints: area of oocytes (B), clutch size (C), and gonadosomatic index (D), among 2011–2014 year classes. Delta Smelt collected in a wet (2011 year class), normal (2012 year class), dry (2013 year class), and critically dry year (2014 year class), were used for the comparison. Only the fish at Stage 4 Late (late vitellogenic stage) were used for the comparison. Different letters indicate statistically significant differences between year classes. Error bars are ±SE.

A) 2011

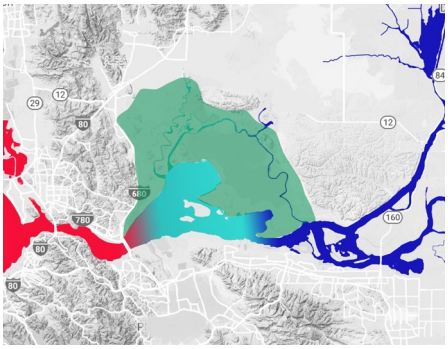

B) 2012

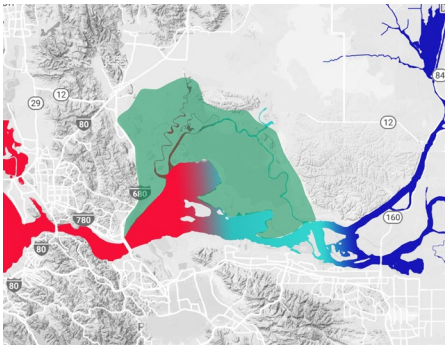

C) 2013

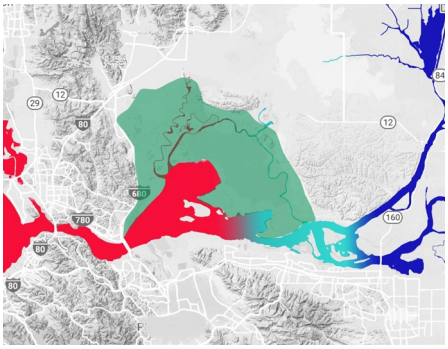

D) 2014

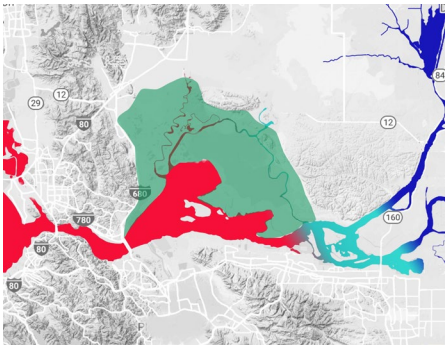

Fig 6. Comparison of area and location of the mixing zone (salinity 1.0-6.0 ppt) among 2011–2014 (A-D), October. The area with red, light blue, and dark blue color represent salinity >6.0, 1.0-6.0, and <1.0, respectively. The Suisun Marsh/Montezuma Slough area is indicated by green. The basemap was downloaded from Google LLC. Salinity data were obtained from the California Department of Fish and Wildlife FTP server (ftp://ftp.dfg.ca.gov/TownetFallMidwaterTrawl/).

Chapter 4: Otolith-Based Approaches Indicate Strong Effects of Environmental Variation on the Growth of a Critically Endangered Estuarine Fish

Submitted to *Marine Ecology Progress Series*

TITLE: Otolith-based approaches indicate strong effects of environmental variation on the growth of a critically endangered estuarine fish

AUTHORS

Levi S. Lewis[1*], Christian Denney[1], Malte Willmes[1,2], Wilson Xieu[1], Rachel Fichman[1], Feng Zhao[1], Bruce Hammock[3], Andrew A. Schultz[4], Nann Fangue[1], James A. Hobbs[1,5]

[1] Wildlife, Fish and Conservation Biology, University of California, Davis, 1 Shields Ave, Davis, CA 95616
[2] Institute of Marine Sciences/NOAA Fisheries Collaborative Program, University of California, Santa Cruz, 156 High Street, Santa Cruz, CA, 95064
[3] Cell Biology, School of Veterinary Medicine, University of California, 1089 Veterinary Medicine Drive, VetMed 3B, Davis, CA 95616, USA
[4] U.S. Bureau of Reclamation, Bay-Delta Office, Science Division, 801 I St., Suite 140, Sacramento, CA 95814
[5] California Department of Fish and Wildlife, 2109Arch Airport Road, Suite 100, Stockton, CA 95206, USA

*corresponding author: lewis.sci@gmail.com

Running page head: Environmental effects on Delta Smelt growth

ABSTRACT

In estuaries, fluctuating environmental conditions exact strenuous physiological demands on the fishes that call these oft-impacted habitats their home, including California's critically endangered Delta Smelt (*Hypomesus transpacificus*). Using an archive of otoliths spanning 2011-2019, we examined how growth rates of wild subadult Delta Smelt vary ontogenetically, regionally, and in relation to variation in the physical environment during late-summer and fall in the upper San Francisco Estuary. Recent growth rates were quantified using otolith increment analysis and modeled as functions of both intrinsic (age) and extrinsic (temperature, salinity, clarity, and region) factors using a suite of generalized additive models. Age explained 60% of the variation in $\log_{10}$-transformed growth rates, which peaked at 50-80 days post-hatch. Overall, age-adjusted growth rates declined at temperatures > 20 ºC, increased with practical salinity values of 0-4, and exhibited interactive patterns with water clarity. Growth rates appeared highest in the West and Central Delta, and lowest in the North Delta, also corresponding with patterns in environmental conditions. Here, we provide new evidence for how vital rates of wild Delta Smelt vary spatially and in relation to abiotic environmental variation. Such otolith-based growth reconstructions often provide the first direct look at how the vital rates of wild fish respond to environmental variation *in situ*, and how future changes are likely to affect the dynamics of wild populations.

Keywords: biological intercept, Delta Smelt, Generalized Additive Model, marginal increment, salinity, San Francisco, temperature, turbidity, water quality

INTRODUCTION

Intersections among structural and dynamic features in estuaries largely determine their suitability for the growth, survival, and production of estuarine fishes (Beck et al. 2001, Peterson 2003, Niklitschek & Secor 2009, Nagelkerken et al. 2015). Dynamic estuarine gradients in water quality (e.g., temperature, salinity, and clarity) vary in response to natural variation in climatic and oceanographic drivers that affect local patterns in precipitation, air temperature, wind, and upwelling. Anthropogenic changes to the climate and local hydrology of estuaries, however, can alter these gradients, thus impacting habitat suitability for estuarine species (Gillanders et al. 2011, Brown et al. 2013, 2016, James et al. 2013, Robins et al. 2016, Muhling et al. 2017). For example, temperature increases metabolic rates and subsequent growth rates (Jain & Farrell 2003, Green & Fisher 2004) until thermal limits are reached, after which, growth rate is suppressed (Houde 1989, Pörtner & Farrell 2008, Thresher et al. 2011, Wenger et al. 2016, Neubauer & Andersen 2019, Dahlke et al. 2020). Similarly, changes in salinity can influence metabolic demands, contingent upon the osmoregulatory physiology of a given species (Lankford & Targett 1994, Baltz et al. 1998, Labonne et al. 2009, Komoroske et al. 2016), and turbidity can enhance growth and survival by reducing predation risk and enhancing foraging success of larval fishes (Blaber & Blaber 1980, Cyrus & Blaber 1987, 1992, Rypel et al. 2007, Gregory 2011, Tigan et al. 2020). Suitable habitat, therefore, can become limiting when anthropogenic modifications uncouple key structural (e.g., habitat) and dynamic (e.g. water quality) features of estuaries that affect the growth, survival, and recruitment of fishes.

The Delta Smelt (*Hypomesus transpacificus*) is a pelagic osmerid fish that is endemic to the tidal fresh and low-salinity waters of the "upper" San Francisco Estuary (SFE), including open-water, slough, and wetland habitats of Suisun Bay and the Sacramento-San Joaquin Delta (Delta) (Moyle et al. 1992, 2016, Hobbs et al. 2019)(Fig. 1). Due to precipitous population declines since the 1980s (Mac Nally et al. 2010, Thomson et al. 2010, Hobbs et al. 2017), Delta Smelt are currently listed as threatened, endangered, and critically endangered according federal, state, and international conservation assessments, respectively (U.S. Fish and Wildlife Service 1993, CDFG 2010, NatureServe 2014). Multiple factors have likely contributed to this decline, including hydrologic alteration, habitat degradation, non-native competitor and predator species, agricultural and municipal pollution, climate change and direct mortality due to water exports (Knowles & Cayan 2002, Bennett 2005, Feyrer et al. 2007, Cloern & Jassby 2012, Fong et al. 2016, Moyle et al. 2016, 2018, Smith et al. 2020). Conservation efforts have occasionally impacted freshwater deliveries to California's multi-billion-dollar agriculture industry and 29 million southern residents, thus putting this endangered species in the political crossfire between advocates of species conservation versus those focused on water conveyance and agriculture (Feyrer et al. 2011, Moyle et al. 2018, Reis et al. 2019, Scoville 2019). In order to effectively manage the system for water conveyance while also protecting sensitive species such as Delta Smelt, an understanding of how species respond to natural and anthropogenic variation in environmental conditions is needed.

The responses of species to environmental variation (e.g., temperature, salinity, and clarity) are often assessed empirically using distribution models based on field survey data (e.g., occupancy modeling) or mechanistically using controlled laboratory studies. Based on field surveys, Delta Smelt are typically captured at temperatures < 25 ºC, practical salinities < 15, and clarity (Secchi depth) < 0.25 m (Bennett 2005, Feyrer et al. 2007, Nobriga et al. 2008, Komoroske et al. 2014). Similarly, acute critical thermal maxima of cultured Delta Smelt in laboratory experiments range from 24-30 ºC, depending on acclimation temperature and

ontogenetic stage (Komoroske et al. 2014), and sublethal physiological stress responses are can be elicited at temperatures as low as 23 ºC (Komoroske et al. 2015, 2016). For younger life stages, foraging activity and success in cultured Delta Smelt are generally maximized at low-light levels and higher turbidities of 18-80 NTU (Lindberg et al. 2013 20, Tigan et al. 2020). Foraging by older life stages, however, may be less sensitive to turbidity and even reduced at very high (e.g., > 80 NTU) turbidity values (Hasenbein et al. 2013, Hammock et al. 2019).

Though field-occupancy and laboratory studies of cultured fish are valuable and informative, it remains important to address likely limitations of these studies for understanding the responses of wild Delta Smelt to variation in the abiotic environment, *in situ*. In surveys, fish often occur in lower-quality habitats, especially if they cannot detect or move freely across suitability gradients or behaviors are modified due to physiological stress. Thus, empirical habitat suitability models based on occurrence may be insensitive to sublethal physiological effects of stressors on fish condition and population dynamics. Similarly, acute mechanistic thresholds established by short-term laboratory experiments using cultured fish may not account for the importance of chronic exposures to sublethal levels of stress, or complex interactions *in situ*, and thus may also mischaracterize the responses of wild populations to environmental patterns (Speers-Roesch & Norin 2016, Morgan et al. 2019). To address these limitations, studies examining the biological responses of wild specimens to variation in ambient environmental conditions are needed.

Growth is a key vital rate in the early life stages of fishes that integrates the physiological responses of fishes to environmental variation. For example, rapid growth corresponds with increased survival due to enhanced predator avoidance and prey capture and, given the high mortality rates experienced by early life-stages of fishes, small differences in growth and survival rates can lead to large variation in recruitment and year-class strength (Hjort 1914, Anderson 1988, Houde 1989, Cushing 1990). In annual fishes, such as Delta Smelt, growth rate in the first year also determines the size, fecundity, and reproductive condition of the spawning population, thus having strong effects on subsequent population dynamics (Rose et al. 2013b a). Growth rate, therefore, can be used as a biologically meaningful metric for assessing habitat suitability for wild specimens in their natural habitats. By understanding how environmental conditions influence the growth rates of wild fishes, we better understand how human activities are likely to impact their population dynamics.

A powerful tool for assessing the growth rates of wild fishes is otolith microstructural analysis (Pannella 1971). Otoliths ("ear stones") are bone-like structures found in the inner ear of fishes that are used for hearing and balance. They are formed by the accretion of calcium carbonate and proteins around a primordium, creating daily light and dark bands (increments) that can be used to estimate the age and reconstruct prior growth for early life stages of fishes. Since otolith accretion is often correlated with somatic growth (Campana & Jones 1992), the widths of daily increments can be used to reconstruct the growth history of individual fish. Such otolith-based approaches have been previously validated and applied to Delta Smelt to describe their life history and the timing of migrations (Hobbs et al. 2007, 2019)

To enhance our understanding of how wild Delta Smelt respond to natural and anthropogenic variation in their physical environment, we examined otolith-based growth rates among regions and as functions of water quality (salinity, temperature, and clarity) in the upper SFE. We then contrasted patterns in the vital rates of the wild population with existing hypotheses based on occupancy and laboratory studies which indicate upper water temperature thresholds of 24-25 ºC due to thermal stress (Feyrer et al. 2007, Komoroske et al. 2015), optimal

growth conditions at practical salinities of 1-4 where osmoregulatory stress is limited and foraging is enhanced (Komoroske et al. 2016, Hammock et al. 2017), and varying effects of water clarity (Hasenbein et al. 2013, Tigan et al. 2020). By contrasting the responses of wild individuals with predictions based on previous models, we aimed to verify or modify our current understanding of habitat suitability, population dynamics, and the most promising options for conserving this critically endangered species.

MATERIALS AND METHODS

Study Site

The SFE is the largest coastal estuary on the California coast, characterized by an "upper estuary" which receives the majority of freshwater inputs from the Sacramento River and San Joaquin River watersheds that each flow into the North and South Delta, respectively (Fig. 1). The two rivers meet at their confluence in the Central Delta and are tidally mixed downstream into the more brackish waters of the West Delta, and eventually out into the saltier bays of the lower estuary. The estuary is a "radically transformed" ecosystem serving 7.5 million local residents, a large commercial shipping industry, several coastal fisheries, and the final destination of 50 municipal sewage treatment plants (Cloern & Jassby 2012). Over 95% of its tidal marsh habitats have been degraded and its hydrograph has been highly altered. Over 100% of the mean annual rainfall can be captured behind major dams that exist on most tributaries, and over 30% of the freshwater flowing into the estuary is diverted annually by state and federal pumping facilities to support agricultural and municipal needs in the southern part of the state, thus impacting the many species that live within or migrate through the upper estuary. To monitor the ecological effects of these anthropogenic alterations, several long-term state and federal monitoring programs have been established, each yielding detailed records of fish abundances, environmental conditions, and historical archives of specimens that can be analyzed by researchers to better inform management and policy decisions (Supplement 1).

Environmental conditions in the SFE are highly dynamic. In general, the estuary exhibits a salinity gradient from freshwater upstream habitats in the North and South Delta to low-salinity (e.g., practical salinities of 1-10) brackish habitats in the West Delta, with variable conditions in between in the Central Delta. Interannual variation in precipitation and freshwater runoff, however, is high, varying form 7.6 km^3 (1977) to 65 km^3 (1983). Therefore, freshwater inflow and spatial salinity gradients vary seasonally, marked primarily by wet winters and dry summers (Cloern & Jassby 2012). Similarly, water temperatures and clarity vary spatially and seasonally, with temperatures varying by more than 20 ºC and water clarity varying from cm to several meters in Secchi Depth. Native species, such as Delta Smelt, have evolved to cope with these dynamic physical attributes; however, anthropogenic alterations to the hydrograph and local climate are increasingly compressing the quality and quantity of habitats available to native species (Cloern et al. 2011). For example, as the estuary continues to warm, thermal stress is likely to increasingly impact the population dynamics of sensitive species (Brown et al. 2016). Reductions in freshwater outflow due to diversions, combined with sea level rise due to climate change, are likely to push salinity gradients further inland, reducing the amount of low-salinity habitat, and further exacerbating warming trends (Nobriga et al. 2008, Feyrer et al. 2011, Brown et al. 2016). Continuing increases in water clarity due to sediment capture by dams and expanding aquatic vegetation, as well as changes in weather patterns, are also likely to impact

turbidity-seeking species such as Delta Smelt (Hestir et al. 2016, Bever et al. 2018). Improved understandings of relationships between species and environmental conditions can yield better predictions about the likely impacts of future environmental change, as well as the responses of species to specific water management and conservation actions.

Sample Collection and Processing

We used a long-term archive of wild Delta Smelt otoliths to explore variation in growth rate in relation to the region and environmental conditions at capture. Wild Delta Smelt of 51.2 ± 6.8 mm (mean ± s.d.) fork length were collected throughout their range during August-November of 2011-2019 (Fig. 1, Table 1) by several long-term monitoring programs and special studies conducted by the California Department of Fish and Wildlife (CDFW) and US Fish and Wildlife Service (Supplement 1, Table S1). This time period and life stage were selected because they represent a critical period in the life cycle of this fish, when environmental variation is likely to influence vital rates such as individual growth, fecundity, and subsequent population growth (Rose et al. 2013b), and when management actions (e.g., flow augmentation) have been focused to improve environmental conditions to help restore the Delta Smelt population. During surveys, each fish was generally given a unique serial number upon capture, its fork-length measured to the nearest 1 mm, and its body preserved in either 95% ethanol or liquid nitrogen. If a field fork-length could not be identified, it was estimated using standard conversion equations for ethanol or liquid nitrogen-preserved specimens (Supplement 1).

Water quality parameters, including temperature (°C), practical salinity (calculated from specific conductance in µS/m), and Secchi depth (m) were measured during each collection event using standard practices. Temperature and specific conductance were measured by each survey using boat-deployed sondes (e.g., YSI Pro30 by YSI Inc. or a CTD by Sea-Bird Scientific), and salinity was calculated from specific conductance using standard equations for low (0-2) and high (2-42) practical salinity values (Lewis & Perkin 1981, Hill et al. 1986). Water transparency (clarity, in cm) was measured using a standard 20 cm Secchi disk. Measurements at capture were assumed to represent an approximation of the recent local environmental conditions experienced by each fish. Due to the rarity of this critically endangered fish and the fact that samples were archived across multiple independent surveys, archived specimens were often distributed unevenly in space and time, thus limiting our ability to account for fine-scale variation among years, months, and regions (Table 1, Supplement 2). However, specimens were collected across broad regions and gradients in environmental conditions, providing an opportunity to examine how vital rates, such as growth, vary regionally and in relation to the physical environment (Table 1).

Otolith Preparation

Otolith preparation and analysis followed standard protocols previously described for Delta Smelt (Hobbs et al. 2007, 2019). Sagittal otoliths (Fig. 2a) were dissected from fish and stored dry in tissue culture trays or in 95% ethanol in 1 ml polypropylene tubes. Before mounting, dry otoliths were soaked in 95% ethanol for up to 24 hours, and adherent tissue was removed from all otoliths. Otoliths were then air dried and mounted onto glass slides with Crystal Bond® thermoplastic resin in the sagittal plane. Each otolith was sanded to the core on both sides with 1,200 grit wet-dry sandpaper and polished with 0.3-µm alumina on a polishing

wheel (MTI Corp). Otoliths were imaged at 200x magnification using a 10-Megapixel AM Scope digital microscope camera attached to an Olympus CH30 compound microscope. Multiple images of each otolith were merged into a single composite image using Adobe Photoshop (ver. 21.1.1) and an aging transect was drawn from the core to the dorsal edge at approximately 90° to the rostral-postrostral axis of the otolith (Fig. 2a-b).

Analysis of Otolith Microstructures

Daily increments were annotated along the dorsal lobe (core to edge) of each composite otolith image using Image-J 4.0 (United States National Institutes of Health; https://imagej.nih.gov/ij/) (Fig. 2b). The total number of increments represented each specimen age (in days) and increment widths, converted from pixels to microns using a stage micrometer, represented the daily otolith growth rate (in µm/day). Prior to analysis, image quality at the dorsal edge of each otolith (Fig. 2c) was scored from 1 to 3, with 1 being highest quality, and images with the lowest-quality edges (3) were excluded from analysis. Multiple increment profiles were generated for each otolith by two or more independent analysts, and the inter-operator precision was evaluated for each sample using the average coefficient of variation (ACV) (Welch et al. 1993, Herbst & Marsden 2011). If consensus (ACV < 10%) was not achieved for all age readings, the estimate furthest from the mean was discarded and ACV was recalculated until consensus was achieved among a minimum of 2 reads, or the sample was excluded from analysis. ACV was evaluated similarly for edge distance of the last 14 days of growth. Following all QAQC procedures, the final dataset included otoliths from a total of 459 Delta Smelt (Table 1, Supplement 1).

Growth Rate

Recent growth rate was quantified for each specimen using the widths of the last 14 daily increments accreted prior to capture. The 14-day interval was chosen as a compromise to maximize both the precision of growth estimates and their temporal proximity to environmental measurements (Fig. S2) (Baltz et al. 1998). Daily otolith growth rates (µm/d) were converted into somatic growth rates (mm/d) using the Biological Intercept Model (BIM, eqn. 1)

$$L_a = L_c + (O_a - O_c)(L_c - L_i)(O_c - O_i)^{-1} \quad (1)$$

where L_a is the back-calculated length of the fish at age a, O_a is the otolith size at age a, L_c and O_c are the size of the fish and otolith at capture, respectively, and L_i and O_i are the size of the fish and otolith at the biological intercept, respectively (Campana 1990, Campana & Jones 1992, Hobbs et al. 2007). This method assumes consistent proportionality in the otolith-somatic size relationship over the size range of fish examined, which has been confirmed for Delta Smelt in contemporary validation studies (Xieu et al. *in prep*). Recent growth rate (G) of a given fish was calculated as the $\log_{10}$-transformed mean somatic growth rate:

$$G = \log_{10}\left(\frac{1}{n}\sum_i^n y_i\right) \quad (2)$$

where y_i is the somatic growth rate (mm/d) for day i and n is the number of days included in the growth interval (n = 14). The $\log_{10}$ transformation was used to meet model assumptions. Adjusted growth rates (G_a) were estimated using the residuals of the intrinsic model (see Statistical Analyses).

Statistical Analyses

We used generalized additive models (GAMs) to quantify how Delta Smelt growth rates varied in relation to intrinsic and extrinsic factors. GAMs were preferred over linear models because they are more flexible for describing complex non-linear relationships between response and predictor variables (Wood 2017). Intrinsic factors included prior growth and daily age, which accounted for inherent individual and ontogenetic variation in growth rates. Extrinsic factors included region, year, temperature, salinity, and clarity; together, representing many of the spatial, temporal, and environmental factors over which growth rates are likely to vary. Water quality attributes were transformed to limit leverage and improve model performance, and correlations among each transformed metric were examined to assess collinearity among predictors. Density plots of water quality attributes were used to identify and exclude outlying values that were too sparse to yield confident predictions.

All GAMs were constructed using a Gaussian distribution, identity link function, thin-plate regression spline, and restricted maximum likelihood (REML) to estimate smooth parameters in the mgcv package (Wood 2017) in R version 3.6.3. Model complexity was limited to a basis dimension of $k = 4$ for main effects or $k = 3$ for interactions to limit over-smoothing and maintain generalizability (Grimaldo et al. 2017). Interactive effects of environmental conditions on growth rates were modeled using tensor product smooths (ti in mgcv). Growth responses were examined by plotting partial residual smooths for each of the variables in the model (2-D plots) and their interactions (3-D plots), and model assumptions were assessed using the gam.check and concurvity functions in mgcv.

Intrinsic Models

Growth rates were first modeled as individual and combined functions of two intrinsic factors, age-at-capture (hereon "age") and prior (larval) growth rate (0-30 dph), that often explain significant variation in the growth rates of young fishes (Hinrichsen et al. 2010, Schismenou et al. 2014, 2016). For example, intrinsic models account for the inherent dependence structure of otolith increments with age (ontogenetic effect) and previous growth rates (e.g., individual variation or increment autocorrelation) (Morrongiello & Thresher 2015, Barrow et al. 2018). Adjusted growth rate (G_a) for each fish was calculated as the residual variation in growth after accounting for the selected intrinsic model (Shima & Swearer 2019).

Extrinsic Growth Models

Several extrinsic models were constructed to examine how growth rates (G_a) of Delta Smelt vary as functions of the individual and interactive effects of ambient physical environmental conditions (i.e., water temperature, salinity, and clarity), aggregated regions (West Delta-WD, Central Delta-CD, North Delta-ND, and South Delta-SD, see Table 1) and among years (2011-2019). First, a series of hierarchical "environment-only" models were constructed, which included temperature, salinity, and clarity as fixed additive and interactive smooth factors, with parameters selected using a maximum likelihood (method = 'ml') estimator. Models were compared using the dredge function from the MuMIn package in R (Bartoń 2019), with model criteria (estimated degrees of freedom-EDF, coefficient of determination-R^2, and corrected Akaike Information Criterion-AIC_c) used to select the preferred model that was logical, parsimonious, and provided a relatively good fit to the data (Pedersen et al. 2019). These

environment-only models were constructed under the simplifying assumption that any variation observed in growth rate was related to variation in the observed physical environmental conditions, independent of other spatiotemporal variation (e.g., years and regions) or environmental conditions (e.g., prey abundance, toxins, etc.) that could influence growth.

Other unmeasured environmental conditions (e.g., prey abundance, etc.), however, may have also varied in time and space and influenced the observed growth patterns. To assess potential spatial variation in growth rates, we constructed a generalized additive mixed effects model (GAMM), the "global-regional model," which included strata that were aggregated into regions as parametric fixed effects, year as a random smooth effect (bs = "re"), as well as the main effects of temperature, salinity, and clarity, each modeled as a fixed smooth effect. By including region as a fixed effect and year as a random effect in this, we aimed to test for evidence of significant spatial variation in growth while controlling for the main fixed effects of environmental conditions and random interannual variation (Pedersen et al. 2019). Since regions exhibited evidence of different growth responses given global environmental smooths, but also varied greatly in the ranges of each environmental metric (especially salinity, see Results), as well as variation in the respective years with available Delta Smelt specimens, growth rate was also modeled separately for each region as a function of the environmental variables and random effect of year, the "region-specific models," thus allowing us to assess region-specific responses in G_a to environmental conditions, without assuming global smooth functions or equivalent ranges for each environmental metric (as in previous models).

RESULTS

Intrinsic Growth Model

Intrinsic models varied in complexity with 1-7 estimated degrees of freedom (Fig. 3A), explaining 20-60% of the variation in growth. Age alone ($\chi^2 = 442.3$, df = 3.03, $p < 0.001$) explained greater than 60% ($R^2 = 0.61$) of the variation in log-transformed Delta Smelt growth rates (G). Prior growth ($R^2 = 0.18$) and its additive ($R^2 = 0.63$) and interactive ($R^2 = 0.64$) effects with age contributed little to the fit of intrinsic growth models (Fig. 3B), indicating that marginal growth rates were largely independent of early growth history. Though additive and interactive intrinsic models explained 2-3% more variance than age alone, the complexity (EDF) of these models was considerably higher, resulting in similar AIC values (Fig. 3C); therefore, the age intrinsic model was selected as the most parsimonious model for describing intrinsic drivers of Delta Smelt growth rates (Fig. 3D-F).

Environmental Attributes

Archived wild Delta Smelt specimens used in this study were collected across broad ranges of environmental conditions that varied in both space and time (Fig. 4). Water temperatures ranged from 12.5-23.9, practical salinity ranged from 0.06-6.38, and clarity ranged from 0.16-0.67 m Secchi depth. Since distributions of temperature and salinity were left- and right- skewed, respectively, each was transformed (temperature-cubic, salinity-log) to improve model performance and reduce leverage of clustered values. Transformed water quality metrics

associated with Delta Smelt collections were largely uncorrelated, thus allowing us to examine the individual and combined effects of each metric (Fig. 4d-f, Table 2).

Extrinsic Growth Models: 'Environment-Only' Model

Extrinsic abiotic habitat attributes (temperature, salinity, clarity) in the environment-only models explained up to 20% of the variance in adjusted growth rates (Fig. 5, Fig. S2 in Supplement 3). Though models including the three-way interaction resulted in a lower AIC_c and higher R^2, the limited sample size and dispersion across all three dimensions, and high (> 0.9) concurvity for many terms suggested this model was likely over-fit. Therefore, we selected the tsc interactive model with each of the two-way interactions (tsc*, Model 18), which was similar in all evaluation criteria to Models 12 and 15, yet allowed for visualization of interactive effects on growth for each pair of predictor variables (Fig. 5, Table 3). The tsc* model explained 16% of the variance in G_a and was significantly different from the null model ($\chi^2 = 281.8$, df = 14.13, $p < 0.001$, Table 3). Overall, G_a declined with increasing temperatures above approximately 20 ºC, ($p < 0.001$, Fig. 5D), increased with practical salinity values of 0.1-6 ($p = 0.007$, Fig. 5E), and exhibited a non-significant decreasing trend with water clarity ($p = 0.217$, Fig. 5F, Table 3). A significant temperature-clarity interaction ($p = 0.005$, Table 3) indicated that growth rates were highest in turbid-cool, clear-cool, and even turbid-warm conditions, but lowest in clear-warm environments (Fig. 5G). Other interactions were not significant ($p > 0.05$).

Extrinsic Growth Models: 'Global-Regional' Model

Qualitative exploration of spatial and temporal variation in growth indicated that, overall, growth appeared to vary more within years and regions than among years and regions, though some trends were worth noting (Table 1, Fig. S1 in Supplement 2). Annual patterns in growth indicated a potential decline in growth rates during warm drought conditions from 2013-2016, and recovery following several wet years in 2017-2019. In 2012, growth was generally higher in the western portion of the Delta Smelt range (i.e., Lower Sacramento River and Suisun Bay/Marsh) than in the North Delta. In Suisun Bay/Marsh and the Lower Sacramento River, growth was higher in 2012 vs. 2017. There were a few fish collected from the Upper Sacramento River in 2015 (during the warmest drought period), many of which exhibited low growth rates. Conversely, a few fish were collected in the Far Western region in 2011, many of which exhibited high growth rates.

The "global-regional" model (Fig. 6, Table 4), which accounted for environmental, interannual, and spatial effects, accounted for 30.0% of the variance in G_a ($\chi^2 = 168.0$, df = 15.4, $p < 0.001$, Table 4) and indicated a significant positive effect of salinity on Delta Smelt growth ($p = 0.049$, Fig. 6C), whereas the effects of temperature, salinity, and region did not contribute significantly to the model ($p > 0.05$). In contrast, removing the random year term from the model resulted in model that explained 12% of the variance in G_a ($\chi^2 = 59.5$, df = 7.2, $p < 0.001$, Table 4) and included significant region and temperature effects (Fig. 6E,F). For this model, Delta Smelt captured in the West Delta and Central Delta exhibited higher growth rates than those captured in the North Delta ($p = 0.001$, Fig. 6A) and reduced growth at higher temperatures. The contrasting results of these two models (with and without the random year term) indicated a significant negative effect of temperature that partially co-varied among years, as well as a positive effect of salinity that largely co-varied among regions (Fig. S1 in Supplement 2).

Extrinsic Growth Models: 'Region-specific' Models

As demonstrated previously, G_a of Delta Smelt varied among regions when also incorporating global environmental smooths and random year effects across the full dataset (Fig. 6, Table 4). The subset of years and ranges of environmental conditions corresponding with the sample set, however, also varied among regions (Table 1, Fig. S1 in Supplement 2). For example, Delta Smelt were not captured in all regions in all years (Table 1), thus the number of years with specimens for each region were 8, 9, and 5 for ND, CD, and WD, respectively. Furthermore, the ranges of each environmental metric from which Delta Smelt were captured also varied among regions; most notably practical salinity, where Delta Smelt from the ND were mostly captured in waters at values < 0.5 and the CD at values < 4, whereas fish from the WD were captured in the full range of salinities in the dataset, from values of 0.1-6.4 (Fig. S1G in Supplement 2). Temperatures were generally warmer for fishes captured in the ND and clarity was generally higher in the CD; however, the ranges of these metrics exhibited more overlap among regions than salinity (Fig, S1F,H in Supplement 2).

Due to the potential effects of this region-specific variation, we fit separate region-specific GAMs that examined G_a as a function of the additive smooth effects of the physical environmental attributes (temperature, salinity, and clarity), and the random effect of year (2011-2019), thus allowing us to assess region-specific and year-independent responses of G_a to environmental variation without assuming global smooth functions or similar ranges for each environmental attribute across regions. Models for all three regions were significantly different from the null ($p < 0.001$) and accounted for 20-45% of the variance in growth (G_a) (Table 5). In the Central Delta, G_a declined significantly at temperatures above 20 ºC (Fig. 7D) and increased linearly with increasing salinity values from 0.1-6 (Fig. 7E), while exhibiting no significant effects of clarity (Fig 7C). In contrast to the Central Delta, the North and West Delta exhibited only significant interannual variation in growth, with no significant effects of the environmental metrics (Fig. 7A-C).

DISCUSSION

Growth is a key vital rate of fishes. It can, therefore, serve as an integrated proxy for the effects of environmental variation on both individual fitness and subsequent population dynamics (Hjort 1914, Houde 1989, 2008, Rose et al. 2013a). In Delta Smelt, poor growth likely leads to higher mortality rates, delayed maturity, reduced size at maturity, fewer batches of eggs, and reduced total fecundity and population growth (Bennett 2005, Rose et al. 2013b a, Damon et al. 2016). Here, we utilized a long-term archive of wild Delta Smelt otoliths to assess how growth rates of this critically endangered fish vary ontogenetically and in relation to *in situ* environmental conditions experienced at capture. Results from the environment-only model indicated that temperature, salinity, and clarity each can explain a significant fraction of the age-independent variation in growth rates. Growth rate declined rapidly as temperatures exceeded 20 ºC, increased linearly with practical salinity values of 0.1-4, and exhibited a complex temperature-dependent response to clarity (at Secchi depths of 0.2-0.7 m). Results of a spatially explicit global model indicated that growth rates were highest in the West Delta and lowest in the North Delta, while region-specific models indicated distinct patterns among regions in growth-environment relationships.

These results suggest that the vital rates of wild Delta Smelt may be suppressed at even lower temperatures than previously described (Feyrer et al. 2007, Nobriga et al. 2008, Komoroske et al. 2014, 2015, Brown et al. 2016, Jeffries et al. 2016), and that increasing water clarity (Hestir et al. 2016, Bever et al. 2018) is likely to further exacerbate the negative effects of current and future warming on the wild population. All individuals were captured at suitable, non-stressful salinities (Hasenbein et al. 2013, Komoroske et al. 2016), thus the general increase in growth rates in downstream, low-salinity brackish habitats support a biological-trophic mechanism, such as enhanced foraging success (Hammock et al. 2015, 2017, 2019), for downstream migration. Such otolith-based growth reconstructions can provide a first direct look at how the vital rates of wild populations of fishes respond to environmental variation, and how future changes, natural or anthropogenic, are likely to affect population dynamics.

Intrinsic Effects

We first assessed and controlled for a dominant intrinsic ontogenetic pattern in growth rate, which is a critical initial step in assessing variation in daily growth rates of young fishes (Weisberg et al. 2010, Morrongiello et al. 2015, Barrow et al. 2018, Shima & Swearer 2019). Using a 2-step modelling approach (Morrongiello & Thresher 2015, Shima & Swearer 2019), we were able to partition the variance between intrinsic ontogenetic and extrinsic abiotic environmental and regional factors to assess relationships between environmental conditions and age-independent growth rates of wild Delta Smelt. Approximately 60% of the variation in growth rates was explained by age, alone, with growth rates ranging from 0.1-0.6 mm/d, decreasing rapidly with daily age from 50 to 200 dph. Inclusion of prior growth rates did not improve the intrinsic growth models, suggesting that the age-specific pattern in growth was largely independent of an individual's prior growth history. Though age-specific growth rates are often correlated with an individual's prior growth history (e.g., for inherently fast and slow growing fish), variation in daily growth can exhibit little correlation with prior growth if separated by longer time intervals (Hinrichsen et al. 2010, Schismenou et al. 2014, 2016), likely explaining why the 14-d recent growth interval did not exhibit autocorrelation with prior larval growth.

Extrinsic Effects: Temperature

Otolith-based reconstructions of growth rates for wild Delta Smelt indicated that growth declined rapidly as temperatures increased to over 20 °C (Fig. 5D), especially in the Lower Sacramento River (Fig. 7D). In ectothermic fishes, growth rate is typically strongly and positively correlated with water temperature due to the kinetic effects of temperature on metabolism. Both growth and metabolism increase with temperature until a maximum growth rate is reached, after which, growth rate is suppressed due to thermal stress or metabolic imbalance between energy expense and consumption (Brett & Groves 1979, Pörtner & Peck 2010, Schismenou et al. 2016).

We did not observe a positive response in growth as temperature increased from 13-20 °C. Instead, growth rate remained relatively high and stable up until approximately 20 °C, after which, growth declined rapidly with increasing temperature. These results suggest that wild adult Delta Smelt may grow best in cooler waters and exhibit suppressed growth at temperatures above 20 °C, either due to physiological limits or other interacting environmental conditions. This

observed decline in growth may indicate that wild Delta Smelt are chronically stressed throughout much of the upper SFE during the warmest summer-fall conditions, especially in the Lower Sacramento River. For example, rapid warming of the upper SFE during the 2014-2015 drought likely reduced growth rates, survival, and shortened the maturation window of Delta Smelt, possibly explaining the low abundances observed during these warmer years.

Delta Smelt have been captured in trawl surveys at temperatures as high as 27 °C in the summer, however most subadult fish are observed at temperatures below 22-24 °C (Bennett 2005, Komoroske et al. 2014). Such catch data, combined with environmental covariates, have been used to describe habitat suitability for Delta Smelt, suggesting that temperatures below 24-25 °C are generally suitable (Feyrer et al. 2007). Nobriga et al. (2008), however, indicated that temperature during summer was "the poorest predictor of Delta Smelt distribution" in the wild, though this was due in part to the limited, high temperature ranges (mostly > º20 C) observed in July and a likely non-linear decline in predicted capture probabilities at approximately 25 °C that was not captured well by the model. Though informative, such habitat suitability models based on occupancy may not reflect the population-level effects of exposure to specific environmental conditions (Neubauer & Andersen 2019). For example, the presence of fish in waters with temperatures above 25 °C does not indicate that conditions are favorable, as it is possible that such fish were trapped in unsuitable conditions that negatively impacted their growth, survival, and future reproductive output. Physiological impairment could decrease swimming activity or net avoidance, thus making fish easier to capture in more stressful conditions. Thus, high catches in suboptimal conditions could obscure important patterns in physiological condition. To complement inferences from occupancy models, additional studies are needed to describe the physiological limits most likely to influence population dynamics.

Laboratory studies using cultured fish have examined a variety of behavioral and metabolic responses to acute lethal and sublethal levels of thermal stress. Such experiments have demonstrated a critical thermal maximum (CT_{max}) of 25-30 °C for cultured Delta Smelt (Swanson et al. 2000, Komoroske et al. 2014). In contrast, sublethal responses in behavior and gene expression have been consistently observed at temperatures of 23-25 °C (Komoroske et al. 2015, Jeffries et al. 2016, 2018). The results of these laboratory studies corroborated prior field occupancy models, each suggesting that physiological limits constrain optimal Delta Smelt habitat to < 25°C in the wild (Feyrer et al. 2007, Nobriga et al. 2008), with adults being more sensitive than juvenile life stages (Komoroske et al. 2014). As observed in field studies (Bennett 2005), nearly all Delta Smelt included in our study were observed at < 22°C , which is slightly cooler than the sublethal thresholds (23-25 ºC) identified in laboratory experiments using cultured fish.

Though growth rates began to decline at just 20 ºC in the environment-only model (Fig. 5D), fish captured in waters > 22°C exhibited the greatest reductions in growth, and the thermal inflection in the Central Delta region-specific model suggested a slightly higher threshold (e.g., 21 ºC, Fig. 7D). Though few laboratory studies have examined physiological thermal thresholds below 20 ºC, an increase in disease (ich) susceptibility in a laboratory setting was observed at 18 ºC relative to fish reared at 16 ºC (Frank et al. 2017), and growth rates of cultured fish were highest at 20 ºC, with lower growth rates at both lower (16 ºC) and higher (23 ºC) temperatures. These results suggest that a lower thermal threshold for growth may be linked to mechanisms other than commonly measured physiological traits. In sum, our results using otolith-based growth rates of wild fish corroborate previous laboratory and field occupancy studies, each indicating that Delta Smelt commonly experience stressful thermal conditions in situ that are

likely to impact fitness and population dynamics. Our results also suggest that growth rates of wild Delta Smelt may be suppressed at temperatures below commonly used thresholds established using field occupancy models and physiology experiments with cultured specimens.

Extrinsic Effects: Salinity

Delta Smelt are euryhaline, and thus can tolerate short-term exposures to the full range of salinities from 0-32 ppt, and exhibit little evidence of physiological stress at practical salinity values < 15 (Swanson et al. 2000, Nobriga et al. 2008, Hasenbein et al. 2013, Komoroske et al. 2016, Hammock et al. 2017). At practical salinities > 15, however, Delta Smelt exhibit significant molecular and physiological impairment, suggesting that prolonged exposure at higher salinities would be energetically detrimental, likely leading to reduced growth rates and other measures of fitness (Hasenbein et al. 2013, Komoroske et al. 2016). This likely limits the range of Delta Smelt to lower salinities of the upper estuary. In the wild, however, relatively few wild fish are ever observed at practical salinities > 6, suggesting that Delta Smelt avoid even lower salinities than those predicted by laboratory studies examining physiological responses to salinity (Kimmerer 2002, Bennett 2005, Komoroske et al. 2016).

In our study, all specimens were captured at practical salinities of 0.1-6.5 (Fig. S1 in Supplement 2). This range lies well-within the "suitable" range for Delta Smelt described above. Growth rates in the environment-only model exhibited a positive, significant relationship with salinity (Fig. 5D). This result corroborated prior studies indicating that foraging success in downstream low-salinity brackish habitats is higher than in upstream freshwater habitats (Hammock et al. 2017). Together, these results indicate that enhanced foraging by Delta Smelt in low-salinity brackish habitats also confers a measurable and significant increase in individual growth rates. This joint variation in feeding and growth may therefore be a mechanism selecting for the downstream migration of many juvenile-subadult Delta Smelt from fresh to low-salinity brackish habitats (Hammock et al. 2017, Hobbs et al. 2019). Similarly, by including region as a parametric fixed term in the global-regional model, results indicated that growth was highest in the West and Central Delta and lowest in the North Delta (Fig. 6A), also suggesting that growth rates of Delta Smelt are maximized further downstream, where higher foraging success is correlated with low-salinity brackish habitats (Hammock et al. 2017, 2019). Since salinity varied strongly with region (Fig. S1 in Supplement 2), however, a significant salinity effect was not detected in the global-regional model.

In contrast to the positive salinity-growth relationship in the environment-only model, region-specific models indicated different salinity effects (Fig. 7, Table 5). In the North Delta, growth rates were generally low and practical salinity values only varied from 0.1-0.5, thus no region-specific effects of salinity were observed (Fig. 7a). In addition to higher foraging success downstream, there is also evidence that higher exposure to contaminants in upstream habitats may also result in poorer fitness (Hammock et al. 2015). In the Central Delta, where most fish were sampled, growth rate exhibited similar patterns as the environment-only model, increasing with practical salinity values of 0.1 to 4 (Fig. 7b). In the West Delta, however, where salinity was highest and most variable, growth rates did not vary significantly with environmental conditions (Fig. 7c), possibly due to the lower sample size and the presence of most fish in downstream habitats only in high-flow years (year effects). It is also possible that finer-scale interactions with other habitat features (e.g., tidal marshes) that influence foraging and growth (Hammock et al. 2019) could complicate such analyses. Future observational and experimental studies examining

differences in growth rates among habitat types within the West Delta are needed to shed further light on such habitat-environment interactions.

Extrinsic Effects: Clarity

Turbid conditions can enhance growth and survival of fishes by reducing predation risk and enhancing foraging success (Moore & Moore 1976, Rypel et al. 2007). In the wild, Delta Smelt occurrence is positively correlated with higher turbidity (Feyrer et al. 2007, 2011, Nobriga et al. 2008), and in laboratory studies of larval Delta Smelt, foraging activity and success are maximized in low-light or highly turbid (e.g., 18-80 NTU) conditions (Lindberg et al. 2013, Komoroske et al. 2016, Tigan et al. 2020). Turbidity *per se* may have less of an effect on foraging by adult Delta Smelt, and at very high turbidities (e.g., 125-250 NTU), foraging success may be reduced for adult Delta Smelt (Hasenbein et al. 2013). The non-significant main effect of water clarity in the environment-only, global-regional, and region-specific model appears to support this previous result.

Growth rates of wild Delta Smelt, however, appeared to respond to a significant interactive effect of water clarity and temperature, with individuals exhibiting stable growth rates when captured in more turbid conditions (e.g., Secchi depths < 0.2 m), even when water temperatures were high (Fig. 5F,G). In contrast, wild Delta Smelt exhibited the strongest decline in growth rate with temperature in clearer waters with higher Secchi depths. This significant temperature-clarity interaction suggests that enhanced foraging or reduced energetic costs (e.g., due to reduced predation risk or higher prey availability) in turbid conditions may help facilitate growth compensation during periods of thermal stress, as has been shown for other temperate fishes (Lusardi et al. 2019). If so, this may explain, in part, the ability of some freshwater resident Delta Smelt to survive otherwise thermally stressful conditions during warm summer conditions (Mahardja et al. 2019, Hobbs et al. 2019).

Statistical Considerations

Catches of this critically endangered species are rare and patchy in the wild, thus, samples were often unbalanced in time, space, and in relation to environmental variation. For this reason, we constructed multiple models to examine specific patterns in the data given varying assumptions. Since Delta Smelt are not known to school, individuals were assumed to have been dispersed within regions with similar environmental conditions for the last 14 days prior to capture and were thus treated as independent to maximize the information provided by each fish. It is possible, however, that individual fish experienced different recent environmental histories, thus limiting the relevance of the measured environmental data to each individual; or to the contrary, that tow-specific variation may have resulted in a lack of independence among individuals for reasons other than similarity in environmental histories. Next, samples were distributed unevenly among years, subregions, regions, and environmental conditions. For example, most specimens were from just three subregions including the Lower Sacramento River, Suisun Bay and Marsh, and the Cache Slough and Liberty Island complex. Therefore, smaller strata were aggregated up into regions, possibly obscuring finer-scale subregional patterns (e.g., Suisun Marsh versus Suisun Bay). Furthermore, most Delta Smelt captured furthest downstream in the West Delta region were primarily collected following the wettest years (e.g., 2011-2012, 2017) with highest freshwater outflows that dispersed fish and low-

salinity habitats further downstream. Similarly, salinity was spatially structured, with specimens from the North Delta having only experienced freshwater conditions, whereas specimens from Lower Sacramento River experienced both fresh and low salinity values, and specimens from the West Delta experienced an even broader range of salinity values.

Our modeling approach included (a) an environmental-only model, (b) a global-regional mixed effects model, and (c) separate region-specific mixed effects models, allowing us to examine how inferences regarding growth responses to environmental and spatiotemporal variation might change given different modeling assumptions. Though hierarchical factor-smooth models can be informative for these types of questions (Pedersen et al. 2019), we chose this modeling approach as the most conservative way to account for the nuances described above. Environment-only models assumed that environmental drivers, alone, explained the variation observed in growth rates, while ignoring temporal and spatial structure in the data. In contrast, the global-regional model assumed all environmental smooths were identical among regions, and that only the intercepts were affected by region and the global random effect of year. Region-specific models accounted for interannual variation and had the fewest assumptions, but also the smallest samples sizes and lowest power to estimate environmental and interannual effects. The use of multiple models allowed us to examine how growth varies in relation to the environmental attributes when accounting for different structures in the data, thus providing additional confidence in consistent patterns that emerge, and shining caution on results that appear less stable. We believe, therefore, that the conclusions reported herein are conservative, yet we also emphasize the importance of expanding upon this study, where feasible, to enhance statistical power and to better partition fine-scale spatiotemporal and environmental patterns in Delta Smelt growth rates.

Management Implications

Conservation efforts for Delta Smelt have largely focused on managing freshwater flows to maintain suitable low-salinity habitats further downstream during summer-fall. During this period, juvenile and subadult Delta Smelt often occur in low-salinity habitats (e.g., salinities of 0.1-4 ppt) of the upper San Francisco Estuary (Moyle et al. 1992), and it is during this period that variation in vital rates, such as growth, are likely to have strong effects on future reproductive output and subsequent population growth rates (Rose et al. 2013b). Prior studies suggest that higher freshwater flows into the estuary during summer-fall could significantly improve the quantity and quality of low-salinity habitats for Delta Smelt by improving the abiotic environment (Feyrer et al. 2007, 2011) and increasing food availability (Miller et al. 2012). For example, the highest-quality summer-fall habitats for Delta Smelt are believed to occur near the 2-ppt isohaline ("X2"), with both the quantity and quality of low-salinity habitats further enhanced when X2 is geographically located westward (e.g., < river kilometer 81) toward Suisun Bay-Marsh (Moyle et al. 1992, Jassby et al. 1995, Kimmerer 2002, Dege & Brown 2004). Field studies linking the vital rates of wild Delta Smelt to dynamic and static habitat features are needed to explore these hypotheses and the mechanisms likely to confer the theorized benefits of specific freshwater flow management actions.

The patterns in otolith-based growth rates of Delta Smelt described herein shed additional light on the responses of this species to environmental and geographic habitat attributes, thus improving inferences regarding likely responses to different management actions. Environment-only models indicated that Delta Smelt grow faster in low-salinity brackish versus freshwater

habitats, corroborating previous observations of enhanced foraging by individuals captured further downstream (Hammock et al. 2017). Global-regional models indicated that geographic patterns matched the above predictions, with Delta Smelt growing slowest in upstream freshwater habitats of the North Delta, and fastest in the saltier downstream habitats of the Central and West Delta. Though growth rates increased with practical salinity in the Central Delta, this pattern was not evident in the West Delta region-specific model, possibly due to its lower sample size. In aggregate, these results confirm that improved feeding and growth in downstream low-salinity habitats are likely key mechanisms selecting for a migratory life history in Delta Smelt (Hammock et al. 2017, Hobbs et al. 2019). Our results suggest that water management actions designed to enhance downstream dispersal and the extent and quality of low-salinity habitats in the summer-fall are likely to benefit Delta Smelt.

We did not, however, identify clear evidence for a unique effect of salinity on growth rates between the Central Delta and West Delta; therefore, our results do not provide clear evidence for or against a geographic location for X2 (e.g., relative to river km 81) that maximizes Delta Smelt growth. Nevertheless, our results further indicate that reductions in freshwater outflow due to droughts and diversions, especially combined with rising sea levels, increasing transparency, and continued warming due to climate change, are likely to exacerbate eastward intrusion of more saline waters, which is likely to further compress and degrade the remaining limited habitats of Delta Smelt (Feyrer et al. 2011, Hasenbein et al. 2013, Brown et al. 2016, Komoroske et al. 2016). Specifically, our results suggest that such changes in the upper SFE are likely to negatively impact growth rates of Delta Smelt, which will likely correspond with reduced fitness and net reproductive output (Hjort 1914, Houde 1989, Cushing 1990, Leggett & Deblois 1994, Rose et al. 2013b). Our results, therefore, suggest that flow management actions that are designed to increase the extent of suitable low-salinity habitats (Kimmerer et al. 2009) and enhance downstream transport to higher-quality habitats are likely to benefit wild Delta Smelt. Several hypotheses regarding the benefits of such flow actions focus on associated increases in the intersection of dynamic low-salinity conditions with fixed geographic habitat features such as wetlands and marshes that occur further downstream (e.g. Suisun Marsh). Future otolith-based studies that examine the growth rates of fishes captured across these different fixed geographic features, while also controlling for intrinsic growth effects and dynamic environmental attributes such as salinity, could shed further light on the potential benefits of brackish wetland habitats and associated flow management actions for this species.

We are still discovering new facets of the basic biology of Delta Smelt that have yet to be accounted for in life-cycle and population models, conservation efforts, and the captive breeding program (Hobbs et al. 2019). The presence of multiple life-history phenotypes including freshwater residents (FWR) suggests that year-round residence of Delta Smelt in freshwater habitats is likely an important mechanism for population resilience and stability (Nobriga et al. 2008, Hobbs et al. 2019). However, our findings support previous studies suggesting that freshwater habitats are becoming increasingly unsuitable in summer-fall due to multiple factors, including thermal stress (Nobriga et al. 2008, Moyle et al. 2016, Hobbs et al. 2019). The likely loss of this life-history phenotype in the South Delta and its continuing decline in the North Delta are likely critical blows to population resilience that pushes Delta Smelt ever-closer toward extinction. This is especially true if growth is suppressed at temperatures above 20 ºC, and further still if this effect is exacerbated in clearer waters, as indicated in this study. FWR Delta Smelt may, however, compensate for reduced growth rates by avoiding the energetic costs and mortality risk associated with migrating upstream to freshwater spawning grounds. Furthermore,

since FWR Delta Smelt live adjacent to optimal spawning habitats and mature earlier (Hobbs et al. 2019), they may also compensate for reduced growth and size-at-spawning by producing a greater number of broods per spawning season (Damon et al. 2016). Comparative studies of the reproductive biology of different life history phenotypes would shed further light on their relative fitness and per capita contributions to Delta Smelt population dynamics.

CONCLUSIONS

Temperatures throughout the upper San Francisco Estuary are now commonly > 20 ºC during summer-fall in most years (Nobriga et al. 2008, Brown et al. 2016), possibly explaining the persistent decline of Delta Smelt despite several recent years of favorably high freshwater outflow. Whether this lower thermal threshold is due to greater thermal sensitivity of wild versus cultured Delta Smelt, other ambient habitat features that co-vary with temperature, or interactive effects of thermal stress with other stressors, remains to be explored. Though salinity and clarity exhibited more complex relationships with growth, our results corroborate others indicating that future increases in water clarity (Hestir et al. 2016, Bever et al. 2018) and landward intrusion of higher-salinity waters (Brown et al. 2016, Moyle et al. 2016, Komoroske et al. 2016), are likely to exacerbate the negative effects of future warming on Delta Smelt vital rates and population dynamics. Thus, future changes to the upper SFE environment are likely to increasingly limit the extent and quality of suitable habitats for Delta Smelt, while management actions have the potential to either mitigate or further exacerbate these imminent effects. Bold and creative actions for thermal mitigation, including flow actions that distribute low-salinity habitat, food, and fish to optimal, cooler downstream regions, as well as novel approaches for maintaining the thermal suitability of upstream freshwater habitats year-round, are likely needed if Delta Smelt are to remain in their Delta for much longer.

ACKNOWLEDGEMENTS

We are grateful to our collaborators at the California Department of Fish and Wildlife (CDFW) and U.S. Fish and Wildlife Service for providing Delta Smelt specimens from field collections for use in this study, and the Teh Lab at UC Davis (UCD) who helped obtain, dissect, and archive specimens. We also thank the many past and present students and staff in the Otolith Geochemistry and Fish Ecology Laboratory at UCD who contributed to fish dissections, otolith preparation, and growth analysis. We thank N. Bertrand for review of the manuscript. Otolith archives were maintained in accordance with an approved California Department of Fish and Wildlife Service Section 2081a Memorandum of Understanding to L. Lewis, M. Willmes, and J. Hobbs. Funding for this project was provided in part by grants from the CDFW contracts E1183004, D1583004 and P1696005, and the U.S. Bureau of Reclamation (USBR) contracts R13AP20022 and R17AC00129 to J. Hobbs, S. Teh, and L. Lewis. Additional support was provided by the Delta Stewardship Council (DSC) via postdoctoral fellowships to M. Willmes (Grant No. 1167) and L. Lewis (Grant Nos. 2279, 5298). The content of this material and views described herein do not necessarily reflect the views and policies of the CDFW, USBR, DSC, or UCD; nor does mention of trade names or commercial products constitute endorsement or recommendation for use.

REFERENCES

Anderson JT (1988) A review of size dependent survival during pre-recruit stages of fishes in relation to recruitment. Journal of Northwest Atlantic Fishery Science 8:55–66.

Baltz DM, Fleeger JW, Rakocinski CF, McCall JN (1998) Food, density, and microhabitat: factors affecting growth and recruitment potential of juvenile saltmarsh fishes. Environmental Biology of Fishes 53:89–103.

Barrow J, Ford J, Day R, Morrongiello J (2018) Environmental drivers of growth and predicted effects of climate change on a commercially important fish, Platycephalus laevigatus. Marine Ecology Progress Series 598:201–212.

Bartoń K (2019) MuMIn: Multi-Model Inference, Version 1.43.6. R package.

Beck MW, Heck KL, Able KW, Childers DL, Eggleston DB, Gillanders BM, Halpern B, Hays CG, Hoshino K, Minello TJ, Orth RJ, Sheridan PF, Weinstein MP (2001) The Identification, Conservation, and Management of Estuarine and Marine Nurseries for Fish and Invertebrates. BioScience 51:633.

Bennett WA (2005) Critical Assessment of the Delta Smelt Population in the San Francisco Estuary, California. SFEWS 3:1–71.

Bever AJ, MacWilliams ML, Fullerton DK (2018) Influence of an Observed Decadal Decline in Wind Speed on Turbidity in the San Francisco Estuary. Estuaries and Coasts 41:1943–1967.

Blaber SJM, Blaber TG (1980) Factors affecting the distribution of juvenile estuarine and inshore fish. Journal of Fish Biology 17:143–162.

Brett JR, Groves TDD (1979) 6 - Physiological Energetics. In: *Fish Physiology*. Hoar WS, Randall DJ, Brett JR (eds) Academic Press, p 279–352

Brown LR, Bennett WA, Wagner RW, Morgan-King T, Knowles N, Feyrer F, Schoellhamer DH, Stacey MT, Dettinger M (2013) Implications for Future Survival of Delta Smelt from Four Climate Change Scenarios for the Sacramento-San Joaquin Delta, California. Estuaries and Coasts 36:754–774.

Brown LR, Komoroske LM, Wayne Wagner R, Morgan-King T, May JT, Connon RE, Fangue NA (2016) Coupled downscaled climate models and ecophysiological metrics forecast habitat compression for an endangered estuarine fish. PLoS ONE 11.

Campana SE (1990) How reliable are growth back-calculations based on otoliths? Canadian Journal of Fisheries and Aquatic Sciences 47:2219–2227.

Campana SE, Jones CM (1992) Analysis of otolith microstructure data. Otolith Microstructure Examination and Analysis 117:13–17.

CDFG (2010) State & federally listed endangered & threatened animals of California. California Department of Fish & Game,State of California, The Natural Resources Agency, California. The Natural Rsources Agency, California.

Cloern JE, Jassby AD (2012) Drivers of change in estuarine-coastal ecosystems: discoveries from four decades of study in San Francisco Bay. Reviews of Geophysics 50.

Cloern JE, Knowles N, Brown LR, Cayan D, Dettinger MD, Morgan TL, Schoellhamer DH, Stacey MT, van der Wegen M, Wagner RW, Jassby AD (2011) Projected Evolution of California's San Francisco Bay-Delta-River System in a Century of Climate Change. PLoS ONE 6:e24465.

Cushing DH (1990) Plankton production and year-class strength in fish populations: An update of the match/mismatch hypothesis. Advances in Marine Biology 26:249–293.

Cyrus DP, Blaber SJM (1987) The influence of turbidity on juvenile marine fishes in estuaries. Part 2. Laboratory studies, comparisons with field data and conclusions. Journal of Experimental Marine Biology and Ecology 109:71–91.

Cyrus DP, Blaber SJM (1992) Turbidity and salinity in a tropical northern Australian estuary and their influence on fish distribution. Estuarine, Coastal and Shelf Science 35:545–563.

Dahlke FT, Wohlrab S, Butzin M, Pörtner H-O (2020) Thermal bottlenecks in the life cycle define climate vulnerability of fish. Science 369:65.

Damon LJ, Slater SB, Baxter RD, Fujimura RW (2016) Fecundity and reproductive potential of wild female Delta smelt in the upper San Francisco Estuary, California. California Fish and Game 102:188–210.

Dege M, Brown LR (2004) Effect of outflow on spring and summertime distribution and abundance of larval and juvenile fishes in the upper San Francisco Estuary. In: *Early Life History of Fishes in the San Francisco Estuary and Watershed*. Feyrer F, Brown LR, Brown RL, Orsi JJ (eds) p 49–65

Feyrer F, Newman K, Nobriga M, Sommer T (2011) Modeling the Effects of Future Outflow on the Abiotic Habitat of an Imperiled Estuarine Fish. Estuaries and Coasts 34:120–128.

Feyrer F, Nobriga ML, Sommer TR (2007) Multidecadal trends for three declining fish species: habitat patterns and mechanisms in the San Francisco Estuary, California, USA. Can J Fish Aquat Sci 64:723–734.

Fong S, Louie S, Werner I, Davis J, Connon RE (2016) Contaminant effects on California bay-delta species and human health. San Francisco Estuary and Watershed Science 14.

Frank DF, Hasenbein M, Eder K, Jeffries KM, Geist J, Fangue NA, Connon RE (2017) Transcriptomic screening of the innate immune response in delta smelt during an Ichthyophthirius multifiliis infection. Aquaculture 473:80–88.

Gillanders BM, Elsdon TS, Halliday IA, Jenkins GP, Robins JB, Valesini FJ (2011) Potential effects of climate change on Australian estuaries and fish utilising estuaries: a review. Marine and Freshwater Research 62:1115.

Green BS, Fisher R (2004) Temperature influences swimming speed, growth and larval duration in coral reef fish larvae. Journal of Experimental Marine Biology and Ecology 299:115–132.

Gregory R (2011) Effect of Turbidity on the Predator Avoidance Behaviour of Juvenile Chinook Salmon (Oncorhynchus tshawytscha). Canadian Journal of Fisheries and Aquatic Sciences 50:241–246.

Grimaldo L, Feyrer F, Burns J, Maniscalco D (2017) Sampling Uncharted Waters: Examining Rearing Habitat of Larval Longfin Smelt (Spirinchus thaleichthys) in the Upper San Francisco Estuary. Estuaries and Coasts 40:1771–1784.

Hammock BG, Hartman R, Slater SB, Hennessy A, Teh SJ (2019) Tidal Wetlands Associated with Foraging Success of Delta Smelt. Estuaries and Coasts 42:857–867.

Hammock BG, Hobbs JA, Slater SB, Acuna S, Teh SJ (2015) Contaminant and food limitation stress in an endangered estuarine fish. Science of The Total Environment 532:316–326.

Hammock BG, Slater SB, Baxter RD, Fangue NA, Cocherell D, Hennessy A, Kurobe T, Tai CY, Teh SJ (2017) Foraging and metabolic consequences of semi-anadromy for an endangered estuarine fish. PLoS ONE 12:e0173497.

Hasenbein M, Komoroske LM, Connon RE, Geist J, Fangue NA (2013) Turbidity and salinity affect feeding performance and physiological stress in the endangered delta smelt. Integr Comp Biol 53:620–634.

Herbst S, Marsden JE (2011) Comparison of precision and bias of scale, fin ray, and otolith age estimates for lake whitefish (Coregonus clupeaformis) in Lake Champlain. Lancet 37:386–389.

Hestir EL, Schoellhamer DH, Greenberg J, Morgan-King T, Ustin SL (2016) The Effect of Submerged Aquatic Vegetation Expansion on a Declining Turbidity Trend in the Sacramento-San Joaquin River Delta. Estuaries and Coasts 39:1100–1112.

Hill KD, Dauphinee TM, Woods DJ (1986) The Extension of the Practical Salinity Scale 1978 to Low Salinities. IEEE Journal of Oceanic Engineering 11:109–112.

Hinrichsen H-H, Voss R, Huwer B, Clemmesen C (2010) Variability of larval Baltic sprat (Sprattus sprattus L.) otolith growth: a modeling approach combining spatially and temporally resolved biotic and abiotic environmental key variables. Fisheries Oceanography 19:463–479.

Hjort J (1914) Fluctuations in the great fisheries of northern Europe viewed in the light of biological research. ICES 20:1–228.

Hobbs JA, Bennett WA, Burton JE, Baskerville-Bridges B (2007) Modification of the biological intercept model to account for ontogenetic effects in laboratory-reared delta smelt (Hypomesus transpacificus). Fishery Bulletin 105:30–38.

Hobbs JA, Lewis LS, Willmes M, Denney C, Bush E (2019) Complex life histories discovered in a critically endangered fish. Scientific Reports 9:16772.

Hobbs JA, Moyle PB, Fangue N, Connon RE (2017) Is Extinction Inevitable for Delta Smelt and Longfin Smelt? An Opinion and Recommendations for Recovery. SFEWS 15:1–19.

Houde E (1989) Comparative growth, mortality, and energetics of marine fish larvae: temperature and implied latitudinal effects. Fishery Bulletin 87:471–495.

Houde ED (2008) Emerging from Hjort's Shadow. J Northw Atl Fish Sci 41:53–70.

Jain KE, Farrell AP (2003) Influence of seasonal temperature on the repeat swimming performance of rainbow trout Oncorhynchus mykiss. Journal of Experimental Biology 206:3569–3579.

James N, Van Niekerk L, Whitfield A, Potts W, Götz A, Paterson A (2013) Effects of climate change on South African estuaries and associated fish species. Climate Research 57:233–248.

Jassby A, Kimmerer W, Monismith S, Armor C, Cloern J, Powell T, Schubel J, Vendlinski T (1995) Isohaline position as a habitat indicator for estuarine populations. Ecological Applications 5:272–289.

Jeffries KM, Connon RE, Davis BE, Komoroske LM, Britton MT, Sommer T, Todgham AE, Fangue NA (2016) Effects of high temperatures on threatened estuarine fishes during periods of extreme drought. Journal of Experimental Biology 219:1705–1716.

Jeffries KM, Fangue NA, Connon RE (2018) Multiple sub-lethal thresholds for cellular responses to thermal stressors in an estuarine fish. Comparative Biochemistry and Physiology - Part A: Molecular & Integrative Physiology 225:33–45.

Kimmerer W (2002) Effects of freshwater flow on abundance of estuarine organisms: physical effects or trophic linkages? Marine Ecology Progress Series 243:39–55.

Kimmerer WJ, Gross ES, MacWilliams ML (2009) Is the Response of Estuarine Nekton to Freshwater Flow in the San Francisco Estuary Explained by Variation in Habitat Volume? Estuaries and Coasts 32:375–389.

Knowles N, Cayan D (2002) Potential effects of global warming on the Sacramento/San Joaquin watershed and the San Francisco estuary. Geophysical Research Letters 29.

Komoroske L, Connon R, Lindberg J, Cheng B, Castillo G, Hasenbein M, Fangue N (2014) Ontogeny influences sensitivity to climate change in an endangered fish. Conservation Physiology 2:cou008.

Komoroske LM, Connon RE, Jeffries KM, Fangue NA (2015) Linking transcriptional responses to organismal tolerance reveals mechanisms of thermal sensitivity in a mesothermal endangered fish. Molecular Ecology 24:4960–4981.

Komoroske LM, Jeffries KM, Connon RE, Dexter J, Hasenbein M, Verhille C, Fangue NA (2016) Sublethal salinity stress contributes to habitat limitation in an endangered estuarine fish. Evolutionary Applications 9:963–981.

Labonne M, Morize E, Scolan P, Laë R, Dabas E, Bohn M (2009) Impact of salinity on early life history traits of three estuarine fish species in Senegal. Estuarine, Coastal and Shelf Science 82:673–681.

Lankford TE, Targett TE (1994) Suitability of estuarine nursery zones for juvenile weakfish (Cynoscion regalis): effects of temperature and salinity on feeding, growth and survival. Marine Biology 119:611–620.

Leggett WC, Deblois E (1994) Recruitment in marine fishes: Is it regulated by starvation and predation in the egg and larval stages? Netherlands Journal of Sea Research 32:119–134.

Lewis EL, Perkin RG (1981) The practical salinity scale 1978: conversion of existing data. Deep Sea Research Part A, Oceanographic Research Papers 28A:307–328.

Lindberg JC, Tigan G, Ellison L, Rettinghouse T, Nagel MM, Fisch KM (2013) Aquaculture Methods for a Genetically Managed Population of Endangered Delta Smelt. North American Journal of Aquaculture 75:186–196.

Lusardi RA, Hammock BG, Jeffres CA, Dahlgren RA, Kiernan JD (2019) Oversummer growth and survival of juvenile coho salmon (Oncorhynchus kisutch) across a natural gradient of stream water temperature and prey availability: an in situ enclosure experiment. Can J Fish Aquat Sci 77:413–424.

Mac Nally R, Thomson JR, Kimmerer WJ, Feyrer F, Newman KB, Sih A, Bennett WA, Brown L, Fleishman E, Culberson SD, Castillo G (2010) Analysis of pelagic species decline in the upper San Francisco Estuary using multivariate autoregressive modeling (MAR). Ecological Applications 20:1417–1430.

Mahardja B, Hobbs JA, Ikemiyagi N, Benjamin A, Finger AJ (2019) Role of freshwater floodplain-tidal slough complex in the persistence of the endangered delta smelt. PLOS ONE 14:e0208084.

Miller WJ, Manly BFJ, Murphy DD, Fullerton D, Ramey RR (2012) An Investigation of Factors Affecting the Decline of Delta Smelt (Hypomesus transpacificus) in the Sacramento-San Joaquin Estuary. Reviews in Fisheries Science 20:1–19.

Moore JW, Moore IA (1976) The basis of food selection in flounders, Platichthys flesus (L.), in the Severn Estuary. Journal of Fish Biology 9:139–156.

Morgan R, Sundin J, Finnøen MH, Dresler G, Vendrell M, Dey A, Sarkar K, Jutfelt F (2019) Are model organisms representative for climate change research? Testing thermal tolerance in wild and laboratory zebrafish populations. Conservation Physiology 7.

Morrongiello JR, Thresher RE (2015) A statistical framework to explore ontogenetic growth variation among individuals and populations: a marine fish example. Ecological Monographs 85:93–115.

Morrongiello JR, Thresher RE, Hobbs NT (2015) A statistical framework to explore ontogenetic Growth variation among individuals and populations: A marine fish example. Ecological Monographs.

Moyle PB, Brown LR, Durand JR, Hobbs JA (2016) Delta smelt: Life history and decline of a once abundant species in the San Francisco Estuary. San Francisco Estuary and Watershed Science 14:1–30.

Moyle PB, Herbold B, Stevens DE, Miller LW (1992) Life History and Status of Delta Smelt in the Sacramento-San Joaquin Estuary, California. Transactions of the American Fisheries Society 121:67–77.

Moyle PB, Hobbs JA, Durand JR (2018) Delta Smelt and Water Politics in California. Fisheries 43:42–50.

Muhling B, Gaitan C, Stock C, Saba V, Tommasi D, Dixon K (2017) Potential Salinity and Temperature Futures for the Chesapeake Bay Using a Statistical Downscaling Spatial Disaggregation Framework. Estuaries and Coasts 41:349–372.

Nagelkerken I, Sheaves M, Baker R, Connolly R (2015) The seascape nursery: a novel spatial approach to identify and manage nurseries for coastal marine fauna. Fish and Fisheries 16:362–371.

NatureServe (2014) Hypomesus transpacificus (errata version published in 2020). The IUCN Red List of Threatened Species 2014:e.T10722A174778740.

Neubauer P, Andersen KH (2019) Thermal performance of fish is explained by an interplay between physiology, behaviour and ecology. Conservation Physiology 7.

Niklitschek E, Secor D (2009) Dissolved oxygen, temperature and salinity effects on the ecophysiology and survival of juvenile Atlantic sturgeon in estuarine waters: II. Model development and testing. Journal of Experimental Marine Biology and Ecology 381:S161–S172.

Nobriga ML, Sommer TR, Feyrer F, Fleming K (2008) Long-Term Trends in Summertime Habitat Suitability for Delta Smelt, Hypomesus transpacificus. San Francisco Estuary and Watershed Science 6:1–13.

Pannella G (1971) Fish otoliths: daily growth layers and periodical patterns. Science 173:1124–1127.

Pedersen EJ, Miller DL, Simpson GL, Ross N (2019) Hierarchical generalized additive models in ecology: an introduction with mgcv. PeerJ 7:e6876.

Peterson MS (2003) A Conceptual View of Environment-Habitat-Production Linkages in Tidal River Estuaries. Reviews in Fisheries Science 11:291–313.

Pörtner H, Peck M (2010) Climate change effects on fishes and fisheries: towards a cause-and-effect understanding. Journal of fish biology 77 8:1745–79.

Pörtner HO, Farrell AP (2008) Physiology and Climate Change. Science 322:690.

Reis G, Howard J, Rosenfield J (2019) Clarifying Effects of Environmental Protections on Freshwater Flows to—and Water Exports from—the San Francisco Bay Estuary. San Francisco Estuary and Watershed Science 17:1–22.

Robins P, Skov M, Lewis M, Enez L, Davies A, Malham S, Neill S, McDonald J, Whitton T, Jackson S, Jago C (2016) Impact of climate change on UK estuaries: A review of past trends and potential projections. Estuarine Coastal and Shelf Science 169:119–135.

Rose KA, Kimmerer WJ, Edwards KP, Bennett WA (2013a) Individual-Based Modeling of Delta Smelt Population Dynamics in the Upper San Francisco Estuary: I. Model

Description and Baseline Results. Transactions of the American Fisheries Society 142:1238–1259.

Rose KA, Kimmerer WJ, Edwards KP, Bennett WA (2013b) Individual-Based Modeling of Delta Smelt Population Dynamics in the Upper San Francisco Estuary: II. Alternative Baselines and Good versus Bad Years. Transactions of the American Fisheries Society 142:1260–1272.

Rypel AL, Layman CA, Arrington DA (2007) Water depth modifies relative predation risk for a motile fish taxon in Bahamian Tidal Creeks. Estuaries and Coasts 30:518–525.

Schismenou E, Giannoulaki M, Tsiaras K, Lefkaditou E, Triantafyllou GS, Somarakis S (2014) Disentangling the effects of inherent otolith growth and model-simulated ecosystem parameters on the daily growth rate of young anchovies. Marine Ecology Progress Series 515:227–237.

Schismenou E, Palmer M, Giannoulaki M, Alvarez I, Tsiaras K, Triantafyllou G, Somarakis S (2016) Seasonal changes in otolith increment width trajectories and the effect of temperature on the daily growth rate of young sardines. Fisheries Oceanography 25:362–372.

Scoville C (2019) Hydraulic society and a “stupid little fish”: toward a historical ontology of endangerment. Theory and Society 48:1–37.

Shima JS, Swearer SE (2019) Moonlight enhances growth in larval fish. Ecology 100:e02563.

Smith WE, Newman KB, Mitchell L (2020) A Bayesian hierarchical model of postlarval delta smelt entrainment: integrating transport, length composition, and sampling efficiency in estimates of loss. Can J Fish Aquat Sci 77:789–813.

Speers-Roesch B, Norin T (2016) Ecological significance of thermal tolerance and performance in fishes: new insights from integrating field and laboratory approaches. Functional Ecology 30:842–844.

Swanson C, Reid T, Young PS, Cech Jr JJ (2000) Comparative environmental tolerances of threatened delta smelt (Hypomesus transpacificus) and introduced wakasagi (H. nipponensis) in an altered California estuary. Oecologia 123:384–390.

Thomson JR, Kimmerer WJ, Brown LR, Newman KB, Mac Nally R, Bennett WA, Feyrer F, Fleishman E (2010) Bayesian change point analysis of abundance trends for pelagic fishes in the upper San Francisco Estuary. Ecological Applications 20:1431–1448.

Thresher R, Lyle J, Semmens J, Neuheimer A (2011) Tolerance limit for fish growth exceeded by warming waters. Nature Climate Change 1:110–113.

Tigan G, Mulvaney W, Ellison L, Schultz A, Hung T-C (2020) Effects of light and turbidity on feeding, growth, and survival of larval Delta Smelt (Hypomesus transpacificus, Actinopterygii, Osmeridae). Hydrobiologia 847:2883–2894.

U.S. Fish and Wildlife Service (1993) Determination of Threatened Status for the Delta Smelt. Federal Register 58:12854–12864.

Weisberg S, Spangler G, Richmond LS (2010) Mixed effects models for fish growth. Can J Fish Aquat Sci 67:269–277.

Welch TJ, van den Avyle MJ, Betsill RK, Driebe EM (1993) Precision and Relative Accuracy of Striped Bass Age Estimates from Otoliths, Scales, and Anal Fin Rays and Spines. North American Journal of Fisheries Management 13:616–620.

Wenger AS, Whinney J, Taylor B, Kroon F (2016) The impact of individual and combined abiotic factors on daily otolith growth in a coral reef fish. Scientific Reports 6:28875.

Wood SN (2017) Generalized Additive Models: An Introduction with R, 2nd ed. Chapman and Hall/CRC, New York.

Table 1. Total Delta Smelt (N = 459) included in the study by year, region, and subregion (EDSM 2017 "Strata"). Regions and subregions are ordered from upstream (top) to downstream (bottom): ND-North Delta, SD-South Delta, CD-Central Delta, WD-West Delta (Fig. 1).

Region	Subregion	Subreg_Code	2011	2012	2013	2014	2015	2016	2017	2018	2019	Total
ND	Cache Sl. and Liberty Is.	CSLI	15	6	1	21	2	0	0	32	1	78
ND	Sac. Deep Water Ship. Channel	SDWSC	0	0	0	0	0	0	2	27	1	30
CD	Lower Sacramento R.	LSR	5	62	43	72	22	3	36	17	2	262
CD	Lower San Joaquin R.	LSJR	0	0	2	0	0	0	1	0	0	3
WD	Suisun Bay and Marsh	SBM	34	4	0	0	0	0	33	6	4	81
WD	Carquinez Strait & San Pablo Bay	CSSPB	5	0	0	0	0	0	0	0	0	5
		Total	59	72	46	93	24	3	72	82	8	459

Table 2. Results of correlation analyses among pairs of the abiotic environmental attributes measured with each sample, including their respective transformations: temperature (cubic), salinity (log10), and Secchi depth (none). The Pearson's correlation coefficient (r), t-statistic (t), degrees of freedom (df), and p-value (p) are provided for each correlation. All pairwise correlations were relatively weak (|r| = 0.04-0.07), and none were significant.

Correlation	r	t	df	p
Temperature-Salinity	-0.03	-0.43	159	0.665
Temperature-Secchi	-0.07	-0.85	159	0.394
Secchi-Salinity	-0.05	-0.58	159	0.560

Table 3. Statistical results of the selected "environment-only" model (Model 18, tsc*) examining variation in age-independent growth rates (Ga) of wild Delta Smelt as the additive and interactive function of the physical environmental attributes measured at capture (t-temperature, s-salinity, c-clarity) ($\chi 2 = 79.6$, df = 15.6, R2 = 0.159, $p < 0.001$). Estimated degrees of freedom (EDF), referenced degrees of freedom (RDF), F-ratio (F), and p-values (P) are provided for each term in the model. Significant p-values ($P < 0.05$) for each coefficient and smooth term are in bold. Additional models are described and compared in Fig. S2 in Supplement 3.

Factor	EDF	RDF	F	P	R^2	P2
Temperature	1.86	2.24	10.46	**<0.001**	0.159	**<0.001**
Salinity	2.60	2.86	5.35	**<0.001**		
Clarity	2.29	2.63	1.79	0.217		
Temperature*Clarity	1.92	1.99	5.68	**0.005**		
Temperature*Salinity	1.00	1.00	0.04	0.844		
Clarity*Salinity	2.60	3.21	1.29	0.312		

Table 4. Statistical results of the "global-regional" GAM examining variation in Ga as a function of the fixed parametric effect of region, additive smooth effects of temperature, salinity, and clarity; both with and without the random effect of year (Model). The estimated coefficients (coefficient), standard error of the estimate (SE), t-statistic (t), and p-value (P1) are provided for each parametric term. Estimated degrees of freedom (EDF), referenced degrees of freedom (RDF), F-ratio (F), and p-values (P1) are provided for each smooth term in in the model. The overall R2 and p-value (P2) of each model are also provided. Significant p-values (P < 0.05) are shown in bold.

Model	Parametric Terms	Coefficient	SE	t	P1	R^2	P2
+ Year	Intercept (WD)	-0.031	0.026	-1.170	0.243		
	CD	0.029	0.021	1.359	0.175		
	ND	-0.006	0.023	-0.251	0.802		
	Smooth Terms	EDF	RDF	F	P1	0.30	**< 0.001**
	Temperature	1.000	1.000	2.331	0.128		
	Salinity	2.226	2.593	3.896	**0.028**		
	Secchi	1.001	1.001	2.590	0.108		
	Year	7.014	8.000	14.273	**<0.001**		

Model	Parametric Terms	Coefficient	SE	t	P1	R^2	P2
- Year	Intercept (WD)	0.024	0.015	1.623	0.105		
	CD	-0.017	0.018	-0.943	0.346		
	ND	-0.061	0.021	-2.947	**0.003**		
	Smooth Terms	EDF	RDF	F	P1	0.12	**<0.001**
	Temperature	1.002	1.004	17.382	**<0.001**		
	Salinity	2.576	2.863	2.026	0.084		
	Secchi	1.000	1.000	0.845	0.358		

Table 5. Statistical results of separate "region-specific" GAMs examining variation in growth (Ga) as a function of the additive effects of physical environmental attributes (temperature, salinity, and clarity) and the random year effect. Significant p-values ($p < 0.05$) are in bold. are: ND – North Delta, CD – Central Delta, WD – West Delta. The estimated degrees of freedom (EDF), referenced degrees of freedom (RDF), F-ratio (F), and p-values (P1) are provided each term in each region-specific model, as well as the coefficient of determination (R2) and p-value (P2) for the overall model compared to the null model (Ga ~ 1) using a likelihood ratio test. Regions are as in Fig. 1 and Table 1.

Region	Factor	EDF	RDF	F	P_1	R^2	P_2
ND	Temperature	1.465	1.784	0.461	0.644	0.450	**< 0.001**
	Salinity	1.000	1.000	0.081	0.777		
	Secchi	1.000	1.000	2.471	0.119		
	Year	5.376	7.000	6.400	**<0.001**		
CD	Temperature	2.565	2.851	3.880	0.011	0.302	**< 0.001**
	Salinity	1.308	1.527	4.124	0.037		
	Secchi	1.000	1.000	1.747	0.187		
	Year	5.854	8.000	7.343	**<0.001**		
WD	Temperature	1.043	1.082	1.608	0.191	0.197	**< 0.001**
	Salinity	1.000	1.000	0.037	0.848		
	Secchi	1.000	1.000	0.013	0.909		
	Year	2.594	4.000	3.220	**0.002**		

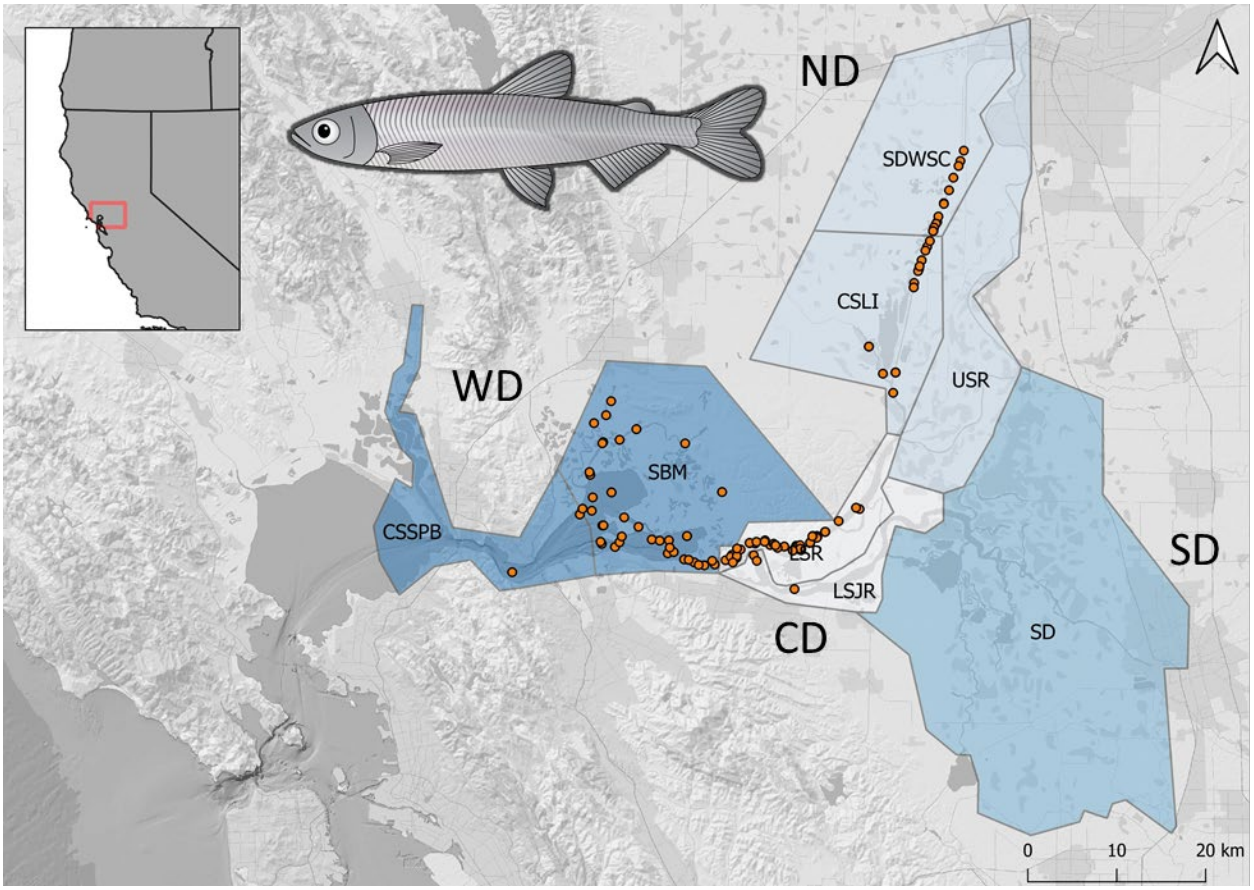

Figure 1. Map of the "upper" San Francisco Estuary. Polygons indicate subregions: CSSPB-Carquinez Strait and San Pablo Bay, SBM – Suisun Bay and Marsh, LSR—Lower Sacramento River, LSJR—Lower San Joaquin River, CSLI—Cache Slough and Liberty Island, SDWSC—Sacramento Deep Water Shipping Channel, USR—Upper Sacramento River, SD—South Delta. Strata of similar shades represent broader regions: West Delta (WD), Central Delta (CD), North Delta (ND), and South Delta (SD) (Table 1). All specimens included in this study were collected in the WD, CD, and ND regions of the SFE (orange circles). Subregions adapted from the EDSM 2017 Survey "strata" (Supplement 1). Delta Smelt artwork by Adi Khen.

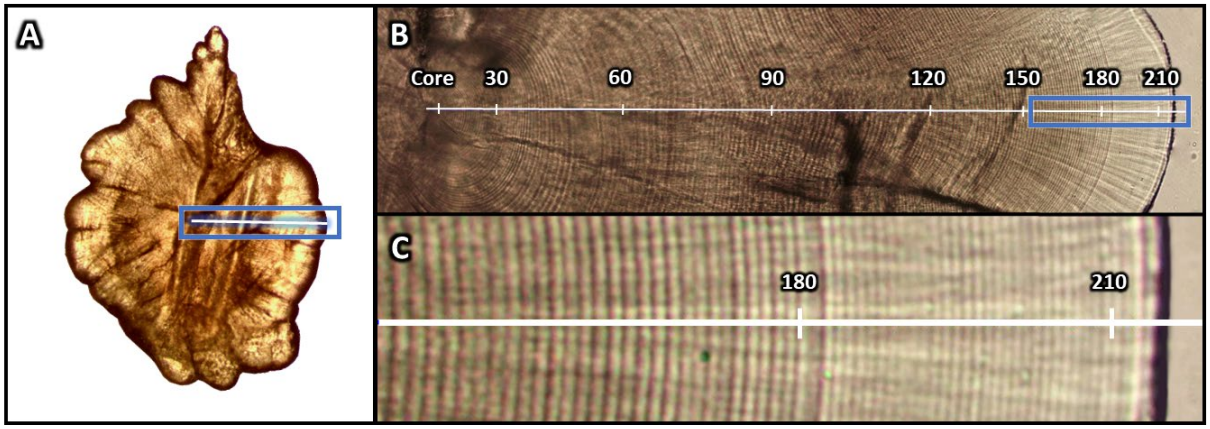

Figure 2. Otolith of a 215 day-post-hatch Delta Smelt. (a) Whole otolith showing dorsal age trajectory (inset). (b) Polished dorsal age trajectory (inset from a) showing daily rings and last ~ 60 days prior to capture (inset). (c) Zoomed-in edge of the polished age trajectory (inset from b) showing the last ~60 daily increments prior to collection.

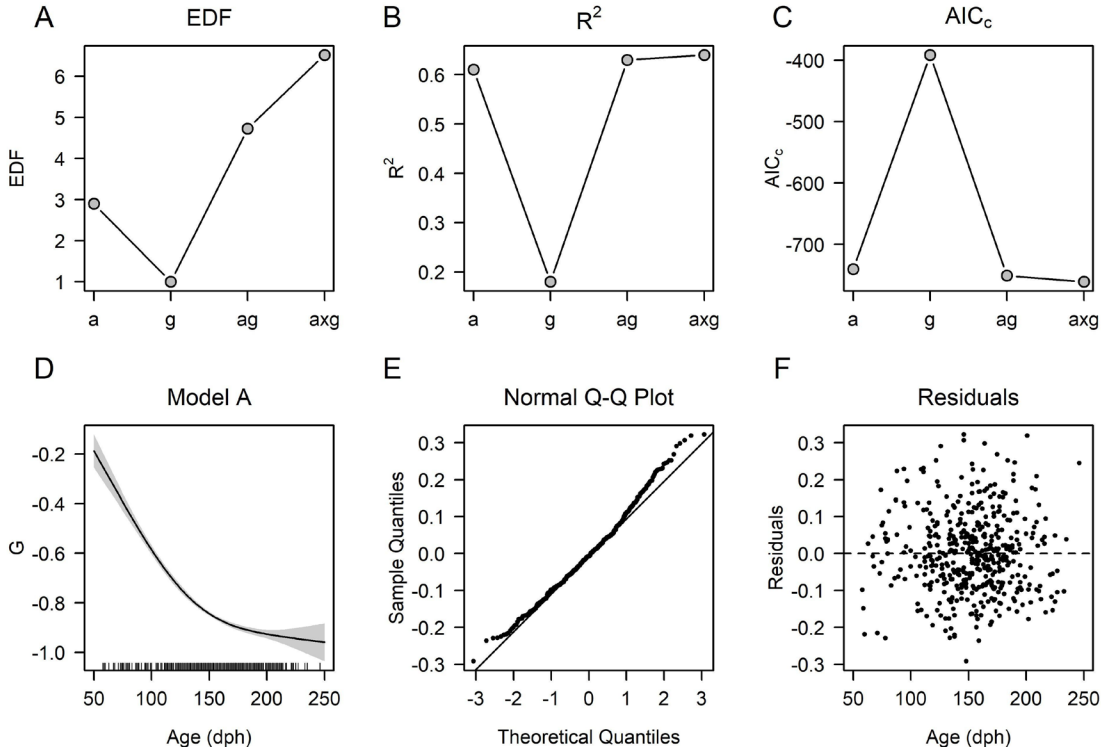

Figure 3: Intrinsic generalized additive models (GAMs) examining the response of log-transformed recent growth rates (G) to age and prior growth rate. Intrinsic models included age ("a"), prior growth ("g"), and their additive ("ag") and interactive ("axg") effects. Models were evaluated by examining complexity (estimated degrees of freedom, EDF), fit (coefficient of determination, R2), and quality (corrected Akaike information criterion, AICc) (A-C, respectively). The intrinsic relationship between growth rate and age (preferred model, "a") is shown (D), along with assessments of normality and homogeneous variance of this model (E-F, respectively). The centered residuals of the intrinsic model (F) represented the age-independent ("age-adjusted") growth rate (Ga).

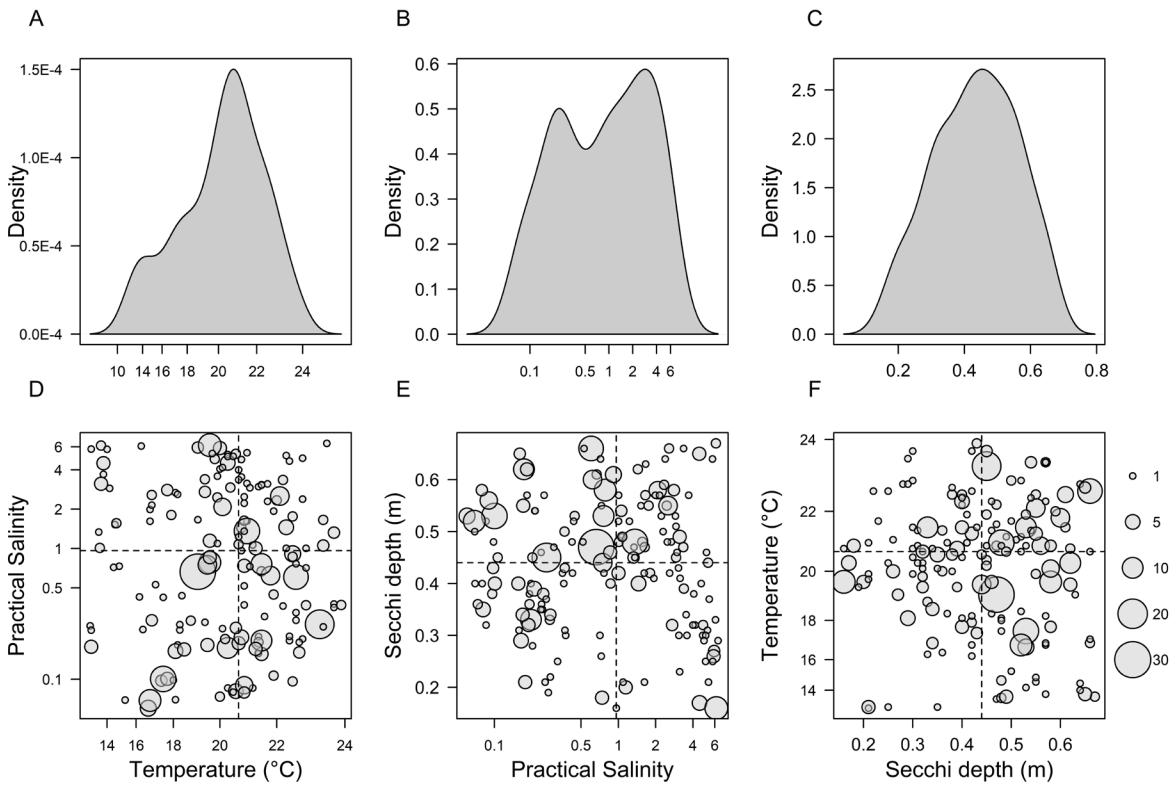

Figure 4: Distribution of environmental conditions from which Delta Smelt were collected. Axis scales reflect the respective transformations for temperature (cubic), salinity (log10), and Secchi depth (none). Kernel density plots of temperature, salinity, and Secchi depth (a-c, respectively) and biplots of each pairwise combination of these metrics (d-f) are shown. Vertical and horizontal lines represent median values. Points reflect individual tows and point size reflects the number of fish associated with a given tow.

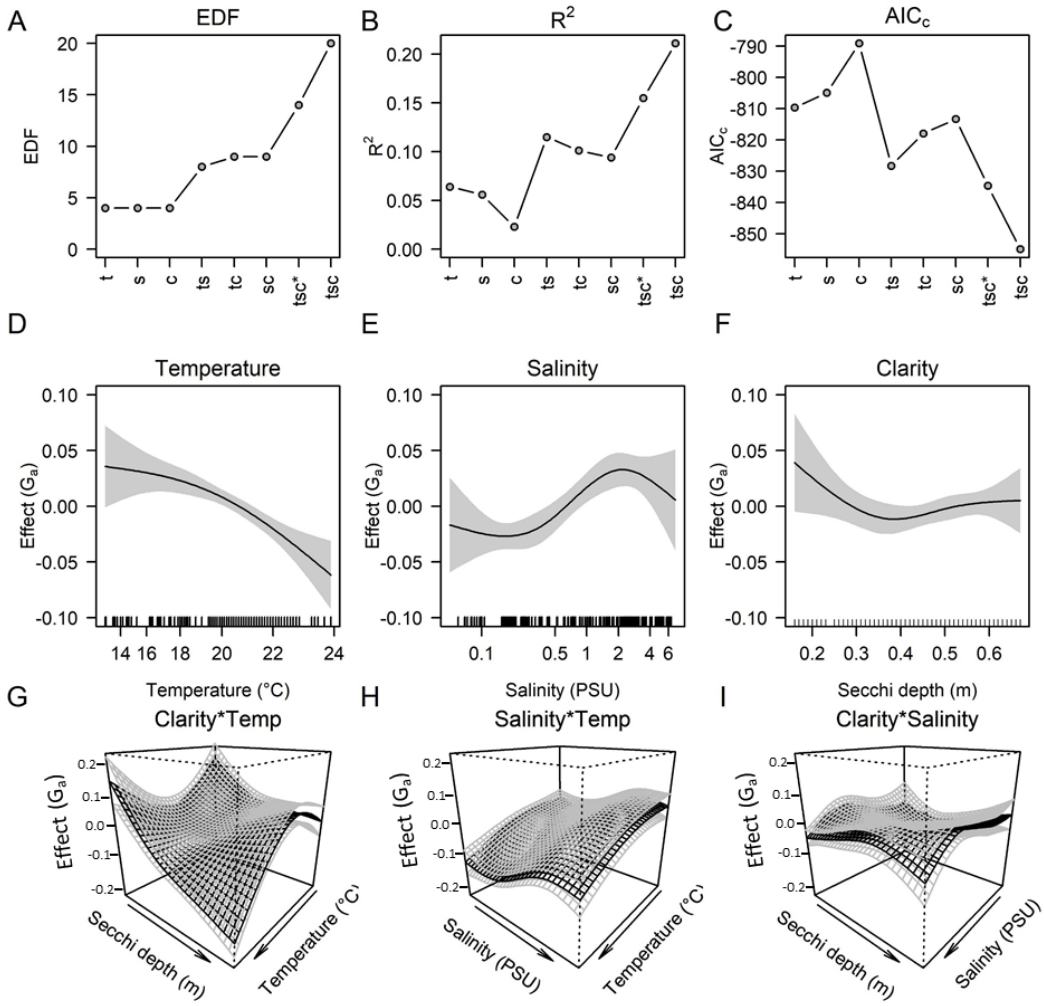

Figure 5: Results of the "environment-only" GAM examining variation in age-independent growth rates (Ga) of wild Delta Smelt as additive and interactive functions of the physical environmental attributes measured at capture ("environment-only models"). Model selection criteria, including (A) the estimated degrees of freedom (EDF), (B) coefficient of determination (R2), and (C) corrected Akaike Information Criterion (AICc) are shown for the univariate and fully interactive two-way and three-way subsets of models, along with the selected 2-way model without the 3-way interaction (tsc*)(t-temperature, s-salinity, c-clarity). Partial residual smooth plots of the main effects of temperature (D), salinity (E), and clarity (F) are shown along with the two-way interactive effects modeled as surfaces using tensor product smooths (G-I) for the selected tsc* model. Solid smooth lines indicate significant effects ($p < 0.05$), shading and errors bars reflects 95% confidence intervals. Light grey polygons (D-F) and surfaces (G-I) reflect the 95% Bayesian credible intervals. Note that x-axes in D-I are scaled according to respective transformations (Fig. 4). Additional models are described and compared in Fig. S2 in Supplement 3.

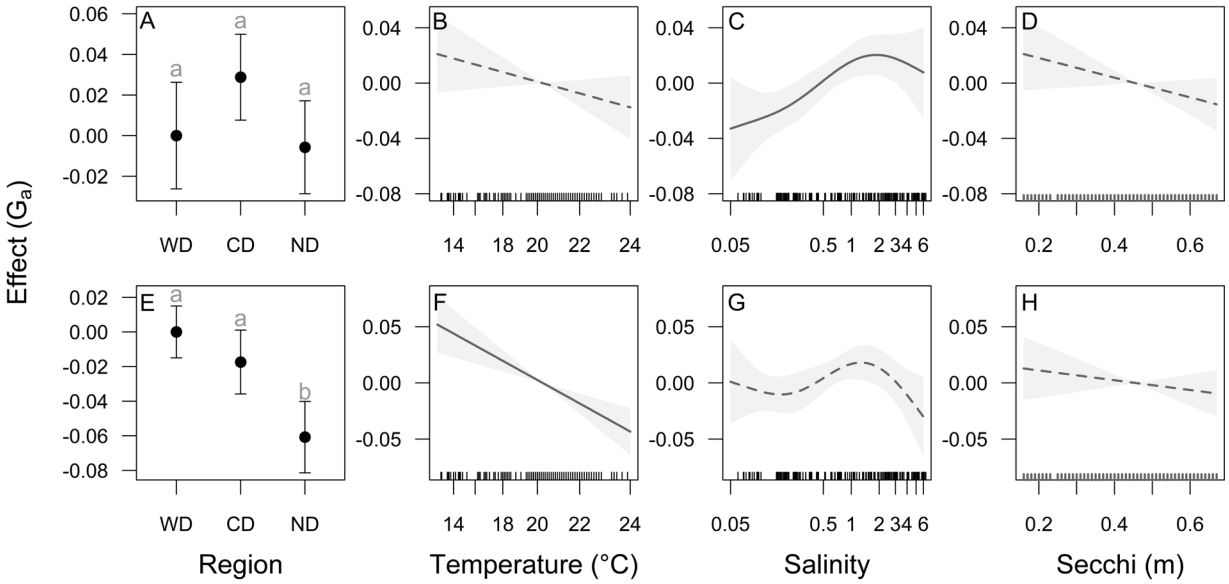

Figure 6: Results of the "global-regional" GAMs examining variation in Ga as a function of the fixed parametric effect of region (A), additive smooth effects of temperature (B), salinity (C), and clarity (D), while including a random year effect. Results of the same model when excluding the random year term are also provided (E-H, respectively). Regional effects (A,E) are represented by the parametric coefficients ± s.e., with letters indicating significant differences among regions ($p < 0.05$). Significant smooth effects are indicated by solid lines ($p < 0.05$), with shading indicating the 95% Bayesian credible intervals. Regions are as in Table 1. By including the random effect of year (A-D), variance associated with temperature was assigned to the year effect, and variance associated with regional differences was assigned to the year and salinity effects.

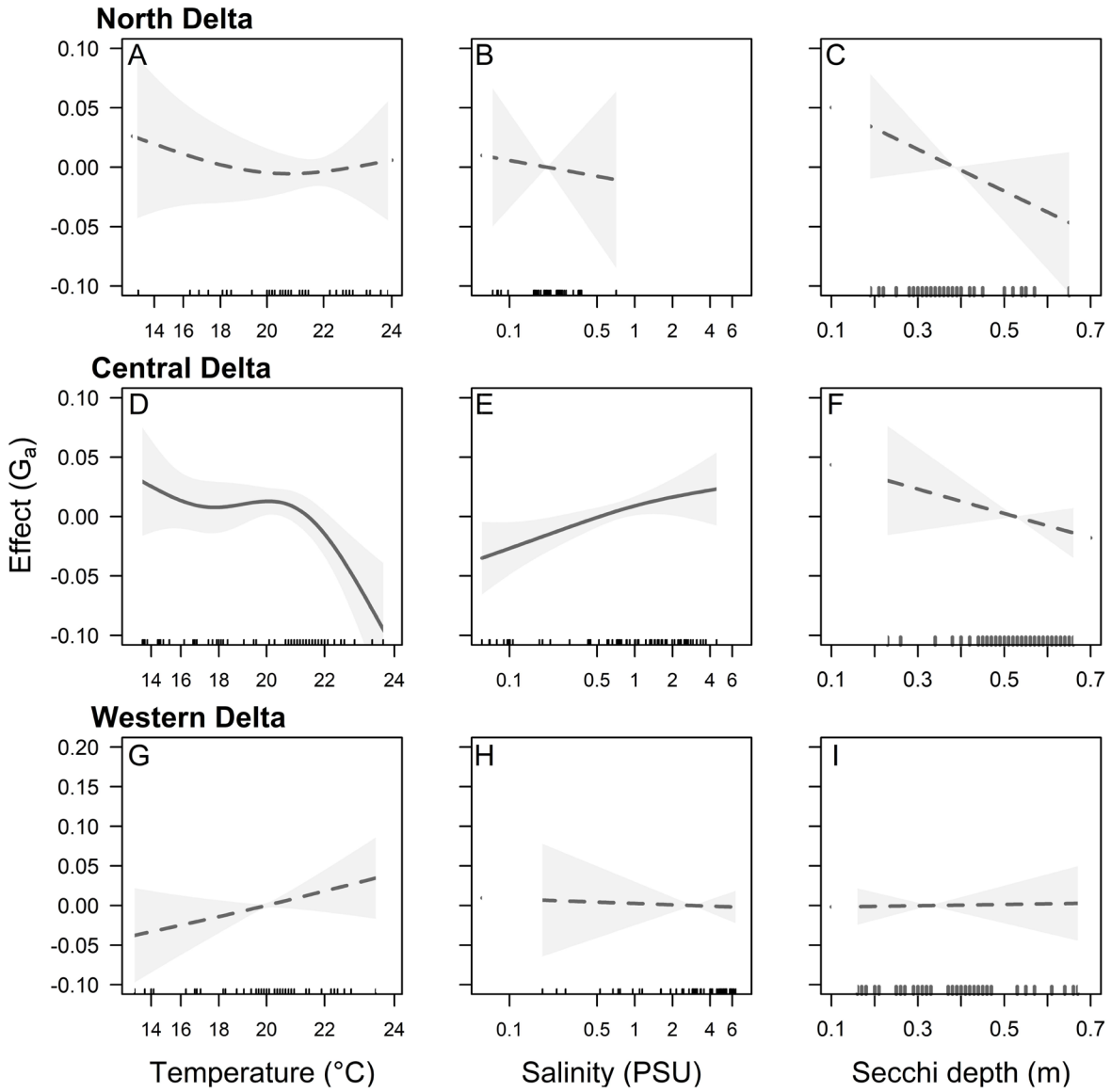

Figure 7. Results of separate "region-specific" GAMs examining variation in growth (Ga) as a function of the additive smooth effects of physical environmental attributes (temperature, salinity, and clarity) and the random year effect. Partial residual smooths demonstrating the effect of each environmental metric on the growth response are shown for the North Delta (A-C), Central Delta (D-F), and West Delta (G-I) regions of the upper SFE. Solid and dashed lines indicate significant and non-significant smooth trends ($\alpha = 0.05$), respectively, and shading reflects the 95% Bayesian credible intervals. Sample sizes are provided in Table 1.

SUPPLEMENTARY INFORMATION

Supplement 1. Field Collections of Delta Smelt and Methods Across Surveys

Archived Delta Smelt specimens were provided by several surveys conducted by the California Department of Fish and Wildlife (CDFW) and the U.S. Fish and Wildlife Service (USFWS). Surveys were conducted across a variety of spatial and temporal scales (Tables S1, S2) using several gear types. Surveys were designed with different purposes, but due to the conservation status of Delta Smelt, Delta Smelt were often preserved and archived for future analyses.

San Francisco Bay Study (SFBS)

The San Francisco Bay Study is conducted by the CDFW and surveys once a month throughout the year. The survey samples 52 sites from the southeastern bay up through the Delta. Each survey takes 7 days to complete. The survey uses a midwater trawl and bottom otter trawl. The midwater trawl has a 3.7 m^2 mouth and mesh size decreases from 20.3 cm at the mouth to 1.3 cm at the code end. The SFBS also uses a four-seam otter trawl with a 4.9-m headrope, a 2.5-cm stretch mesh body and a 13-mm stretch mesh cod end. Tows are conducted for 12 minutes (midwater trawl) and 5 minutes (otter trawl) (Honey et al. 2004).

Fall midwater trawl (FMWT)

The Fall Midwater Trawl survey is conducted by the CDFW during the months of September through December, once monthly. Each survey takes 8 days to complete. They sample 116 sites from San Pablo Bay up through the Lower Sacramento River and the Lower San Joaquin River. It uses the same midwater trawl net and trawling method as in the SFBS (Honey et al. 2004).

Summer Townet Survey (TNS):

The Summer Townet survey is conducted by the CDFW and samples every other week from June through August. The survey takes 5 days to complete and samples 32 locations from San Pablo Bay through the Lower Sacramento River and Lower San Joaquin River. The survey uses a 4.3m long net attached to a skid mounted frame with a 1.5m^2 mouth. Mesh size is20mm woven mesh for the 2.1 meters of the body of the net and 4mm for the 2.1m cod end. At each location, three 10-minute oblique tows are conducted, unless no fish are caught, in which case only two tows are completed (Honey et al. 2004).

Enhanced Delta Smelt Monitoring (EDSM)

The Enhanced Delta Smelt Survey is conducted by the USFWS between the months of July and November using a Kodiak Trawl towed for up to 10 minutes between 2 boats. EDSM surveys sample 24-37 random sites per week using a GRTS spatial sampling procedure (Stevens and Olsen 2004), with at least 2 tows conducted in each stratum. The Kodiak net has a 1.83m x 7.62m mouth Mesh ranges from 5.1cm at mouth to 0.3cm at cod end, which consists of a live box with baffles and flow holes to reduce mortality. Up to three crews sample concurrently at 2 or more sites per day with 2-8 tows per site (10 minutes max tow length). Towing ceases if at least 1 DS is caught in the first 2 tows.

Gear Evaluation Survey (GES)

The gear evaluation survey used a variety of nets and protocols of several other surveys in 2012-2013 to assess relative capture efficiencies for conversion of abundance estimates among gear types including the TNS, FMWT, SFBS, and EDSM Kodiak gears described above.

Covered Cod End survey (CCE)

Samples were conducted at two FMWT sites in the Sacramento Delta. They used the FMWT net and methodology with an additional fine mesh cover over the cod end to capture smaller fish. Surveys were conducted with paired surface tows and oblique tows with the goal of calculating the FMWT contact selectivity curves (Mitchell et al. 2017).

Table S1: Sample size of Delta Smelt included in this study by year and capture survey

Survey	2011	2012	2013	2014	2015	2016	2017	2018	2019	Total
CCE	0	0	0	83	0	0	0	0	0	83
EDSM	0	0	0	0	0	0	60	82	8	150
FMWT	29	14	0	3	4	3	0	0	0	53
GES	0	46	42	0	0	0	0	0	0	88
SFBS	2	0	0	0	19	0	0	0	0	21
TNS	28	12	4	7	1	0	12	0	0	64
Total	59	72	46	93	24	3	72	82	8	459

Table S2: Sample size of Delta Smelt included in this study by subregion (EDSM 2017 Strata) and survey.

EDSM Stratum	CCE	EDSM	FMWT	GES	SFBS	TNS	Total
Carquinez Straight and San Pablo Bay	0	0	3	0	0	2	5
Suisun Bay/Marsh	0	31	14	0	2	34	81
Lower San Joaquin	0	1	0	0	0	2	3
Lower Sacramento	63	55	26	88	19	11	262
Cache Slough/Liberty Island	20	33	10	0	0	15	78
Sac Deep Water Shipping Channel	0	30	0	0	0	0	30
Total	83	150	53	88	21	64	459

Table S3: Sample size of Delta Smelt included in this study by year and month

Year	Aug	Sep	Oct	Nov	Total
2011	30	12	7	10	59
2012	12	28	28	4	72

2013	4	33	0	9	46
2014	55	34	4	0	93
2015	10	13	1	0	24
2016	0	0	0	3	3
2017	31	17	21	3	72
2018	21	40	14	7	82
2019	3	2	3	0	8
Total	166	179	78	36	459

Fork Length Measurements

Of the 459 fish included in this study, 93% could be linked with fork lengths measured in the field. For those missing field measurements, lengths were measured post-preservation and converted into field lengths using standard conversion equations. For the 21 ethanol-preserved fish, field fork lengths were calculated as $FL_{Field} = 1.0225 * FL_{EtOH} + 0.3368$ (N = 175, R^2 = 0.994), based on shrinkage observed for a similar species (Longfin Smelt). The 13 fish preserved in liquid nitrogen were converted to field fork lengths using a previously published conversion for Delta Smelt: $FL_{Field} = 0.972 * FL_{LN} + 2.558$ (Teh et al. 2016).

References

Honey, K., Baxter, R., Hymanson, Z., Sommer, T., Gingras, M. and Cadrett, P., 2004. IEP long-term fish monitoring program element review. Interagency Ecological Program.

Mitchell, L., Newman, K. and Baxter, R., 2017. A Covered Cod-End and Tow-Path Evaluation of Midwater Trawl Gear Efficiency for Catching Delta Smelt (Hypomesus transpacificus). San Francisco Estuary and Watershed Science, 15(4).

Teh SJ, Baxa DV, Hammock BG, Gandhi SA, Kurobe T (2016) A novel and versatile flash-freezing approach for evaluating the health of Delta Smelt. Aquatic Toxicology 170:152–161.

Supplement 2. Variation in growth and water quality among years and regions

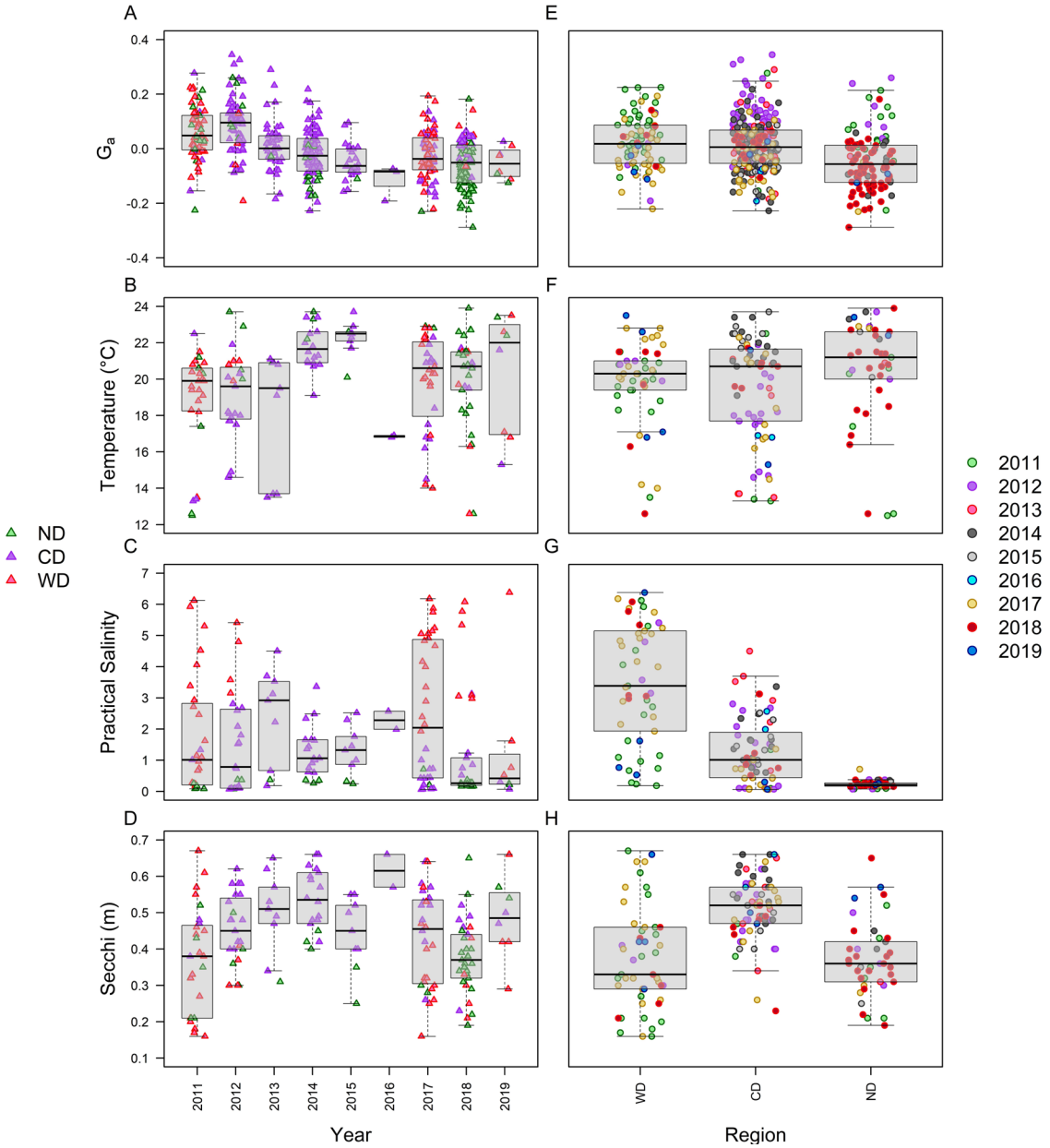

Figure S1. Temporal (A-D) and spatial (E-H) variation in age-adjusted growth rates (G_a , in log(mm/d)) of subadult Delta Smelt, along with variation in water quality including temperature, salinity, and Secchi depth (top-bottom, respectively) at capture. Colors indicate region (left legend, A-D) for temporal plots or year (right legend, E-H) or regional plots. Age-adjusted growth rates (G_a) are the residuals of the intrinsic model for Delta Smelt captured in August-November. Strata are as in Table 1 and Fig. 1.

Supplement 3. Environment-only Model Comparisons

We used generalized additive models (GAMs) to examine G_a as smooth functions of three physical water quality metrics: temperature (t) in ºC, practical salinity (s), and clarity (c) in m Secchi Depth (Table S4). Model structures were specified using the gam() function of the mgcv package in R, and the dredge function of the MuMIn package was used to conduct model comparisons and selection. Dredge evaluates the fully interactive model and then contrasts results among all simpler nested model structures, providing the coefficient of determination (R^2), estimated degrees of freedom (EDF), and corrected Akaike information criterion (AIC_c), which are commonly used to inform model selection (Fig. S2). The fully interactive model included a total of 7 terms including three main effects, the three 2-way tensor product smooths, and one 3-way tensor product smooth; however, all models including a 3-way interaction exhibited high concurvity (> 0.9) for many terms, and were thus excluded from further consideration. As is common, several models appeared similarly valid for describing the effects of abiotic environmental attributes on G_a. Here, Model 18 (tsc*), including each main effect and the three two-way interactions, was selected as the preferred model as it exhibited the lowest AIC_c, highest R^2, and allowed for visualization and comparison of each of the 2-way interaction surfaces.

Table S4: Generalized additive environment-only models constructed using the dredge function in the MuMIn R package. Factors include temperature (t), salinity (s), and clarity (c). Main and interactive effects were fit using ti() in the mgcv gam() package. The preferred model (Model 18) is identified with an asterisk (*).

Model Name	Model Structure
Model 1	$G_a \sim 1$
Model 2	$G_a \sim$ ti(t)
Model 3	$G_a \sim$ ti(s)
Model 4	$G_a \sim$ ti(c)
Model 5	$G_a \sim$ ti(t) + ti(s)
Model 6	$G_a \sim$ ti(t) + ti(c)
Model 7	$G_a \sim$ ti(s) + ti(c)
Model 8	$G_a \sim$ ti(t) + ti(s) + ti(c)
Model 9	$G_a \sim$ ti(t) + ti(c) + ti(t,c)
Model 10	$G_a \sim$ ti(t) + ti(s) + ti(s,c)
Model 11	$G_a \sim$ ti(s) + ti(c) + ti(t,s)
Model 12	$G_a \sim$ ti(t) + ti(s) + ti(c) + ti(t,c)
Model 13	$G_a \sim$ ti(t) + ti(s) + ti(c) + ti(s,c)
Model 14	$G_a \sim$ ti(t) + ti(s) + ti(c) + ti(t,s)
Model 15	$G_a \sim$ ti(t) + ti(s) + ti(c) + ti(t,c) + ti(s,c)
Model 16	$G_a \sim$ ti(t) + ti(s) + ti(c) + ti(t,s) + ti(s,c)
Model 17	$G_a \sim$ ti(t) + ti(s) + ti(c) + ti(t,s) + ti(t,c)
Model 18*	$G_a \sim$ ti(t) + ti(s) + ti(c) + ti(t,s) + ti(t,c) + ti(s,c)
Model 19	$G_a \sim$ ti(t) + ti(s) + ti(c) + ti(t,s,c)
Model 20	$G_a \sim$ ti(t) + ti(s) + ti(c) + ti(t,s) + ti(t,s,c)
Model 21	$G_a \sim$ ti(t) + ti(s) + ti(c) + ti(t,c) + ti(t,s,c)
Model 22	$G_a \sim$ ti(t) + ti(s) + ti(c) + ti(s,c) + ti(t,s,c)
Model 23	$G_a \sim$ ti(t) + ti(s) + ti(c) + ti(t,s) + ti(t,c) + ti(t,s,c)
Model 24	$G_a \sim$ ti(t) + ti(s) + ti(c) + ti(t,s) + ti(s,c) + ti(t,s,c)
Model 25	$G_a \sim$ ti(t) + ti(s) + ti(c) + ti(t,c) + ti(s,c) + ti(t,s,c)
Model 26	$G_a \sim$ ti(t) + ti(s) + ti(c) + ti(t,s) + ti(t,c) + ti(s,c) + ti(t,s,c)

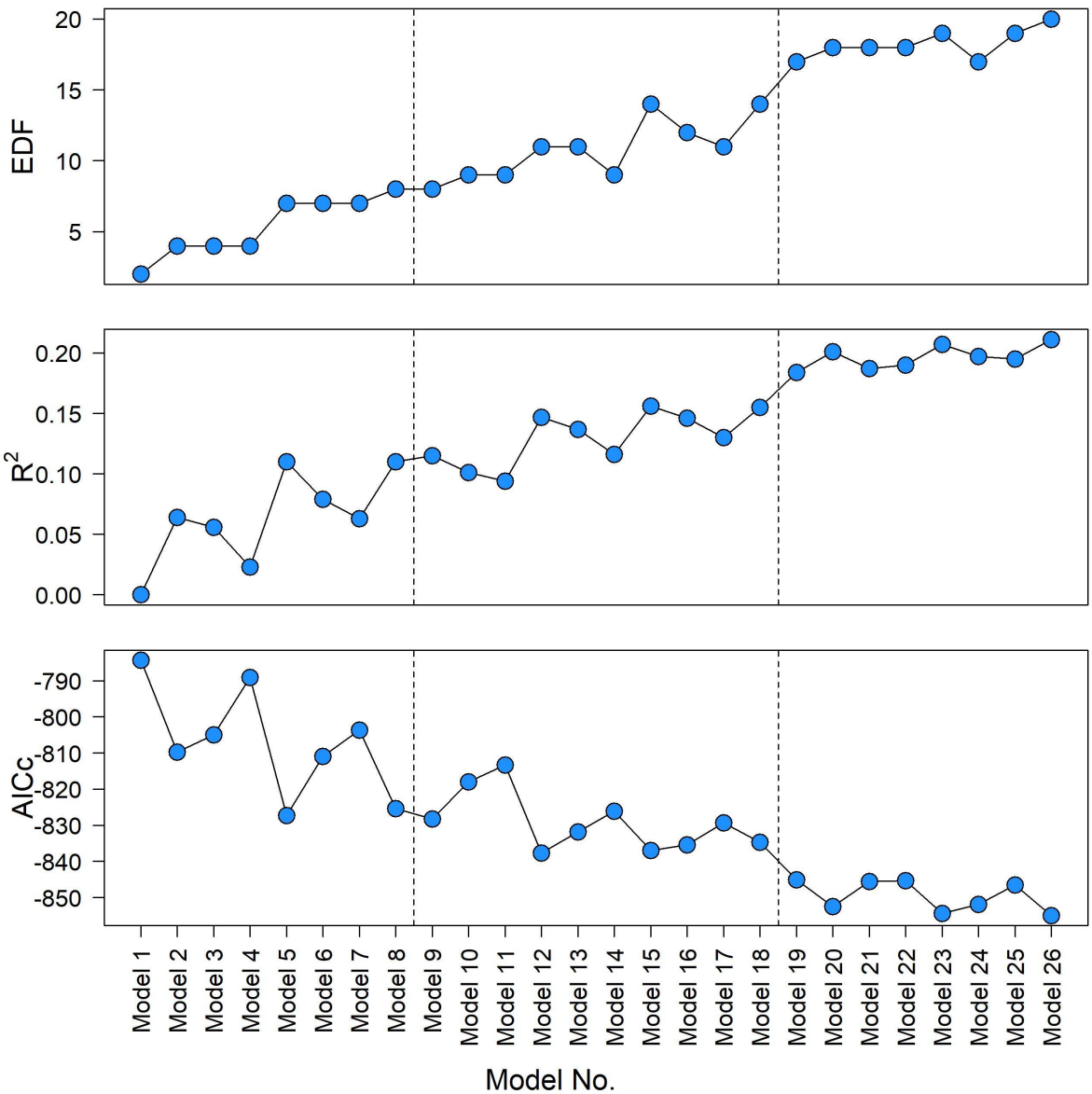

Figure S2: Estimated degrees of freedom (A), coefficient of determination (B), and corrected Akaike information criterion (C) for generalized additive models examining adjusted growth rates as additive and interactive effects of environmental conditions (temperature, salinity, and clarity) (Fig. Table S4). Models are ordered by the number of terms, generally increasing complexity from left to right. Vertical dashed lines delineate models including main effects only (left), two-way interactions (middle), and 3-way interactions (right).

Supplement 4. Model Evaluation

The assumptions of each model were evaluated using by examining normal Q-Q plots of residuals, plots of residuals versus estimated values, and histograms of the residuals for each model (left to right, respectively). (A) Models included the interactive tsc* (Model 18) environmental model (A), the model including additive effects of environment, region, and year (random) (B) and the three separate models examining responses to environmental conditions and year (random) for the North Delta, Central Delta, and West Delta (C-D, respectively). All models appeared to satisfy the assumptions of the approach.

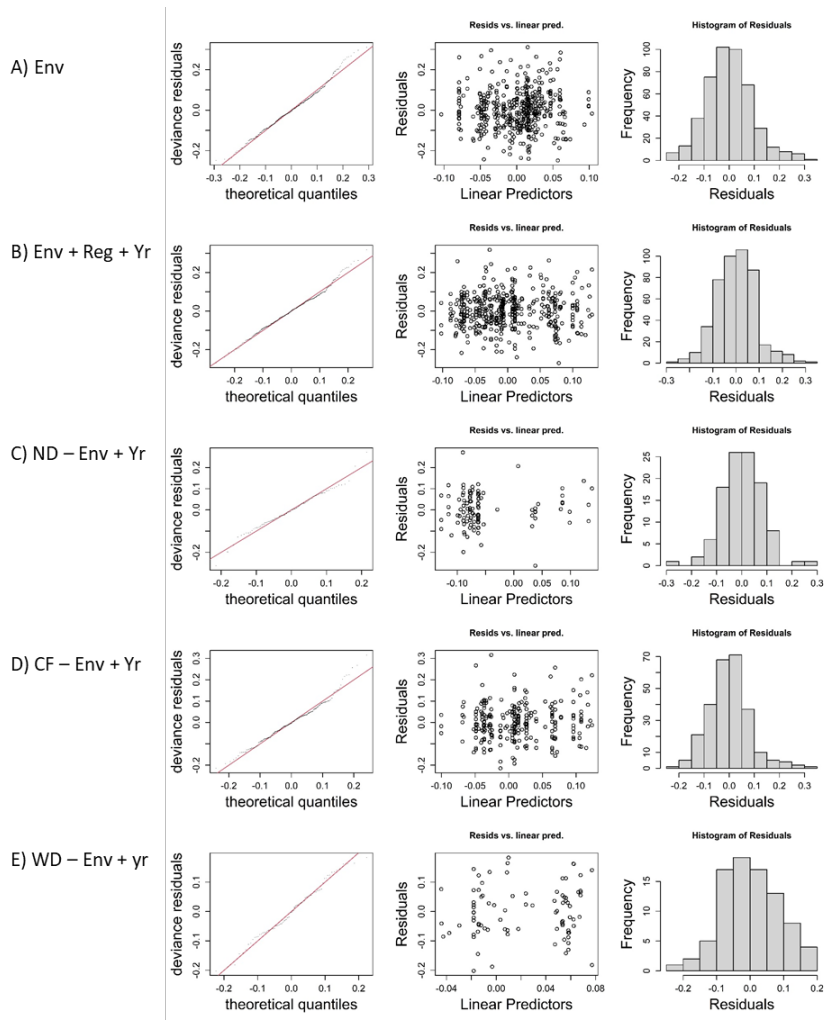

Figure S3: Evaluation of the assumptions associated with each generalized additive model: (A) the selected "environment-only" model with all main effects and two-way interactions (Model 18, tsc*), (B) the "global-regional" model with fixed parametric effects of region, the fixed smooths of temperature, salinity, and clarity, and the random effect of year, (C-E) the three "region-specific" models examining the fixed smooth effects of temperature, salinity, and clarity, and the random effect of year, for each region of the upper SFE, separately (ND, CF, and WD, respectively).

This page intentionally left blank

Chapter 5: Experimental Validation of Otolith-Based Size and Age Reconstructions Across Multiple Life Stages of a Critically Endangered Estuarine Fish

Submitted to *PeerJ*

Chapter 5: Otolith-Based Approaches Indicate Strong Effects of Environmental Variation on the Growth of a Critically Endangered Estuarine Fish

Experimental validation of otolith-based size and age reconstructions across multiple life stages of a critically endangered estuarine fish

Wilson Xieu[1], Feng Zhao[1], Rachel A. Fichman[1], Malte Willmes[2], James Hobbs[1], Tien-Chieh Hung[3], Luke Ellison[3], Troy Stevenson[3], Galen Tigan[3], Andrew A. Schultz[4], Levi S. Lewis[1*]

[1] Department of Wildlife, Fish and Conservation Biology, University of California Davis, Davis, CA, 95616
[2] Institute of Marine Sciences/NOAA Fisheries Collaborative Program, University of California Santa Cruz, Santa Cruz, CA, 95064
[3] Fish Conservation and Culture Laboratory, University of California Davis, Byron, CA 94514
[4] United States Bureau of Reclamation, Bay-Delta Office, Sacramento, CA 95814

* Corresponding Author: lewis.sci@gmail.com

Key Words: otolith, smelt, fish, estuarine, age, growth, validation, endangered

ABSTRACT

The application of otolith analyses to reconstruct the age, growth, and migration of fishes first requires taxon-specific validation of established aging protocols. The Delta Smelt (*Hypomesus transpacificus*) is an endangered fish endemic to the upper San Francisco Estuary (SFE). As a key indicator of the health of the SFE, understanding its vital rates and population dynamics can inform important management decisions. Otolith-based tools are being applied to a wide range of Delta Smelt life stages for which methods, assumptions, and inferences remain unvalidated, thus limiting confidence in otolith-derived metrics that are intended to inform important management decisions. Using known-age cultured individuals, we examined otolith formation, otolith-somatic proportionality, aging accuracy and precision, left-right symmetry, and the effects of image magnification for larval, juvenile, and adult Delta Smelt. In general, otolith size varied linearly with fish size (from 10-60 mm), explaining 99% of the variation in fish length, despite a unique slope for yolk-sac larvae < 10 mm. Aging precision among independent analysts was 98% and aging accuracy relative to known fish ages was 96%, with age estimates exhibiting negligible differences among left and right otoliths. Though error in days increased with age, percent error decreased from 0-30 dph, with precision remaining relatively high (≥ 95%) thereafter. Increased magnification (400x) further improved aging accuracy for the oldest, slowest-growing individuals. Results confirm that the otolith-based techniques described herein provide reliable age and size reconstructions for larval, juvenile, and subadult Delta Smelt. Such experimental assessments across multiple developmental stages are critical for assessing confidence in otolith-derived metrics used to inform our understanding of the dynamics of wild fish populations.

Keywords: otolith, fish, estuarine, freshwater, growth, validation, Delta Smelt, San Francisco

INTRODUCTION

Otoliths (ear stones) are paired calcium carbonate structures found in the inner ears of bony fishes (Pannella, 1971; Campana & Neilson, 1985). They accrete continuously throughout the life of a fish, are metabolically inert, and can preserve a permanent record of its age, hatch date, growth rate, and past environmental conditions (Campana, 1999; Starrs, Ebner & Fulton, 2016). Otoliths, therefore, can be used to reconstruct the life history and vital rates of fishes, thus improving our understanding of a species' population dynamics (Campana & Thorrold, 2001) and even movement patterns (Campana, 1999; Starrs, Ebner & Fulton, 2016). This is particularly important for developing effective management plans for imperiled species such as California's Delta Smelt (*Hypomesus transpacificus*), an estuarine osmerid fish that is endemic to the San Francisco Estuary. Delta Smelt exhibit an annual life cycle and a complex life-history (Moyle et al., 1992; Hobbs et al., 2019). Though historically abundant, the population has steeply declined since the 1980s, likely due to multiple factors including pollution, invasive species, habitat loss, hydrologic alterations (e.g., dams, channelization, and water exports), as well as changing environmental and climatic conditions (Feyrer, Nobriga & Sommer, 2007; Sommer et al., 2007; Moyle et al., 2016; Hobbs et al., 2017; Moyle, Hobbs & Durand, 2018). As a result, Delta Smelt are listed as threatened, endangered, and critically endangered under the federal Endangered Species Act (ESA), the California Endangered Species Act (CESA), and the International Union for Conservation of Nature (IUCN) Red List, respectively (U.S. Fish and Wildlife Service, 1993; CDFG, 2010; NatureServe, 2014).

The conservation status of Delta Smelt has resulted in numerous efforts to study and conserve the species, including setting limits on freshwater exports that directly and indirectly impact the Delta Smelt population through entrainment and habitat modification (Grimaldo et al., 2009; Sommer et al., 2011; Miller et al., 2012; Moyle, Hobbs & Durand, 2018; Hammock et al., 2019; Smith, Newman & Mitchell, 2020). Restrictions on water exports have placed Delta Smelt in the crossfire between conserving species and providing a stable water supply to California's 25 million southern residents and multi-billion dollar agriculture industry (Moyle, Hobbs & Durand, 2018). As a result, studies addressing the habitat needs and responses of Delta Smelt to natural and anthropogenic perturbations have become a priority focus for managers and researchers in the region (Hobbs et al., 2017). Key elements of this include quantifying the age structure, hatch dates, movement patterns, and growth rates of Delta Smelt, all of which can be obtained via otolith analysis.

To assess confidence in otolith-based reconstructions, validation of microstructure periodicity (accuracy), verification of the repeatability (precision), and consistency in otolith-somatic size relationships are necessary (Campana, 2001; Campana & Thorrold, 2001). This is critical for assessing the confidence of any study using otolith-based age and growth analyses. Daily ring deposition has been validated for many fish species including larval Delta Smelt (Miller & Storck, 1982; Campana, 2001; Roberts et al., 2004; Hobbs et al., 2007; Sakaris, Buckmeier & Smith, 2014). However, otolith-based approaches are now being applied to older life stages using updated protocols, none of which have been rigorously validated (Hobbs et al., 2019). With Delta Smelt on the brink of extinction, it is necessary to address increasingly

complex questions for a wider variety of life stages, thus requiring further assessment of the accuracy and precision of otolith-derived metrics.

Here, we expand upon previous work by experimentally evaluating multiple aspects of otolith-based techniques using age estimates by multiple independent analysts of a sample of cultured known-age larval, juvenile, and adult Delta Smelt (ages 0 to 271 dph). Specifically, we examined otolith-somatic proportionality, left-right symmetry, initial increment formation, accuracy, precision, and bias of age estimates, and the effects of image magnification for older, slower growing individuals. Results of this study are necessary for assessing confidence in past and future otolith-based age, growth, and geochemical studies that provide important metrics that inform population models and key policy and management decisions.

MATERIALS & METHODS

Known-age Delta Smelt were cultured in 2017-2018 at the UC Davis Fish Conservation and Culture Laboratory (FCCL) using standard methods approved by the UC Davis Institutional Animal Care and Use Committee Protocol No. 19747 (Lindberg et al., 2013). In short, eggs were fertilized and hatched, and larvae were reared in fresh water at 16 °C. Larval Delta Smelt were fed rotifers and *Artemia sp.* nauplii, ad libitum, with juvenile fish fed *Artemia sp.* Nauplii and Bio-Oregon Mash (pellet food) starting at 80 dph and weaned to only Bio-Oregon MASH at 120 dph. Fish were collected at 0, 5, 10, 30, 61, and 90 dph (n=20 per age class), euthanized in 500 mg/L MS-222, and preserved in 95% ethanol in 2018-2019. Sub-adult Delta Smelt were collected at 180, 215, 243, and 271 dph (n = 20 per age class), euthanized in 500 mg/L MS-222, and frozen at -20 °C in 2018. When feasible, a minimum of 10 fish were sampled from each age class for otolith analyses, thus allowing for otolith techniques to be evaluated across multiple life stages (Table 1).

Fish Length Measurements

Adults (≥ 180 dph) were imaged with a mounted Canon Powershot digital camera (Canon Solutions America Inc., Melville, New York, USA) and larvae (≤ 90 dph) were imaged at 20x magnification with an AmScope MU1000 10MP camera (AmScope, Irvine, California, USA) on a Leica StereoZoom7 dissecting microscope (Leica Camera Inc., Allendale, New Jersey, USA). All images included millimeter markers to facilitate image calibration and measurements. Digital measurements of standard length (SL), fork length (FL), and total length (TL) (Fig. 1A) were collected for each fish using ImageJ (version 1.8.0) (Abramoff, Magelhaes & Ram, 2006). Digital and hand measurements of standard length yield nearly identical measurements (mean difference = 0.57 mm or 1.08%) (Fig. S1 in Supplement 1, thus digital and hand measurements could be used interchangeably as needed. To correct for preservation effects (Fowler & Smith, 1983; Fey, 1999), fresh "corrected" standard lengths (SL_c) were calculated using empirical linear models developed in the laboratory for specimens that were preserved in 95% ethanol (SL_e, slope = 1.018, intercept = 0.952, R^2 = 0.977, n=35) or were frozen at -20 ºC (SL_z, slope = 1.018, intercept = 1.524, R^2 = 0.980, n=36) (Fig. S2 in Supplement 2).

Otolith Preparation

Sagittal otoliths from larval, juvenile, and adult Delta Smelt (Fig. 1A) were dissected and mounted using standard methods, adapted for the size of each age class. Otoliths from larvae were dissected using 30-gauge hypodermic needles and mounted on top of a drop of Loctite Super Glue and imaged with a drop of glycerin at 1000x magnification. Adults and juveniles were dissected using size 10 scalpel blades and super fine tip forceps. Prior to sanding and polishing, whole, intact otoliths of fish ≥ 180 dph were imaged at 40x magnification, while those of fish between 30-90 dph were imaged at 200x magnification. All whole otolith images were taken with an Amscope MU1000 10-Megapixel camera on an Olympus CH30 compound microscope. The rostrum-postrostrum and dorsal-ventral measurements were digitally measured using ImageJ (version 1.8.0). After imaging, otoliths were mounted in the sagittal plane to glass microscope slides using Crystal Bond thermoplastic glue and stored in plastic microscope slide boxes.

Mounted otoliths were wet sanded with 600, 800, and 1200 grit Buehler MicroCut silicon carbide paper and polished with 0.3-µm Buehler MicroPolish alumina on a Buehler Microcloth (Buehler, Lake Bluff, Illinois, USA) on the sulcus side, then flipped and sanded to expose the core and daily increments. All polished otoliths were imaged at 200x, with additional images captured at 400x magnification for 271 dph fish (Table 1). All images were taken using an Amscope MU1000 10MP camera on an Olympus CH30 compound microscope and stitched together using the photo merge function in Adobe Photoshop 2020 (v. 21.1.1). Left otoliths were initially sanded; however, if the left otolith was broken, lost, or of poor quality, the right otolith was prepared in its place. For the comparison of otolith symmetry, a subset of fish had both the left and right otoliths prepared: 90 dph (n=5) and 180 dph (n=5) age groups (Table 1). In total, 108 Delta Smelt (120 otoliths) were examined achieving approximately 10 samples in each age classes (Table 1) covering 0-271 dph and 5.93 to 56.75 mm in standard length.

Otolith Age and Growth Analyses

The quality of each otolith image was ranked on a scale of 0 to 3 (low to high, respectively) based on the clarity of the core and edge increments, with only quality 2 and 3 otoliths used in analyses. All otoliths were analyzed with ImageJ by three independent analysts without prior knowledge of each fish's age. Images were calibrated from pixels to µm using a stage micrometer. Increments were counted from the core to the dorsal edge, which provided the most consistent and clear age trajectory on the otolith (Hobbs et al., 2007) (Fig. 1B). A distinct hatch mark, indicating the moment larvae emerge from eggs into the ambient environment, was observable in each otolith as a thick, dark band approximately 8 µm from the core. This was used to identify the first daily increment from which the growth profile was constructed for each otolith (Fig. 1B).

Accuracy

Accuracy was quantified to assess how well otolith-based age estimates reflect the known ages of cultured Delta Smelt. Error in accuracy (EA_{fi}) of a given age estimate for a given fish,

reflecting both accuracy and bias (in days), was calculated as the raw deviation from the known age of the fish:

Equation 1: $EA_{fi} = a_{fi} - \widehat{a_f}$

where a_{fi} is the *i*th age estimate and $\widehat{a_f}$ is the known age of the *f*th fish. Percent error in accuracy (PEA_{fi}) of a given age estimate, an age-normalized estimate of the absolute error, was calculated as 100 times the ratio of the absolute error and the known age of the *f*th fish.

Equation 2: $PEA_{fi} = \frac{|EA_{fi}|}{\widehat{a_f}} * 100$

Precision

Precision was quantified to assess the reproducibility of repeated age estimates among the three independent analysts (Campana, 2001). Error in precision (EP_{fi}) of a given age estimate for a given fish was calculated as the raw deviation (in days) from the mean age estimate of the fish:

Equation 4: $EP_{fi} = a_{fi} - \overline{a_f}$

where $\overline{a_f}$ is the mean age estimate for the *f*th fish. Percent error in precision (PEP_{fi}) for a given fish, an age-normalized estimate of the absolute inter-operator error, was calculated as 100 times the ratio of the absolute precision error and mean age estimate of a given fish:

Equation 5: $PEP_{fi} = \frac{|EP_f|}{\overline{a_f}} * 100$

Statistical Analyses

First, to describe the general somatic growth curve for cultured Delta Smelt, size-at-age was modeled using a Gompertz growth function with the known ages (t – time in days-post-hatch) of cultured fish and their standard lengths (SL_c) where μ is absolute growth rate at inflection, A is the upper asymptote, and λ is the lag time (Eqn. 6). Fish size was then contrasted with otolith size using linear regression to assess otolith-size to fish-size (OS-FS) proportionality.

Equation 6: $SL_c \sim A * e^{-e^{\left(\frac{\mu * e}{A}\right)(\lambda - t) + 1}}$

Next, to examine the additive and interactive contributions of analyst identity, otolith side, and fish age on the accuracy (*PEA*) of otolith-based age estimates, a subset of larval (90 dph, n = 5) and sub-adult (180 dph, n = 5) Delta Smelt were selected to have both the left and right otoliths analyzed. Both otoliths from each fish were aged by each of the three analysts, and a linear model was constructed to examine the additive and interactive effects of analyst identity (*I*), otolith side (*O*), and age class (*A*) on the accuracy (*PEA*) of ages estimates:

Equation 7: PEA ~ $I + O + A + I*O + I*A + O*A + I*O*A$

To examine the interactive effects of microscope magnification and analyst identity on the accuracy (*PEA*) of otolith-based age estimates for the oldest, slowest growing individuals (with the smallest rings), one otolith for each of the age-271 dph Delta Smelt (N=9) was imaged at both 200x and 400x magnification, with both images being aged by each of the three analysts, and a linear model was constructed to examine the additive and interactive effects of analyst identity (*I*) and image magnification (*M*) on the accuracy (*PEA*) of ages estimates:

Equation 8: PEA ~ $M + I + M*I$

All ordination and modeling were conducted in the R software environment version 3.6.3 (R Core Team, 2019). The Gompertz model was fit using the "nls" function, which determines the nonlinear (weighted) least-squares estimates of the parameters of a nonlinear model. Models were run and compared using maximum likelihood estimation while assuming a Gaussian distribution. Model assumptions were examined using Q-Q and residual plots. Likelihood ratio tests were used to assess the significance of each model relative to the null model (intercept only) with $\alpha = 0.05$.

RESULTS

Somatic and Otolith Growth

The Gompertz growth model provided a reasonable fit to size-at-age of cultured Delta Smelt ($A = 1.769$, $\mu = 0.0089$, $\lambda = -79.4$, $R^2 = 0.993$), using $\log_{10}(SL)$ to fit model assumptions (Fig. 2A, Fig. S2 in Supplement 2). Overall, otolith size varied strongly and linearly with fish size (slope = 0.070 ± 0.001, intercept = 6.84, $R^2 = 0.988$), indicating that otolith growth is generally proportional to fish growth across most size classes examined (Fig. 2B). Inspection of the smallest larval size classes, however, indicated an inflection at approximately 10 mm SL (otolith radius = 18.96 µm), with newly-hatched yolk-sac larvae < 10 mm (~ 10 dph) exhibiting a steeper slope of 2.85 ± 0.03, and all older individuals exhibiting a constant slope of 0.068 ± 0.001, similar to the global slope (Supplement 3). Delta Smelt otoliths exhibited single primordia with core sizes (otolith radius at hatch) of 8.5 ± 1.5 µm (mean ± s.d.) (Fig. 2C), corresponding with a size-at-hatch of 5.93 ± 0.5 mm (mean ± s.d.) standard length. Otolith growth profiles exhibited ontogenetic variation in accretion rates, with slower rates of 1-2 µm/d for fish < 30 dph, increasing to over 8 µm/d in 50-100 dph fish, followed again by a gradual decrease back to 2 µm/d as fish matured toward 270 dph (Fig. 2D).

Accuracy and Precision

Error in accuracy decreased from 0 to -10 days as age increased from 5 to 271 dph, indicating negative bias in older specimens (Fig. 3A). Absolute percent error in accuracy declined from 20% to 2% in fishes of age 5-90 dph, increasing to 3-4% in older 245-271 dph fish

(Fig. 3B). Due to the sensitivity of percent error to small deviations in fish < 10 dph, mean error and percent error in accuracy and precision were only contrasted for fish ≥ 10 dph. Mean EA and PEA across all age classes (10-271 dph) and the three analysts were -3.6 days and 3.9%, respectively, and values for each were similar among analysts (Fig. 4a-b). Mean percent error in precision across all age classes and analysts was 2.2% (Fig. 4c), and also was similar among analysts. These errors correspond with relatively high accuracy (96.1%) and precision (97.8%), thus confirming the proper identification of the hatch mark and first increment, daily periodicity of increment formation, and both accurate and repeatable age estimation by multiple independent analysts.

Effects of Otolith Symmetry, Image Magnification, and Life Stage on Aging Accuracy Among Analysts

The 90-dph and 180-dph fish for which both otoliths were analyzed exhibited mean error (PEA) of 1-2%, which did not vary as additive or interactive functions of life stage, otolith side, or analyst (Table 2, Fig. 5). For the oldest fishes examined (271 dph), however, error was often biased 7-10 days lower than the known age (Fig. 4A), suggesting that the smaller increments in these slower-growing specimens were often inconspicuous and overlooked. Re-imaging of older specimens at higher magnification (400x versus 200x) yielded significant improvement in age estimates for older fish, reducing mean bias to 0.25% (Table 3, Fig. 5).

DISCUSSION

Experimental Validation of Otolith-based Metrics

Validation studies are essential for assessing confidence in otolith-derived metrics (Campana, 1990, 2001). Our results build upon prior work to refine and expand our understanding of the accuracy and precision of otolith-based tools for a critically endangered estuarine fish. Using cultured, known-age specimens and multiple independent analysts, we demonstrated daily periodicity of increment formation and high accuracy and precision of age estimates. Left-right otolith symmetry indicated that either otolith can be utilized, and increased magnification improved aging precision, indicating that otolith approaches can be applied to older fish with slower accretion rates. In aggregate, our results indicate that the application of otolith-based techniques to archived collections of Delta Smelt can yield repeatable, accurate, and valuable estimates of the hatch dates, age structure, growth rates, and timing of movements (when paired with otolith chemistry) across life stages (Hobbs et al., 2007, 2019). Such experimental approaches using multiple independent analysts and known-age specimens across key developmental stages can greatly improve confidence in otolith-derived metrics that are valuable for informing resource management and species conservation.

Interpretation of Otolith Microstructures

For many fish species, the first otolith increment is visible following a dark, thick “hatch check” which is assumed to form when larvae emerge from eggs into the ambient environment

(Campana & Neilson, 1985; Ohama, 1990). However, verification of the timing of such features is necessary to facilitate accurate age reconstructions for each species. For example, features identified as hatch checks may correspond with other processes, such as the end of the yolk-sac stage or first-feeding (Moksness, 1992; Sepulveda, 1994; Hirose & Kawaguchi, 2001), and embryonic rings can form prior to hatch and with unknown periodicity (Stevenson & Campana, 1992). In Delta Smelt otoliths, a distinct hatch check was consistently observed at approximately 8-9 µm from the center of the otolith primordium. We also observed embryonic rings of unknown periodicity that are generally excluded from increment analyses (Stevenson & Campana, 1992). Following the hatch check, increments were accreted daily as evidenced by strong agreement between increment counts and known ages of each fish. Though the first observations of Delta Smelt otoliths suggested that increments first formed at 5 dph (Hobbs et al., 2007), we believe this was likely due to the lower quality of images used (e.g., 1 versus 10 megapixels) that obscured the first and smallest larval increments. Thus, Delta Smelt exhibit clear microstructures including a single primordium, a prominent hatch check, and daily increments that, together, facilitate accurate reconstructions of hatch dates and size-at-age.

Otolith-Somatic Proportionality

A simple linear model indicated that > 99% of the variation in fish size (SL) could be explained by otolith size across the full range of age classes examined (0-271 dph). This result indicated that, for Delta Smelt, otolith-somatic proportionality is largely constant—a key assumption of standard models used to estimate size and growth rates from otolith radii and accretion rates, respectively (Campana, 1990). Closer inspection of otolith-somatic proportionality immediately after hatch (e.g., fish < 10 mm or 10 dph), however, indicated that pro-larvae exhibited rapid somatic growth despite low rates of otolith accretion; a phenomenon also observed in early otolith work on Delta Smelt larvae (Hobbs et al., 2007). During this period, larval elongation (growth) was proportional to otolith growth, but with a much higher slope relative to that of fish > 10 mm (Supplement 3). During this early larval period, fish are largely reliant on endogenous sources of nutrition (e.g., yolk and oil globule) (Mager et al., 2004). At approximately 10 dph, when endogenous reserves are exhausted and larvae become dependent on exogenous feeding (Mager et al., 2004) the somatic-otolith relationship decreased abruptly and remained constant thereafter for all age classes (i.e., 10-271 dph). This short-lived discontinuity in slopes had little influence on the overall somatic-otolith relationship ($m = 0.068$ vs 0.070) for estimating the growth of older life stages, but would be important for otolith-based growth and size estimates for the youngest larvae. Thus otoliths of Delta Smelt exhibited constant proportionality for all exogenously feeding life stages (10-271 dph), verifying their use in back-calculating individual growth histories (Campana, 2001; Hobbs et al., 2007).

Accuracy and Precision of Otolith-based Age Estimates

Validation experiments can be exceptionally challenging for sensitive, critically endangered species such as Delta Smelt. Here, we leveraged on-going efforts by the UC Davis Fish Conservation and Culture Laboratory to maintain a captive population of Delta Smelt for both conservation and research purposes, which provided unique opportunity to build an archive

of otoliths from known-age individuals across multiple age classes. that could be used to assess the accuracy and repeatability otolith-based size and age reconstructions. Using known-age cultured fish and multiple independent analysts, we demonstrated relatively high (> 95%) accuracy and precision of otolith-based age estimates for Delta Smelt.

Obtaining high accuracy and precision in otolith age estimates requires finely calibrated otolith preparation and imaging protocols, and subsequent training of analysts, to facilitate clear and accurate interpretations of daily increments. As for many fishes (Stevenson & Campana, 1992), with careful preparation, daily increments can be observed in otoliths of Delta Smelt as fine rings (microstructures) that exhibit a consistent and readily-interpretable appearance. Poor preparation, however, can result in multi-day check marks or smaller sub-daily rings that generate systematic bias in age and growth reconstructions. For example, under-sanding can result in thick samples that emphasize larger multi-day checks that obscure the true daily increments, while over-sanding can result in extra thin samples that emphasize sub-daily otolith features or image artifacts that occur at a higher frequency than the true daily increments. For these reasons, archives of known-age specimens are needed, proper quality assurance and control (QAQC) procedures should be employed, and only high-quality preparations and highly trained analysts should be used in otolith-based studies of wild populations, where precision is assessed but accuracy is often assumed (Campana, 1990; Hobbs et al., 2019).

Otolith Symmetry

Paired otoliths in fishes may exhibit varying degrees of asymmetry (Lychakov et al., 2006, 2008; Díaz-Gil et al., 2015). Symmetrical otoliths can be valuable for studying rare species, where each specimen is highly valuable. For example, to control for potential effects of asymmetry (Mahé et al., 2019), otolith protocols often use only left or right otoliths, replacing entire specimens if the selected otolith is lost, damaged, or otherwise unusable for growth analysis. For valuable specimens of endangered species; however, each specimen is difficult to replace, thus the use of either otolith (e.g., if the preferred otolith is lost or damaged) is often valuable, when shown to be appropriate (Hobbs et al., 2007, 2019). If left and right otoliths exhibit systematic asymmetrical accretion patterns, however, this can greatly affect otolith-based inferences when otolith side cannot be standardized. Here, we showed that age estimates from paired left and right Delta Smelt otoliths were similar, with no evidence for differences in accuracy or precision. These results suggest that reliable age and growth estimates can be constructed from either left or right otoliths of Delta Smelt.

Image Magnification

During QAQC of image quality, older Delta Smelt specimens (e.g., 271 dph) often exhibited increment compaction toward the otolith edge, indicative of the ontogenetic reduction of growth rate in older fish. These rings were occasionally flagged as “low quality” by analysts due to their poor appearance when imaged at 200x magnification. Though these samples exhibited acceptable percent precision and accuracy (~ 95%), the increase in the raw daily error rate and consistent negative aging bias for these older individuals indicated that the finest daily rings were often missed by each analyst for these slow-growing specimens. By re-imaging the

otoliths from the oldest 271 dph fish at twice the magnification (400x) and re-analyzing the microstructures, the accuracy of age estimates increased significantly and exhibited no measurable bias. Though higher-resolution imaging requires additional time and computing power for capturing, storing, and processing larger datafiles, our results indicate that this additional effort significantly improved otolith-based age and growth estimates for subadult Delta Smelt.

Cultured Versus Wild Fish

The use of cultured fish was valuable for providing known-age specimens to verify the interpretation of otolith microstructures; however, increment patterns in wild populations could be more complex than those in controlled laboratory environments (Campana, 2001). For example, environmental variability may influence otolith shape, increment appearance, or the timing of the first increment (Campana & Casselman, 1993; Otterlei, 2002; Vignon & Morat, 2010). Standard back-calculation tools such as the Biological Intercept Model, however, explicitly account for individual variation in otolith shape by adjusting growth estimates for individual somatic-otolith relationships (Campana, 1990), and prior work has indicated that such variation is likely negligible for reconstructing size-at-age in Delta Smelt ≤ 90 mm (Hobbs et al., 2007). Nevertheless, future studies should examine if and how otolith-based size and growth estimates might vary between wild and cultured specimens, and in relation to environmental variability.

CONCLUSIONS

Assessments of the accuracy and repeatability of schlerochronological reconstructions are key to their application in science and management. For fishes, otolith-derived metrics such as hatch dates, growth rates, and migration patterns provide valuable data for evaluating factors that are likely to impact the recovery of endangered species. For Delta Smelt, we experimentally demonstrated that otoliths provide accurate and precise estimates of individual size, age, growth, and phenology—each of which are likely to be impacted by changes in water management, local environmental conditions, and the regional climate. Furthermore, we demonstrated this across multiple life stages, left and right otoliths, and image resolutions. Such experimental approaches greatly improve the interpretation of otolith-derived metrics for fisheries ecology and conservation, facilitating valuable reconstructions of hatch dates, growth rates, and movement patterns of wild fish populations.

ACKNOWLEDGEMENTS

We thank the many staff of UC Davis Fish Conservation and Culture Laboratory for their assistance in rearing and archiving known-age Delta Smelt for this study. The UC Davis Department of Wildlife, Fish, and Conservation Biology (N. Fangue) and Center for Aquatic Biology and Aquaculture (L. Deanovic) provided laboratory space and logistical support. Constructive reviews from N. Bertrand and several anonymous reviewers greatly improved the

manuscript. Otolith archives were maintained in accordance with an approved California Department of Fish and Wildlife Service Section 2081a Memorandum of Understanding. This work was funded by the U.S. Bureau of Reclamation Grant # R17AC00129. The views expressed herein are those of the authors and do not represent the official opinion of any employer, institution, or government agency.

REFERENCES

Abramoff MD, Magelhaes PJ, Ram SJ. 2006. Image Processing with ImageJ. In: *Optical Imaging Techniques in Cell Biology*. CRC Press, 249–258. DOI: 10.1201/9781420005615.ax4.

Campana SE. 1990. How Reliable are Growth Back-Calculations Based on Otoliths? *Canadian Journal of Fisheries and Aquatic Sciences* 47:2219–2227. DOI: 10.1139/f90-246.

Campana SE. 1999. Chemistry and composition of fish otoliths: pathways, mechanisms and applications. *Marine Ecological Progress Series* 188:263–297.

Campana SE. 2001. Accuracy, precision and quality control in age determination, including a review of the use and abuse of age validation methods. *Journal of Fish Biology* 59:197–242. DOI: 10.1006/jfbi.2001.1668.

Campana SE, Casselman JM. 1993. Stock Discrimination Using Otolith Shape Analysis. *Canadian Journal of Fisheries and Aquatic Sciences* 50:1062–1083. DOI: 10.1139/f93-123.

Campana SE, Neilson JD. 1985. Microstructure of Fish Otoliths. *Canadian Journal of Fisheries and Aquatic Sciences* 42:1014–1032. DOI: 10.1139/f85-127.

Campana SE, Thorrold SR. 2001. Otoliths, increments, and elements: keys to a comprehensive understanding of fish populations? *Canadian Journal of Fisheries and Aquatic Sciences* 58. DOI: https://doi.org/10.1139/f00-177.

CDFG. 2010. State & federally listed endangered & threatened animals of California. California Department of Fish & Game,State of California, The Natural Resources Agency, California. *The Natural Rsources Agency, California*.

Díaz-Gil C, Palmer M, Catalán IA, Alós J, Fuiman LA, García E, Gil M del M, Grau A, Kang A, Maneja RH, Mohan JA, Morro B, Schaffler JJ, Buttay L, Riera-Batle I, Tolosa B, Morales-Nin B. 2015. Otolith fluctuating asymmetry: a misconception of its biological relevance? *ICES Journal of Marine Science* 72:2079–2089. DOI: 10.1093/icesjms/fsv067.

Fey DP. 1999. Effects of preservation technique on the length of larval fish: Methods of correcting estimates and their implication for studying growth rates. *Archive of Fishery and Marine Research* 47:17–29.

Feyrer F, Nobriga ML, Sommer TR. 2007. Multidecadal trends for three declining fish species: Habitat patterns and mechanisms in the San Francisco Estuary, California, USA. *Canadian Journal of Fisheries and Aquatic Sciences* 64:723–734. DOI: 10.1139/F07-048.

Fowler GM, Smith SJ. 1983. Length Changes in Silver Hake (Merluccius bilinearis) Larvae: Effects of Formalin, Ethanol, and Freezing. *Canadian Journal of Fisheries and Aquatic Sciences* 40:866–870.

Grimaldo LF, Sommer T, Van Ark N, Jones G, Holland E, Moyle PB, Herbold B, Smith P. 2009. Factors Affecting Fish Entrainment into Massive Water Diversions in a Tidal Freshwater

Estuary: Can Fish Losses be Managed? *North American Journal of Fisheries Management* 29:1253–1270. DOI: 10.1577/m08-062.1.

Hammock BG, Moose SP, Solis SS, Goharian E, Teh SJ. 2019. Hydrodynamic Modeling Coupled with Long-term Field Data Provide Evidence for Suppression of Phytoplankton by Invasive Clams and Freshwater Exports in the San Francisco Estuary. *Environmental Management* 63:703–717. DOI: 10.1007/s00267-019-01159-6.

Hirose T, Kawaguchi K. 2001. Daily otolith increments and growth of reared chika Hypomesus japonicus larvae. *Bulletin of the Japan Sea National Fisheries Research Institute*:141–144.

Hobbs JA, Bennett WA, Burton JE, Baskerville-Bridges B. 2007. Modification of the biological intercept model to account for ontogenetic effects in laboratory-reared delta smelt (Hypomesus transpacificus). *Fishery Bulletin* 105:30–38.

Hobbs JA, Lewis LS, Willmes M, Denney C, Bush E. 2019. Complex life histories discovered in a critically endangered fish. *Scientific Reports* 9:1–12. DOI: 10.1038/s41598-019-52273-8.

Hobbs JA, Moyle PB, Fangue N, Connon RE. 2017. Is Extinction Inevitable for Delta Smelt and Longfin Smelt? An Opinion and Recommendations for Recovery. *San Francisco Estuary and Watershed Science* 15:1–19. DOI: 10.15447/sfews.2017v15iss2art2.

Lindberg JC, Tigan G, Ellison L, Rettinghouse T, Nagel MM, Fisch KM. 2013. Aquaculture Methods for a Genetically Managed Population of Endangered Delta Smelt. *North American Journal of Aquaculture* 75:186–196. DOI: 10.1080/15222055.2012.751942.

Lychakov DV, Rebane YT, Lombarte A, Demestre M, Fuiman LA. 2008. Saccular otolith mass asymmetry in adult flatfishes. *Journal of Fish Biology* 72:2579–2594. DOI: 10.1111/j.1095-8649.2008.01869.x.

Lychakov DV, Rebane YT, Lombarte A, Fuiman LA, Takabayashi A. 2006. Fish otolith asymmetry: Morphometry and modeling. *Hearing Research* 219:1–11. DOI: 10.1016/j.heares.2006.03.019.

Mager RC, Doroshov SI, Van Eenennaam JP, Brown R. 2004. Early Life Stages of Delta Smelt. In: *Early Life History of Fishes in the San Francisco Estuary and Watershed*. American Fisheries Society, 296.

Mahé K, Ider D, Massaro A, Hamed O, Jurado-Ruzafa A, Gonçalves P, Anastasopoulou A, Jadaud A, Mytilineou C, Elleboode R, Ramdane Z, Bacha M, Amara R, de Pontual H, Ernande B. 2019. Directional bilateral asymmetry in otolith morphology may affect fish stock discrimination based on otolith shape analysis. *ICES Journal of Marine Science* 76:232–243. DOI: 10.1093/icesjms/fsy163.

Miller WJ, Manly BFJ, Murphy DD, Fullerton D, Ramey RR. 2012. An Investigation of Factors Affecting the Decline of Delta Smelt (Hypomesus transpacificus) in the Sacramento-San Joaquin Estuary. *Reviews in Fisheries Science* 20:1–19. DOI: 10.1080/10641262.2011.634930.

Miller SJ, Storck T. 1982. Daily Growth Rings in Otoliths of Young-of-the-Year Largemouth Bass. *Transactions of the American Fisheries Society* 111:527–530. DOI: 10.1577/1548-8659(1982)111<527.

Moksness E. 1992. Validation of daily increments in the otolith microstructure of norwegian spring-spawning herring (Clupea harengus l.). *ICES Journal of Marine Science* 49:231–235.

Moyle PB, Brown LR, Durand JR, Hobbs JA. 2016. Delta smelt: Life history and decline of a once abundant species in the San Francisco Estuary. *San Francisco Estuary and Watershed Science* 14:1–30. DOI: 10.15447/sfews.2016v14iss2art6.

Moyle PB, Herbold B, Stevens DE, Miller LW. 1992. Life History and Status of Delta Smelt in the Sacramento-San Joaquin Estuary, California. *Transactions of the American Fisheries Society* 121:67–77. DOI: 10.1577/1548-8659(1992)121<0067:LHASOD>2.3.CO;2.

Moyle PB, Hobbs JA, Durand JR. 2018. Delta Smelt and Water Politics in California. *Fisheries* 43:42–51. DOI: 10.1002/fsh.10014.

NatureServe. 2014. Hypomesus transpacificus (errata version published in 2020). *The IUCN Red List of Threatened Species* 2014:e.T10722A174778740. DOI: https://dx.doi.org/10.2305/IUCN.UK.2014-3.RLTS.T10722A174778740.en.

Ohama H. 1990. Age determination of Japanese smelt with daily otolith increment. *Nippon Suisan Gakkaishi* 56:1053–1057.

Otterlei E. 2002. Temperature dependent otolith growth of larval and early juvenile Atlantic cod (Gadus morhua). *ICES Journal of Marine Science* 59:851–860. DOI: 10.1006/jmsc.2001.1300.

Pannella G. 1971. Fish Otoliths: Daily Growth Layers and Periodical Patterns. *Science* 173:1124. DOI: 10.1126/science.173.4002.1124.

R Core Team. 2019. R: A language and environment for statistical computing.

Roberts ME, Wetzel JE, Brooks RC, Garvey JE. 2004. Daily Increment Formation in Otoliths of the Redspotted Sunfish. *North American Journal of Fisheries Management* 24:270–274. DOI: 10.1577/m02-197.

Sakaris PC, Buckmeier DL, Smith NG. 2014. Validation of Daily Ring Deposition in the Otoliths of Age-0 Alligator Gar. *North American Journal of Fisheries Management* 34:1140–1144. DOI: 10.1080/02755947.2014.951806.

Sepulveda A. 1994. Daily growth increments in the otoliths of European smelt Osmerus eperlanus larvae. *Marine Ecology Progress Series* 108:33–42. DOI: 10.3354/meps108033.

Smith WE, Newman KB, Mitchell L. 2020. A Bayesian hierarchical model of postlarval delta smelt entrainment: integrating transport, length composition, and sampling efficiency in estimates of loss. *Canadian Journal of Fisheries and Aquatic Sciences* 77:789–813. DOI: 10.1139/cjfas-2019-0148.

Sommer T, Armor C, Baxter R, Breuer R, Brown L, Chotkowski M, Culberson S, Feyrer F, Gingras M, Herbold B, Kimmerer W, Mueller-Solger A, Nobriga M, Souza K. 2007. The collapse of pelagic fishes in the Upper San Francisco Estuary. *Fisheries* 32:270–277. DOI: 10.1577/1548-8446(2007)32[270:TCOPFI]2.0.CO;2.

Sommer T, Mejia F, Nobriga ML, Feyrer F, Grimaldo LF. 2011. The Spawning Migration of Delta Smelt in the Upper San Francisco Estuary. *San Francisco Estuary and Watershed Science* 9:1–16.

Starrs D, Ebner BC, Fulton CJ. 2016. All in the ears: Unlocking the early life history biology and spatial ecology of fishes. *Biological Reviews* 91:86–105. DOI: 10.1111/brv.12162.

Stevenson DK, Campana SE. 1992. *Otolith Microstructure Examination and Analysis*. Ottawa, Canada: Department of Fisheries and Ocean.

U.S. Fish and Wildlife Service. 1993. Determination of Threatened Status for the Delta Smelt. *Federal Register* 58:12854–12864. DOI: http://ecos.fws.gov/docs/federal_register/fr2751.pdf.

Vignon M, Morat F. 2010. Environmental and genetic determinant of otolith shape revealed by a non-indigenous tropical fish. *Marine Ecology Progress Series* 411:231–241.

List of Tables

Table 1: Samples used in the present study. Sample size (N) is shown by age class, along with the mean standard length for the subsample from each age class. The number of specimens for which paired left and right otoliths (L/R) were used to examine symmetry and paired images at 200x and 400x magnification (200x/400x) to examine magnification are also provided.

Table 2. Effects of observer, otolith side, and life stage on aging accuracy. Results of a linear model examining the effects of observer (obs), otolith side (left vs. right), and fish life stage (90 vs 180 dph) on the accuracy of age estimates (PEA). Factors include: obs—analyst, oto—otolith side, known—known age. No significant effects were detected (P > 0.05).

Table 3. Effects of observer and image magnification on aging accuracy. Statistical results of the linear model examining the additive and interactive effects of observer (obs) and image magnification (mag: 200x vs 400x) on accuracy of age estimates (percent error) for slower growing 271 dph Delta Smelt (with small rings). Significant P-values are in bold. DF-degrees of freedom, SS-sum-of-squares, MS-mean squares.

List of Figures

Figure 1. Morphological features of Delta Smelt and their otoliths. (A) Larval (left) and adult (right) Delta Smelt and associated length measurements: standard length (SL), total length (TL), fork length (FL, adult only). (B) Ontogenetic development and morphology of sagittal otoliths from individuals of ages 30 to 271 days-post-hatch (dph). Dorsal-ventral (DV) and rostral-postrostral (RP) dimensions, and the dorsal aging trajectory (black/white line) are shown for the 180 dph otolith. (C) A polished sagittal section of the dorsal lobe of a Delta Smelt otolith exhibiting 180 daily rings from the core (hatch) to the outer edge (death). Tick marks in (C) represent 30-day intervals along the aging trajectory. Delta Smelt artwork by Adi Khen.

Figure 2. Somatic and otolith size and growth in Delta Smelt. (A) Log10 standard length versus age and fitted Gompertz growth curve, (B) otolith size (radius) versus corrected fish standard length, (C) density plot of otolith core sizes, and (D) otolith growth trajectories with known ages (vertical dashed lines) examined in the present study.

Figure 3. Aging accuracy across life stages. Mean ± SD error (A) and percent error (B) in the accuracy of age estimates for Delta Smelt are plotted in relation to the known age of each age group.

Figure 4. Aging accuracy and precision among analysts. Error in days (left) and absolute percent error (right) in relation to known ages (accuracy, A-B) and mean age estimates among analysts (precision, C-D) for each Delta Smelt analyzed by each of the 3 analysts (x-axis). Points represent the mean error value foreach analyst and segments represent 1 s.d. The global mean for all analysts is shown by the gray dashed line. Only specimens ≥ 10 dph were included in the analysis.

Figure 5. Effects of otolith side and image magnification on aging accuracy. Comparison of the accuracy (raw %, to reflect normalized bias) of age estimates from (a) left versus right otoliths for 90 and 180 dph Delta Smelt and (b) between images of otoliths taken at different magnifications for older (271-dph), slower-growing individuals.

Table 1.

Age (dph)	N (fish)	SL_c (mm)	L/R	200x/400x
0	10	5.9		
5	10	6.9		
10	13	8.4		
30	10	12.5		
61	10	20.8		
90	11	26.0	5	
180	14	50.3	5	
215	10	53.2		
243	11	52.5		
271	9	57.9		9

Table 2.

Factor	df	SumSq	MeanSq	F	P
obs	2	4.39	2.1965	0.3039	0.7393
oto	1	0.01	0.0051	0.0007	0.9788
known	1	0.13	0.1286	0.0178	0.8944
obs:oto	2	20.87	10.4372	1.4441	0.2460
obs:known	2	12.17	6.0854	0.8420	0.4371
oto:known	1	1.16	1.1574	0.1601	0.6908
obs:oto:known	2	6.51	3.2562	0.4505	0.6400
Residuals	48				

Table 3.

Factor	DF	SS	MS	F	P
obs	2	213.645	106.823	20.5102	**<0.001**
mag	1	192.175	192.175	36.8980	**<0.001**
obs:mag	2	8.592	4.296	0.8248	0.4438
Residuals	54	281.246	5.208		

Figure 1.

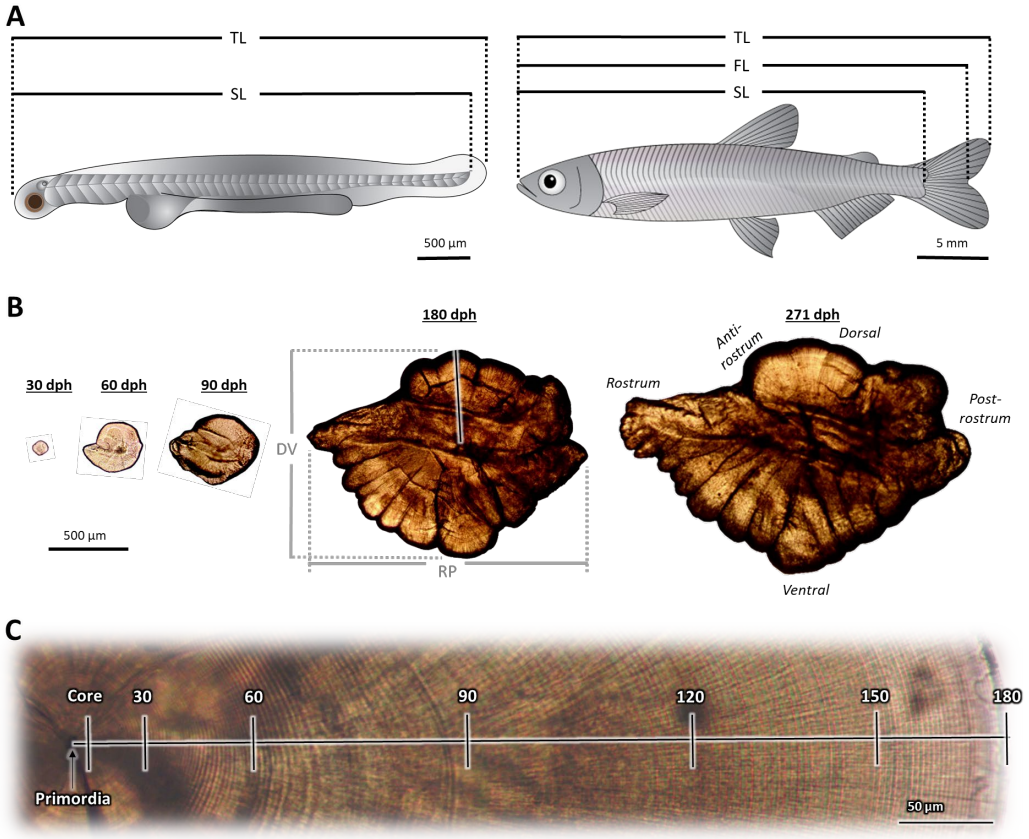
A
TL
SL
500 µm
TL
FL
SL
5 mm
B
30 dph
60 dph
90 dph
500 µm
DV
180 dph
RP
271 dph
Anti-rostrum
Dorsal
Rostrum
Post-rostrum
Ventral
C
Core
30
60
90
120
150
180
Primordia
50 µm

Figure 2.

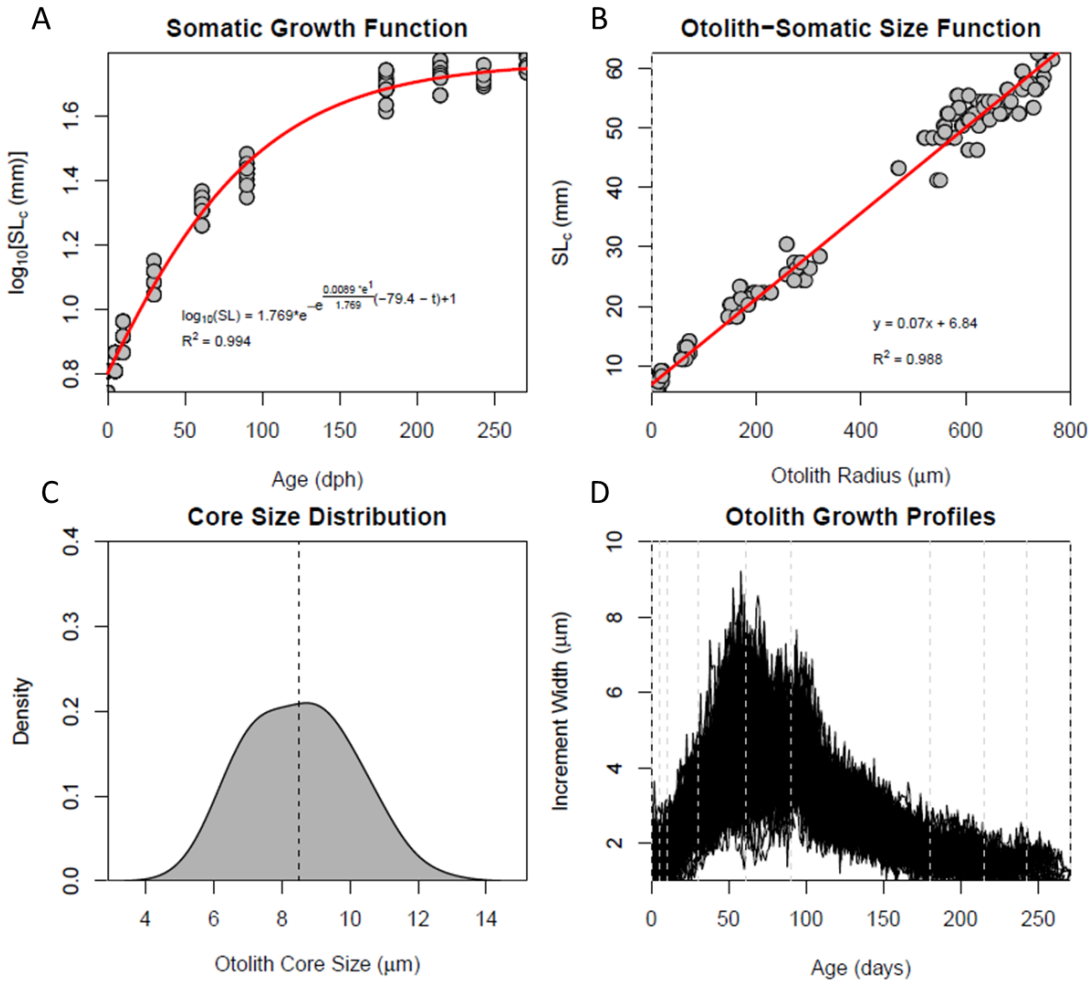
A
Somatic Growth Function
log10[SLc (mm)]
Age (dph)
log10(SL) = 1.769*e^(−e^(0.0089*e^1/1.769)(−79.4 − t)+1)
R2 = 0.994
B
Otolith−Somatic Size Function
SLc (mm)
Otolith Radius (µm)
y = 0.07x + 6.84
R2 = 0.988
C
Core Size Distribution
Density
Otolith Core Size (µm)
D
Otolith Growth Profiles
Increment Width (µm)
Age (days)

Figure 3.

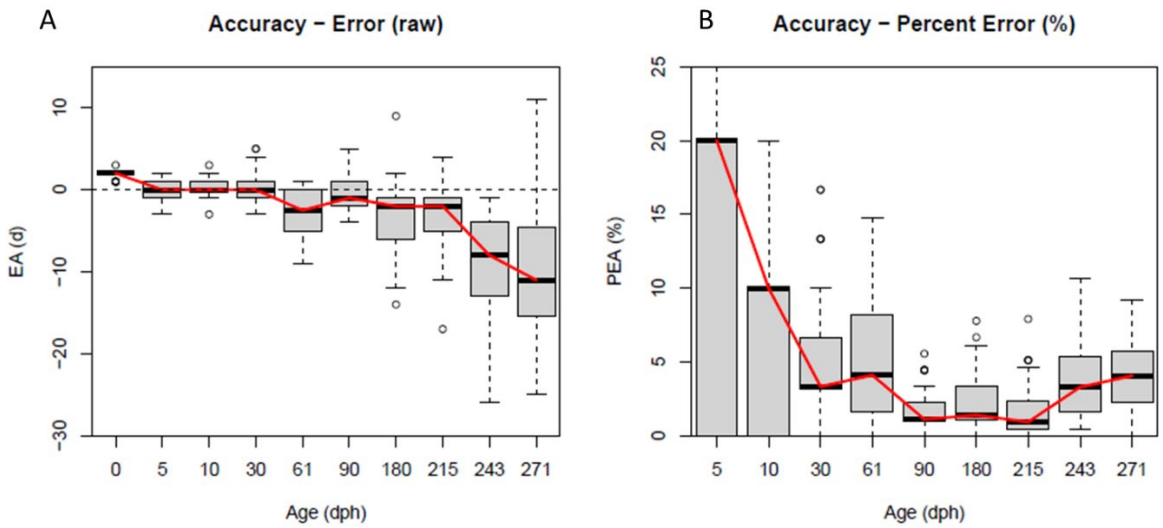
A
Accuracy – Error (raw)
EA (d)
10
0
−10
−20
−30
0
5
10
30
61
90
180
215
243
271
Age (dph)
B
Accuracy – Percent Error (%)
PEA (%)
25
20
15
10
5
0
5
10
30
61
90
180
215
243
271
Age (dph)

Figure 4.

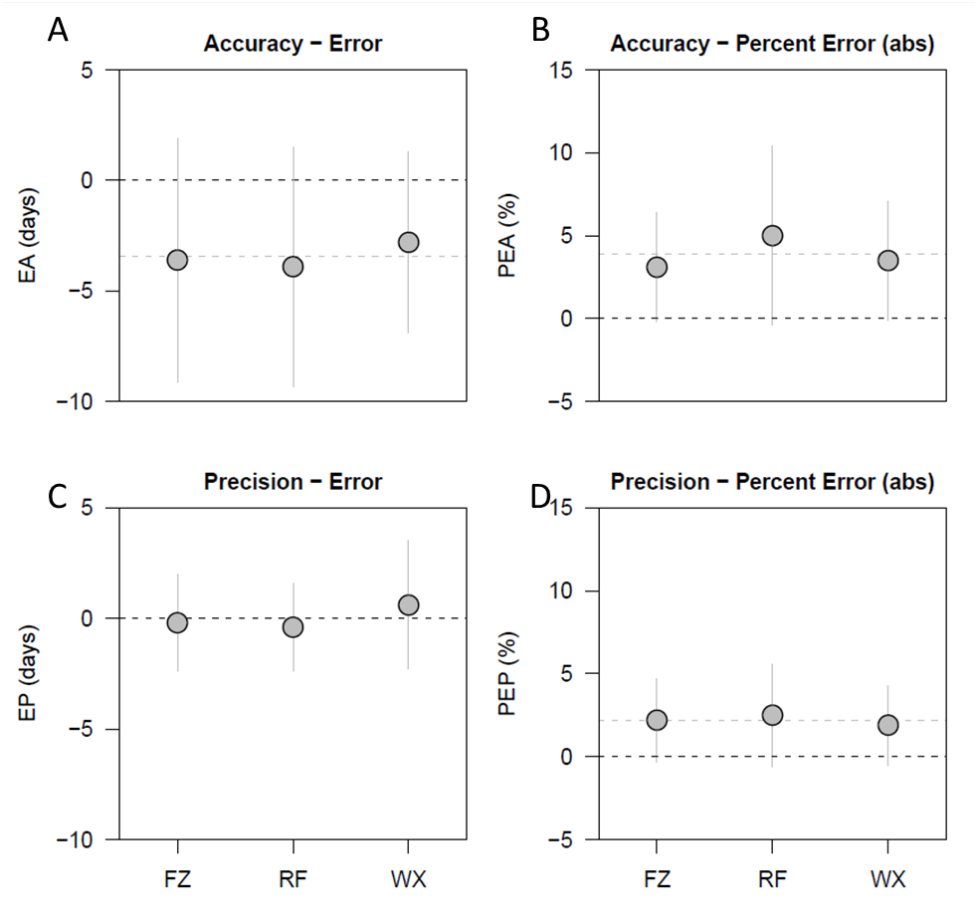
A
Accuracy – Error
EA (days)
5
0
−5
−10
B
Accuracy – Percent Error (abs)
PEA (%)
15
10
5
0
−5
C
Precision – Error
EP (days)
5
0
−5
−10
FZ
RF
WX
D
Precision – Percent Error (abs)
PEP (%)
15
10
5
0
−5
FZ
RF
WX

Figure 5.

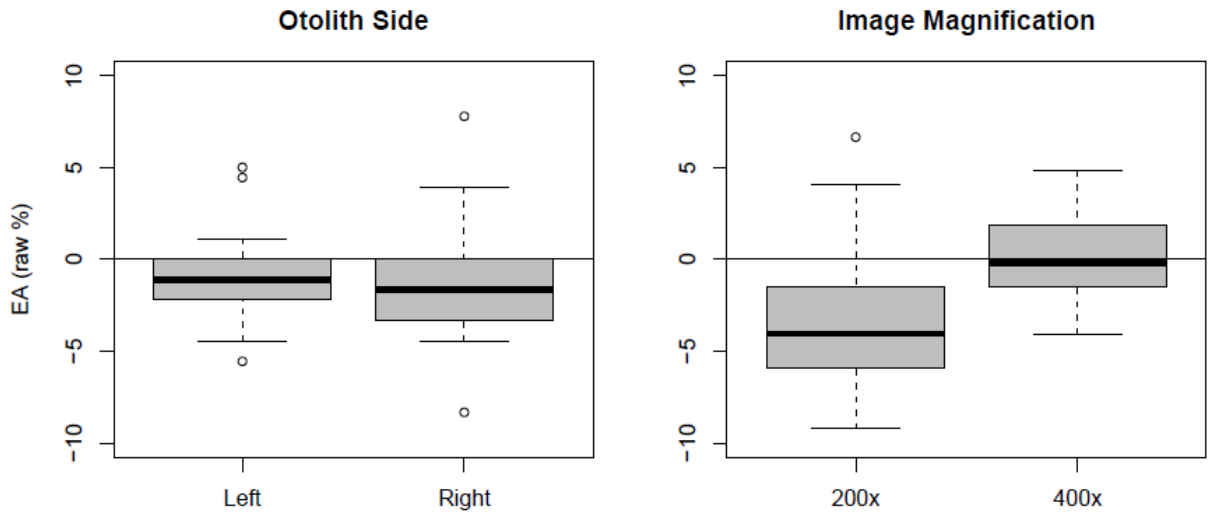
Otolith Side
Image Magnification
EA (raw %)
10
5
0
−5
−10
Left
Right
200x
400x

Supplement 1

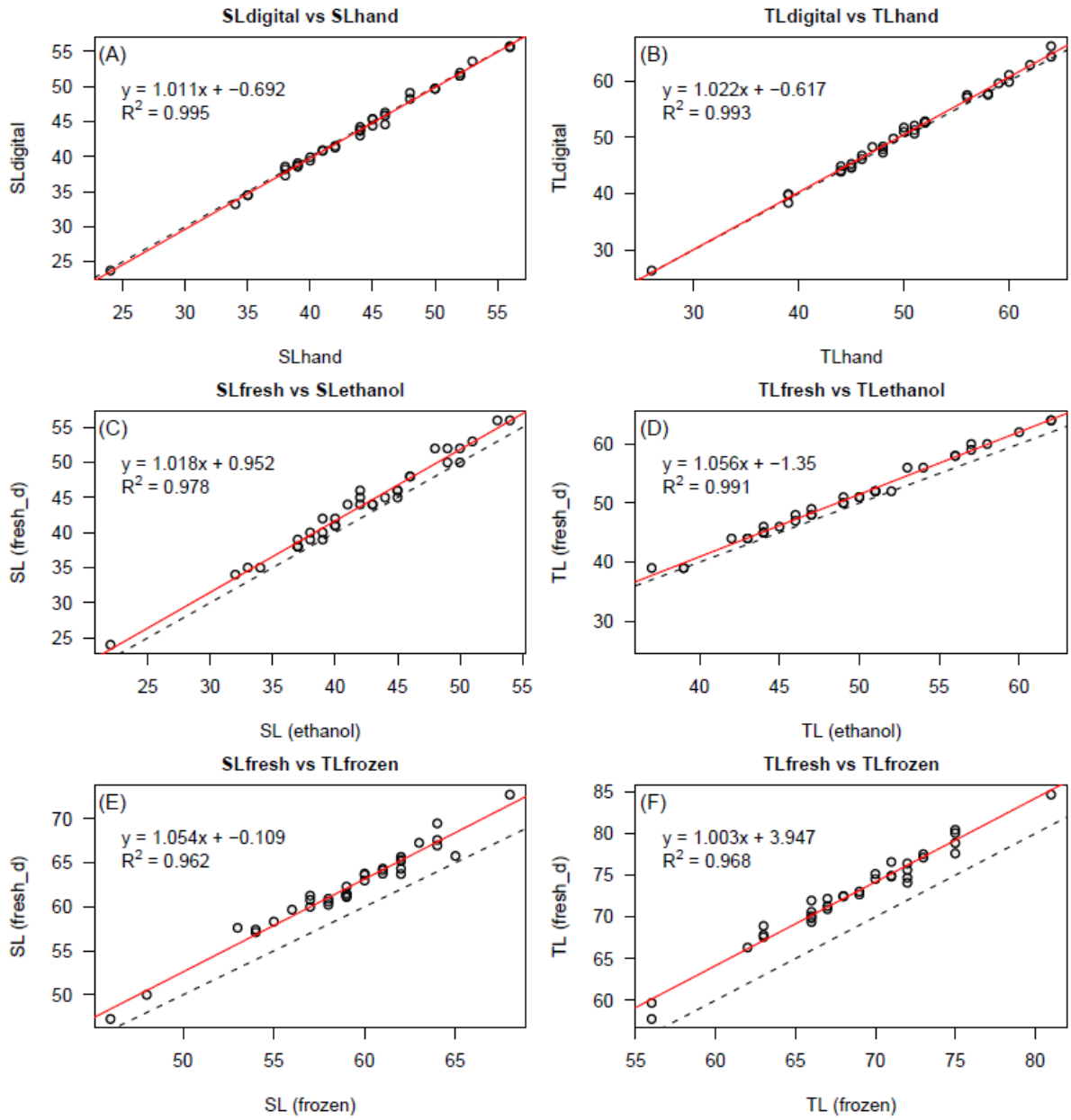

Figure S1. Standard (SL) and total (TL) length conversion equations for larval and adult Delta Smelt measured fresh by hand or digitally using image analysis (a-b) and either preserved in ethanol (c-d) or frozen at -20 ºC (e-f). Dashed lines represent 1:1; red lines represent the respective linear models.

Supplement 2

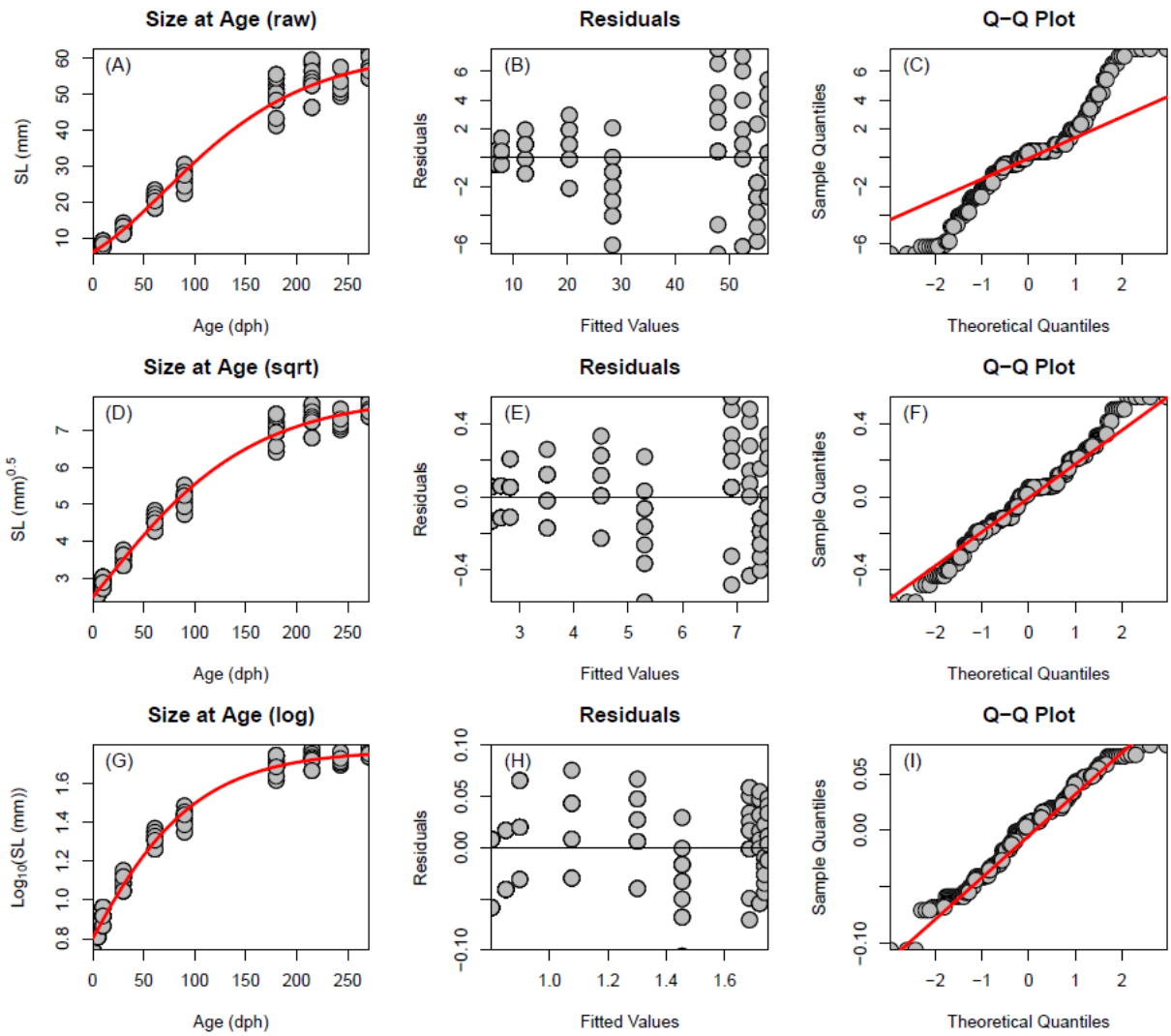

Figure S2. A Gompertz size-at-age curve was fit to fish size (standard length, SL_c) and known age using raw (a-c), square-root transformed (d-f), and $\log_{10}$-transformed (g-i) sizes. Model assumptions were evaluated using plots of residual versus fitted values (middle) and Q-Q plots of residuals (bottom). The $\log_{10}$ transformation was chosen as the best fit given the improved variance structure of the residuals.

Supplement 3

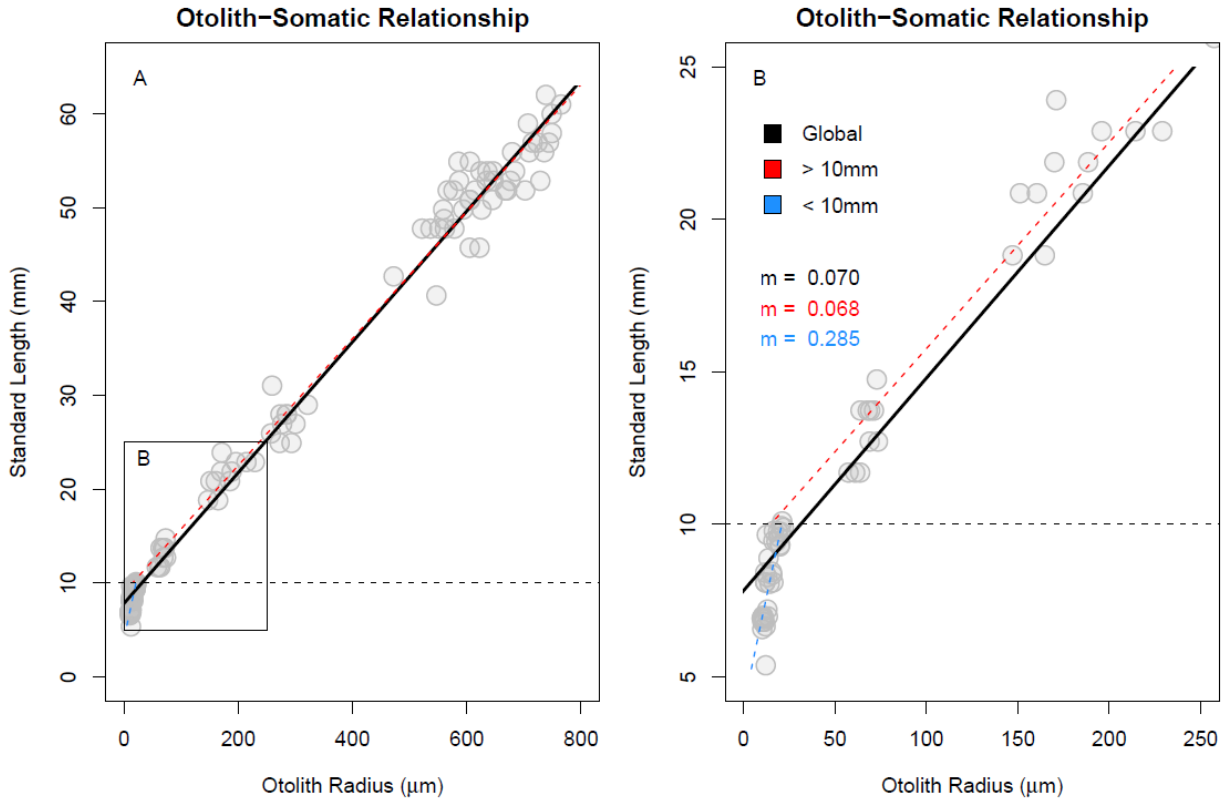

Figure S3. Examination of stage-specific somatic-otolith size relationships for (A) all size classes and (B) zoomed to fish < 25 mm. Three models were fit including a global model (all size classes as in Fig. 1b, black), a model for pro-larval fish ≤10 mm (blue), and a model for all fish > 10mm (red). Slopes (m) of each model are provided in (b) (see table S3 for model details).

Table S3. Results of stage-specific linear models examining somatic-otolith size relationships. Table headings include: Model = fish size class, Coefficient = slope or intercept for each linear model, Estimate = coefficient value, Error = standard error, t = t-value, P_1= p-value for each coefficient, n = sample size, F = F-statistic, P_2 = p-value and R^2 = coefficient of determination for the model. SL = standard length.

Model	Coefficient	Estimate	Error	t	P_1	n	F	P_2	R^2
All Sizes	Intercept	7.830	0.316	24.770	< 0.001	108	8694.2	< 0.001	0.989
	Slope	0.070	0.001	93.240	< 0.001				
> 10 mm SL	Intercept	8.997	0.576	15.620	< 0.001	76	3508.1	< 0.001	0.979
	Slope	0.068	0.001	59.230	< 0.001				
≤ 10 mm SL	Intercept	4.053	0.544	7.449	< 0.001	32	61.1	< 0.001	0.671
	Slope	0.285	0.036	7.817	< 0.001				

Chapter 6: The Effect of Outflow on Subsidy of a Key Calanoid Copepod Prey Item for Delta Smelt in the San Francisco Estuary

Submitted to *Estuaries and Coast*

The effect of outflow on subsidy of a key calanoid copepod prey item for Delta Smelt in the San Francisco Estuary

Jason L. Hassrick[1*], Josh Korman[2], Wim Kimmerer[3], Edward Gross[4], Lenny F. Grimaldo[5], Calvin Lee[1], and Andrew Schultz[6]

[1] 201 Mission Street, Suite 1500, San Francisco, CA 94105 USA
[2] Ecometric Resarch, 3560 W 22nd Ave, Vancouver, BC, V6S 1J3
[3] Estuary & Ocean Science Center, San Francisco State University, 3150 Paradise Drive, Tiburon CA 94920 USA
[4] Resource Management Associates, 1756 Picasso Avenue, Suite G, Davis, CA 95618, USA
[5] State Water Project Long-term Operations, 1416 9th Street, Sacramento, CA 95814
[6] Science Division, U.S. Bureau of Reclamation Bay-Delta Office; 801 I Street, Suite 140, Sacramento, CA 95814
[*] corresponding author: jason.hassrick@icf.com, (530) 312-3275

Abstract

Freshwater outflow in the San Francisco Estuary has been supplemented in the fall of recent wet years to try to bolster the population of endangered Delta Smelt *Hypomesus transpacificus*. This augmentation was intended in part to increase spatial subsidies of the copepod *Pseudodiaptomus forbesi* from its freshwater population center into the low-salinity habitat of much of the Delta Smelt population. This study combined hydrodynamic and particle-tracking modeling with Bayesian analysis in a box-model approach to estimate the transport of copepods to the low-salinity box and its response to flow augmentation. Net gains of *P. forbesi* into the low-salinity box, mostly from landward boxes of higher copepod abundance, were higher than those into other boxes because mortality rates of early life stages were highest in the low-salinity box. Proportional net gain was insensitive to flow augmentation across four scenarios. This study supports previous analyses showing that increasing outflow can increase food subsidies to the low-salinity zone resulting in higher abundance there; however, flow levels required for a substantial net gain are too high to be feasible through flow releases from reservoirs or manipulation of export flows in the Delta.

Keywords: spatial subsidies, box model, zooplankton, *Pseudodiaptomus forbesi*, low-salinity zone, Delta Smelt

Introduction

Spatial subsidies of nutrients and prey populations are common in marine and estuarine ecosystems where rates of exchange can be high. Subsidies are manifested in a variety of cases including outwelling of dissolved organic carbon from marshes to open water (Odum 1980), nutrient subsidies from terrestrial organisms entering lakes (Carpenter et al. 2005), and subsidies of pelagic nutrients to oceanic islands (Polis et al. 1997) and kelp forests (Zuercher and Galloway 2019). Subsidies can also be found in marine-derived nutrients transported in the bodies of migrating spawning salmon to freshwater tributaries (Gende et al. 2002), in larval recruitment (Cowen et al. 2006; Morgan et al. 2017), and in subsidies of zooplankton to nearshore communities (Morgan et al. 2017). Subsidies must cross a boundary between biologically distinct habitats and they usually increase primary and secondary productivity, indirectly and directly (Polis et al. 1997). This has important implications for an open population, in which rates of birth, growth, and mortality are complicated by immigration and emigration. In the upper San Francisco Estuary biomass of phytoplankton and calanoid copepods in the low-salinity zone (LSZ, salinity 0.5-6, Practical Salinity Scale) are subsidized from freshwater habitats in the Sacramento San Joaquin Delta (Delta; Fig. 1). Productivity in the LSZ is low, a result of top-down grazing effects from the introduced overbite clam Potamocorbula amurensis (Alpine and Cloern 1992; Carlton et al. 1990; Kimmerer and Lougee 2015; Thompson 2005). Without subsidies, net producitivity of zooplankton would be negative (Kimmerer et al. 2019). The decline of primary productivity in the LSZ has been implicated as one of the major factors contributing to decline in pelagic fish community in the upper estuary (Sommer et al. 2007).

Copepods such as *Pseudodiaptomus forbesi* are an important food source for small estuarine fishes, comprising ~85% of the prey biomass of the endangered Delta Smelt *Hypomesus transpacificus* (Slater and Baxter 2014). The majority of juvenile Delta Smelt rear in the LSZ (Brown et al. 2014; Bush 2017), and declines in Delta Smelt have been attributed to poor feeding conditions there, particularly during summer and fall (Hammock et al. 2015; Mac Nally et al. 2010; Slater and Baxter 2014). Copepods other than *P. forbesi* can be important in Delta Smelt diets (Slater and Baxter 2014), notably the small cyclopoid copepod *Limnoithona tetraspina* and the predatory copepod *A. sinensis*. However, both of these species are most abundant at salinities of 0.5–15 (Slaughter et al. 2016) so their abundance in the LSZ is unlikely to be increased by increasing outflow. No other copepod is abundant in the LSZ during summer-fall, and *P. forbesi* is the only one that arrives there from a denser population in fresh water.

Abundance of *P. forbesi* in the LSZ is low because of high mortality in early life stages due to low food supply and consumption by clams and predatory copepods (Kimmerer et al. 2019). *P. forbesi* have occupied the upper San Francisco Estuary and lower Delta continuously since they were first reported in 1987 (Orsi 1991). Since 1989, they have been the most abundant calanoid copepod in the upper estuary during late spring to early autumn, although their distribution shifted landward in 1994 following the introduction of a predatory brackish-water copepod (Kayfetz and Kimmerer 2017). They may retain an estuarine distribution through tidal vertical migration to overcome net seaward transport in waters saline enough to stratify (Kimmerer et al. 2014).

Most Delta Smelt undergo a diffuse migration into fresh (or less brackish) water in advance of spawning, and some fraction of juveniles remain in fresh water during summer–fall (Sommer et al. 2011). Bush (2017) found three life-history phenotypes through otolith analysis on 1109 adult Delta Smelt collected during seven years from 2006 to 2015. These comprised a

freshwater resident (23% of samples, mean for all years), a brackish resident (7%), and a phenotype that migrated to waters of salinity > 0.5 around 3 months after hatching (Bush 2017). That is, about three quarters of the population was in the LSZ from about June until the end of the year. Data from fish surveys confirm that Delta Smelt occupy low-salinity waters during the fall (Feyrer et al. 2007; Kimmerer et al. 2009; Kimmerer et al. 2013; Nobriga et al. 2008; Sommer et al. 2011).

Regulatory permits for the State Water Project (SWP) and Central Valley Project (CVP) now include flow actions to improve low-salinity habitat and food availability for Delta Smelt during the summer and fall (CDFW 2020; USFWS 2019). In September–October of recent wet years, net Delta outflow, hereafter outflow, has been augmented through manipulations of reservoir flow releases and export flows. These augmentations are intended to improve the low-salinity habitat of Delta Smelt, partly through an anticipated increase in copepod abundance due to an increased subsidy at higher flows.

The objective of this study was to estimate the magnitude of the subsidy in *P. forbesi* that resulted from the flow augmentation. We evaluated subsidies of *P. forbesi* into the low-salinity zone during 2017, an extremely wet year. Our study used the approach of Kimmerer et al. (2019), in which the upper estuary was divided into a series of boxes with internal boundaries determined by salinity to reflect the organization of habitat for pelagic organisms. Three-dimensional hydrodynamic and particle-tracking models were used to estimate tidal and net movement of water between pairs of boxes. We collected zooplankton samples in the spatial boxes to provide data for estimating mortality within the boxes and, combined with the data on water movement, the magnitudes of subsidies between pairs of boxes. We modeled hydrodynamic conditions corresponding to positions of the low-salinity zone (indexed by X2, Jassby et al. 1995, MacWilliams et al. 2015) at three target positions for flow augmentation (U.S. Bureau of Reclamation 2012) at 74 km, 81 km, and a low-flow baseline scenario of 85 km. A hypothetical X2 of 67 km was also included as an extreme value to investigate the effect on net gain of flow augmentation over a wider range.

This study builds on Kimmerer et al. (2019) in two ways. First, the focus of Kimmerer et al. (2019) was mortality and its potential causes. A key finding was the very high mortality of early life stages of *P. forbesi* in the low-salinity zone. Here we are more concerned with estimating the magnitudes and effects of the subsidies in overcoming mortality to enhance abundance, and thereby evaluating the effectiveness of the flow actions for this purpose. Second, because the earlier paper revealed the importance of movement to estimates of mortality, we sampled for copepods using a design intended to best characterize spatial patterns of abundance and therefore the magnitude of that movement.

Methods

We sampled for zooplankton in five boxes in the Delta during four surveys in the fall of 2017: Oct. 11 to 16, Oct. 23 to 26, Nov. 6 to 10, and Nov. 20 to 22 (Fig. 1). In each box ten sites were sampled following a generalized random stratified tessellated sampling (GRTS) design (Stevens and Olsen 2004). Five sites were located in shallow water (< 3 m) and five in deeper water (> 3 m). At each site a vertical tow was taken with a 50-cm diameter, 50-micron mesh net pulled from the bottom or at most from a depth of 10 m to the surface. Volume of water filtered was determined from distanced towed. We corrected for net efficiency using a value of 70% previously determined following Kimmerer and Slaughter (2016). Upon retrieval, the net was washed down and the sample concentrated into labeled jars with formaldehyde to make the final concentration ~4%. Water-quality variables (temperature, turbidity, salinity, dissolved oxygen,

and chlorophyll-*a* fluorescence) at each site were measured using a handheld sonde (EXO 2 YSI, Xylem, Inc). Chlorophyll samples were taken by filtering whole water samples through 25-mm Whatman grade GF/F glass fiber filters (nominal pore size 0.7-µm) under gentle vacuum pressure (<10 mm Hg). Depending on the observed chlorophyll concentration from the YSI sonde, between 10 and 200 ml of water was filtered.

In the laboratory, quantitative subsamples of the zooplankton samples were taken using an adjustable pipette, and in each subsample the life stages of *P. forbesi* were identified and counted as in Kimmerer et al. (2019): adults were sexed and counted; copepodites were staged and counted; and nauplii and the individual number of eggs in both loose and attached egg sacs were counted. To provide high enough counts of each stage for mortality estimates, we took additional subsamples to obtain at least 30 of each life stage. Abundance (m^{-3}) was determined by dividing the count of each life stage by the product of the subsample fraction for that life stage and the volume filtered in the original sample.

Our box model approach closely followed methods in Kimmerer et al. (2019; Fig. 2). The three seaward boxes represented: (i) very low-salinity zone (VLSZ, salinity 0.2–0.5); (ii) low-salinity zone (LSZ, 0.5–5.0); and (iii) high salinity (SAL, >5.0). These zones, and hence the box boundaries, varied in location with X2. The two most landward boxes were the Sacramento River box (SAC) and the San Joaquin River box (SJ). Both had seaward boundaries within the legal Delta and adjoined the VLSZ box at its landward margin (salinity 0.2; Fig. 1).

Hydrodynamics were simulated using the three-dimensional RMA UnTRIM San Francisco Estuary Model (Andrews et al. 2017; Gross et al. 2010; Kimmerer et al. 2019). UnTRIM solves the discretized Reynolds-averaged shallow water equations on an unstructured grid (Casulli and Walters 2000). It allows for wetting and drying of computation cells, and sub-grid scale representation of bathymetry (Casulli and Stelling 2011). Vertical turbulent mixing in the model is parameterized using a k-ε closure, which solves one equation for turbulent kinetic energy (k) and another for turbulent dissipation (ε) using published parameter values (Warner et al. 2005). The model domain extends from the coastal ocean through the San Francisco Estuary including the Delta. The model was applied to simulate hydrodynamics from October 18, 2016 to December 1, 2017 using idealized tides with M2 tidal period modified to 12 hours so that tides repeat daily and therefore do not vary on a spring-neap cycle. Winds also repeated a daily pattern, representative of average summer and fall wind conditions. This approach allows transport to be estimated for a single day of representative tidal and wind conditions (Kimmerer et al. 2019). Predicted salinity distributions and X2 varied throughout the simulation with varied tributary inflows to the model.

Using calculated velocities and eddy diffusivities from the UnTRIM model at a half-hour interval, the Flexible Integration and Staggered-grid Hydrodynamics Particle Tracking Model (FISH-PTM) was used to simulate individual particle trajectories in the study area through time (Ketefian et al. 2016). These particles represented *P. forbesi* under two alternative swimming behaviors: tidal migration for copepodites and adults and passive behavior for nauplii. Tidal migration had an upward swimming speed of 0.25 mm s^{-1} during flood tide and a downward swimming speed of 0.75 mm s^{-1} during ebb tide, which resulted in the closest match between simulated particles and vertical distributions of copepods observed in the estuary (Kimmerer et al. 2014). Nauplii (< 0.2 mm long) were assumed to be too small to swim at speeds required to overcome vertical turbulence and were therefore treated as passive (neutrally buoyant) particles. The modeled tidal migration behavior is effective at retaining copepods in regions of salinity stratification but less so in freshwater regions.

The FISH-PTM model was initialized by seeding each box with a spatially uniform density of particles of one particle per 5000 m^3, resulting in approximately 400,000 particles for each of the eight combinations of simulated behavior and X2. The FISH-PTM then simulated forward over 24 hours, or exactly two semi-diurnal tidal cycles for the idealized tidal pattern. Particles were transported between boxes by tidal and net currents. At the end of the run, the number of particles present in a destination box from each source box was divided by the original number of particles from the source boxes. This fraction represented the proportional exchange from a source box to a destination box. The calculation was repeated for all source and destination boxes to populate a "Gross Exchange Matrix" (Kremer et al. 2010). Losses of particles at water diversion locations (sinks) were also estimated. At these points [e.g., water export facilities (Fig.1)] particles were permanently removed from the simulation.

The two swimming behaviors were applied for each of the four X2 scenarios, resulting in eight Gross Exchange Matrices. Omitting X2 and life-stage subscripts for simplicity, we calculated the proportional loss entries for one cell of this exchange matrix as

$$E_{bjk} = \frac{P_{bk,t=1}}{P_{bj,t=0}} \tag{1}$$

where E_{bjk} is the proportion of particles with swimming behavior b that originated from source box j and moved to destination box k. $P_{bj,t=0}$ is the number of particles seeded in box j during initiation at time zero, and $P_{bk,t=1}$ is the number of particles in box (or sink) k that originated in box j after one day's simulation.

The methods used to compute subsidies and net gains assume the population is at steady state on each sampling survey. Under this assumption the abundance of *P. forbesi* in each box is not changing over time. Thus, the proportional subsidy and net gain described below is relative to the assumed equilibrium density in each box. The proportional subsidy in each box depends on exchange rates but also on differences in copepod densities and the relative box volumes between the source and destination boxes. Following the notation in Eqn. 1, the gains were,

$$g_{bkj} = \frac{n_k E_{bkj} V_k}{n_j V_j} \tag{2}$$

where g_{bkj} is the proportional gain in numbers in box j due to transport from box k. E_{bkj} is from Eqn. 1, n_j and n_k give the mean abundance (m^{-3}) (density) boxes j and k respectively, and V_j and V_k give the volumes (m^3) of boxes j and k respectively. Calculations used both the mean of copepod densities across all survey periods from a box, and from survey-specific means. Subscripts for sampling survey are not shown in the equations for clarity of presentation. Note that the exchange proportions and box volumes in Eqn. 2 vary with the X2 scenario, but the mean abundances in each box are assumed not to vary. There is strong support for this assumption (see Figure 4 of Kimmerer et al. 2019).

The proportional net spatial gain into box j is the sum of subsidies (Eqn. 2) from all other boxes combined, less the sum of proportional losses (Eqn. 1) from box j to the other boxes:

$$G_{bj} = \sum_{j \neq k} g_{bkj} - \sum_{j \neq k} E_{bjk} \tag{3}$$

We calculated apparent mortality from counts of each life stage and the stage durations using the vertical-life-table method of Kimmerer et al. (2019). Apparent mortality is the value calculated from demographics of the population determined from the samples, ignoring the effects of transport. The two key assumptions in the approach are that the apparent mortality rate is constant within a life stage and that the population is at steady state. Given this latter assumption, the stage distribution is stable and therefore the decline in abundance across stages is not influenced by temporal variation in the number of *P. forbesi* entering each stage. For reasons discussed in Kimmerer and Lougee (2015) we used a Bayesian hierarchical approach to

estimate apparent mortality for copepodites (based on abundance by stage and estimated stage durations) and adults (based on the results for copepodites and abundance of copepodites and adults). Apparent mortality could not be calculated for nauplii, because counts of nauplii were lower than expected from the counts of other life stages.

The actual mortality rate, which we term the in-situ mortality rate, M_{bi}, was calculated as the sum of apparent mortality m_i and the proportion net gain G_i based on:

$$M_{bi} = m_i + G_i \tag{4}$$

where 'i' is an index for each unique site-survey sample. G_i values were computed by linear interpolation using the box-specific values from eqn. 3 with X2 values that spanned the X2 value at station 'i' at the time of sampling.

Uncertainty in estimates of proportional subsidies, proportional net gain, an *in-situ* mortality were computed by boostrapping. The subsidy and net gain calculations are based on mean *P. forbesi* densities for each box on a given sampling survey (Eqn 2.). However, these means are uncertain owing to variation in density estimates among sites within each box on each survey. We computed the mean and the standard error of the mean for each box and survey and used these values in the rnorm() function in R (R Core Team 2019) to return random samples of the mean densities. These values were used in eqn. 2 to compute uncertainty in proportional subsidy and therefore net gain. Uncertainty in in-situ mortality estimates depends on both the uncertainty in apparent mortality determined from the Bayesian model, and uncertainty in net gain. We combined these uncertainties by using random samples from the posterior distribution of m_i, and the distribution of G_i values from boostrapping, in Eqn. 4.

Results

The particle-tracking model predicted very little transport from seaward boxes (LSZ, VLSZ) into San Joaquin and Sacramento boxes (Fig. 3). Exchange from the very-low-salinity box to the low-salinity box, was substantial and increased with outflow (i.e. lower X2). There was a small exchange of particles from the low-salinity box to the high-salinity box, which increased modestly with X2.

Observed densities of *P. forbesi* were highest in the landward boxes (Sacramento, San Joaquin) and decreased to seaward (Fig. 4). Within surveys and boxes, densities of copepodites were higher than adults as expected. Densities of nauplii were sometimes lower than those of copepodites which likely reflects a sampling bias because the development times for each of those life stages are about the same. There was generally very high variability in densities among sites within boxes and surveys, as seen by relatively high values of coefficient of variation in log-transformed densities. Variation in nauplius densities was generally much greater than for copepodites or adults.

Subsidy calculations depend on box volume (Eqn. 2) which varied among boxes but also among X2 levels within boxes (Table 1). Volumes of San Joaquin and Sacramento boxes at the highest X2 level were 30 and 40% lower than at the lowest X2 level due to an eastward contraction of the boxes as X2 increased. In contrast, the volume of the high-salinity box was 86% higher at the highest X2 level than at the lowest. The volumes of very low-salinity box and low-salinity box varied less, and in different directions, across X2 levels.

Proportional subsidies of *P. forbesi* varied by life stage, box, and X2 level. We focused on the low-salinity zone given its importance for Delta Smelt (Fig. 5). Proportional subsidies for nauplii were highly uncertain due to extensive variation in densities among sites within the LSZ and VLSZ boxes (see CV's in Fig. 4). Proportional subsidies for copepodites and adults were

better defined and often large. Subsidies declined with increasing X2 because of reduced exchange from the VLSZ to the LSZ (Fig. 3).

The largest proportional net gain in the low-salinity box was greatest for nauplii and smallest for adults (Fig. 6). In the LSZ the median net gain declined with increasing X2 for copepodites and adults, although there was considerable uncertainty in X2-specific estimates and substantial overlap in net gain distributions among X2 levels. Proportional net gains in the low-salinity zone varied among survey periods due to differences in copepod densities (Fig. 6). As for the survey-averaged results, median net gain decreased with increasing X2 but there was considerable overlap in distributions among X2 scenarios.

Apparent mortality estimates for *P. forbesi* nauplii were not reliable because counts were lower than required to support the rate of production estimated for the first copepodite stage. Therefore we show mortality rates only for copepodites and adults. *In-situ* mortality rates for copepodites in the VLSZ and LSZ boxes were often considerably greater than they were in the SAC and SJ (Fig. 7). This pattern was less evident for adults, although higher values in the VLSZ or LSZ were apparent on surveys when the net gain in these boxes was higher (e.g. Nov 20-22).

Discussion

We combined predictions of movement from a particle tracking model with empirical observations from four carefully designed surveys to assess the role of freshwater outflow in subsidizing the food supply available to Delta Smelt in the Low-Salinity Zone. This study was designed to evaluate the efficacy of flow augmentation in fall (USFWS 2008) for supporting Delta Smelt through supplementing their food supply, although the results apply more broadly to any flow effects on transport of copepods. We have shown that abundance for all life stages of *P. forbesi* is low throughout the fall period relative to freshwater habitats and that exchange between boxes does not appear to respond to flow augmentation (i.e. lower X2; Fig. 3). X2 values ranging from 74-85 km can realistically be achieved by flow augmentation, and the considerable overlap in distributions among X2 scenarios (Fig. 5) imply that within operational ranges there is little difference in subsidy. Higher subsidies to the low-salinity box with greater outflow are partially offset by greater losses (Fig. 6). Higher net gain in the low-salinity box also resulted in greater in situ mortality compared to other boxes (Fig. 7). Copepod exchange in a landward direction tended to be less than exchange seaward, suggesting increasing subsidy by advection in wet years (Fig. 3). Net gain of copepods seaward tended to increase with increasing X2 in high outflow conditions observed in this study (Fig. 6) and in high outflows associated with 2011 by Kimmerer et al. (2019).

Using the same zooplankton box model for different years and data from sampling programs with three different designs, Kimmerer et al. (2019) also found that subsidies to the Low-Salinity Zone was relatively insensitive to X2. We found that mortality rates of *P. forbesi* copepodites in the low-salinity box were higher than in other boxes, with nauplii showing the most variation. These findings are consistent with the conclusion that predation by invasive clams and copepods (e.g., *Acartiella sinensis*) depletes zooplankton densities in the LSZ (Kayfetz and Kimmerer 2017; Kimmerer et al. 1994; Kimmerer et al. 2019; Slaughter et al. 2016), increasing the importance of subsidies from landward sources to the LSZ.

Our expectation was that the subsidy from zooplankton-rich freshwater sources to the LSZ would be greater for lower X2 values (more outflow) and thus there would be a negative relationship between X2 and proportional net gain. Our modeling results suggest that subsidies of *P. forbesi* do not differ between the 74 and 81 X2 scenarios. While net gain did decrease

between an X2 of 85 km and 81 km in the very low-salinity box, the general trend was flat except at a hypothetical X2 of 67 km that was chosen as an extreme value to investigate the effect on net gain of flow augmentation over a wider range. Such a target seems unrealistic because moving X2 from 74 to 67 km for two months would require about 20% of the capacity of Shasta Reservoir, based on a steady-flow analysis of MacWilliams et al. (2015).

Our analysis is based on some inputs that are highly reliable and on some that should be considered with a degree of uncertainty. Volumes of modeled boxes are known accurately and exchange of particles between boxes can be estimated reliably by the well calibrated and validated hydrodynamic model and particle-tracking model used in this analysis (Gross et al. 2019; Ketefian et al. 2016). The particles were passive to represent the small nauplii, and moved up on the flood and down on the ebb to represent copepodites and adults. This behavior results in a good match with the vertical distributions of the copepods (Kimmerer et al. 2002) and causes retention in the deeper, more saline parts of the estuary. For this reason the migratory behavior had an increasing effect on copepod movements going from fresh water to the high-salinity zone.

The estimates of proportional net gain are largely driven by differences in zooplankton densities among boxes, which were well defined by the robust sampling effort in 2017. However, the coarse spatial representation of the estuary by five rather large boxes, although consistent with the spatial scales at which copepod abundance can be differentiated, results in an approximate representation of transport, introducing some uncertainty to the estimates of spatial subsidy.

This study builds on that of Kimmerer et al. (2019) to reinforce the finding that spatial transport processes are an essential element of the population dynamics of *P. forbesi*, and probably other pelagic species besides zooplankton. These processes are now seen to be important at a range of spatial scales, from the entire habitat of the species, as here, to the scale of individual wetlands and their connections to open water (Kimmerer et al. 2018). Transport processes are heavily dependent on the interaction of tidal flows with spatio-temporal variation in abundance and distribution, presenting a challenge for analysis. Given the availabity of robust transport modeling described above, and growing knowledge and understanding of the population ecology of this species, a logical next step would be to derive a more mechanistic model of copepod production and subsidy. This would combine transport modeling with better understanding of vertical movements of copepods, reinforced by data on abundance by life stage and vital rates to develop spatial mass-balance models.

Acknowledgements

We thank A. Slaughter for providing guidance on experimental design and J. Smith for guidance on setting up a random stratified sampling program. C. Brennan and J. Sousa assisted with field work and taxonomic expertise. R. Miller, D. Maniscalco helped with field work and A. Kalmbach with data quality control. J. Brandon provided internal review and assistance with the life table. We thank Kristin Arend (United States Bureau of Reclamation [USBR]) for helpful review of the manuscript. We thank R. Rachiele for guidance on model calibration and R. Holleman for providing Python tools for analysis of model results. V. Casulli developed the UnTRIM hydrodynamic model and S. Andrews led the development of the RMA UnTRIM model interface. This study was funded by USBR as part of the Directed Outflow Project. The views expressed are those of the authors and do not represent official opinion of any employer, institution or government agency.

References

Alpine, A. E., and J. E. Cloern. 1992. Trophic interactions and direct physical effects control phytoplankton biomass and production in an estuary. Limnology and Oceanography 37(5):946-955.

Andrews, S., E. Gross, and P. Hutton. 2017. Modeling salt intrusion in the San Francisco Estuary prior to anthropogenic influence. Continental Shelf Research 146:58-81.

Brown, L. R., and coauthors. 2014. Synthesis of studies in the fall low-salinity zone of the San Francisco Estuary, September–December 2011. US Geological Survey Scientific Investigations Report 5041:136.

Bush, E. E. 2017. Migratory life histories and early growth of the endangered Estuarine Delta Smelt (Hypomesus transpacificus). University of California, Davis.

Carlton, J. T., J. K. Thompson, L. E. Schemel, and F. H. Nichols. 1990. Remarkable invasion of San Francisco Bay (California, USA) by the Asian clam Potamocorbula amurensis. I. Introduction and dispersal. Marine Ecology Progress Series:81-94.

Carpenter, S. R., and coauthors. 2005. Ecosystem subsidies: terrestrial support of aquatic food webs from 13C addition to contrasting lakes. Ecology 86(10):2737-2750.

Casulli, V., and G. S. Stelling. 2011. Semi-implicit subgrid modelling of three-dimensional free-surface flows. International journal for numerical methods in fluids 67(4):441-449.

Casulli, V., and R. A. Walters. 2000. An unstructured grid, three-dimensional model based on the shallow water equations. International journal for numerical methods in fluids 32(3):331-348.

CDFW. 2020. Incidental Take Permit No. 2081-2019-066-00 for the Long-term Operation of the State Water Project in the Sacramento San Joaquin Delta. California Department of Fish and Wildlife, Sacramento, California.

Cowen, R. K., C. B. Paris, and A. Srinivasan. 2006. Scaling of connectivity in marine populations. Science 311(5760):522-527.

Feyrer, F., M. L. Nobriga, and T. R. Sommer. 2007. Multidecadal trends for three declining fish species: habitat patterns and mechanisms in the San Francisco Estuary, California, USA. Canadian Journal of Fisheries and Aquatic Sciences 64(4):723-734.

Gende, S. M., R. T. Edwards, M. F. Willson, and M. S. Wipfli. 2002. Pacific salmon in aquatic and terrestrial ecosystems: Pacific salmon subsidize freshwater and terrestrial ecosystems through several pathways, which generates unique management and conservation issues but also provides valuable research opportunities. BioScience 52(10):917-928.

Gross, E., and coauthors. 2019. The use of stable isotope-based water age to evaluate a hydrodynamic model. Water 11(11):2207.

Gross, E. S., M. L. MacWilliams, C. D. Holleman, and T. A. Hervier. 2010. POD 3–D particle tracking modeling study. Particle tracking model testing and applications report.Report to the Interagency Ecological Program.

Hammock, B. G., J. A. Hobbs, S. B. Slater, S. Acuña, and S. J. Teh. 2015. Contaminant and food limitation stress in an endangered estuarine fish. Science of The Total Environment 532:316-326.

Kayfetz, K., and W. Kimmerer. 2017. Abiotic and biotic controls on the copepod Pseudodiaptomus forbesi in the upper San Francisco Estuary. Marine Ecology Progress Series 581:85-101.

Ketefian, G., E. Gross, and G. Stelling. 2016. Accurate and consistent particle tracking on unstructured grids. International journal for numerical methods in fluids 80(11):648-665.

Kimmerer, W., J. R. Burau, and W. Bennett. 2002. Persistence of tidally-oriented vertical migration by zooplankton in a temperate estuary. Estuaries 25(3):359-371.

Kimmerer, W., and coauthors. 2018. Zooplankton Dynamics in the Cache Slough Complex of the Upper San Francisco Estuary. San Francisco Estuary and Watershed Science 16(3).

Kimmerer, W., and A. Slaughter. 2016. Fine-scale distributions of zooplankton in the northern San Francisco Estuary. San Francisco Estuary and Watershed Science 14(3).

Kimmerer, W. J., E. Gartside, and J. J. Orsi. 1994. Predation by an introduced clam as the likely cause of substantial declines in zooplankton of San Francisco Bay. Marine Ecology Progress Series:81-93.

Kimmerer, W. J., E. S. Gross, and M. L. MacWilliams. 2009. Is the response of estuarine nekton to freshwater flow in the San Francisco Estuary explained by variation in habitat volume? Estuaries and Coasts 32(2):375.

Kimmerer, W. J., E. S. Gross, and M. L. MacWilliams. 2014. Tidal migration and retention of estuarine zooplankton investigated using a particle-tracking model. Limnology and Oceanography 59(3):901-916.

Kimmerer, W. J., E. S. Gross, A. M. Slaughter, and J. R. Durand. 2019. Spatial subsidies and mortality of an estuarine copepod revealed using a box model. Estuaries and Coasts 42(1):218-236.

Kimmerer, W. J., and L. Lougee. 2015. Bivalve grazing causes substantial mortality to an estuarine copepod population. Journal of Experimental Marine Biology and Ecology 473:53-63.

Kimmerer, W. J., M. L. MacWilliams, and E. S. Gross. 2013. Variation of fish habitat and extent of the low-salinity zone with freshwater flow in the San Francisco Estuary. San Francisco Estuary and Watershed Science 11(4).

Kremer, J. N., and coauthors. 2010. Simulating property exchange in estuarine ecosystem models at ecologically appropriate scales. Ecological Modelling 221(7):1080-1088.

Mac Nally, R., and coauthors. 2010. Analysis of pelagic species decline in the upper San Francisco Estuary using multivariate autoregressive modeling (MAR). Ecological Applications 20(5):1417-1430.

MacWilliams, M. L., A. J. Bever, E. S. Gross, G. S. Ketefian, and W. J. Kimmerer. 2015. Three-dimensional modeling of hydrodynamics and salinity in the San Francisco estuary: An evaluation of model accuracy, X2, and the low–salinity zone. San Francisco Estuary and Watershed Science 13(1).

Morgan, S. G., and coauthors. 2017. Surf zones regulate larval supply and zooplankton subsidies to nearshore communities. Limnology and Oceanography 62(6):2811-2828.

Nobriga, M. L., T. R. Sommer, F. Feyrer, and K. Fleming. 2008. Long-term trends in summertime habitat suitability for Delta Smelt, Hypomesus transpacificus. San Francisco Estuary and Watershed Science 6(1).

Odum, E. P. 1980. The status of three ecosystem-level hypotheses regarding salt marsh estuaries: tidal subsidy, outwelling, and detritus-based food chains. Pages 485-495 *in* Estuarine perspectives. Elsevier.

Orsi, J. 1991. Pseudodiaptomus forbesi and P. marinus (Copepoda Calanoida), the latest copepod immigrants to California's Sacramento-San Joaquin Estuary. Proc. Fourth Internl. Conf. on Copepoda. Bull. Plankton Soc. Jpn.:553-562.

Polis, G. A., W. B. Anderson, and R. D. Holt. 1997. Toward an integration of landscape and food web ecology: the dynamics of spatially subsidized food webs. Annual review of ecology and systematics 28(1):289-316.

R Core Team. 2019. R: A Language and Environment for Statistical Computing. R foundation for statistical computing.

Slater, S. B., and R. D. Baxter. 2014. Diet, prey selection, and body condition of age-0 Delta Smelt, Hypomesus transpacificus, in the Upper San Francisco Estuary. San Francisco Estuary and Watershed Science 12(3).

Slaughter, A. M., T. R. Ignoffo, and W. Kimmerer. 2016. Predation impact of Acartiella sinensis, an introduced predatory copepod in the San Francisco Estuary, USA. Marine Ecology Progress Series 547:47-60.

Sommer, T., and coauthors. 2007. The collapse of pelagic fishes in the upper San Francisco Estuary: El colapso de los peces pelagicos en la cabecera del Estuario San Francisco. Fisheries 32(6):270-277.

Sommer, T., F. H. Mejia, M. L. Nobriga, F. Feyrer, and L. Grimaldo. 2011. The Spawning Migration of Delta Smelt in the Upper San Francisco Estuary. San Francisco Estuary and Watershed Science 9(2).

Thompson, J. K. 2005. One estuary, one invasion, two responses: phytoplankton and benthic community dynamics determine the effect of an estuarine invasive suspension-feeder. Pages 291-316 *in* The comparative roles of suspension-feeders in ecosystems. Springer.

USFWS. 2008. Formal Endangered Species Act Consultation on the Proposed Coordinated Operations of the Central Valley Project (CVP) and State Water Project (SWP). United States Fish and Wildlife Service. Sacramento, California.

USFWS. 2019. Formal Endangered Species Act Consultation on the Proposed Coordinated Operations of the Central Valley Project (CVP) and State Water Project (SWP). United States Fish and Wildlife Service, Sacramento, California.

Warner, J. C., C. R. Sherwood, H. G. Arango, and R. P. Signell. 2005. Performance of four turbulence closure models implemented using a generic length scale method. Ocean Modelling 8(1-2):81-113.

Zuercher, R., and A. W. Galloway. 2019. Coastal marine ecosystem connectivity: pelagic ocean to kelp forest subsidies. Ecosphere 10(2):e02602.

Tables

Table 1. The calculated volume of each box (millions of m^3) at the four modeled X2 scenarios. Boxes are lower San Joaquin River (SJ), lower Sacramento River (SAC), very low-salinity zone (VLSZ), low-salinity zone (LSZ), and high salinity (SAL).

	Box				
X2 (km)	**SJ**	**SAC**	**VLSZ**	**LSZ**	**SAL**
67	658	528	91	391	183
74	601	408	91	424	208
81	499	372	68	333	335
85	463	318	109	312	340

Figures

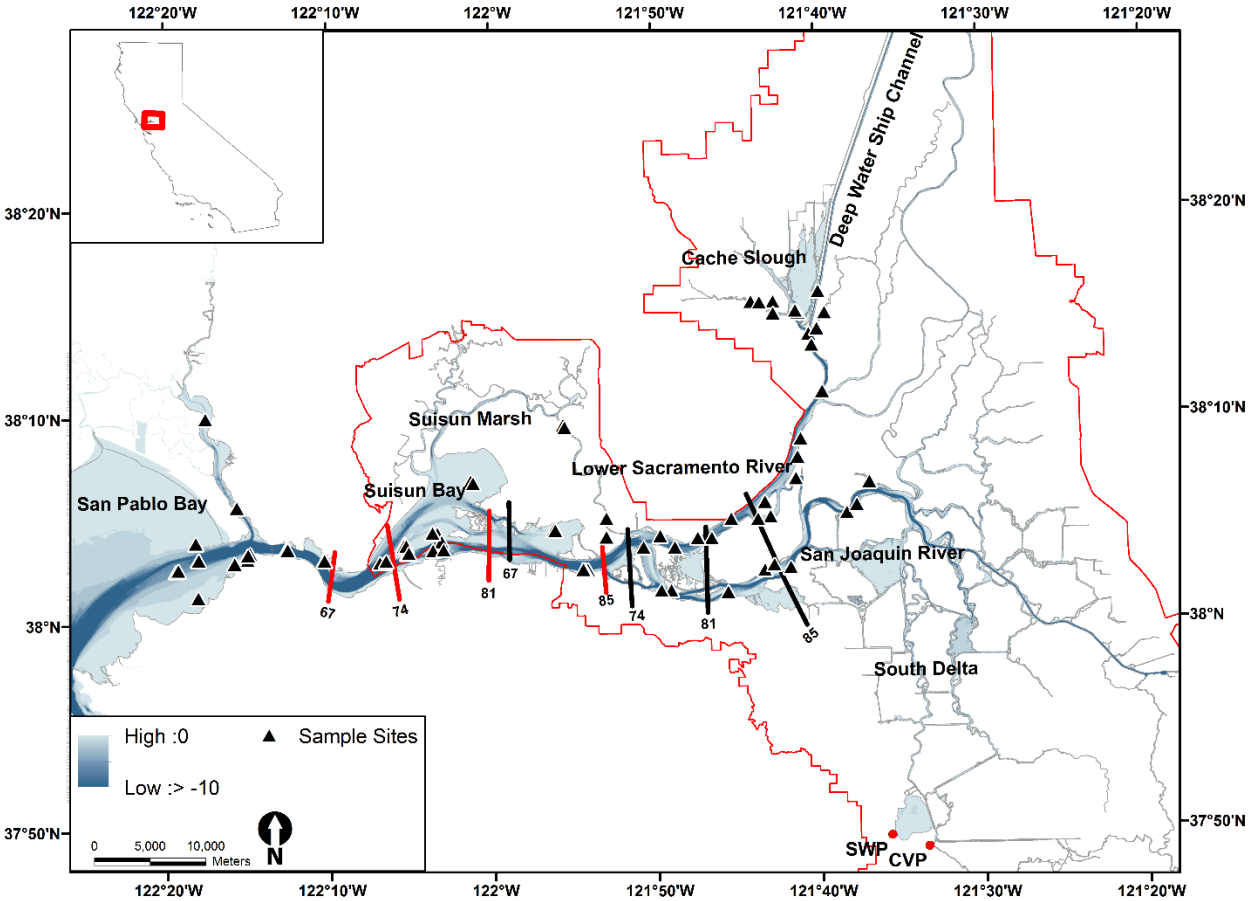

Figure 1. Map of the northern San Francisco Estuary for X2 scenarios at 67, 74, 81, and 85 km with boundaries (red is seaward, black is landward) of the low-salinity box. Black triangles represent sampling stations, red dots indicate the water export facilities of the State Water Project and federal Central Valley Project, and red border line is the boundary of the legal Delta.

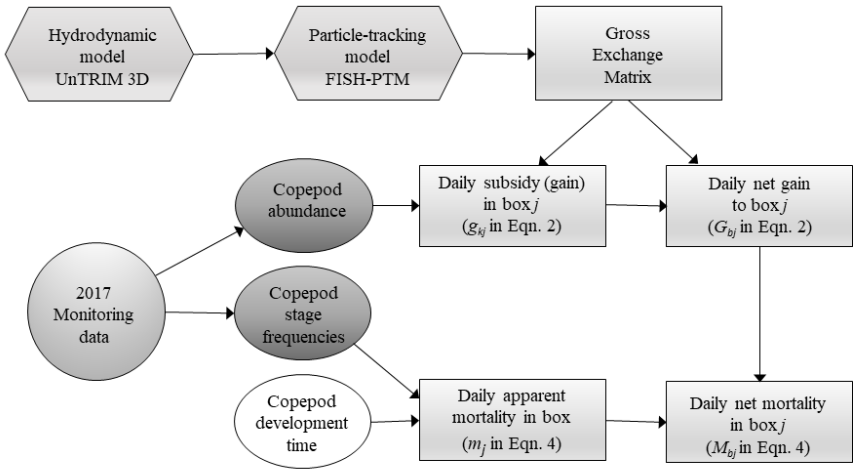

Figure 2. Flow diagram of calculations: Shaded shapes represent calculations made for this paper, whereas copepod development time is unshaded because it involves parameter estimates from Kimmerer et al. (2019); hexagons are three-dimensional simulation models; rectangles are results of calculations based on data and 3-D model output.

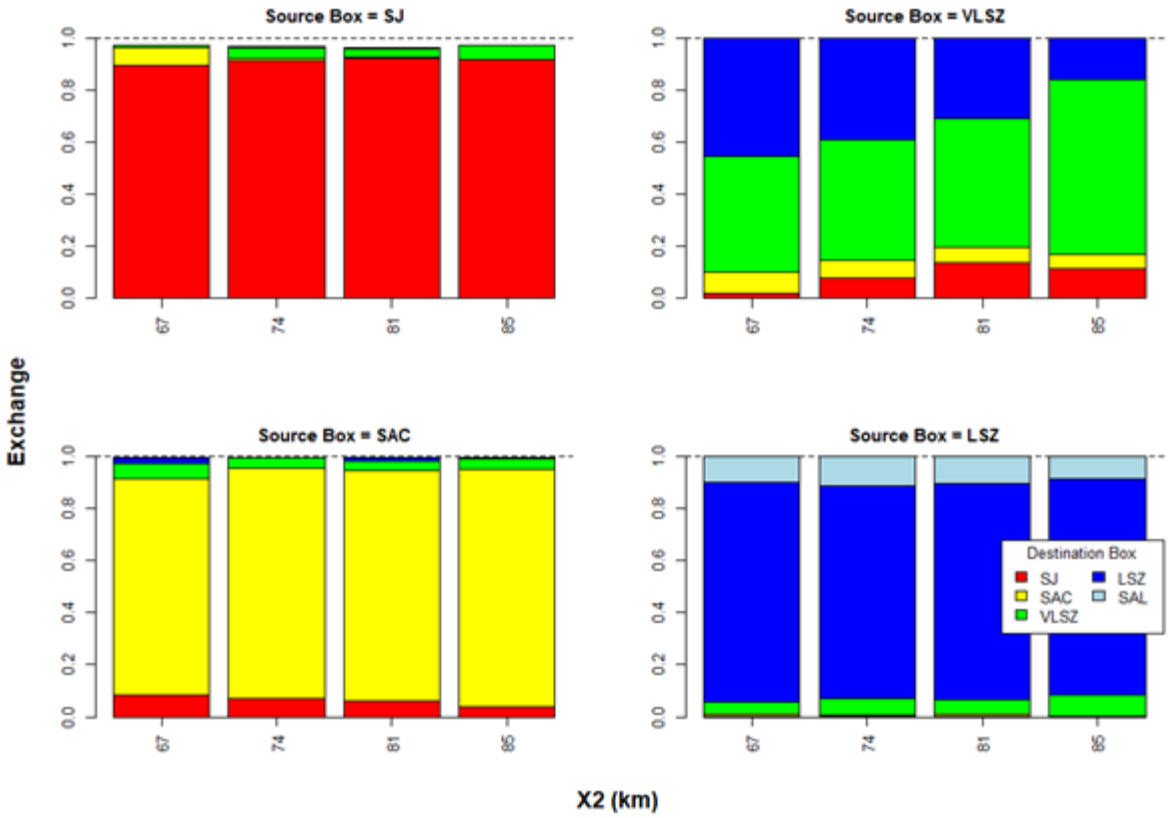

Figure 3. Predicted proportion of particles exchanged from source to destination boxes under four X2 conditions based on tidal behavior. The sum of exchanges from each source box to all destination boxes equals one except in cases where there are losses due to water export and particle sinks. Boxes are lower San Joaquin River (SJ), lower Sacramento River (SAC), very low-salinity zone (VLSZ), low-salinity zone (LSZ), and high salinity (SAL).

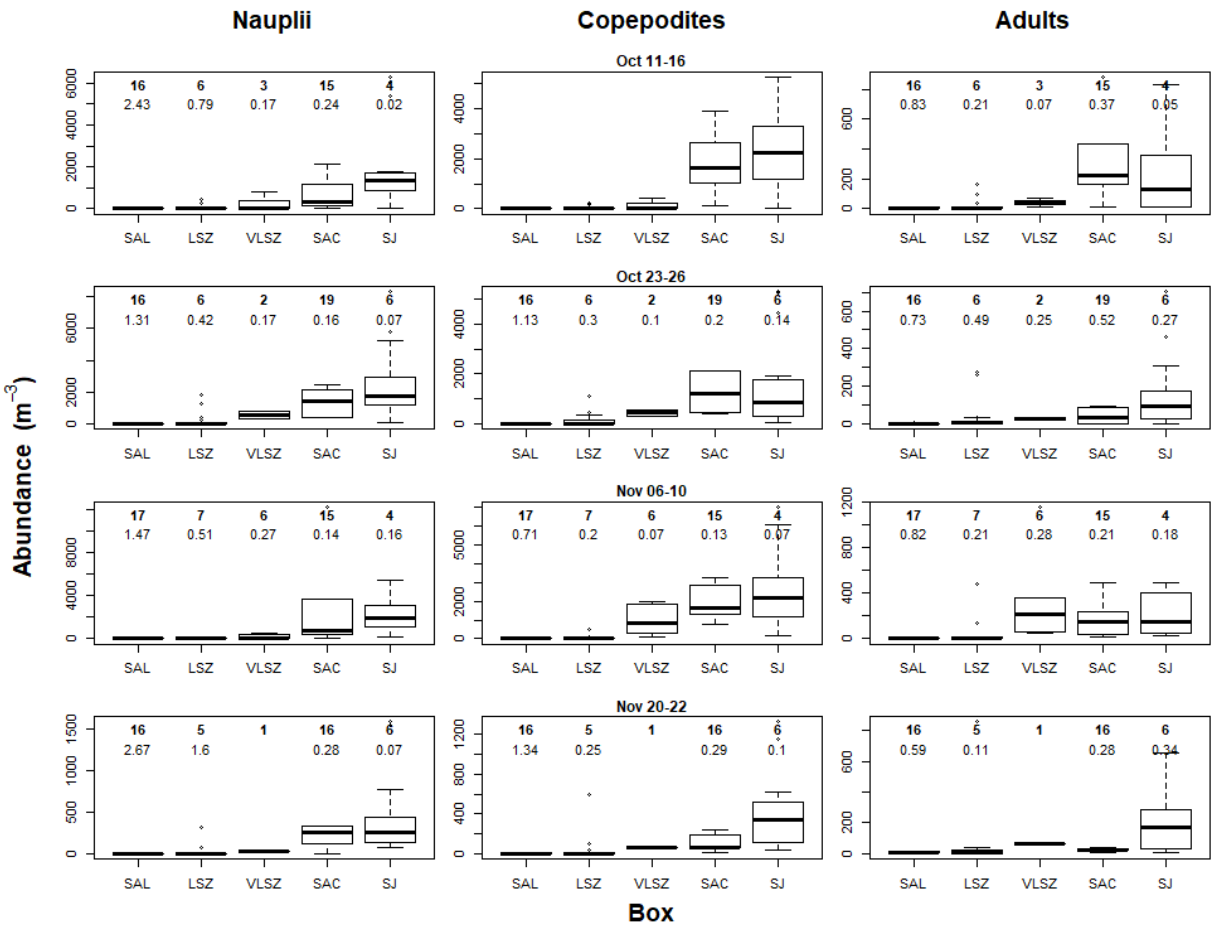

Figure 4. Box plots showing the variability in *P. forbesi* densities across boxes by life stage (columns), sampling survey (rows). The center line in each box plot shows the median and the box shows the interquartile range or IQR. Error bars show Q1-1.5*IQR and Q3+1.5IQR, and points show outliers beyond the error bars. Values at the top of each panel show the number of zooplankton samples used to calculate each distribution (top row) and the coefficients of variation (CV) of log-transformed densities (bottom row).

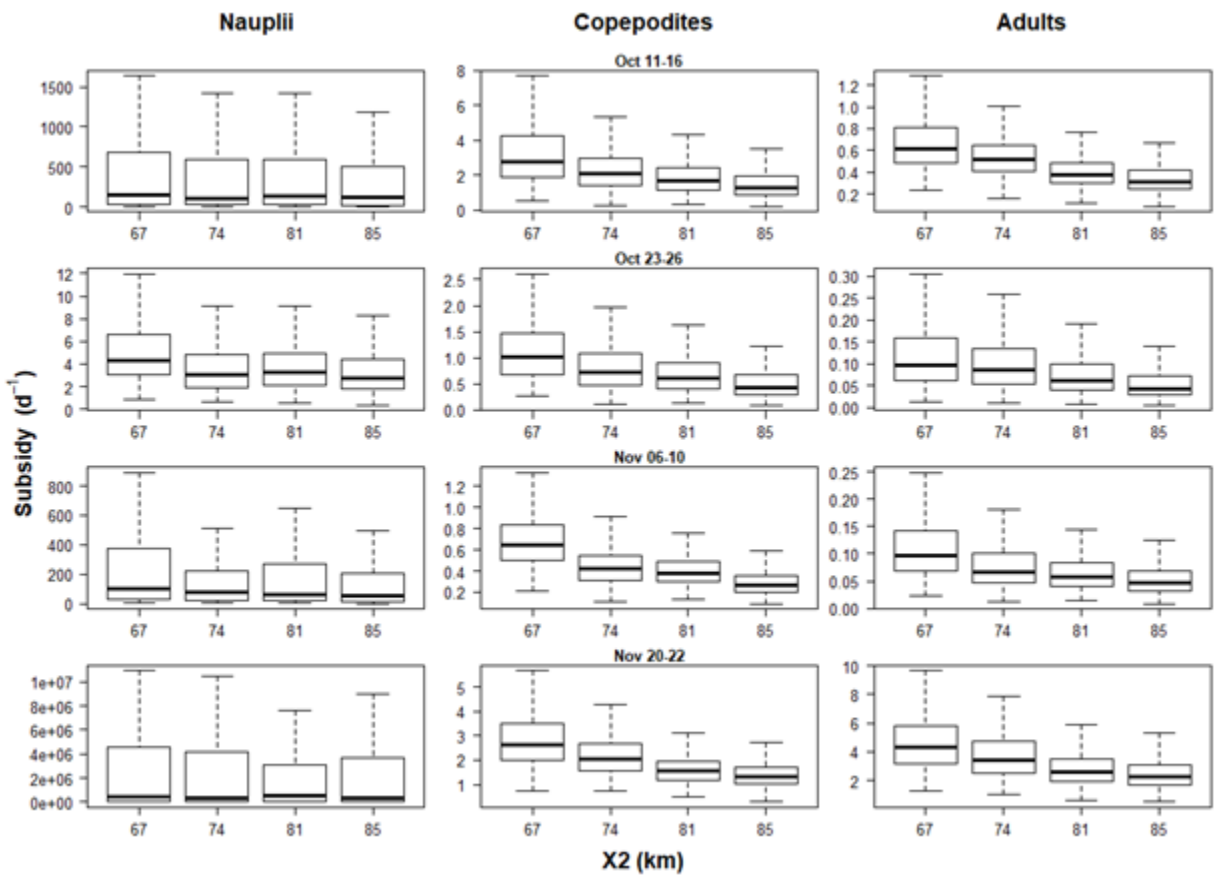

Figure 5. Proportional subsidies of *P. forbesi* (Eqn. 2) to the low-salinity zone (LSZ) by X2 scenario based on passive behavior for nauplii, and the tidal migration behavior for copepodites and adults. Results are shown by life stage (columns) and sampling survey (rows). Boxplots are presented as in Fig. 3 with outliers omitted to show X2 patterns more clearly.

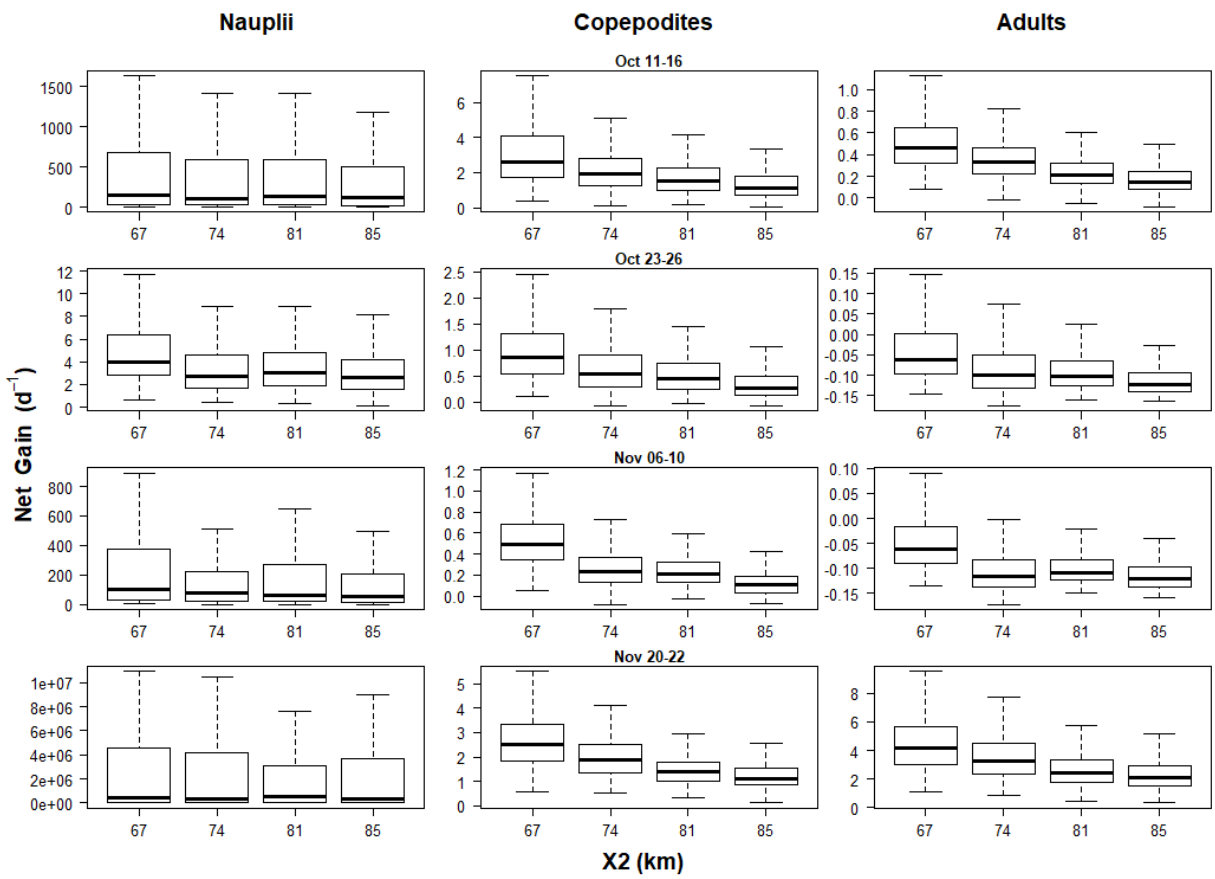

Figure 6. Proportional net gain (Eqn. 3) of *P. forbesi* in the low-salinity zone box (LSZ) by X2 level for each life stage (columns) and sampling survey (rows). Results are shown by life stage (columns) and sampling survey (rows). See caption for Fig. 3 for a description of boxplots. Outliers were omitted to show X2 patterns more clearly.

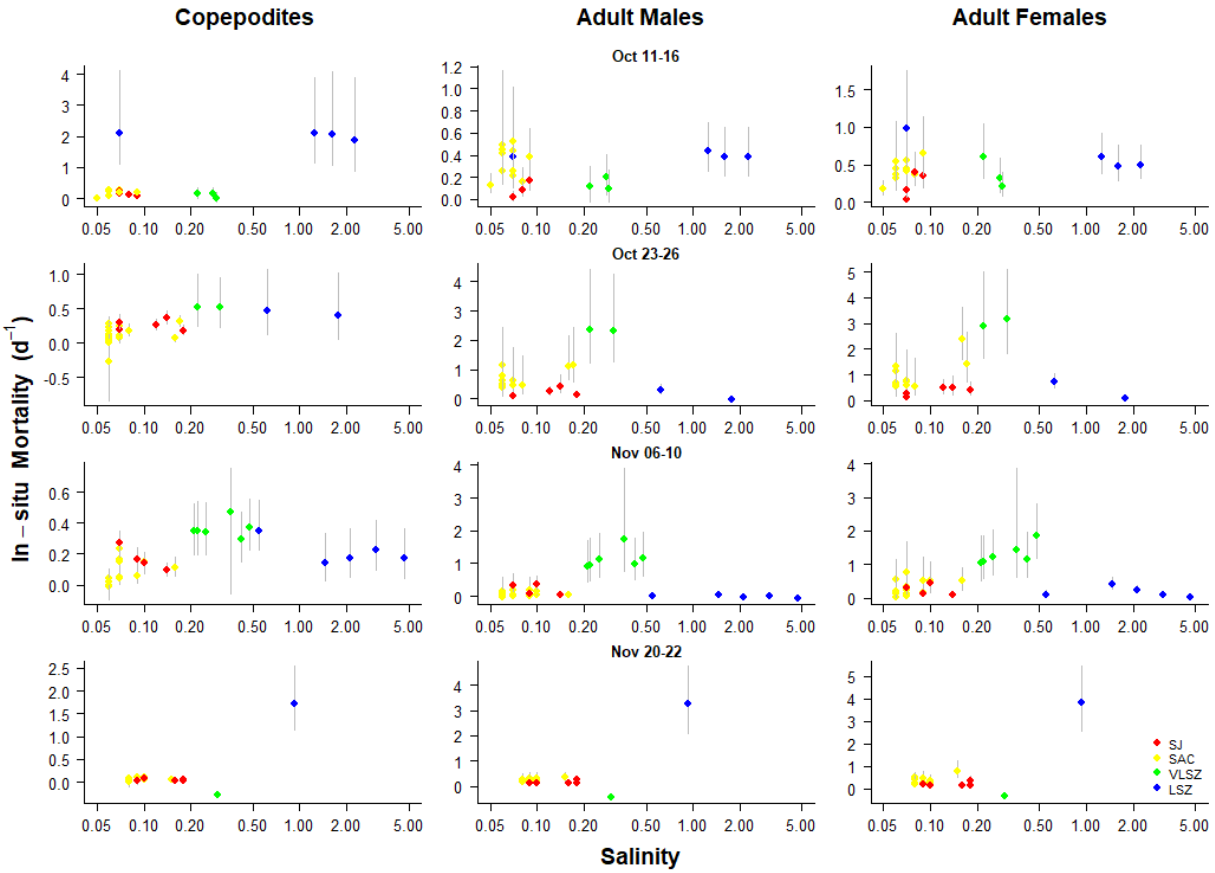

Figure 7. Station-specific estimates of in-situ mortality for *P. forbesi* as a function of salinity by survey (rows) and life stage (columns). The color of points denotes the box the sample was taken in. Points and error bars show the medians and 80% credible intervals, respectively.

Chapter 7: How an Estuarine Prey Field Changes with Managed Freshwater Outflow

How an estuarine prey field changes with managed freshwater outflow

Jason L. Hassrick[1*], April G. Smith[2], Calvin Y. Lee[1], Daniel M. Cox[2], Andrew J. Kalmbach[2], and Andrew A. Schultz[3]
[1] ICF, 201 Mission Street, Suite 1500, San Francisco, CA 94105 USA
[2] ICF, 980 9th Street, Suite 1200, Sacramento, CA 95814 USA
[3] Bureau of Reclamation, Bay-Delta Office, 801 I Street, Sacramento, CA 95814, USA
*Corresponding author: Jason.Hassrick@icf.com

Keywords: zooplankton, *X2*, outflow, estuarine hydrology, Delta Smelt

ABSTRACT

In estuaries with high variation in freshwater inflow, food resources for fish can vary considerably from year to year. Conservation efforts to improve habitat quality for endangered fishes in the tidal San Francisco Estuary have focused on increasing freshwater outflow to expand foraging habitat during the fall season when Delta Smelt body condition for the pre-spawning period has the greatest influence on fecundity. We collected zooplankton abundance and biomass as measures of habitat quality during fall of a high outflow year (2017) and a subsequent low outflow year (2018). Abundance was greater in the high outflow year, but biomass was similar between years. Non-metric multi-dimensional scaling revealed that during the high outflow year, zooplankton communities were more homogeneous across the estuary while in the low outflow year they segregated into distinct low and high salinity groups. Salinity was the primary factor underlying differences between the two years. Deep channel habitat in the low outflow year had higher abundance and biomass than near surface habitat in channels and shoals. Abundance and biomass of macrozooplankton communities (mysids and amphipods) were unaffected by changes in outflow. This paper highlights how managed freshwater outflow during fall can affect distribution and abundance of zooplankton across the estuary in ways that influence habitat dynamics of endangered planktivorous fishes. Salinity appears to influence the structure and composition of the lower trophic community in response to managed outflow in ways that provide insight to impacts from future sea level rise.

INTRODUCTION

Estuaries are especially vulnerable to climate change because they are cumulatively affected by climatic factors that independently affect marine and freshwater systems (Gillanders et al. 2011). This influence of climate change may be exacerbated in regions where freshwater is in scarce supply. Interactions at the interface of fresh and marine waters serve to structure estuarine planktonic prey communities, which influence the quality of habitat for estuarine fishes (Jassby 2008; Kimmerer 2002). Tidal estuaries can be highly productive and dynamic environments that provide critical habitat for many ecologically and economically important species (Barbier et al. 2011; Kimmerer 2004). In tidal estuaries with managed freshwater flows, understanding these processes is critical to developing water management strategies directed at protecting estuarine fishes (Peterson 2003).

The San Francisco Estuary (the estuary) is situated in a Mediterranean climate, in which habitat availability for the lower trophic prey community is dynamic and driven by an interaction of freshwater advection and tidal dispersion of nutrients and organic matter (Kimmerer et al. 2019). Outflow from the Sacramento-San Joaquin Delta (the delta) is the primary source of freshwater to the estuary and some 40 million residents of California. Net outflow is controlled by a combination of inputs from upstream dam releases and exports from two pumping stations in the south delta, from which water is conveyed to water users in other parts of the state through one of the world's most complex and highly managed water conveyance systems.

Changes to estuarine hydrology from managed outflow can influence habitat functionality for estuarine fishes by altering the position and stability of prey phytoplankton and zooplankton assemblages (Cloern 2007; Jassby et al. 1995; Kimmerer 2002; Kimmerer et al. 1998). Understanding how the distribution of the lower trophic community responds to managed freshwater outflow conditions can clarify the effectiveness of management actions aimed at recovering native estuarine fish populations. The state and federally protected endangered Delta Smelt (*Hypomesus transpacificus*) is subject to targeted efforts to improve habitat quality, including increasing prey availability (Feyrer et al. 2003; Grimaldo et al. 2009; Slater and Baxter 2014).

As the Delta Smelt abundance index from state and federal monitoring surveys declined to critical levels in recent years, the species has been thrust into the forefront of water resource management concerns (USFWS 2019b). Increased food availability in the fall season is thought to positively affect the survival of pre-spawning Delta Smelt and the degree of this association appears to strengthen in high outflow years (MAST 2015).

We surveyed distribution, abundance, and biomass of zooplankton assemblages that comprise the Delta Smelt prey field as a proxy for Delta Smelt habitat quality because their scarcity makes it increasingly difficult to directly determine distribution changes of the population in response to environmental conditions (Hobbs et al. 2017). We compared fall conditions between a relatively high outflow year in 2017 and drier conditions in the following low outflow year. We focused on the north estuary where outflow dictates the position of low-salinity habitat (0.5-6 ppt) that juvenile and sub-adult Delta Smelt generally occupy at relatively higher densities (Merz et al. 2011).

During the fall period of "wet" water years, the position of *X2*, defined as the distance (km) from the Golden Gate Bridge to the tidally averaged 2 ppt salinity isohaline (Jassby et al. 1995), is managed to range between 74 to 81 km so that low-salinity water overlaps with Suisun Bay and Suisun Marsh. Within this area, shallow-water shoal habitats, where advection and dispersion are reduced, are known to be important nursery habitat for the successful recruitment of larval estuarine fishes (Grimaldo et al. 2020). In estuarine channel habitats, behavioral mechanisms like diurnal vertical migration can help zooplankton maintain position and make use of dispersive processes associated with tidal exchange and advection from net-positive freshwater inflow to obtain food (Kimmerer et al. 2002). In this paper we address four questions to understand how the Delta Smelt prey field changes in response to managed outflow: [1] How does freshwater outflow affect physical habitat between years and among regions? [2] What prey taxa were influenced by these differences? [3] Is there a difference in prey community abundance and biomass distribution across regions of the estuary that Delta Smelt occupy? and [4] Did the outflow action during the high outflow year enhance the Delta Smelt prey field across low-salinity habitats?

MATERIALS AND METHODS

The San Francisco Estuary is the largest estuary on the west coast of North America. Its watershed extends from the Sierra Nevada range to the Golden Gate Bridge, an area that covers 60,000 square miles and nearly 40% of California. Within the estuary, Suisun Bay and Suisun Marsh, situated just west of the confluence of the delta, combine to form the largest tidal marsh on the west coast. To effectively sample an area this large, we used a generalized random tessellation stratified design (Starcevich et al. 2016; Stevens Jr and Olsen 2004) to randomly select sample stations in the upper estuary (Fig. 1), also known as the North Delta Arc (Moyle et al. 2016). Sampling occurred within and around low-salinity habitat (salinity 0.5-6, Practical Salinity Scale) during the fall period across the North Delta Arc. We focused on five regions that include the Cache Slough Complex, the Sacramento Shipping Channel, the Lower Sacramento River, Suisun Bay and Suisun Marsh (Fig. 1). Three stations in each region were sampled once a week, in tandem with the United States Fish and Wildlife Service (USFWS) Enhanced Delta Smelt Monitoring program. In 2017, sampling occurred on a biweekly basis and in 2018 sampling occurred weekly. We sampled from Sep 24-Nov 29 in 2017 and Sep 5-Nov 30 in 2018.

Habitat Sampling

Habitat sampling methods are listed in Schultz et al. (2019). At each sampling station, individual tows were conducted in three habitat types (surface channel, deep channel, and shoal) when depth conditions were met. Tows were conducted at fixed depths to vertically segregate channel habitats. In channels deeper than 3 m, nets were towed just under the surface, followed by a deep tow along the same transect that sampled the bottom half of the water column. The open-mouth configuration of our nets did not exclude zooplankton during deployment and retrieval to and from the target depth. For deep channel tows, the bridle of the net was weighted with a lead weight of approximately 5 kg. Measures of the warp length and wire angle from the stern tow bar were used to target desired fishing depths,

$$D = sin\ (rad[A]) * L$$

where depth (D) is determined by the product of the sin of the wire angle (A) and the warp length (L) of the tow line. In addition, pressure loggers (HOBO, Bourne, Massachusetts USA) were attached to the net frame to verify and record the sampling depth of each tow. Paired shoal samples were taken when shallow areas less than 2 m deep existed within 0.8 km of the station.

Macro- and meso-zooplankton were sampled using a 50-cm diameter macrozooplankton net frame attached to a smaller 20-cm diameter mesozooplankton net frame and were constructed with 500-µm mesh and 150-µm mesh nets, respectively. Each net was equipped with a flowmeter (General Oceanics, Miami, Florida USA) to determine the volume of water filtered through each net. Five-minute tows were conducted for each habitat and the nets were systematically washed towards the cod end. The contents were preserved with 10% formaldehyde and transferred to the lab for processing.

Spot measurements of temperature, turbidity (NTU), salinity (psu), dissolved oxygen (DO; mg/L), and Chlorophyll-*a* (mg/L) were taken at each habitat prior to the tow using a EXO2 multiparameter sonde (Yellow Springs Inc., Yellow Springs, Ohio USA)). Water samples were filtered by vacuum pressure <10 mm Hg through 0.2 µm, 47-mm diameter polycarbonate filters at each site for surface channel and shoal habitats. The water samples were later analyzed using colorimetric assays for ammonium (NH_4^+, mg/L), nitrate (NO_3^-, mg/L), phosphorous (PO_4^{3-}, mg/L) (Verdouw et al. 1978, Doane and Horwath 2003, Murphy and Riley 1962). Dissolved organic carbon (DOC, mg/L) was analyzed by high temperature catalytic oxidation (Bird et al.

2003). The daily position of *X2* was obtained from California Department of Water Resources (DWR) Dayflow program (CDWR 2020).

Zooplankton samples were identified using methods described in the Interagency Ecological Program's Environmental Monitoring Program (Kayfetz et al. 2020), however, 10 aliquot counts were used instead of 20 aliquot counts due to high densities. All organisms were identified to the lowest taxonomic level possible and zooplankton were further separated by life stage, all of which are hereafter referred to as taxa. Prey taxa noted in this study were confirmed in gut contents of Delta Smelt collected between 0.5 ppt and 6 ppt from September to November for 2011-2017 by Slater et al. (2019)

Data Analysis

Analyses were conducted for two measures of the zooplankton community; abundance by volume (count/m^3) and biomass by volume (µg/m^3), herein referred to as abundance and biomass, respectively. Biomass was calculated by multiplying species specific grams of carbon by the abundance value as outlined in Kayfetz et al (2020) using values from Kimmerer et al. (2011). Covariate analyses of water quality variables, outflow year, taxa, abundance, biomass, and Shannon's diversity index (H′, which accounts for evenness of taxa distributions, vegan package, version 2.5-6; Oksanen et al. 2019), were evaluated using a non-parametric Kruskal-Wallis test (*H* stat) in R version 3.5.3 (R Core Team 2019) followed by a Dunn's pairwise comparison (Ogle et al. 2021). Tests were conducted with Bonferroni corrections for multiple comparisons for all covariates.

The degree of dissimilarity between macro- and meso-zooplankton in the high and low outflow years for abundance and biomass were analyzed with similarity percentage (SIMPER, vegan package, version 2.5-6; Oksanen et al. 2019) in R version 3.5.3 (R Core Team 2019), with permutations following (Clarke 1993; Oksanen et al. 2013). SIMPER identifies a taxa's contribution to dissimilarity between groupings. We identified the top five taxa with the highest contribution to groupings and tested for significant relationships between their abundance and biomass with temperature, turbidity, salinity, dissolved oxygen, dissolved organic carbon, nitrate, phosphate, Chlorophyll-*a*, and ammonium using a negative binomial General Additive Model. We used a negative binomial error distribution because our data were slightly over-dispersed with restricted maximum likelihood estimation (REML; GAM, 'mgcv package version 1.8-31) (Wood 2017).

We performed six separate non-parametric multidimensional scaling (NMDS) ordinations using Bray-Curtis dissimilarity matrices to reduce the dimensionality of a complex dataset and characterize key differences in lower trophic community abundance and biomass across the estuary and within Suisun Bay. NMDS was first run on all prey samples in the estuary and then using only data collected within Suisun Bay. Rare taxa were retained in the analysis because removal of rare species has been shown to alter interpretation of multivariate analysis results significantly; additionally, rare species can be greater indicators of ecosystem stress compared to common species (Poos and Jackson 2012). Prior to calculating the Bray-Curtis dissimilarity matrix used in NMDS, prey samples were square root transformed, followed by a Wisconsin double standardization to equalize emphasis of dominant sites and taxa on the ordination space (Bray and Curtis 1957). The NMDS dissimilarity matrix was performed using 'metaMDS' from the Vegan package following the methods of Oksanen et al. (2019). A two-dimensional solution was selected as the final solution for all six ordinations as it reduced the solution stress to < 0.20 (Kruskal 1964).

Relationships between zooplankton abundance or biomass and environmental covariates were examined by fitting vectors to the ordination space from the NMDS analysis, using the function `envfit` from the vegan package (Oksanen et al. 2019). Vectors indicate the direction with the most significant positive change and were assessed for significance with a permutation test that generates a p-value for the percent of randomly permuted fitted vector lengths that exceed raw fitted vector lengths. The relationship between the environmental covariates, habitat-year and region-year groups with zooplankton abundance or biomass were then visualized by overlapping environmental covariate vectors with convex hulls formed by connecting the vertices of the habitat-year and region-year groups within the two ordination spaces.

RESULTS

Over the course of the study, 194 paired macro- and meso-zooplankton samples were collected in 2017 and 321 pairs were collected in 2018 across five regions and three habitat types. Of these, 193 were from deep in channels, 102 were from shoals, and 220 were from the channel surface (Table 1). The spatial extent of these samples extends from the terminus of the Sacramento Deepwater Ship Channel in the top of the North Delta Arc seaward to Carquinez strait on the western edge of Suisun Bay (Fig. 1). Average fall *X2* was 76.0 km (+/- 0.12 km) and 83.8 km (+/- 0.12 km) in 2017 and 2018, respectively (CDWR 2020). Temperatures were similar across both years and regions, except when Cache Slough was significantly cooler than Suisun Marsh in the 2017 high outflow year (Fig. 2; Table 2). Turbidity was higher in the Sacramento Shipping Channel, Suisun Bay and Suisun Marsh under high outflow but did not change in Cache Slough or the Lower Sacramento. Salinity within a given region was significantly lower in the high outflow year only for the three most seaward regions (Table 2). Dissolved oxygen remained unchanged between the two years for all regions except Suisun Bay, where it was significantly higher in the high outflow year. Chlorophyll-*a* varied by regions in response to outflow conditions with higher values in the high outflow year for the Sacramento Shipping Channel and lower values for Suisun Bay. All other regions were unchanged across the two outflow years. Within each region, concentrations of nitrate, ammonium and phosphate, and DOC were similar between the two years.

Five taxa accounted for 52% of the variation in abundance between outflow years (Fig. 3). These included *Limnoithona tetraspina* copepodites*, Pseudodiaptomus forbesi* copepodites, nauplii, and adults, and *Acartiella sinensis* copepodites. Five taxa accounted for 62% of the variation in biomass between outflow years, including *P. forbesi* adults and copepodites, *A. sinensis* adults and copepodites, and *Tortanus spp.* copepodites.

Abundance and biomass tracked each other closely for a given taxa in response to water quality measures (Fig. 4). *P. forbesi* copepods were more common in freshwater and less common between 4 and 7 psu (Fig. 4). *Acartiella sinensis* and *Limnoithona tetraspina* were more common in salinities above 5 and *Tortanus spp.* was more common in higher salinity water. All taxa were more common at dissolved oxygen levels between 6 and 9 mg/L and at temperatures between 13 and 16°C. *P. forbesi* adults and copepodites also showed an additional increase in abundance at temperatures up to 22.5°C. *P. forbesi* abundance and biomass were correlated with phosphate, where maximum values were centered between concentrations of 0.18 and 0.20 mg/L that corresponded with minimum values for *A. sinensis*, which had maximum values at 0.4 to 0.5 mg/L. Similarly, *P. forbesi* was mostly found in water with low nitrate concentrations, while the other taxa appeared to be more abundant at nitrate concentrations centered around 0.3 mg/L.

Total abundance, total biomass and Shannon's diversity index varied differently by region between the high outflow and low outflow years (Table 2). Overall, the high outflow year had significantly greater abundance for each region (Fig. 5). In the high outflow year, total abundance was similar across all five regions whereas in the low outflow year, total abundance in the Sacramento Shipping Channel was significantly greater than the three more seaward regions. We did not observe a change in biomass for a particular region from one year to the next. All regions were similar in biomass for a given year except in 2017 where the Sacramento Shipping Channel had significantly greater biomass than Suisun Bay. Shannon's diversity was similar within a region across the years. In the high outflow year, Shannon diversity index was greater at Sacramento Shipping Channel relative to the Lower Sacramento River in both years. Shannon's diversity in the lower Sacramento for the low outflow year was significantly lower than all other regions.

Non-metric multidimensional scaling revealed differences in regional taxa abundance/biomass along a salinity gradient, with relatively weak differences along temperature, nitrate, and dissolved oxygen vectors (Fig. 6). None of the other water quality parameters, including phosphate, dissolved organic carbon, ammonium, Chlorophyll-*a*, turbidity, and *X2* contributed significantly to differences in community composition. In the high outflow year, taxa composition overlapped for the three landward regions of Cache Slough, Sacramento Shipping Channel, and Lower Sacramento, whereas Suisun Marsh did not overlap with these regions and was separated along the salinity axis. In the low outflow year, Suisun Bay and Suisun Marsh were separated along the salinity axis from the other regions.

P. forbesi was the most abundant mesozooplankton taxon in the freshwater regions of Cache Slough, Sacramento Shipping Channel, and Lower Sacramento River in both years of the study (Fig. 7, Table 2). Densities of adult *P. forbesi* copepods in Suisun Bay and Suisun Marsh during fall of the high outflow year were not unlike densities observed in other regions except for the Sacramento Shipping Channel, which was substantially higher. In the low outflow year, there were significantly lower densities of all life stages of *P. forbesi* in Suisun Bay and Suisun Marsh relative to all other regions. Conversely, adult and copepodites of the congener, *P. marinus*, were observed in the seaward regions in the low outflow year after having not been present in any of the study regions in the high outflow year. Abundance of all life stages of *A. sinensis* were significantly greater in Suisun Bay and Suisun Marsh than in more freshwater regions during both years of the study (Fig. 7). All life stages of *Eurytemora affinis* were uniformly abundant across regions in the high outflow year, becoming more variable between regions in the low outflow year. Landward regions in that year generally had lower densities of this species relative to Suisun Bay and were significantly less abundant relative to Suisun Marsh. In the high outflow year, adult *Sinocalanous doerrii* were significantly more abundant in Sacramento Shipping Channel than in Cache Slough, Lower Sacramento River and Suisun Bay (Fig. 7). Their copepodite and nauplii were significantly less abundant in Lower Sacramento River and Suisun Bay than in Cache Slough and Sacramento Shipping Channel. Abundances of all life stages of *S. doerrii* in the low outflow year were significantly greater in Sacramento Shipping Channel than all other regions. This species was not observed in Suisun Marsh in either year. The extent of *Tortanus spp.* in the high outflow year was limited to Suisun Bay and Suisun Marsh with abundance significantly greater there in the low outflow year when copepodites were also present in Lower Sacramento River.

Adults and copepodites of *L. tetraspina* were significantly more abundant in Suisun Bay and Suisun Marsh than in other regions during fall of the high outflow year. The same regional

gradient in abundance existed in fall of the low outflow year, however, both life stages of *L. tetraspina* were significantly less abundant in seaward regions relative to the prior high outflow year. The congener, *Limnoithona sinensis*, was significantly less abundant in the high outflow year in Suisun Bay and Suisun Marsh relative to all other regions. In the low outflow year, *L. sinensis* abundance in Cache Slough, Sacramento Shipping Channel, and Lower Sacramento River was significantly lower than the prior year and densities in Suisun Bay and Suisun Marsh remained low.

Macrozooplankton abundances were low in most regions throughout our study. In the high outflow year, *Hyperacanthomysis longirostris* was more abundant in Sacramento Shipping Channel and in the seaward regions, significantly less abundant in Lower Sacramento River, and not present in our samples for Cache Slough. This species was observed at similar densities in both years and were present in very low abundances at Cache Slough. Greater densities of *Neomysis kadiakensis* were detected in Suisun Bay than for Lower Sacramento River. This species expanded to all regions in the low outflow year. Amphipods that were present in all regions during both years included *Americorophium spinicorne*, *Gammarus daiberi*, and *Hyalella* spp.

Cladocerans and rotifers generally decreased in abundance from landward regions to seaward regions in both years. In contrast, barnacle nauplii had significantly greater densities in Suisun Bay and Suisun Marsh. Ostracod abundance was significantly lower in Suisun Bay than Cache Slough. Variation in biomass of individual taxa across regions and between years varied similarly with abundance (Fig. 8, Table 2).

In the low outflow year of 2018, variation in the total abundance and biomass of zooplankton between habitats was greatest in Sacramento Shipping Channel, Lower Sacramento River, and Suisun Bay (Fig. 9). Total biomass in the deep portion of the channels in the low outflow year was significantly greater than the channel surface, though this was not true in the high outflow year. Surface habitats of channels in Suisun Bay had significantly lower biomass than at depth during low outflow, however, the decrease was less pronounced for shoal habitats. Shannon diversity indices were lowest in the Lower Sacramento River in both years, particularly in deep channel habitat during low outflow conditions. Suisun Bay, however, had slightly greater diversity at depth than at the surface of channels and shoals during the low outflow year. Shoal habitat was only examined for Suisun Bay because shoal habitats were less frequently found and sampled in other regions (Table 1).

No substantial differences were observed between the macrozooplankton communities in Suisun Bay across years with high and low outflow or across habitats between years (Fig. 10). Deep channel habitats during the high outflow year had a more constrained community composition relative to assemblages in channel surface and shoal habitats. There was, however, a strong influence on the community abundance along a salinity gradient ($r^2 = 0.43$) and weak associations with temperature, nitrate, *X2*, ammonium, and phosphate. Macrozooplankton community biomass had similar relationships as abundance to the water quality variables.

The composition of the mesozooplankton assemblage in Suisun Bay changed between the two outflow years to a greater extent than macrozooplankton (Fig. 10). Salinity had the greatest influence in the structuring of these two assemblages, followed by *X2* and dissolved oxygen. Salinity and *X2* were autocorrelated to an extent ($r^2 = 0.67$) but the lack of overlap between the gradient vectors within the NMDS suggested that both variables be included (Fig. 10). There were small differences in zooplankton community composition between habitat types as well for each year. In the high outfow year, mesozooplankton assemblages in the channel surface and

deep habitats were similar to shoal habitat but diverged mostly along the DO gradient and only slightly along the *y*-component of the salinity gradient. Conversely, all three habitat types in Suisun Bay were similar in the low outflow year. Mesozooplankton in the deep channel habitats during the high outflow year were less similar in composition to assemblages in channel surface and shoal habitats relative to the low outflow year. Salinity, *X2*, and DO were the underlying factors that separated the composition of the zooplankton community in all habitats across the two outflow years.

DISCUSSION

The San Francisco Estuary remains one of the largest tidal marshes on the west coast of North America and still exhibits habitat complexity that is lacking in most other areas of the estuary. Many native fishes that historically characterized this marsh complex have undergone severe declines (Matern et al. 2002; Meng et al. 1994). For example, the prey field for Delta Smelt has changed dramatically over time. In the 1980s, introduced copepods like *P. forbesi* began to replace *E. affinis*, also introduced, as the dominant copepod in the estuary (Moyle et al. 1992). Since then, the non-native overbite clam, *Potamocorbula amurensis*, contributed to the decimation of mysids (Kimmerer and Orsi 1996). Introductions of other invasive copepods such as *A. sinensis* and *L. tetraspina* have further altered the prey field through new food web dynamics (Orsi and Ohtsuka 1999; Slaughter et al. 2016). Here, we have shown the extent to which outflow actions can differentially affect mesozooplankton and macrozooplankton as the salinity gradient shifts across habitats.

Outflow actions taken in fall of 2017 altered the physical environment by depressing average *X2* and mobilizing the salinity gradient further seaward (Fig. 2), which was expected as the outflow action was targeted to increase low-salinity habitat for pre-spawning Delta Smelt in Suisun Bay (Brown et al. 2014; USFWS 2019a). The seaward expansion of the low-salinity zone into the Suisun Bay and Suisun Marsh complex was accompanied by increased turbidity and low chlorophyll-*a*, however, larger and more nutritious diatoms constituted a greater proportion of the phytoplankton community (Kalmbach et al. 2021). These shifts in the salinity gradient were associated with the variable distributions of several important zooplankton taxa that compose the prey field available to Delta Smelt.

Enhanced freshwater outflow redistributes the mesozooplankton assemblage throughout the upper estuary primarily by advection along the surface of channels, but it does not appear to have a similar effect on macrozooplankton. The prey base for planktivorous fish in the low-salinity habitat of the upper estuary defined by the position of *X2* is relatively poor, due in part to non-native clams that outcompete zooplankton for phytoplankton and also prey on zooplankton nauplii (Kimmerer and Orsi 1996; Kimmerer et al. 1994; Kimmerer and Lougee 2015; Kimmerer and Thompson 2014). Since the introductions of *P. amurensis* in 1986 and *A. sinensis* in 1993, the population center of *P. forbesi* shifted further up the salinity gradient away from the low-salinity zone (Kimmerer et al. 1998; Slaughter et al. 2016). In the present study, the shift in distribution of this taxa to low-salinity habitat in Suisun Bay during high outflow (Fig. 7) is best explained by Kimmerer et al. (2019) who determined that when flows are high, movement of *P. forbesi* from areas of high abundance can subsidize areas of low abundance. Moreover, the broader width of Suisun Bay increases the area and volume of low-salinity habitat under outflow conditions as in 2017. These favorable environmental conditions overlap with low current speeds and allow organisms to retain position in the estuary and overcome net seaward transport.

The relatively small, non-native cyclopoid copepod, *L. tetraspina*, which is a common prey item of Delta Smelt in the low-salinity zone during fall (Slater and Baxter 2014; Slater et al. 2019), was more abundant during the high outflow year in Suisun Bay and Suisun Marsh (Fig. 7). Despite its abundance, direct consumption of *L. tetraspina* yields poor nutritional value because it feeds on ciliates, a nutritionally impoverished food source, and it carries a bioenergetic cost because similar energetic effort is required to capture a prey item of low or high quality (Bouley and Kimmerer 2006; Winder and Jassby 2011). Predation of *L. tetraspina* by the large calanoid copepod *A. sinensis* is an important trophic link for adult Delta Smelt (Gould and Kimmerer 2010; Slaughter et al. 2016). Augmented outflow had no effect on the abundance or biomass of *A. sinensis* in the seaward regions of our study (Fig. 7), which may be attributed to its tolerance of salinities between 0 and 20 with maximum densities observed in salinities ranging between 2.5 and 8.6 (Orsi and Ohtsuka 1999). Lower outflow in 2018 and higher salinities in the Lower Sacramento Region meant the preferred habitat for adult *A. sinensis* extended landward and could have limited *Psuedodiaptomus* nauplii numbers in that region (Fig. 7 and 8). Similarly, *Tortanus* spp. can range from mesohaline salinities between 1.2 to 13 (Orsi and Ohtsuka 1999) and was more commonly encountered in the low outflow year. While this taxon is a large contributor to biomass in the lower trophic community in Suisun Bay and Suisun Marsh, it is not a common prey item for Delta Smelt in low-salinity habitat during fall (Slater et al. 2019). Instead, a higher proportion of cyclopoid and harpacticoid copepods as well as cladocerans, to some extent, tend to appear in diets of Delta Smelt (Slater and Baxter 2014; Slater et al. 2019).

Among macrozooplankton, mysids represent most of the biomass in the diets of Delta Smelt in the low-salinity habitat during fall (Slater et al. 2019). The low abundance and biomass of mysids reported here are consistent with observations recorded since their decline began in the 1980s, which subsequently led to a significant decrease in consumption of mysids by Delta Smelt (Feyrer et al. 2003). Mysids have been important supplemental prey items in the past (Feyrer et al. 2003; Moyle et al. 1992). The slightly decreasing trend we saw in abundance and biomass of the amphipod *Americorophium stimpsoni* from high to low outflow conditions may be a response to salinity (Hymanson et al. 1994). A lack of a response during the fall period of 2017 and 2018 by mysids, cladocerans, and rotifers to changes in outflow within regions suggests that this component of the prey field is controlled by factors that are either not sensitive to changes in flow or respond at a time lag beyond our ability to detect with temporal extent of this study. The high variability in macrozooplankton indicates that greater sampling over more years is required to achieve sufficient power to resolve the effects of flow. Future work on the distribution and abundance of mysids throughout the estuary would provide insight to what other factors that may be limiting the low numbers observed.

Mechanisms behind a seasonal flow response of estuarine organisms in the upper estuary has been a subject of much investigation. Castillo (2019) showed fall outflow resulting in an *X2* of 74 km during fall can improve the potential carrying capacity in low-salinity habitat for Delta Smelt and their supporting lower trophic prey communities, though this does not necessarily equate with increased Delta Smelt catch (Schultz et al. 2019). Greater abundances of zooplankton observed during the period when the low-salinity zone overlapped Suisun Bay and Suisun Marsh in the high outflow year is consistent with previous findings by Kimmerer et al. (2018b) that greater abundances of zooplankton are found during a wet year compared to a dry year. Indeed, densities of lower trophic communities in Suisun Bay and Suisun Marsh were greater in 2017 relative to 2018 (Fig. 5), which support the importance of connectivity between landward and seaward regions with respect to improved productivity that sustain higher trophic

levels (Cloern 2007; Lopez et al. 2006), including Delta Smelt (Moyle et al. 2016). However, variability between regions suggests that other factors, such as clam predation and grazing, may be more limiting for recovering the lower food web than outflow.

The magnitude of flow in the low-salinity habitat of the Delta determines over-wintering success and subsequent prevalence of the invasive overbite clam, *P. amurensis* (Kimmerer and Thompson 2014). Prior to our study, benthic monitoring efforts by the Interagency Ecological Program Environmental Monitoring Program found them in high abundance during the entire low outflow year of 2018 but did not detect them from the confluence of the Sacramento and San Joaquin rivers seaward prior to the fall of 2017 (Arena and Wells 2018; Watkins and Wells 2019). Relatively low success in over-wintering by adult clams in wet years like 2017 may reduce fall grazing pressure on primary producers to some extent and predation pressure on microzooplankton by limiting clam populations to the recruits that recolonize the low-salinity habitat. Community structure and function in Suisun Bay and Suisun Marsh during fall of 2017 likely benefited from the interaction of landward subsidies and reduced competition among lower trophic levels due to clam populations of smaller size-classes in fall. Conversely, overwintering of adults in the dry conditions of 2018 may have contributed to greater impacts from larger-sized clam populations on seaward zooplankton assemblages in addition to the reduction in subsidies from landward regions. Ongoing monitoring of *P. amurensis* has revealed that successful recruitment is restricted to the fall season in non-drought years (Crauder et al. 2016). Targeted sampling of plankton resources and *P. amurensis* during recolonization in the low-salinity zone would improve our understanding of how variability in flow may affect lower trophic levels in the low-salinity zone.

Delta Smelt are known to aggregate at the shoal-channel interface to facilitate their position in the estuary by moving laterally with the tides (Bennett and Burau 2015). Channelization of the delta, formerly a dendritic system, has reduced the complexity of the estuarine landscape (Brown et al. 2016). Shoal habitat in the freshwater regions of our study was scarce relative to Suisun Bay (Table 1) thereby limiting habitat comparisons to this region.

Within Suisun Bay, similarities in abundance and biomass metrics of the lower food web across habitats in the high outflow year (Fig. 9) suggest that habitat assemblages reflect the overall structure of the community in that region. Bever et al. (2016) demonstrated that depth-averaged salinities in the Suisun Bay and Suisun Marsh complex fell below 6 psu for a greater percentage of time during fall of a wet year (2011) relative to a dry year (2010). Minimal variation in the prey field as well as the salinity field across Suisun Bay habitats in 2017 may be a result of greater mixing. In 2018, differences in biomass may have resulted from advection of high primary production in shoals into deep channel habitats where currents are weaker (Lopez et al. 2006). While average salinities across all habitats were elevated in 2018, the sustained higher biomass in the deep channels may have resulted from potentially greater stratification, which may develop in Suisun Bay channels during low flow conditions, as well as increased variability in turbidity. The lower turbidity in shoals and the channel surface during the dry year may increase the visibility of zooplankton to predators such that zooplankton are less likely to migrate vertically to habitats with greater clarity (Williamson et al. 2011). It should be noted that the loss of phytoplankton by clam grazing is fastest in shallow habitats (Kimmerer and Thompson 2014) and this limitation on production and flux of energy between habitats across varying outflow conditions remains to be investigated.

Management Implications and Future Directions

Under low outflow conditions, Suisun Bay and Suisun Marsh have relatively low abundance and biomass in the lower food web. Flow augmentation to Suisun Bay and Suisun Marsh in a high outflow year was effective at increasing these metrics for some known prey items of Delta Smelt, however, this did not coincide with greater catches of the endangered planktivorous fish (Schultz et al. 2019). Increased zooplankton during high flow years is attributed to subsidies from upstream, however, predation by non-native clams may be diminishing the effect of the subsidy (Hassrick et al. 2020; Kimmerer et al. 2018b)

The invasive clam population has a large effect on not only zooplankton communities but also phytoplankton, ultimately leading to alterations at multiple levels of the food web as evidenced by decreased Chlorophyll-*a* levels, the decline of mysid populations, and changes in seasonality and range of calanoid copepod species (Jassby et al. 2002; Kimmerer et al. 1994; Orsi and Mecum 1996). Salinity can affect abundance and distribution of *P. amurensis* by affecting recruitment success (Baumsteiger et al. 2017; Crauder et al 2016), but it may take multiple years to see a significant ecosystem-wide effect due to source/sink dynamics and climate change, which may result in long drought periods.

Restoration of tidal marshes could benefit Delta Smelt by supplementing their zooplankton diet with larval fish prey. Tidal marshes serve as nurseries for many fish species that may in turn become sources of nutrition for Delta Smelt (Hammock et al. 2019). Data paired with current profiles from Suisun Marsh across wet and dry years can provide greater resolution about lower trophic community dynamics as they pertain to changes in advection with varying outflow.

Certain regions had high abundance and biomass throughout both wet and dry years such as Cache Slough and the Sacramento Shipping Channel. Studies have shown these regions can be very productive and suggest certain habitats such as terminal channels could be highly productive (Feyrer et al. 2017; Kimmerer et al. 2018a). Some Delta Smelt reside in these areas year-round but the abiotic and biotic factors that drive high productivity and zooplankton abundance require further study.

Future investigations that focus on the effectiveness of habitat restoration, particularly on how it affects availability of nursery shoal habitat and clam abundance, may provide insight to other factors that are limiting Delta Smelt recovery. Flow is often used as a master variable to manage fish populations. While managed flows can affect the prey field, further actions to complement these efforts in the recovery of Delta Smelt include restoring habitat complexity and productivity as well as mitigating the effects of non-native clams.

ACKNOWLEDGEMENTS

This work was conducted as part of the Interagency Ecological Program (IEP) annual work plan. Early reviews of related study plans were supported by the IEP Flow Alteration Project Work Team and the Collaborative Adaptive Management Team (special thanks to Larry Brown [United States Geological Survey), and USFWS, DWR, California Department of Fish and Wildlife (CDFW), and U.S. Bureau of Reclamation (USBR). We thank Kristin Arend (USBR) for helpful review of the manuscript. Permitting for this work was facilitated through CDFW, USWFS and IEP. This study was supported by the contribution of multiple IEP agency field sampling activities of fish and zooplankton (CDFW, USFWS, DOP [USBR]), as well as informed by DWR DAYFLOW. Funding and contractual support was provided by USBR, DWR, State Water Contractors (special thanks to Jennifer Pierre) and State and Federal Contractors Water Agency (special thanks to Laura Valoppi). We acknowledge the support of

many people from the Delta science community. Contributors from ICF include Colin Brennan, Rob Miller, Athena Maguire, Andrew Winston, Ramona Zeno, Jake Sousa, Angelina Ravani, Tim Carrara, Katherine Maniscalco, Donna Maniscalco, Eric Chapman and Stephanie Owens. We thank Catherine Johnston and Lara Mitchell (USFWS) on timely guidance for site selection, coordination, and data; April Hennessy, Steve Slater, and Christina Burdi (CDFW) for assistance with zooplankton and data; and Michael Beakes (USBR) for statistical advice and reviews; and Tom Philippi (National Park Service) for sampling and GRTS advice. Any use of trade, product, or firm names is for descriptive purposes only and does not imply endorsement by the U.S. Bureau of Reclamation or the U.S. Government. The views expressed are those of the authors and do not represent the official opinion of the USBR.

LITERATURE CITED

Arena, B., and B. Wells. 2018. Benthic monitoring, 2017. Interagency Ecological Program for the San Francisco Estuary, 6-13: IEP Newsletter.

Barbier, E.B., S.D. Hacker, C. Kennedy, E.W. Koch, A.C. Stier, and B.R. Silliman. 2011. The value of estuarine and coastal ecosystem services. *Ecological monographs* 81: 169-193.

Baumsteiger, J., R.E. Schroeter, T. O'Rear, J.D. Cook, and P.B. Moyle. 2017. Long-term surveys show invasive overbite clams (Potamocorbula amurensis) are spatially limited in Suisun Marsh, California. *San Francisco Estuary and Watershed Science* 15.

Bennett, W.A., and J.R. Burau. 2015. Riders on the storm: selective tidal movements facilitate the spawning migration of threatened Delta Smelt in the San Francisco Estuary. *Estuaries and Coasts* 38: 826-835.

Bever, A.J., M.L. MacWilliams, B. Herbold, L.R. Brown, and F.V. Feyrer. 2016. Linking hydrodynamic complexity to Delta Smelt (Hypomesus transpacificus) distribution in the San Francisco Estuary, USA. *San Francisco Estuary and Watershed Science* 14.

Bird, S. M., M. S. Fram, and K. L. Crepeau, K. L. 2003. *Method of Analysis by the US Geological Survey California District Sacramento Laboratory: Determination of Dissolved Organic Carbon in Water by High Temperature Catalytic Oxidation, Method Validation, and Quality-control Practices* (p. 14). US Department of the Interior, US Geological Survey.

Bouley, P., and W. Kimmerer. 2006. Ecology of a highly abundant, introduced cyclopoid copepod in a temperate estuary. *Marine Ecology Progress Series* 324: 219-228.

Bray, J.R., and J.T. Curtis. 1957. An Ordination of the Upland Forest Communities of Southern Wisconsin. *Ecological Monographs* 27: 326-349.

Brown, L., Baxter, G. Castillo, Conrad, S. Culberson, Erickson, Feyrer, Fong, Gehrts, L. Grimaldo, H. Bruce, Kirsch, S. Mueller, S. Slater, Souza, and E. Nieuwenhuyse. 2014. *Synthesis of studies in the fall low-salinity zone of the San Francisco estuary, September–December 2011: U.S. Geological Survey Scientific Investigations Report 2014–5041, 136 p.* Reston, VA: U.S. Geological Survey.

Brown, L.R., W. Kimmerer, J.L. Conrad, S. Lesmeister, and A. Mueller–Solger. 2016. Food webs of the Delta, Suisun Bay, and Suisun Marsh: an update on current understanding and possibilities for management. *San Francisco Estuary and Watershed Science* 14.

California Department of Water Resources. 2020. Dayflow: Environmental Planning and Information Branch. Dayflow Program. https://data.cnra.ca.gov/dataset/dayflow

Castillo, G.C. 2019. Modeling the influence of outflow and community structure on an endangered fish population in the upper San Francisco Estuary. *Water* 11: 1162.

Clarke, K.R. 1993. Non-parametric multivariate analyses of changes in community structure. *Australian Journal of Ecology* 18: 117-143.

Cloern, J.E. 2007. Habitat connectivity and ecosystem productivity: Implications from a simple model. *The American Naturalist* 169: E21-E33.

Cloern, J.E., N. Knowles, L.R. Brown, D. Cayan, M.D. Dettinger, T.L. Morgan, D.H. Schoellhamer, M.T. Stacey, M. Van der Wegen, and R.W. Wagner. 2011. Projected evolution of California's San Francisco Bay-Delta-River system in a century of climate change. *PloS one* 6: e24465.

Crauder, J.S, J.K. Thompson, F. Parchaso, R.I. Anduaga, S.A. Pearson, K. Gehrts, H. Fuller, and E. Wells. 2016. *Bivalve Effects on the Food Web Supporting Delta Smelt: A Long-term Study of Bivalve Recruitment, Biomass, and Grazing Rate Patterns with Varying Freshwater Outflow*: US Department of the Interior, US Geological Survey. Open-File Report 2016-1005, 216 p., http://dx.doi.org/10. 3133/ofr20161005.

Doane, T. A., and W.R. Horwáth, 2003. Spectrophotometric determination of nitrate with a single reagent. *Analytical letters*, *36*(12), 2713-2722.

Feyrer, F., B. Herbold, S.A. Matern, and P.B. Moyle. 2003. Dietary shifts in a stressed fish assemblage: consequences of a bivalve invasion in the San Francisco Estuary. *Environmental Biology of Fishes* 67: 277-288.

Feyrer, F., S.B. Slater, D.E. Portz, D. Odom, T. Morgan-King, and L.R. Brown. 2017. Pelagic nekton abundance and distribution in the northern Sacramento–San Joaquin Delta, California. *Transactions of the American Fisheries Society* 146: 128-135.

Gillanders, B.M., T.S. Elsdon, I.A. Halliday, G.P. Jenkins, J.B. Robins, and F.J. Valesini. 2011. Potential effects of climate change on Australian estuaries and fish utilising estuaries: a review. *Marine and Freshwater Research* 62: 1115-1131.

Gould, A.L., and W.J. Kimmerer. 2010. Development, growth, and reproduction of the cyclopoid copepod Limnoithona tetraspina in the upper San Francisco Estuary. *Marine Ecology Progress Series* 412: 163-177.

Grimaldo, L., J. Burns, R.E. Miller, A. Kalmbach, A. Smith, J. Hassrick, and C. Brennan. 2020. Forage Fish Larvae Distribution and Habitat Use During Contrasting Years of Low and High Freshwater Flow in the San Francisco Estuary. *San Francisco Estuary and Watershed Science* 18.

Grimaldo, L.F., A.R. Stewart, and W. Kimmerer. 2009. Dietary segregation of pelagic and littoral fish assemblages in a highly modified tidal freshwater estuary. *Marine and Coastal Fisheries: Dynamics, Management, and Ecosystem Science* 1: 200-217.

Hammock, B.G., R. Hartman, S.B. Slater, A. Hennessy, and S.J. Teh. 2019. Tidal wetlands associated with foraging success of Delta Smelt. *Estuaries and Coasts* 42: 857-867.

Hassrick, J.L., J. Korman, W. Kimmerer, E.Gross, L.F. Grimaldo, C.Y. Lee, and A.A. Schultz. 2020. The effect of outflow on subsidy of a key calanoid copepod prey item for delta smelt in the San Francisco Estuary. Manuscript submitted for publication.

Hobbs, J., P.B. Moyle, N. Fangue, and R.E. Connon. 2017. Is extinction inevitable for Delta Smelt and Longfin Smelt? An opinion and recommendations for recovery. *San Francisco Estuary and Watershed Science* 15.

Hymanson, Z.P., D. Mayer, and J. Steinbeck. 1994. *Long-term Trends in Benthos Abundance and Persistence in the Upper Sacramento-San Joaquin Estury: Summary Report, 1980-1990*: Interagency Ecological Program for the San Francisco Bay/Delta Estuary.

Jassby, A.D. 2008. Phytoplankton in the Upper San Francisco Estuary: Recent Biomass Trends, Their Causes, and Their Trophic Significance. *San Francisco Estuary and Watershed Science* 6.

Jassby, A.D., J.E. Cloern, and B.E. Cole. 2002. Annual primary production: Patterns and mechanisms of change in a nutrient-rich tidal ecosystem. *Limnology and Oceanography* 47: 698-712.

Jassby, A.D., W.J. Kimmerer, S.G. Monismith, C. Armor, J.E. Cloern, T.M. Powell, J.R. Schubel, and T.J. Vendlinski. 1995. Isohaline Position as a Habitat Indicator for Estuarine Populations. *Ecological Applications* 5: 272-289.

Kalmbach, A.K., D.M. Cox, C.Y. Lee, and A. Schultz. 2021. Comparison of Phytoplankton Community Structure and Nutrient Conditions in the Sacramento River Delta During a Fall Flow Action and Non-action Period. Unpublished manuscript.

Kayfetz, K., S.M. Bashevkin, M. Thomas, R. Hartman, C.E. Burdi, A. Hennessy, T. Tempel, A. Barros, D.S. Council, and E. Burdi. 2020. Zooplankton Integrated Dataset Metadata Report. *IEP Technical Report 93*., ed. C.D.O.W. Resources. Sacramento, California.

Kimmerer, W. 2002. Physical, biological, and management responses to variable freshwater flow into the San Francisco Estuary. *Estuaries* 25: 1275-1290.

Kimmerer, W. 2004. Open water processes of the San Francisco Estuary: from physical forcing to biological responses. *San Francisco Estuary and Watershed Science* 2.

Kimmerer, W., J. Burau, and W. Bennett. 1998. Tidally oriented vertical migration and position maintenance of zooplankton in a temperate estuary. *Limnology and Oceanography* 43: 1697-1709.

Kimmerer, W., J.R. Burau, and W. Bennett. 2002. Persistence of tidally-oriented vertical migration by zooplankton in a temperate estuary. *Estuaries* 25: 359-371.

Kimmerer, W., T.R. Ignoffo, and B. Bemowski. 2018a. Zooplankton Dynamics in the Cache Slough Complex of the Upper San Francisco Estuary. *San Francisco Estuary and Watershed Science* 16: 3.

Kimmerer W, T.R. Ignoffo, and L. Sullivan L. 2011. Length, weight, carbon, and nitrogen content of the common copepods in the San Francisco Estuary. Tiburon, CA: Romberg Tiburon Center, San Francisco State University. Unplublished Manuscript.

Kimmerer, W., and J. Orsi. 1996. Changes in the zooplankton of the San Francisco Bay Estuary since the introduction of the clam Potamocorbula amurensis. *San Francisco Bay: The Ecosystem*: 403-424.

Kimmerer, W.J., E. Gartside, and J.J. Orsi. 1994. Predation by an introduced clam as the likely cause of substantial declines in zooplankton of San Francisco Bay. *Marine ecology progress series*: 81-93.

Kimmerer, W.J., E.S. Gross, A.M. Slaughter, and J.R. Durand. 2019. Spatial subsidies and mortality of an estuarine copepod revealed using a box model. *Estuaries and coasts* 42: 218-236.

Kimmerer, W.J., T.R. Ignoffo, K.R. Kayfetz, and A.M. Slaughter. 2018b. Effects of freshwater flow and phytoplankton biomass on growth, reproduction, and spatial subsidies of the estuarine copepod Pseudodiaptomus forbesi. *Hydrobiologia* 807: 113-130.

Kimmerer, W.J., and L. Lougee. 2015. Bivalve grazing causes substantial mortality to an estuarine copepod population. *Journal of Experimental Marine Biology and Ecology* 473: 53-63.

Kimmerer, W.J., and J.K. Thompson. 2014. Phytoplankton growth balanced by clam and zooplankton grazing and net transport into the low-salinity zone of the San Francisco Estuary. *Estuaries and Coasts* 37: 1202-1218.

Kruskal, J.B. 1964. Nonmetric multidimensional scaling: a numerical method. *Psychometrika* 29: 115-129.

Lavee, H., A.C. Imeson, and P. Sarah. 1998. The impact of climate change on geomorphology and desertification along a Mediterranean-arid transect. *Land degradation & development* 9: 407-422.

Lopez, C.B., J.E. Cloern, T.S. Schraga, A.J. Little, L.V. Lucas, J.K. Thompson, and J.R. Burau. 2006. Ecological values of shallow-water habitats: Implications for the restoration of disturbed ecosystems. *Ecosystems* 9: 422-440.

MacWilliams, M.L., A.J. Bever, E.S. Gross, G.S. Ketefian, and W.J. Kimmerer. 2015. Three-dimensional modeling of hydrodynamics and salinity in the San Francisco estuary: An evaluation of model accuracy, X2, and the low–salinity zone. *San Francisco Estuary and Watershed Science* 13.

MAST. 2015. An updated conceptual model of Delta Smelt biology: our evolving understanding of an estuarine fish, ed. M. Interagency Ecological Program, Analysis, and Synthesis Team, 200. Sacramento, CA, USA: Interagency Ecological Program for the San Francisco Bay/Delta Estuary.

Matern, S.A., P.B. Moyle, and L.C. Pierce. 2002. Native and alien fishes in a California estuarine marsh: twenty-one years of changing assemblages. *Transactions of the American Fisheries Society* 131: 797-816.

Meng, L., P.B. Moyle, and B. Herbold. 1994. Changes in abundance and distribution of native and introduced fishes of Suisun Marsh. *Transactions of the American Fisheries Society* 123: 498-507.

Merz, J.E., S. Hamilton, P.S. Bergman, and B. Cavallo. 2011. Spatial perspective for delta smelt: a summary of contemporary survey data. *California Fish and Game* 97: 164-189.

Moyle, P.B., L.R. Brown, J.R. Durand, and J.A. Hobbs. 2016. Delta smelt: life history and decline of a once-abundant species in the San Francisco Estuary. *San Francisco Estuary and Watershed Science* 14.

Moyle, P.B., B. Herbold, D.E. Stevens, and L.W. Miller. 1992. Life history and status of delta smelt in the Sacramento-San Joaquin Estuary, California. *Transactions of the American Fisheries Society* 121: 67-77.

Murphy, J. A. and J.P Riley, 1962. A modified single solution method for the determination of phosphate in natural waters. *Analytica Chimica Acta*, *27*, 31-36.

Ogle, D.H., P. Wheeler, and A. Dinno. 2021. FSA: Fisheries Stock Analysis. R package version 0.8.32, https://github.com/droglenc/FSA

Oksanen, J., F.G. Blanchet, R. Kindt, P. Legendre, P.R. Minchin, R. O'hara, G.L. Simpson, P. Solymos, M.H.H. Stevens, and H. Wagner. 2013. Package 'vegan'. *Community ecology package, version* 2: 1-295.

Oksanen, J.F., G. Blanchet, M. Friendly, R. Kindt, P. Legendre, D. McGlinn, P.R. Minchin, R.B. O'Hara, G.L. Simpson, P. Solymos, M.H.H. Stevens, E. Szoecs, and H. Wagner. 2019. Ordination methods, diversity analysis and other functions for community and vegetation ecologists.: vegan: Community Ecology Package.

Orsi, J.J., and W.L. Mecum. 1996. Food limitation as the probable cause of a long-term decline in the abundance of Neomysis mercedis the opossum shrimp in the Sacramento-San Joaquin estuary. *San Francisco Bay: the ecosystem. American Association for the Advancement of Science, San Francisco*: 375-401.

Orsi, J.J., and S. Ohtsuka. 1999. Introduction of the Asian copepods Acartiella sinensis, Tortanus dextrilobatus (Copepoda: Calanoida), and Limnoithona tetraspina (Copepoda: Cyclopoida) to the San Francisco Estuary, California, USA. *Plankton Biology and Ecology* 46: 128-131.

Peterson, M.S., 2003. A conceptual view of environment-habitat-production linkages in tidal river estuaries. *Reviews in Fisheries science*, 11: 291-313.

Poos, M.S., and D.A. Jackson. 2012. Addressing the removal of rare species in multivariate bioassessments: the impact of methodological choices. *Ecological Indicators* 18: 82-90.

R Core Team. 2019. R: A language and environment for statistical computing. Vienna, Austria: R Foundation for Statistical Computing.

Schultz, A.A., L. Grimaldo, J.L. Hammock, A.J. Kalmbach, A.G. Smith, O. Burgess, D. Barnard, and J. Brandon. 2019. Effect of Isohaline (X2) and Region on Delta Smelt Habitat, Prey and Distribution During the Summer and Fall: Insights into Managed Flow Actions in a Highly Modified Estuary. In Directed Outflow Project: Technical Report 1. U.S. Bureau of Reclamation, ed. A.A. Schultz, 237-301. Mid-Pacific Region, Sacramento, CA.: U.S. Bureau of Reclamation, Bay-Delta Office.

Slater, S., A.A. Schultz, B. Hammock, A. Hennessy, and C. Burdi. 2019. Patterns of zooplankton consumption by juvenile and adult Delta Smelt (Hypomesus transpacificus). In Directed Outflow Project: Technical Report 1, ed. A.A. Schultz, 9-54. Sacramento, CA.

Slater, S.B., and R.D. Baxter. 2014. Diet, prey selection, and body condition of age-0 delta smelt, Hypomesus transpacificus, in the Upper San Francisco Estuary. *San Francisco Estuary and Watershed Science* 12.

Slaughter, A.M., T.R. Ignoffo, and W. Kimmerer. 2016. Predation impact of Acartiella sinensis, an introduced predatory copepod in the San Francisco Estuary, USA. *Marine Ecology Progress Series* 547: 47-60.

Starcevich, L., G. DiDonato, T. McDonald, and J. Mitchell. 2016. A GRTS user's manual for the SDrawNPS package: a graphical user interface for generalized random tessellation stratified (GRTS) sampling and estimation. *Natural Resource Report NPS/PWRO/NRR–2016/1233. National Park Service, Fort Collins, CO.*

Stevens Jr, D.L., and A.R. Olsen. 2004. Spatially balanced sampling of natural resources. *Journal of the American statistical Association* 99: 262-278.

Teh, S.J., A.A. Schultz, W. Ramirez-Duarte, S. Acuña, D.M. Barnard, B.H. Hammock, and R.D. Baxter. 2019. Patterns of Zooplankton Consumption by juvenile and adult Delta Smelt (Hypomesus transpacificus). In *Directed Outflow Project: Technical Report 1. U.S. Bureau of Reclamation*, ed. A.A. Schultz, 9-54. U.S. Bureau of Reclamation, Bay-Delta Office, Mid-Pacific Region, Sacramento, CA.

USFWS. 2019a. Biological Opinion for the Reinitiation of Consultation on the Coordinated Operations of the Central Valley and State Water Project. U.S. Department of the Interior.

USFWS. 2019b. Formal Endangered Species Act Consultation on the Proposed Coordinated Operations of the Central Valley Project (CVP) and State Water Project (SWP). Sacramento, California: United States Fish and Wildlife Service.

Verdouw, H., C.J.A. Van Echteld, C. J. A., and E. M. J. Dekkers, 1978. Ammonia determination based on indophenol formation with sodium salicylate. *Water Research*, *12*(6), 399-402.

Vicuna, S., E.P. Maurer, B. Joyce, J.A. Dracup, and D. Purkey. 2007. The sensitivity of California water resources to climate change scenarios 1. *JAWRA Journal of the American Water Resources Association* 43: 482-498.

Watkins, B., and B. Wells. 2019. Benthic monitoring, 2018. Interagency Ecological Program for the San Francisco Estuary, 23-30: IEP Newsletter.

Williamson, C.E., J.M. Fischer, S.M. Bollens, E.P. Overholt, and J.K. Breckenridge. 2011. Toward a more comprehensive theory of zooplankton diel vertical migration: Integrating ultraviolet radiation and water transparency into the biotic paradigm. *Limnology and Oceanography* 56: 1603-1623.

Winder, M., and A.D. Jassby. 2011. Shifts in zooplankton community structure: implications for food web processes in the upper San Francisco Estuary. *Estuaries and Coasts* 34: 675-690.

Wood, S.N. 2017. *Generalized additive models: an introduction with R*: CRC press.

TABLES

Table 1. Number of samples taken for each habitat in each region during 2017 and 2018.

		Cache Slough	Sacramento Shipping Channel	Lower Sacramento	Suisun Bay	Suisun Marsh
2017	Channel Surface	11	19	10	34	6
	Channel Deep	5	18	12	31	7
	Shoal	2	0	5	30	4
2018	Channel Surface	25	27	32	36	20
	Channel Deep	15	26	30	33	16
	Shoal	4	1	8	25	23

Table 2. Kruskal-Wallis Rank Sum test results for water quality variables, total abundance, total biomass, and Shannon's diversity indices for all five regions in the northern San Francisco Estuary during the two years of varying hydrology (shaded). Results for zooplankton community metrics are shown for Suisun Bay (not shaded) as a whole (italicized) and its separate habitats (bold).

Predictor Variables	Response Variable	Chi-Squared Statistic	Degrees of Freedom	p-value	Figure #
Region	Temperature	15.1	9	0.09	Figure 2
Region	Turbidity	157.4	9	<0.05	
Region	Salinity	371.1	9	<0.05	
Region	Dissolved Oxygen	158.9	9	<0.05	
Region	Chlorophyll-*a*	181.8	9	<0.05	
Region	Nitrate	54.2	9	<0.05	
Region	Ammonium	38.7	9	<0.05	
Region	Phosphate	64.1	9	<0.05	
Region	Dissolved Organic Carbon	96.4	9	<0.05	
Region	Total Abundance	186.8	9	<0.05	Figure 5
Region	Total Biomass	63.2	9	<0.05	
Region	Shannon's Diversity	64.6	9	<0.05	
Year	*Total Abundance*	*94.0*	*1*	*<0.05*	Figure 9
Year	*Total Biomass*	*0.02*	*1*	*0.88*	
Year	*Shannon's Diversity*	*0.05*	*1*	*0.82*	
Habitat	**Total Abundance**	**100.4**	**5**	**<0.05**	
Habitat	**Total Biomass**	**30.9**	**5**	**<0.05**	
Habitat	**Shannon's Diversity**	**6.6**	**5**	**0.25**	

Table 3. Kruskal-Wallis Rank Sum test results for taxa abundances (Figure 7) and biomasses (Figure 8) across five regions in the San Francisco Estuary over two years of varying hydrology. Taxa that did not have biomass calculated are indicated with the gray shading.

	Abundance			Biomass		
Taxa	Chi-squared statistic	Degrees of Freedom	p-value	Chi-squared statistic	Degrees of Freedom	p-value
Acartia spp. (a)	136.68	9	<0.05	136.68	9	<0.05
Acartia spp. (c)	160.39	9	<0.05	160.39	9	<0.05
Acartiella sinensis (a)	294.32	9	<0.05	294.32	9	<0.05
Acartiella sinensis (c)	352.35	9	<0.05	352.35	9	<0.05
Diaptomidae (a)	61.09	9	<0.05	61.09	9	<0.05
Diaptomidae (c)	82.58	9	<0.05	82.58	9	<0.05
Eurytemora affinis (a)	60.84	9	<0.05	60.84	9	<0.05
Eurytemora affinis (c)	94.36	9	<0.05	94.36	9	<0.05
Eurytemora spp. (n)	195.31	9	<0.05	195.31	9	<0.05
Osphranticum labronectum (a)	15.08	9	0.09			
Osphranticum labronectum (c)	4.83	9	0.85			
Pseudodiaptomus forbesi (a)	205.30	9	<0.05	205.30	9	<0.05
Pseudodiaptomus forbesi (c)	272.50	9	<0.05	272.50	9	<0.05
Pseudodiaptomus marinus (a)	101.93	9	<0.05	101.93	9	<0.05
Pseudodiaptomus marinus (c)	85.97	9	<0.05	85.97	9	<0.05
Pseudodiaptomus spp. (a)	99.12	9	<0.05	99.12	9	<0.05
Pseudodiaptomus spp. (c)	170.99	9	<0.05	170.99	9	<0.05
Pseudodiaptomus spp. (n)	263.44	9	<0.05	263.44	9	<0.05
Sinocalanus doerrii (a)	313.28	9	<0.05	313.28	9	<0.05
Sinocalanus doerrii (c)	312.56	9	<0.05	312.56	9	<0.05
Sinocalanus doerrii (n)	239.05	9	<0.05	239.05	9	<0.05
Tortanus dextrilobatus (a)	254.73	9	<0.05	254.73	9	<0.05
Tortanus dextrilobatus (c)	304.49	9	<0.05	304.49	9	<0.05
Calanoid (a)	21.53	9	<0.05	21.53	9	<0.05
Calanoid (c)	17.42	9	<0.05	17.42	9	<0.05
Acanthocyclops vernalis (a)	32.29	9	<0.05	32.29	9	<0.05
Acanthocyclops vernalis (c)	34.43	9	<0.05	34.43	9	<0.05
Acanthocyclops spp. (a)	12.57	9	0.18	12.57	9	0.18
Limnoithona sinensis (a)	254.49	9	<0.05	254.49	9	<0.05
Limnoithona sinensis (c)	180.25	9	<0.05	180.25	9	<0.05
Limnoithona spp. (a)	4.42	9	0.88	4.42	9	0.88
Limnoithona spp. (c)	8.86	9	0.45	8.86	9	0.45
Limnoithona tetraspina (a)	181.87	9	<0.05	181.87	9	<0.05
Limnoithona tetraspina (c)	319.91	9	<0.05	319.91	9	<0.05
Oithona davisae (a)	260.51	9	<0.05	260.51	9	<0.05

Oithona davisae (c)	94.59	9	<0.05	94.59	9	<0.05
Oithona similis (a)	4.56	9	0.87	4.56	9	0.87
Oithona spp. (a)	8.86	9	0.45	8.86	9	0.45
Oithona spp. (c)	8.86	9	0.45	8.86	9	0.45
Cyclopoid (a)	103.92	9	<0.05	103.92	9	<0.05
Cyclopoid (c)	111.67	9	<0.05	111.67	9	<0.05
Harpacticoid	153.69	9	<0.05	153.69	9	<0.05
Copepod (n)	207.11	9	<0.05	207.11	9	<0.05
Acanthomysis aspera	8.97	9	0.44	8.97	9	0.44
Alienacanthomysis macropsis	40.16	9	<0.05	40.40	9	<0.05
Hyperacanthomysis longirostris	82.80	9	<0.05	97.10	9	<0.05
Neomysis kadiakensis	63.00	9	<0.05	63.81	9	<0.05
Neomysis mercedes	3.46	9	0.94	3.46	9	0.94
Mysid	13.69	9	0.13	6.36	9	0.7
Americorophium spinicorne	67.11	9	<0.05	71.61	9	<0.05
Americorophium spp.	8.86	9	0.45	8.86	9	0.45
Americorophium stimpsoni	23.34	9	<0.05	25.00	9	<0.05
Ampelisca abdita	16.09	9	0.07	16.06	9	0.07
Amphipod	60.95	9	<0.05			
Ampithoe spp.	4.48	9	0.88	4.48	9	0.88
Ampithoe valida	47.74	9	<0.05	43.88	9	<0.05
Corophiidae	7.22	9	0.61	4.28	9	0.89
Corophium alienense	49.94	9	<0.05	49.94	9	<0.05
Crangonyx spp.	47.38	9	<0.05	49.66	9	<0.05
Gammarus daiberi	89.26	9	<0.05	72.02	9	<0.05
Grandidierella japonica	28.86	9	<0.05	29.13	9	<0.05
Hyalella spp.	155.14	9	<0.05	153.70	9	<0.05
Monocorophium acherusicum	8.16	9	0.52	8.24	9	0.51
Pleustidae	23.37	9	<0.05			
Alona spp.	199.42	9	<0.05	199.42	9	<0.05
Bosmina longirostris	303.48	9	<0.05	303.48	9	<0.05
Camptocercus spp.	158.18	9	<0.05	158.18	9	<0.05
Chydorus spp.	178.78	9	<0.05	178.78	9	<0.05
Daphnia spp.	78.01	9	<0.05	78.01	9	<0.05
Daphniidae	266.99	9	<0.05	266.99	9	<0.05
Ilyocryptus spp.	10.62	9	0.3	10.62	9	0.3
Leptodora spp.	9.76	9	0.37	12.92	9	0.17
Macrothrix spp.	67.66	9	<0.05	67.66	9	<0.05
Sididae	239.61	9	<0.05	239.61	9	<0.05
Cladocera	90.03	9	<0.05	90.03	9	<0.05
Asplanchna spp.	92.53	9	<0.05			

Brachionus spp.	54.15	9	<0.05			
Keratella spp.	62.02	9	<0.05			
Trichocerca spp.	142.48	9	<0.05			
Rotifer	93.39	9	<0.05			
Barnacle (n)	358.34	9	<0.05			
Crab zoea	7.52	9	0.58			
Cumacean	40.43	9	<0.05			
Exopalaemon spp.	27.30	9	<0.05			
Isopoda	119.02	9	<0.05			
Ostracoda	66.89	9	<0.05			
Shrimp larvae	53.09	9	<0.05			
Tanaidacea	15.49	9	0.08			

Table 4. Generalized Additive Model (GAM) model output for relationships between individual zooplankton taxa abundances and biomasses with water quality variables in the San Francisco estuary across two years with varying hydrology. Effective degrees of freedom (EDF) of 0.00 indicates no relationship, 1.00 a linear relationship, 2+ indicates increasing complexity in the relationship. RDF- Relative Degrees of Freedom. Life stages are indicated for adult (a), copepodid (c), and nauplii (n). Below the taxa name are the percentages of deviance explained with the model performed with abundance (first) and the model performed with biomass (second). Numbers in italics indicate significant relationships (p-value <0.05)

		Abundance				Biomass			
Taxa (life stage)	Smoothed Covariates	EDF	RDF	Chi. sq	p-value	EDF	RDF	Chi. sq	p-value
Acartiella sinensis (a) (63.7, 60.3)	Ammonium	<0.01	9	2.23^{-3}	0.39	0.61	9	1.05	0.17
	Chlorophyll-*a*	0.65	9	2.01	0.07	0.03	9	0.02	0.45
	Dissolved Organic Carbon	*1.30*	*9*	*19.67*	*<0.05*	*1.27*	*9*	*18.50*	*<0.05*
	Dissolved Oxygen	*3.29*	*9*	*19.98*	*<0.05*	*4.47*	*9*	*32.03*	*<0.05*
	Nitrates	*3.59*	*9*	*22.41*	*<0.05*	*3.41*	*9*	*19.49*	*<0.05*
	Phosphate	*2.18*	*9*	*27.26*	*<0.05*	*2.15*	*9*	*28.41*	*<0.05*
	Salinity	*4.57*	*9*	*79.13*	*<0.05*	*4.23*	*9*	*74.26*	*<0.05*
	Temperature	0.41	9	0.40	0.31	0.29	9	0.24	0.37
	Turbidity	*1.77*	*9*	*18.84*	*<0.05*	*1.67*	*9*	*17.50*	*<0.05*
Acartiella sinensis (c) (78.4, 77.9)	Ammonium	<0.01	9	2.81^{-5}	0.86	<0.01	9	7.31^{-6}	0.81
	Chlorophyll-*a*	<0.01	9	5.04^{-5}	0.69	<0.01	9	1.43^{-5}	0.57
	Dissolved Organic Carbon	*1.21*	*9*	*16.15*	*<0.05*	*1.26*	*9*	*17.74*	*<0.05*
	Dissolved Oxygen	*1.49*	*9*	*3.75*	*<0.05*	1.34	9	2.98	0.07
	Nitrates	*2.29*	*9*	*11.29*	*<0.05*	*2.27*	*9*	*11.10*	*<0.05*
	Phosphate	*1.56*	*9*	*30.79*	*<0.05*	*1.58*	*9*	*32.24*	*<0.05*
	Salinity	*4.63*	*9*	*231.17*	*<0.05*	*4.66*	*9*	*234.96*	*<0.05*
	Temperature	*1.76*	*9*	*25.11*	*<0.05*	*1.48*	*9*	*24.50*	*<0.05*

	Turbidity	*1.05*	*9*	*4.43*	*<0.05*	*1.02*	*9*	*4.01*	*<0.05*
Limnoithona tetraspina (a) (59.9, 67.2)	Ammonium	<0.01	9	1.99^{-6}	1.00	<0.01	9	1.66^{-5}	0.78
	Chlorophyll-*a*	0.72	9	1.55	0.11	0.39	9	0.58	0.20
	Dissolved Organic Carbon	*0.81*	*8*	*3.08*	*<0.05*	*0.90*	*7*	*7.31*	*<0.05*
	Dissolved Oxygen	1.93	9	3.83	0.08	<0.01	9	5.45^{-5}	0.67
	Nitrates	*3.48*	*9*	*21.69*	*<0.05*	*3.32*	*9*	*15.19*	*<0.05*
	Phosphate	<0.01	9	1.06^{-6}	1.00	<0.01	9	6.43^{-6}	0.85
	Salinity	*2.11*	*9*	*14.28*	*<0.05*	*2.68*	*9*	*19.71*	*<0.05*
	Temperature	*3.90*	*9*	*38.18*	*<0.05*	*3.83*	*9*	*42.57*	*<0.05*
	Turbidity	*1.85*	*9*	*26.81*	*<0.05*	*1.78*	*9*	*20.69*	*<0.05*
Pseudodiaptomus forbesi (a) (44.0, 41.6)	Ammonium	0.44	9	0.83	0.16	0.31	9	0.51	0.18
	Chlorophyll-*a*	<0.01	9	1.50^{-4}	0.56	<0.01	9	2.79^{-4}	0.49
	Dissolved Organic Carbon	0.44	7	0.69	0.21	0.39	6	0.50	0.25
	Dissolved Oxygen	*2.30*	*9*	*19.84*	*<0.05*	*2.29*	*9*	*20.03*	*<0.05*
	Nitrates	<0.01	9	1.18^{-5}	1.00	<0.01	9	1.97^{-5}	0.90
	Phosphate	0.74	9	2.43	0.07	*0.78*	*9*	*3.28*	*<0.05*
	Salinity	*3.26*	*9*	*213.62*	*<0.05*	*3.22*	*9*	*209.30*	*<0.05*
	Temperature	1.01	9	2.00	0.10	0.76	9	1.24	0.16
	Turbidity	*1.28*	*9*	*8.99*	*<0.05*	*1.27*	*9*	*8.90*	*<0.05*
Pseudodiaptomus forbesi (c) (55.4, 54.7)	*Ammonium*	*1.19*	*9*	*3.77*	*<0.05*	*1.16*	*9*	*3.59*	*<0.05*
	Chlorophyll-*a*	0.83	9	2.03	0.08	0.78	9	1.79	0.09
	Dissolved Organic Carbon	<0.01	9	1.46^{-4}	0.44	<0.01	9	5.95^{-4}	0.41
	Dissolved Oxygen	*1.38*	*9*	*4.53*	*<0.05*	*1.37*	*9*	*4.52*	*<0.05*
	Nitrates	*1.95*	*9*	*13.82*	*<0.05*	*1.94*	*9*	*14.04*	*<0.05*
	Phosphate	0.56	9	0.97	0.17	0.57	9	1.02	0.16
	Salinity	*3.86*	*9*	*208.14*	*<0.05*	*3.80*	*9*	*205.63*	*<0.05*
	Temperature	*3.36*	*9*	*21.87*	*<0.05*	*3.30*	*9*	*21.12*	*<0.05*
	Turbidity	*2.09*	*9*	*11.57*	*<0.05*	*2.10*	*9*	*11.76*	*<0.05*
Pseudodiaptomus spp. (n) (78.1, 80.9)	Ammonium	*1.55*	*9*	*10.29*	*<0.05*	0.74	9	2.59	0.05
	Chlorophyll-*a*	*2.66*	*9*	*48.26*	*<0.05*	*1.99*	*9*	*29.17*	*<0.05*
	Dissolved Organic Carbon	*0.91*	*9*	*9.14*	*<0.05*	*0.93*	*9*	*8.30*	*<0.05*
	Dissolved Oxygen	*1.70*	*9*	*6.66*	*<0.05*	0.89	9	1.85	0.10
	Nitrates	*0.94*	*9*	*15.24*	*<0.05*	*0.94*	*9*	*15.34*	*<0.05*
	Phosphate	*4.48*	*9*	*41.98*	*<0.05*	*4.27*	*9*	*39.22*	*<0.05*
	Salinity	*4.51*	*9*	*220.07*	*<0.05*	*4.49*	*9*	*202.56*	*<0.05*
	Temperature	*5.89*	*9*	*89.08*	*<0.05*	*5.66*	*9*	*51.94*	*<0.05*
	Turbidity	<0.01	9	9.50^{-6}	1.00	<0.01	9	1.29^{-4}	0.57
Tortanus dextrilobatus (c)	Ammonium	<0.01	9	5.16^{-4}	0.37	0.10	9	0.08	0.36
	Chlorophyll-*a*	<0.01	9	2.32^{-5}	0.63	<0.01	9	4.27^{-6}	0.88

(83.0, 82.7)	Dissolved Organic Carbon	<0.01	9	6.97^{-4}	0.41	<0.01	9	2.35^{-5}	0.62
	Dissolved Oxygen	0.59	9	1.18	0.14	0.56	8	0.96	0.18
	Nitrates	*1.53*	*9*	*4.04*	*<0.05*	*1.67*	*9*	*4.61*	*<0.05*
	Phosphate	0.63	9	1.09	0.18	0.70	9	1.33	0.16
	Salinity	*4.03*	*9*	*137.45*	*<0.05*	*4.45*	*9*	*160.64*	*<0.05*
	Temperature	*2.78*	*9*	*23.06*	*<0.05*	*2.71*	*9*	*21.48*	*<0.05*
	Turbidity	<0.01	9	7.13^{-5}	0.33	<0.01	9	2.38^{-5}	0.46

FIGURES

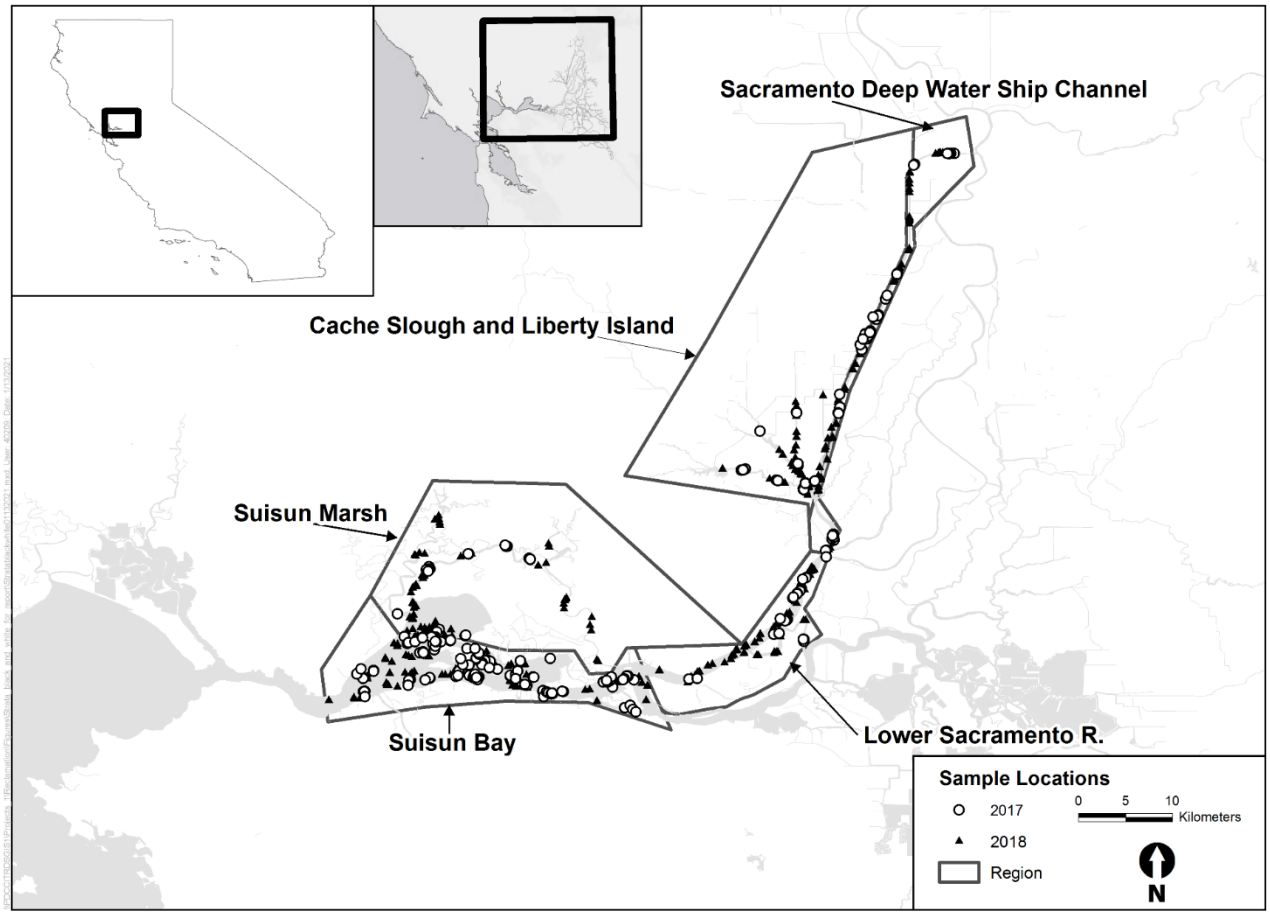

Figure 1. Sampling locations for each region in the San Francisco Estuary.

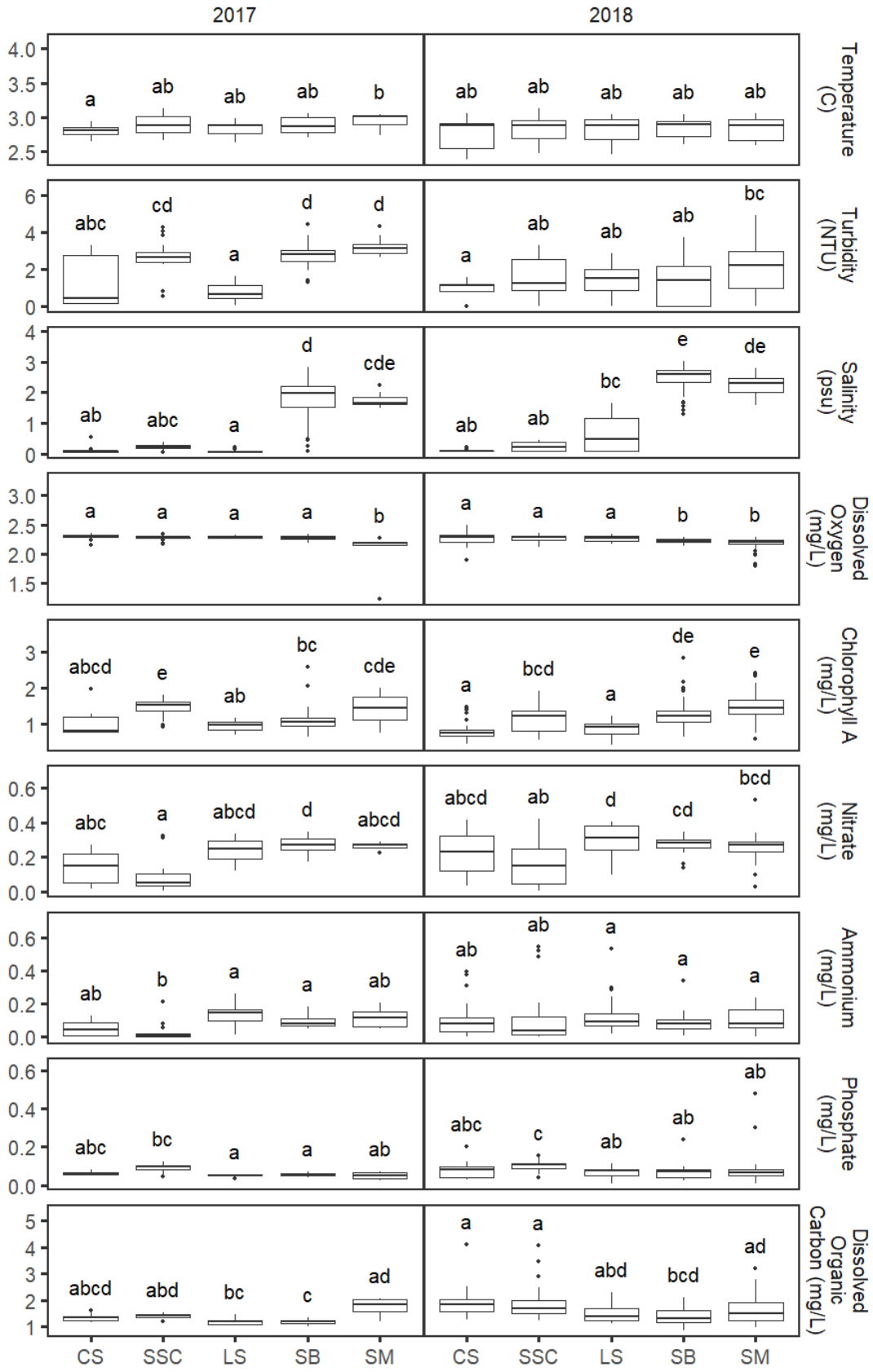
2017
2018
Temperature (C)
Turbidity (NTU)
Salinity (psu)
Dissolved Oxygen (mg/L)
Chlorophyll A (mg/L)
Nitrate (mg/L)
Ammonium (mg/L)
Phosphate (mg/L)
Dissolved Organic Carbon (mg/L)
CS
SSC
LS
SB
SM

Figure 2. Differences in water quality within five regions of the estuary for both years of variable outflow. All values are on the log+1 scale to aid in visualization. Lowercase letters indicate no significant differences were observed between regions that share letters as determined by Dunn's multiple comparison post-hoc test (p-value > 0.05, see Table 2). Group membership is comparable across years not between water quality metrics. Abbreviations: CS- Cache Slough, SSC - Sacramento Shipping Channel, LS - Lower Sacramento River, SB - Suisun Bay, SM - Suisun Marsh.

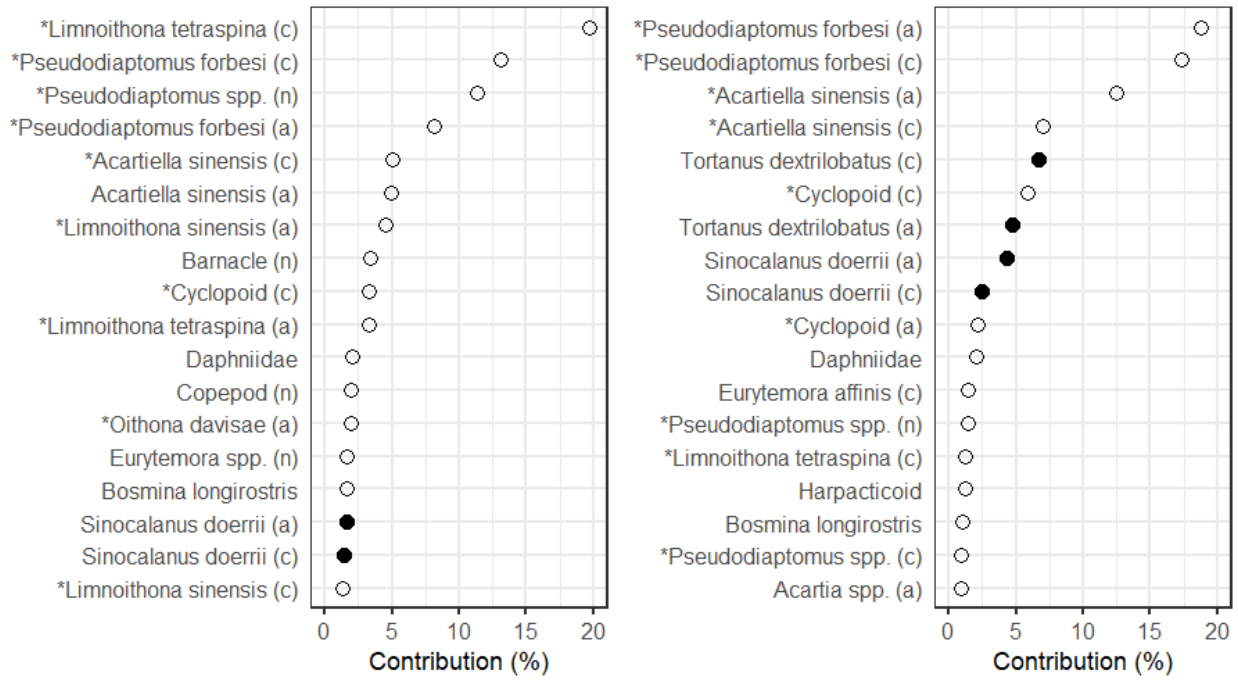

Figure 3. Average contribution to dissimilarity between 2017 and 2018 lower trophic community abundance (left) and biomass (right). A cut-off of 90% cumulative dissimilarity is shown. Taxa with higher abundance/ biomass in 2017 are white, higher abundance/biomass in 2018 are black. Asterisks preceding the names of taxa indicate known Delta Smelt fall prey items. Life stages are indicated for adult (a), copepodite (c), and nauplii (n).

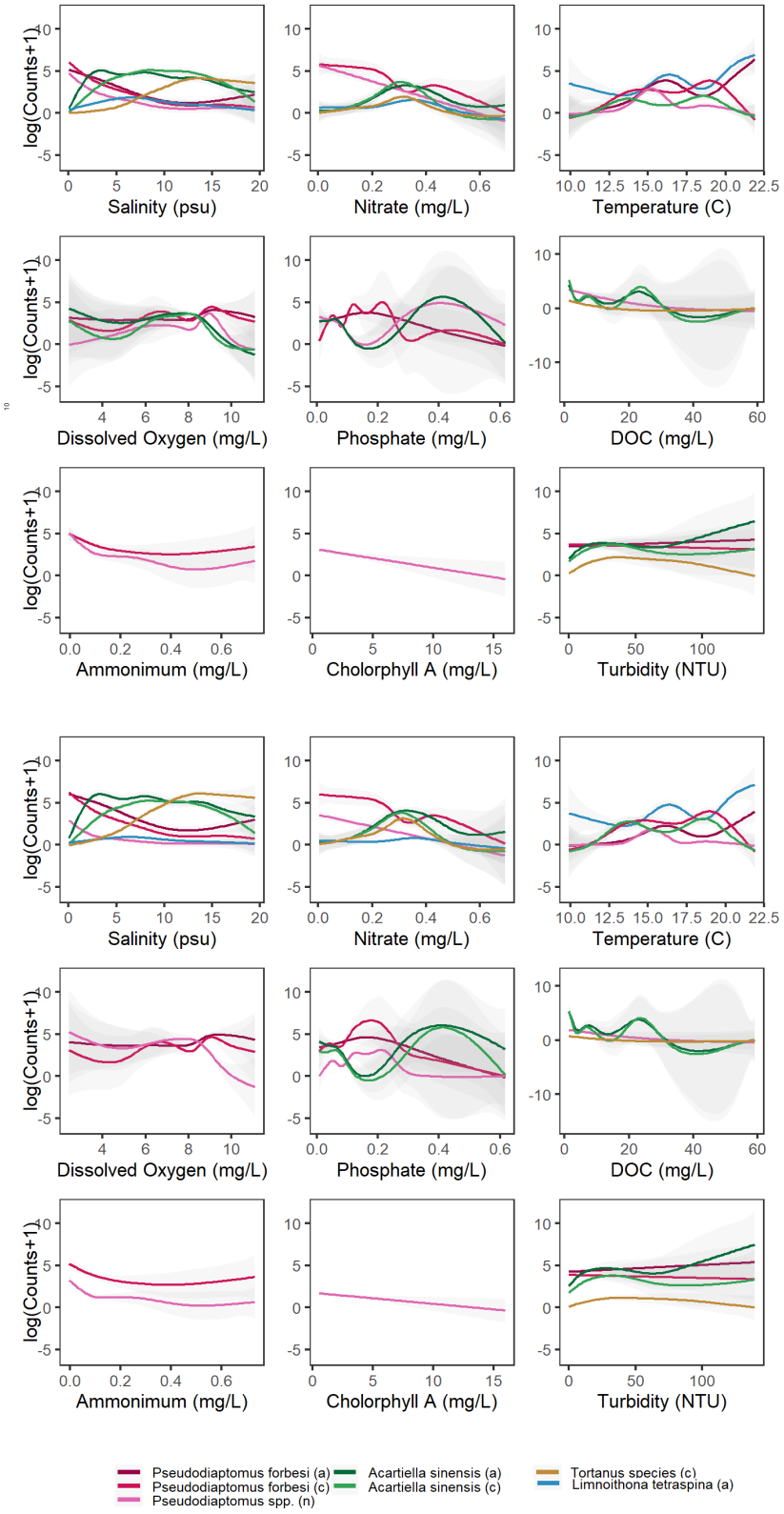

Figure 4. Predicted relationships between lower trophic taxa abundance (top) and biomass (bottom) with water quality metrics. Plots fitted using cubic regression splines and 95% confidence intervals for partial responses generated from general additive models. Taxa are only

shown if the water quality variable was a significant predictor in the model (p-value < 0.05, Table 4.). Life stages are described by letters in the parenthesis following taxa name a- adult, c- copepodite, n- nauplii.

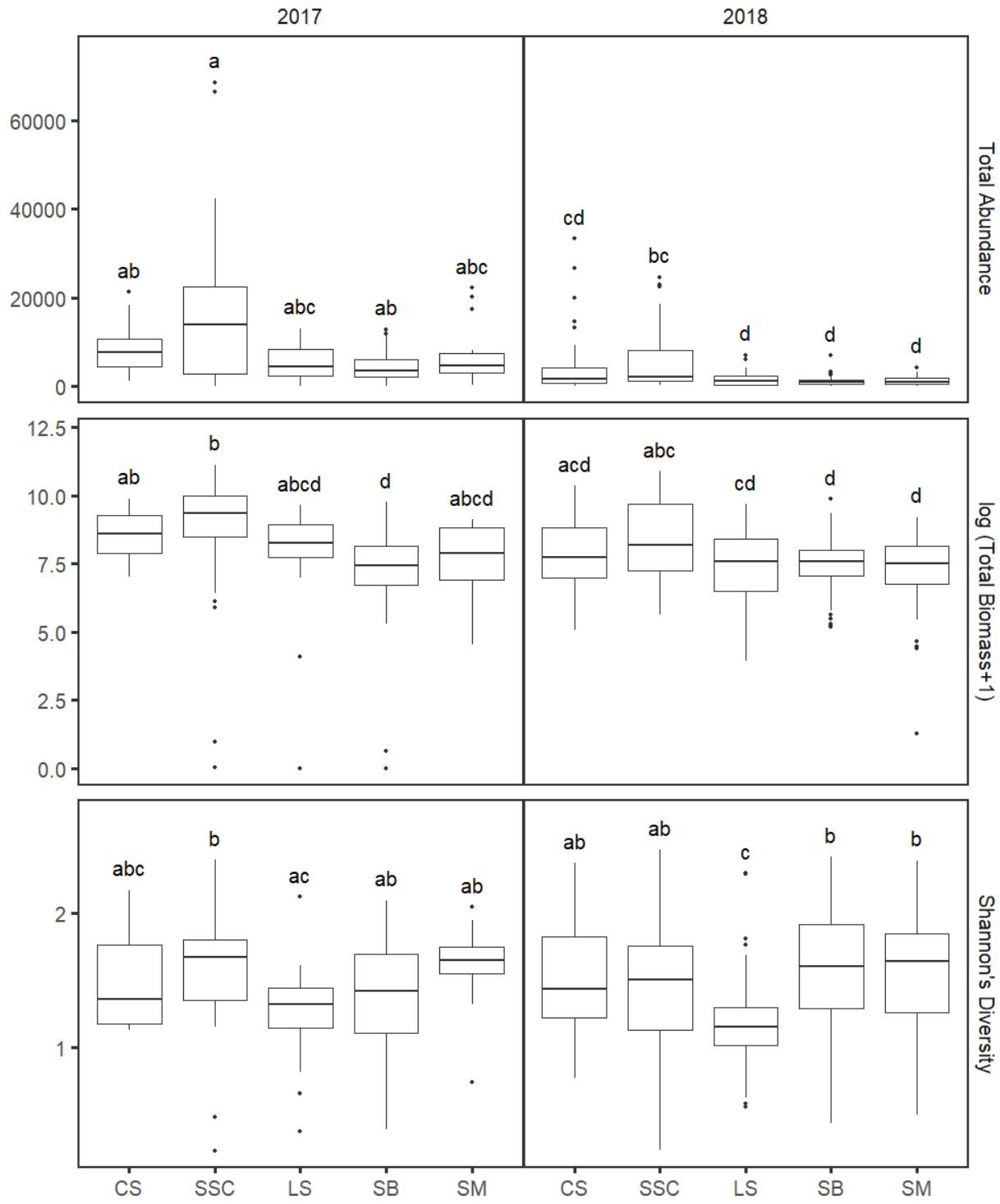

Figure 5. Box plots for total abundance (individuals per m^3), log-transformed total biomass (µg C per m^3), and Shannon's diversity (H') for five regions within the estuary in years with varying hydrology. Lowercase shared letters indicate no significant differences were observed between regions as determined by Dunn's multiple comparison post-hoc test (p-value > 0.05, see Table 2). Group membership is comparable across years not between metrics. Abbreviations: CS - Cache Slough, SSC - Sacramento Shipping Channel, LSR - Lower Sacramento River, SB - Suisun Bay, SM - Suisun Marsh.

2). Group membership is comparable across years not between metrics. Abbreviations: CS - Cache Slough, SSC - Sacramento Shipping Channel, LSR - Lower Sacramento River, SB - Suisun Bay, SM - Suisun Marsh.

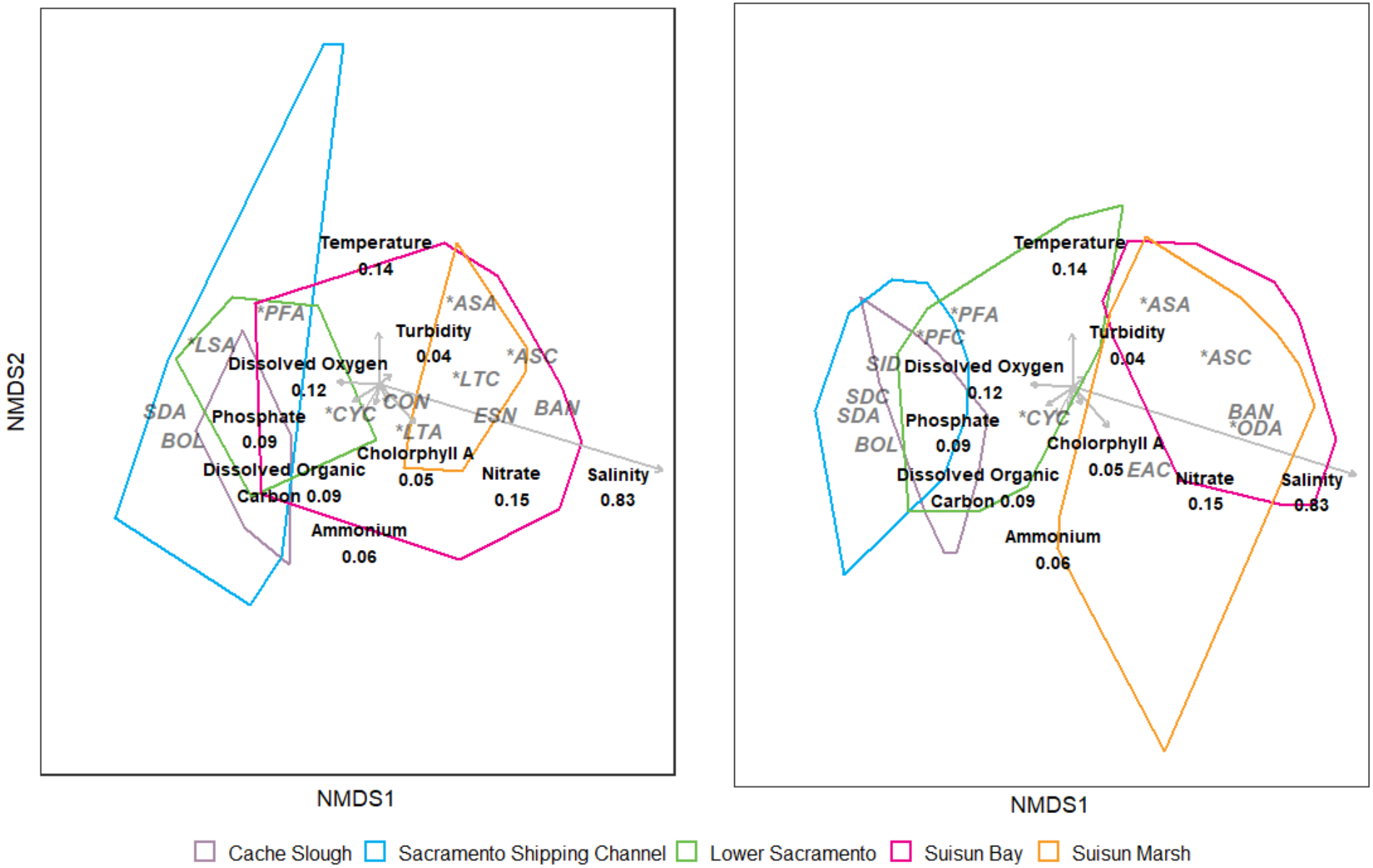
NMDS2
NMDS1
Temperature
0.14
*ASA
*PFA
Turbidity
0.04
*LSA
Dissolved Oxygen
0.12
*ASC
*LTC
SDA
Phosphate
0.09
*CYC
CON
ESN
BAN
BOL
*LTA
Cholorphyll A
0.05
Dissolved Organic
Carbon 0.09
Nitrate
0.15
Salinity
0.83
Ammonium
0.06
NMDS1
Temperature
0.14
*ASA
*PFA
*PFC
Turbidity
0.04
*ASC
SID
Dissolved Oxygen
0.12
SDC
SDA
Phosphate
0.09
*CYC
BAN
*ODA
BOL
Cholorphyll A
0.05
EAC
Dissolved Organic
Carbon 0.09
Nitrate
0.15
Salinity
0.83
Ammonium
0.06
Cache Slough
Sacramento Shipping Channel
Lower Sacramento
Suisun Bay
Suisun Marsh

Figure 6. *NMD*S ordinations depicting differences in 80 lower trophic taxa abundance across five regions in 2017 (left) and 2018 (right) in the San Francisco Estuary in years with varying hydrology (stress= 0.180). Taxa names are in gray and asterisks preceding names indicate known prey items for Delta Smelt in the fall. Abbreviated taxa names are defined as follows, where life stages are indicated by adult (a), copepodid (c), and nauplii (n): ASA- *Acartiella sinensis* (a), ASC- *A. sinensis* (c), BAN- Barnacle (n), BOL- *Bosmina longirostris,* CON-Copepod (n), CYC- Cyclopoid (c), ESN- *Eurytemora* spp. (n), LSA- *Limnoithona sinensis* (a), LTA- *Limnoithona tetraspina* (a), LTC- *L. tetraspina* (c), PFA- *Pseudodiaptomus forbesi* (a), PFC- *P. forbesi* (c), SDA- *Sinocalanus doerrii* (a)

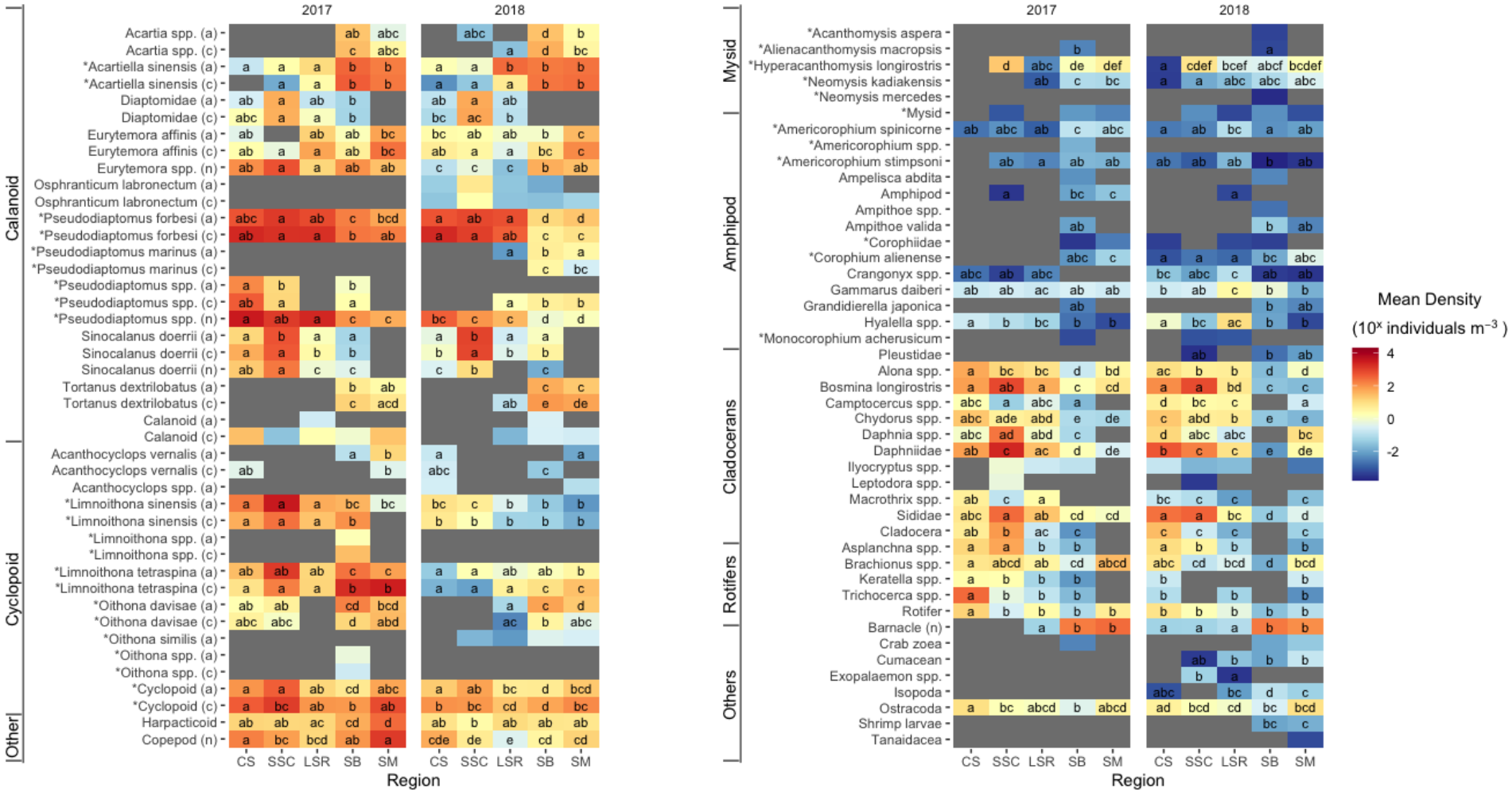

Figure 7. Mean densities of lower trophic taxa observed during fall of 2017 and 2018 across all regions sampled in the San Francisco Estuary. Asterisks preceding the names of taxa indicate known prey items for Delta Smelt in the fall. Lowercase letters indicate no significant differences were observed between regions that share letters as determined by Dunn's multiple comparison post-hoc test (p-value > 0.05, see Table 3). Group membership is comparable across years not between rows. Life stages are life stages are indicated by adult (a), copepodite (c), and nauplii (n). Abbreviations: CS - Cache Slough, SSC - Sacramento Shipping Channel, LSR - Lower Sacramento River, SB - Suisun Bay, SM - Suisun Marsh.

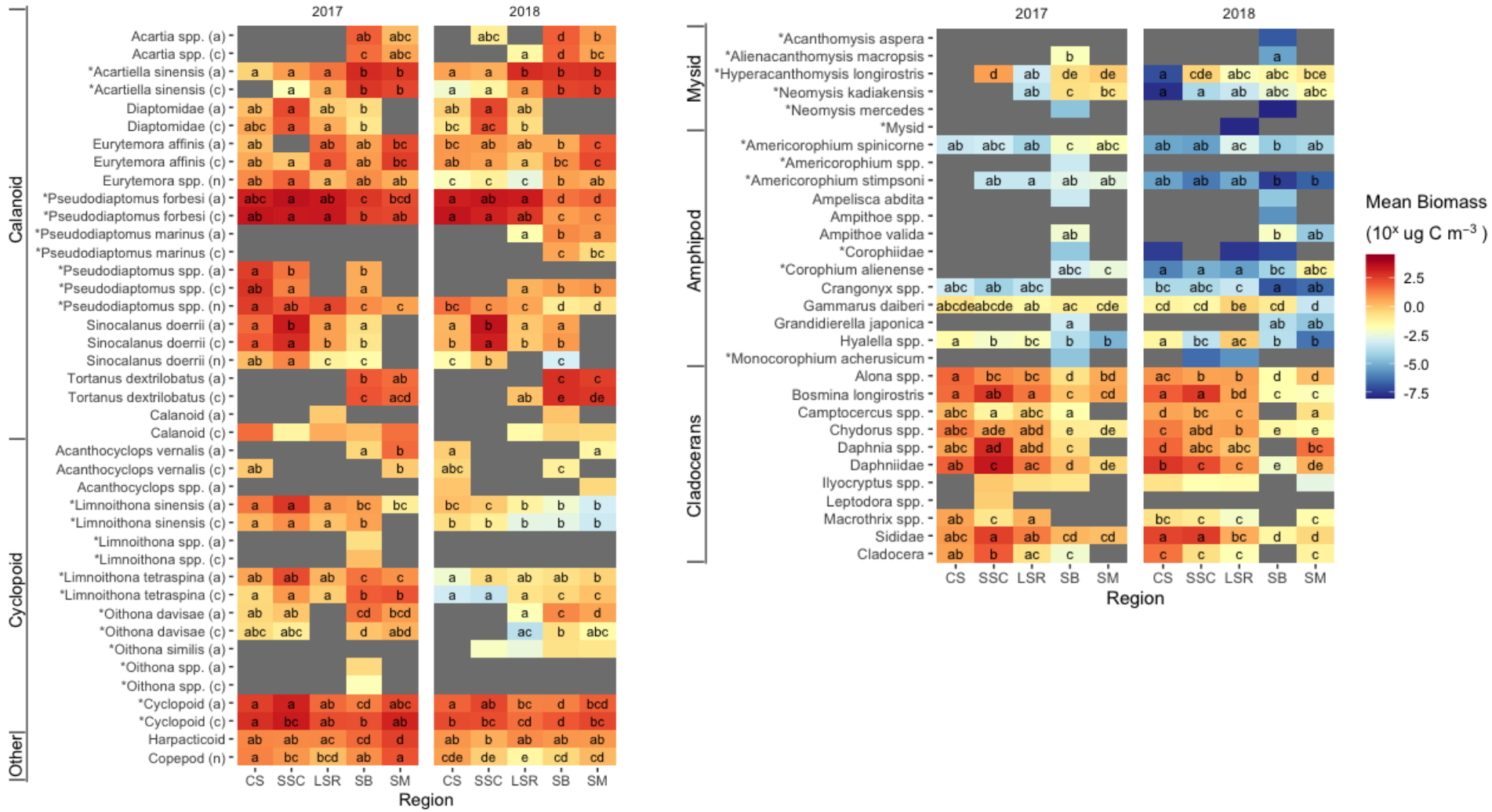

Figure 8. Mean biomass of lower trophic taxa observed during fall of 2017 and 2018 across all regions sampled in the San Francisco Estuary. Asterisks preceding the names of taxa indicate known prey items for Delta Smelt in the fall. Lowercase letters indicate no significant differences were observed between regions that share letters as determined by Dunn's multiple comparison post-hoc test (p-value > 0.05, see Table 3). Group membership is comparable across years but not between rows. Life stages are indicated by adult (a), copepodite (c), and nauplii (n). Abbreviations: CS - Cache Slough, SSC - Sacramento Shipping Channel, LSR - Lower Sacramento River, SB - Suisun Bay, SM - Suisun Marsh

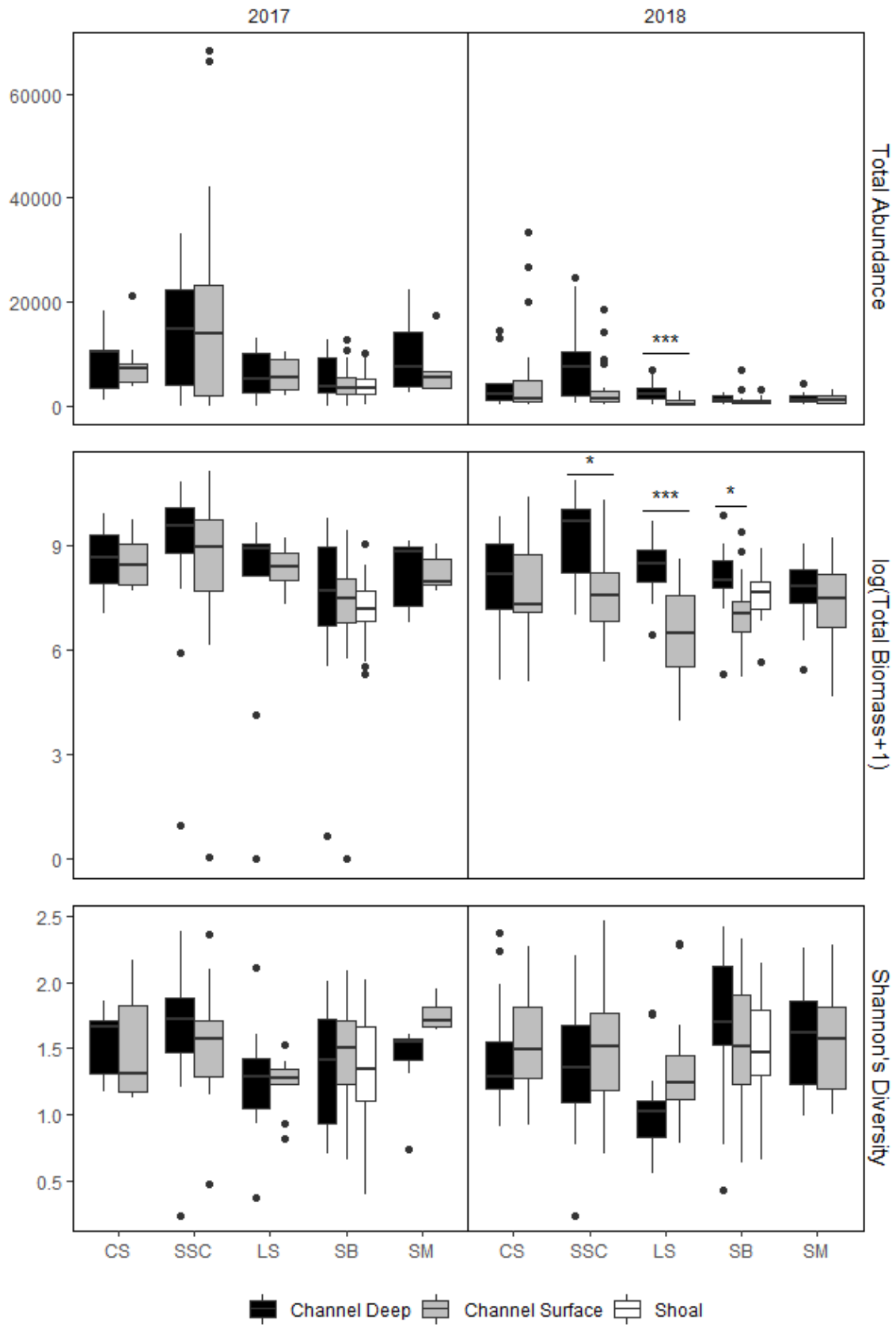
2017
2018
Total Abundance
60000
40000
20000
0
***
log(Total Biomass+1)
9
6
3
0
*
***
*
Shannon's Diversity
2.5
2.0
1.5
1.0
0.5
CS
SSC
LS
SB
SM
CS
SSC
LS
SB
SM
Channel Deep
Channel Surface
Shoal

Figure 9. Box plots for total abundance (individuals per m^3), log-transformed total biomass (µg C per m^3), and Shannon's diversity (H') for habitat in each region across years with varying hydrology. Note that observations for shoal habitats are shown only for Suisun Bay due to comparable sample sizes for that region in both years (see Table 1). Horizontal bars shared by habitats indicate significant differences were observed. '*' ($p < 0.05$), '**' ($p < 0.01$), '***' ($p < 0.001$). Abbreviations: CS - Cache Slough, SSC - Sacramento Shipping Channel, LSR - Lower Sacramento River, SB - Suisun Bay, SM - Suisun Marsh

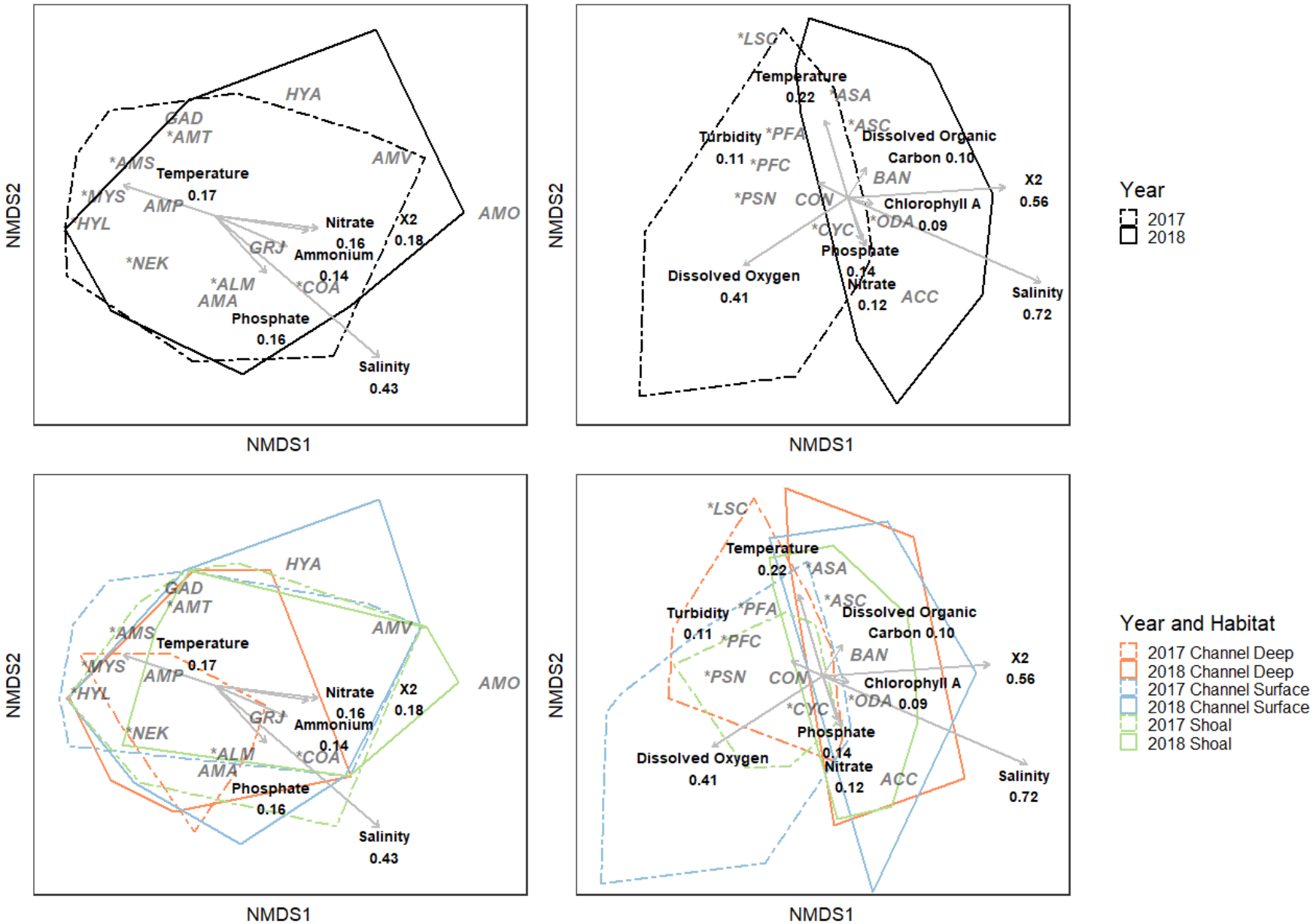
NMDS2
NMDS1
HYA
GAD
*AMT
*AMS
AMV
Temperature
0.17
*MYS
AMP
HYL
Nitrate
0.16
X2
0.18
AMO
GRJ
Ammonium
0.14
*NEK
*ALM
*COA
AMA
Phosphate
0.16
Salinity
0.43
*LSC
Temperature
0.22
*ASA
*ASC
Turbidity
0.11
*PFA
Dissolved Organic
Carbon 0.10
*PFC
BAN
X2
0.56
*PSN
CON
Chlorophyll A
0.09
*ODA
*CYC
Phosphate
0.14
Dissolved Oxygen
0.41
Nitrate
0.12
ACC
Salinity
0.72
Year
2017
2018
Year and Habitat
2017 Channel Deep
2018 Channel Deep
2017 Channel Surface
2018 Channel Surface
2017 Shoal
2018 Shoal

Figure 10. NMDS ordinations depicting differences in 20 mysid/amphipod taxa abundance (left) and 56 zooplankton taxa abundance (right) in Suisun Bay from 2017 to 2018 (top) and in three habitats (bottom) in the estuary in years with varying low-salinity habitat (stress= 0.175). Taxa names are in gray and asterisks preceding names indicate known prey items for Delta Smelt in the fall. Abbreviated taxa names are defined as follows, where life stages are indicated by adult (a), copepodite (c), and nauplii (n): Mysid/amphipod taxa AMS - *Americorophium spinicorne*, AMT - *Americorophium stimpsoni,* AME - *Americorophium* spp., AMA - *Ampelisca abdita*, AMP - Amphipods, AMO - *Ampithoe* spp., AMV - *Ampithoe valida*, COA - *Corophium alienense*, GAD - *Gammarus daiberi,* GRJ - *Grandidierella. japonica*, HYA - *Hyalella* spp., ALM - *Alienacanthomysis macropsis*, HYL - *Hyperacanthomysis longirostris*, MYS - Mysids, NEK- *Neomysis kadiakensis*. Zooplankton taxa: ACC - *Acartia* spp. (c), ASA - *Acartiella sinensis* (a), ASC - *A. sinensis* (c), BAN - Barnacle (n), CON -Copepod (n), CYC - Cyclopoid (c), LSC - *Limnoithona sinensis* (c), ODA - *Oithona davisae* (a), PFA - *Pseudodiaptomus forbesi* (a), PFC - *P. forbesi* (c), PSN - P*seudodiaptomus* spp. (n)

This page intentionally left blank

Chapter 8: Comparisons of Phytoplankton Community Structure and Nutrient Conditions in the Sacramento River Delta During a Fall Flow Action and Non-Action Period

Comparison of Phytoplankton Community Structure and Nutrient Conditions in the Sacramento River Delta During a Fall Flow Action and Non-action Period.

Andrew Kalmbach[1], Daniel M. Cox[1], Calvin Lee[2], Andrew A. Schultz[3]

[1] ICF, 980 9th Street, Suite 1200, Sacramento, CA 95814 USA

[2] ICF, 201 Mission Street, Suite 1500, San Francisco, CA 94105 USA

[3] United States Bureau of Reclamation, Bay-Delta Office, 801 I Street, Suite 140, Sacramento, CA 95814, USA

Abstract

Phytoplankton are a primary component of the aquatic food web in the San Francisco Bay Estuary and the Sacramento-San Joaquin River Delta. Various changes to the ecosystem such as the introduction of invasive clams, nutrient enrichment, and changes in flow regimes have caused shifts in the phytoplankton communities, leading to harmful algal blooms, reduced primary productivity, and declines in fish populations. As part of efforts to improve habitat for the endangered Delta Smelt, managed flow regimes have targeted moving the low salinity field seaward during wet years, which may affect phytoplankton abundances and assemblages in several ways. We sampled nutrients, phytoplankton and *Microcystis spp.* in the upper estuary and delta during the fall period of 2017 (a wet water year) and 2018 (a below normal water year) to assess changes to the phytoplankton assemblage structure and biomass during fall outflow actions. Biomass was lower in the high flow year of 2017 and increased in downstream regions during 2018. Ammonium and nitrate concentrations were higher in 2018 though this varied between different regions, while phosphate concentrations did not significantly vary. Diatoms comprised most of the phytoplankton assemblage during 2017 (except for the Sacramento Shipping Channel) but were only abundant in more landward regions in 2018. Cyanobacteria and cryptophytes were common in 2018. *Microcystis spp.* was more common in the lower flow year of 2018 with higher presence as sampling moved downstream.

Introduction

In the upper San Francisco Estuary and Sacramento-San Joaquin River Delta, hereafter referred to as the Delta, photosynthesis by phytoplankton is the major source of autochthonous primary production (Jassby et al. 2003). Over the past three decades, fish populations in the Delta have declined simultaneously with decreasing phytoplankton and zooplankton biomass, referred to as Pelagic Organism Decline (POD; Sommer et al., 2007; Thomson et al., 2010).

Prior to the onset of POD, phytoplankton biomass often exceeded 10 µg L^{-1} chlorophyll-*a* (a proxy for phytoplankton biomass), with phytoplankton blooms in excess of 20 µg L^{-1} commonly occurring in the spring and summer bloom period (Ball and Arthur 1979; Merz et al. 2016). Following the colonization by the non-native overbite clam, *Potamocorbula amurensis*, in 1986 (Carlton et al. 1990), phytoplankton biomass declined to current chlorophyll-*a* concentrations of $\leq$5 µg L^{-1} with blooms occurring occasionally (Brown et al. 2016).

Historically, diatoms dominated Delta phytoplankton communities in the fall, with the occasional dominance by green algae or small flagellates (Ball and Arthur 1979). Since the onset of POD, phytoplankton assemblages have shifted to include greater contributions by cyanobacteria, chlorophytes, and flagellates (Jassby 2008). These community shifts have been linked to a range of ecosystem perturbations including: dynamics in nitrogen speciation, intense grazing by *P. amurensis*, and modified river flows (Glibert et al. 2014; Lehman 1996).

One such shift involves the recent appearance of summer blooms of *Microcystis aeruginosa* (Lehman et al. 2005; Lehman et al. 2017), which has the potential for major impacts on fish species within the Delta (Acuña et al. 2012). *Microcystis spp.* are colonial cyanobacteria that can produce harmful algal blooms (HABs) due to the release of toxins (microcystins) produced by some strains (Namikoshi et al. 1992), the light-limiting impacts of blooms on other phytoplankton through formation of surface scums, and their resistance to grazing by zooplankton (Ger et al. 2018; Ibelings et al. 1991). In

the Delta, *Microcystis spp.* blooms were first observed in 1999, although the genus was observed in phytoplankton assemblages as early as 1975 (Lehman et al. 2005). Recently, summer blooms of *M. aeruginosa* are commonplace in the Delta where high surface water temperatures > 25°C promote the *Microcystis spp.* growth (Mioni et al. 2011).

As the largest estuary on the west coast of the United States, the Delta is stressed by anthropogenic impacts on the entire ecosystem. Given the semi-arid, Mediterranean climate of California, most agricultural and municipal fresh water is sourced from the Delta (Luoma et al. 2015) via the State Water Project and the Central Valley Project, along with smaller water projects throughout the Delta. Dynamics of this system are further impacted by nutrient loading from agricultural runoff and wastewater treatment (Sobota et al. 2009) as well as the colonization by many non-native plant, invertebrate, and fish species (Cohen and Carlton 1998). Flow rates in the Delta are managed for water resource needs, flood prevention, hydroelectric power generation, and protection of native fish species (Miller et al. 2012). Such manipulations to estuarine hydrology in the Delta can alter the distribution and function of phytoplankton communities in the system (Cloern 2007; Jassby 2008).

Several ongoing or planned management actions involving flow in the Delta are intended to benefit native aquatic species (NMFS 2009; NMFS 2019; USFWS 2008; USFWS 2019) including the endangered fish, Delta Smelt (*Hypomesus transpacificus*). Managed flow projects are designed to increase favorable Delta Smelt habitat where factors including, but not limited to, low-salinity water, food resources, turbidity, and geomorphologic complexity overlap (Baxter et al. 2015). For example, the flow-related Fall *X2* action is intended to improve Delta Smelt fall habitat by managing *X2*, which is the distance of the 2 ppt bottom water isohaline (measured in kilometers) upstream of the Golden Gate Bridge (Jassby et al. 1995). In above-normal water years, the September and October *X2* is maintained to no more than 81 km, and in wet years the fall *X2* action is enacted to move the *X2* seaward to no more than 74 km. An *X2* near 74 km results in the areal augmentation of low-salinity habitat due to superimposition with the

broad shoals of Suisun Bay (Brown et al. 2014; Kimmerer 2002). Such conditions existed in the wet year of 2011, which coincided with greater catches of Delta Smelt in Suisun Bay during the Fall Midwater Trawl annual monitoring survey (Bever et al. 2016).

Increased flow during a Fall *X2* action could impact both the biomass and composition of the phytoplankton assemblage through several parameters. The reduction in salinity may shift communities from marine taxa to more freshwater taxa (Muylaert et al. 2009) whereas reductions in temperature due to cool water releases from upstream reservoirs may promote an increase in diatom growth and overall phytoplankton biomass in the Delta (Lehman 2004) while reducing the potential for *Microcystis spp.* bloom formation. Residence times in the Delta vary with flow thereby altering the distribution of nutrients through variable rates of loss to uptake by primary producers and other microbial pathways (Dahm et al. 2016). Additionally, the degree of dilution of nutrients from agricultural and waste treatment point sources (Novick et al. 2015) may differentially affect constituents of the microalgal assemblage (Glibert et al. 2011) as well as rates of primary production (Liu et al. 2018). Finally, nitrogen speciation may influence phytoplankton assemblages whereby nitrate as the dominant species generally promotes growth of diatoms (Glibert et al. 2014) while cyanobacteria and cryptophytes are more able to utilize ammonium when present as the dominant species (Glibert et al. 2016). Furthermore, the nitrogen source can limit phytoplankton biomass, even when nutrients are abundant, as ammonium concentrations above 4 $\mu mol\ l^{-1}$ inhibit uptake of available nitrate and prevent phytoplankton blooms in the Delta (Dugdale et al. 2007).

These alterations to phytoplankton community composition may affect nutritional quality and trophic transfer efficiency (Cloern and Dufford 2005). The food quality of phytoplankton taxa varies: diatoms and cryptophytes are rich in polyunsaturated fatty acids (PUFA), which improve survival and growth rates in zooplankton and fish (Brett and Müller-Navarra, 1997). In contrast, many taxa are known for potentially harmful effects on the wider food web due to toxicity, eutrophic oxygen

depletion, and shading of competitor phytoplankton (Ibelings and Havens 2008). Due to the rarity of blooms in the modern Delta, risks of eutrophication and shading is low, but many taxa with the potential to produce toxins exist in the region.

Our paper addresses how the Fall *X2* action and the hydrological conditions in an extremely wet water year affect the phytoplankton community and biomass in the Delta relative to conditions in a dry year. We examine the correlations between phytoplankton assemblages and water quality conditions and nutrient distributions. Our study had 3 objectives:

1. Identify and evaluate variations in phytoplankton assemblage structure and biomass throughout the northern Delta and Suisun Bay.
2. Assess the direct causes of community variation through water quality parameters and nutrient concentration.
3. Assess the potential for the Fall *X2* Action to impact harmful algal blooms, especially blooms of the toxic cyanobacteria *Microcystis spp.*

Methods

Study Area and General Sampling Design Location and Sampling Period

Our study area consisted of 5 regions within the Delta (Figure 1). Sampling occurred September 24th through November 29th in 2017 and between September 5th to November 30th in 2018. All 5 regions were sampled within a one-week period, with 2017 sampling occurring on alternating weeks and 2018 sampling occurring weekly. We sampled 2 sites per week within each region in 2017 and 3 per week in each region in 2018. Sites were selected via a generalized random-tessellation stratified sampling method (Starcevich et al. 2016; Stevens Jr and Olsen 2004). Within each site phytoplankton, chlorophyll-*a*, and nutrient samples were collected at up to two habitats (channel and shoal) within 0.5-km of each site. Channels were defined as areas where the depth was greater than ~ 3m and shoals were areas that were less than ~ 3m. Some sites only had one habitat within the vicinity of the site.

Sampling Methods

Water quality parameters at the at 1-m depth were measured via a handheld multiparameter YSI EXO2 (Yellow Springs Inc, Yellow Springs, OH). Upon arrival at the site, measurements were taken for water temperature (± 0.01°C), salinity (calculated from conductivity and temperature; ± 0.1 ppt), turbidity (± 0.3 NTU), and dissolved oxygen (± 0.01 mg L^{-1}).

Whole water samples were collected from one meter below the surface using nylon tubing into a 2-L vacuum flask. Prior to collection of the sample, the vessel was stopped, and water was pumped into the flask 3 times and discarded to rinse the equipment. After rinsing, one liter of sample water was collected into the vacuum flask.

Sample water for nutrient analysis was filtered via gentle vacuum pressure (<10 mm Hg) through 0.2-µm pore size, 47-mm diameter polycarbonate filters into clean 120-ml High Density Polyethylene bottles. Nutrient samples were kept refrigerated until later analysis for nitrate (NO_3^-), ammonium (NH_4^+), phosphate (PO_4^{3-}) and dissolved organic carbon (DOC) within 2 weeks of collection.

Chlorophyll samples were filtered onto 25-mm Whatman grade GF/F glass fiber filters (nominal pore size 0.7-µm) via gentle vacuum pressure (<10 mm Hg). Depending on turbidity and chlorophyll conditions measured in the field, between 10 and 200 ml of water was filtered and stored in the dark on ice until returning to the laboratory.

Forty-five milliliters of whole water was transferred to a 50-mL Falcon tube for phytoplankton identification. Samples were stained and preserved with 1 to 4-mL of Lugol's solution and kept in the dark.

Lab Analysis Methods

Chlorophyll samples were frozen upon returning to the laboratory and analyzed using a Turner Trilogy fluorometer (Turner Designs, San Jose, CA) with an acidified chlorophyll module (Arar and Collins 1992). Chlorophyll was extracted using 90% acetone and the fluorescence read with the fluorometer, then acidified to decompose the chlorophyll into phaeophytin to calculate total chlorophyll-*a*, as a proxy for phytoplankton biomass.

Phytoplankton samples were kept in the dark until analysis via light microscopy following the methods by (Lund et al. 1958). Subsamples were settled for at least 24-h using Utermoehl settling chambers. Phytoplankton were identified to genera or to the best possible taxonomic level (Bellinger and Sigee 2015; Tomas 1997; Wehr et al. 2015). The slide was analyzed over horizontal transects, identifying and counting each cell, as well as trichomes/colonies in the case of cyanobacteria, in each transect until a target of 400 total cells counted or 100 cells of a single genus was met. The entire subsample was counted if neither target was met.

Final phytoplankton counts were recorded in units of cells per milliliter. Phytoplankton were characterized by taxonomy and by potential as harmful algal bloom (HAB) organisms using the IOC/UNESCO taxonomic reference list of harmful micro algae (Moestrup 2009), which includes only taxa associated with toxic blooms, and not algae with have nontoxic harmful blooms (Hallegraeff 2003).

To account for the often-poor representation of *Microcystis spp* due to their colonial morphology, we also incorporated visual observations of surface water. In 2017, water was sampled from the surface with a 5-gallon bucket, and crews noted presence or absence of *Microcystis spp.* In 2018, surface water was collected from the surface during 3-minute tows using a 12.7-cm diameter plankton net with 50-µm mesh, and concentration of *Microcystis spp.* was estimated using a qualitative scale, with 1 being no *Microcystis spp.* observed and 5 as a continuous sheet of the cyanobacteria at the surface.

Statistical Analysis

Contrasts in nutrient concentrations between years and regions were investigated using Analysis of Variance (ANOVA) without interaction effects in R statistical computing environment (R version 4.0.2, R Core Team 2020), which was used in all analyses describe below. We used Bonferroni corrected estimated marginal means (EMM, 'emmeans' package version 1.5.3, Lenth et al. 2020) to compare differences in nutrient concentrations among regions.

Phytoplankton biomass was contrasted with predictor variables using a generalized linear model (GLM) with an identity-linked Gamma distribution. The full model included the following predictor variables: region, habitat, year, *X2*, environmental parameters (temperature, salinity, turbidity, and dissolved oxygen) and nutrient concentrations (nitrate, ammonium, and phosphate). After backwards stepwise regression, the most parsimonious model was selected via Akaike Information Criteria (AIC).

Diversity of phytoplankton assemblages was characterized for each region and year using Shannon's index for diversity, which incorporates species richness as well as evenness. Diversity was evaluated against region, year, *X2*, chlorophyll-*a*, environmental variables, and nutrient concentrations with a GLM using a Gaussian distribution. After backwards selection, the best model was selected with AIC. The presence or absence of *Microcystis spp.* was contrasted with region and year using a GLM with a binomial distribution.

Non-Metric Multidimensional Scaling (NMDS) from the R package "Vegan" (Oksanen et al. 2020) was used to compare the phytoplankton assemblages between sites after standardization of the of the taxa counts via Wisconsin double standardization. Environmental data was fit to the first and second ordination axes via linear model, and the effects of year, location, and habitat on the structure of the assemblage.

Results

In 2017 samples were collected every other week from September 5th to November 30th, for a total of 125 Samples. In 2018 we collected samples weekly from September 24th to November 29th, For a total of 176 samples. Samples were collected from 254 sites, with 208 collected from the channel surface and 93 collected from shoal habitats.

Water Flow

Water exports were reduced to implement the Fall X2 Action criteria in 2017 and flows in the Sacramento and San Joaquin river were higher, resulting in a higher Net Delta Outflow Index (NDOI) and eastward X2 compared to the 2018 season (Figure 2). 2017 was a wet year (CDWR 2020), so the Fall *X2* action was initiated and *X2* averaged 76-km from September through November. Outflow in 2017 was correspondingly high, with a mean NDOI of 10,400 CFS. In contrast, 2018 was characterized as a below normal water year and had no Fall *X2* action, a mean *X2* of 84 km, and a mean NDOI of 6,600 CFS during the study period.

Nutrient and Water Quality Data

Salinity ranged from 0.04 to 17.5 ppt, and water temperatures ranged from 10.9 to 23.9 °C. The observed turbidity range was from below the detection limit to 71.2 NTU, and dissolved oxygen concentrations were between 5.00 and 9.67 mg L^{-1} (Table 1). Turbidity was lower in 2018 than 2017 throughout the study region, and salinity was higher in 2018, especially in the downstream regions. Temperatures were similar between both years and throughout all the regions.

There were higher ammonium and nitrate concentrations in 2018 than 2017, with no significant differences ($p < 0.05$, Table 2) in phosphate between the two years, and the yearly differences vary between regions (Figure 3). Cache Slough and the Sacramento River Shipping Channel had lower nitrate concentrations than the downstream regions, particularly during the 2017 season. The Sacramento River Shipping Channel also had lower ammonium levels than the Lower Sacramento River, Suisun Marsh, and Suisun Bay, and Cache Slough had lower ammonium than the Lower Sacramento River. The Shipping Channel had higher phosphate concentrations than the Lower Sacramento River and Suisun Bay (Figure 3).

Generally nutrient concentrations were lower than or similar to other estuaries in the United States (Barrera et al. 2001). The combined nitrogen concentrations were overwhelmingly within the "good" range for coastal water quality (< 1 mg/L). Phosphate samples had higher concentrations: 53% of samples had good phosphate concentrations (<0.07 mg/L), 28% had fair phosphate concentrations (0.7 – 0.1 mg/L), and 13% had poor phosphate concentrations (> 0.1 mg/L, EPA 2012).

Nutrient ratios were near the 16:1 nitrogen to phosphate Redfield ratio in the downstream regions but was well below the Redfield ratio within Cache Slough in 2017, and during both years in the Sacramento River Shipping Channel. The ratios of nitrate to ammonium concentrations were roughly equal throughout the study region, with the largest range of ratios in the Sacramento River Shipping Channel. (Figure 4).

Biomass

Median chlorophyll concentration by region and year ranged from 1.9 µg/L in Cache Slough 2017 to 6.8 µg/L in Suisun Marsh,2018 (Figure 5). Chlorophyll-*a* was generally higher in 2018 than 2017, particularly in the Suisun Bay and Marsh regions. In 2018, these two downstream regions had the highest chlorophyll-*a* concentrations while Cache Slough had the lowest. In both years, Cache Slough

had lower biomass than most other regions, and the Sacramento River Shipping channel had the highest biomass in 2017.

The most parsimonious biomass model included ammonium concentration, salinity, *X2*, year, region, and habitat as predictors for chlorophyll concentration, and only habitat was non-significant ($p<0.05$) (Figure 6, Table 2). Suisun Bay was the only non-significant region, while Cache Slough predicted lower than average biomass. Year, region, and salinity had significant positive correlations while *X2* and ammonium had negative correlations. Year and regions had some of the largest significant estimated effect sizes while *X2*, salinity and ammonium had some of the smallest effect sizes (Figure 7).

Harmful Algal Blooms

Microsystis was more common in 2018 than 2017, and presence was least likely in the two upper regions, Cache Slough, and the Sacramento River Shipping Channel (Figure 8). In 2018, *Microcystis spp.* was observed at most sites in the Lower Sacramento River, Suisun Bay and Suisun Marsh.

A total of 14 potential HAB genera were observed (Table 3), although all were in low concentrations and a minority of the overall assemblage. Most HAB genera were cyanobacteria (7 genera), followed by dinoflagellates (5 genera), and diatoms (2 genera).

Diversity

Most phytoplankton were identified within 5 taxonomic groups – diatoms (Bacillariophyceae), cyanobacteria (Cyanophyceae), dinoflagellates (Dinophyceae), green algae (Chlorophyceae and Charophyceae), and cryptophytes (Cryptophyceae). Other groups observed included ciliates, Haptophytes, Ochrophytes, and Euglenozoa. In 2017, diatoms comprised the majority of the assemblage in all strata except the Sacramento River Shipping Channel, in which cyanobacteria was the largest component by cell count. In 2018, diatoms were abundant in the Sacramento River Shipping Channel and Suisun Marsh. Cryptophytes comprised the largest group in Suisun Bay, and cyanobacteria were the largest component in Cache Slough and the Lower Sacramento River.

Cyanobacteria and cryptophytes were common in 2018, while dinoflagellates and green algae were rare in both years (Figure 9). Despite the high abundance of cyanobacteria in Cache Slough during the 2018 season, mean chlorophyll concentration was lowest in that region (Figure 7). Both cyanobacteria and cryptophytes have smaller cell sizes than the diatoms present in the system.

There were 63 phytoplankton genera observed at more than 5 sites (Table 3). Diversity was generally higher in 2017 than 2018 and was higher in the Lower Sacramento River than all other regions (Figure 10).

The two study years had distinct community structures. Diatoms were more common in 2017, while cryptophytes and cyanobacteria were larger components in 2018 (Figure 11). The phytoplankton communities shifted with region, roughly along the salinity gradient (Figure 12), with freshwater taxa, including the cyanobacteria *Oscillatoria* and the diatom *Cocconeis* occurring in Cache Slough and the Sacramento Shipping Channel. Moving downstream to Suisun Bay and Marsh, salt tolerant and marine taxa such as the diatom *Coscinodiscus* and dinoflagellates like *Gonyaulax* became more common. The community of the Lower Sacramento River region comprised both freshwater and euryhaline taxa. Channel and shoal samples have wide overlap in the species distribution; the community structures in the two habitats are similar (Figure 13).

Discussion

While overall phytoplankton biomass in Suisun Bay and Suisun Marsh was lower during the fall *X2* action of 2017, the community composition had a larger proportion composed largely of diatoms, which are considered to be an important primary producer due to their large cell diameter and high carbon content (Chow-Fraser and Wong 1985; Lehman 2004). Potential drivers of the contribution of diatoms to phytoplankton community composition include growth inhibition of diatoms due to elevated concentrations of ammonium (Wilkerson and Dugdale 2016). Higher ammonium: nitrate ratios in 2018 may have inhibited diatom growth (Wilkerson and Dugdale 2016) as well as rates of advective transport within the estuary (Cloern et al. 1983).

Dissolved Nutrients

Along with agricultural runoff, effluent from the Sacramento Regional Wastewater Treatment Plant (SRWTP) supplies nitrogen to the Sacramento River (Kendall et al. 2015). The elevated concentrations of ammonium and nitrate in regions seaward of the confluence of Cache Slough and the Sacramento Shipping Channel (Figure 3) further support the importance of introduced nitrogen from landward sources in the Sacramento River. High flows during the in 2017 *X2* action may have quickly advected excess nitrogen to seaward regions.

The low variation in the ratios of nitrate to ammonium centered around 1 throughout the study (Figure 4) suggests that ammonium is present at high enough concentrations to potentially inhibit phytoplankton growth and primary productivity, as well as cause shifts in the phytoplankton assemblages. The high ammonium concentrations observed in the Delta may have contributed to the low phytoplankton biomass and shift in assemblage, especially in the downstream sample strata.

In contrast, phosphate decreased slightly from Cache Slough and the Sacramento River Shipping Channel to downstream areas, indicative of potential nutrient drawdown. Phytoplankton may have drawn down phosphate concentrations moving downstream (Ball and Arthur 1979), although not to

levels that limit phytoplankton growth. Phosphate and nitrogen concentrations were generally moderate, and unlikely to limit phytoplankton growth or to drive eutrophication of the estuary. The nutrient concentrations are unlikely to promote eutrophication, especially with the low standing stock of phytoplankton generally observed in the Delta since the onset of POD.

The near-Redfield nitrogen:phosphorus ratios suggest that nutrient concentration did not limit phytoplankton biomass through most of the study. The exception was the Sacramento River Shipping channel, where N:P ratio was well below the 16:1 ratio in both years (Turner et al. 2003), and in 2017 phosphate concentrations exceeded nitrogen concentrations, which suggests that phytoplankton productivity may occasionally be limited by depleted nitrogen in the Sacramento River Shipping Channel (Ptacnik et al. 2010).

Phytoplankton Biomass

In 2017, phytoplankton biomass was lower than 2018 throughout the study regions, except for the high biomass in the Sacramento River Shipping Channel. Despite high nutrient concentrations and low turbidity, the remaining regions all had low chlorophyll-*a* concentrations. The low phytoplankton biomass in Suisun Bay and Marsh during the 2017 season suggests the primary producer stock was not improved by the action in this target region. The high chlorophyll-*a* concentrations in the downstream regions during the 2018 season and the positive correlation between salinity and biomass may be due to increased residence time resulting from low flow rates.

In Cache Slough, high residence times permit build-up of phytoplankton biomass; however, our study sites did not include the productive flooded islands and we rarely sampled locations farther upstream where Downing et al. (2016) observed the highest chlorophyll concentrations. During both years, Cache Slough had the lowest biomass, possibly due to the short residence times of water in the sampled channels. Consumption by zooplankton or the competition with invasive floating and submerged aquatic vegetation (Montgomery et al. 2015) may also contribute to low phytoplankton

biomass. As part of the North Delta Flow Action in 2018, the California Department of Water Resources released agricultural runoff into upper Cache Slough to increase phytoplankton productivity and downstream transport, with little observed benefit to biomass (Bureau of Reclamation 2019).

Since the invasion of *P. amurensis* in 1986, mean phytoplankton biomass in the northern estuary during summer and fall in the northern estuary has been reduced due to intense grazing pressure (Alpine and Cloern 1992). Low salinity throughout the 2017 water year may have depressed larval *Potamocorbula* development, and high flows may have moved recruitment downstream (Baumsteiger et al. 2017; Parchaso and Thompson 2002), allowing greater phytoplankton biomass in 2018. During fall *X2* action years, however, clam concentrations in Suisun Bay and Grizzly Bay were similar during the two study periods (Arena and Wells 2018; Watkins and Wells 2019).

The decline in biomass when ammonium concentrations exceeded 10 µmol L^{-1} further highlights the importance of ammonium inhibition of nitrate uptake in the northern estuary (Dugdale et al. 2007). Although ammonium may have inhibited biomass at these high concentrations, only 10% of sites had such high concentrations. During both years, ammonium concentrations increased downstream of Cache Slough and the Shipping Channel, due to wastewater effluent from SRWTP into the Sacramento River upstream of its confluence with Cache Slough and the Shipping channel. With improved wastewater treatment at the SRWTP, ammonium discharge from the largest point source in the northern Delta will decline, which may help to mitigate ammonium inhibition of nitrate uptake (Hobbs et al. 2017). In the high flow year of 2017, ammonium peaked in the Lower Sacramento River region and declined further downstream, presumably due to nitrification and perhaps uptake by phytoplankton.

The Sacramento Ship Channel was a unique region with respect to biomass, with the highest chlorophyll-*a* in 2017 and similarly high biomass in 2018. This region also had the lowest N:P ratio during both years. The low dissolved nitrogen concentrations suggest that Nitrogen does limit biomass in the

Ship Channel. High residence time in the channel allows higher primary productivity and biomass growth and supports a robust zooplankton population (Feyrer et al. 2017).

The spatial biomass patterns observed require further examination; if the low downstream chlorophyll concentration observed in 2017 is characteristic of Fall *X2* action years with high-precipitation, low phytoplankton biomass may depress the primary consumers and thus the Delta Smelt food source. The independent impact of a wet water year and the X2 action cannot be distinguished from these data, which will necessitate continued sampling during action and non-action years, as well as analysis of historical data from long-term monitoring programs.

The between-year biomass pattern was most apparent downstream, in Suisun Bay and Suisun Marsh, where 2018 chlorophyll-a concentrations were double that of 2017. Nutrient concentrations were similar between the two years in these regions, although salinity was lower in 2017 due to the Fall *X2* action. Turbidity and outflow were lower in 2018, which may have promoted phytoplankton biomass through both reduced shading and increased residence times of a diverse assemblage within Suisun Bay and Marsh.

Phytoplankton Diversity

Phytoplankton diversity varied with region and *X2*, with the highest diversity in the Lower Sacramento River and the Western Delta. The Lower Sacramento River has variable salinity regimes and had high incidence of both freshwater and euryhaline taxa. Suisun Bay and Suisun Marsh had the highest proportion of the more salt-tolerant diatoms. As *X2* moved downstream, Shannon diversity increased, potentially indicative of more mixing between marine and riverine influenced water, especially in the Lower Sacramento and Suisun Bay/Marsh. Although the trend was not significant, the apparent inverse trend with chlorophyll-*a* is expected; as blooms form from single dominant taxa, species richness and evenness decreases.

There was very little difference between assemblages in the Channel and Shoal habitats; any influence of habitat on the phytoplankton community is minor compared to the larger temporal and geographic trends, due to well mixed waters within the sample sites. Likewise, biomass did not vary between shoal and channel habitats, therefore paired sampling of phytoplankton from nearby habitats may be unnecessary.

The phytoplankton assemblage shifted downstream with region, which was similar to successional patterns previously reported for the northern estuary (Cloern and Dufford 2005). This shift was from freshwater taxa to salt tolerant taxa, although several taxa including *Navicula*, *Cyclotella*, and *Phormidium* were common throughout the study region. Assemblages in Cache Slough and the Shipping Channel were composed of a wide range of taxa, with diatoms, cyanobacteria and euglenophytes being common in these regions. Farther downstream, cryptophytes became more common and occasionally dominated this assemblage. Cyanobacteria were rarer in the higher salinity reaches.

Sample year had a strong impact on the phytoplankton assemblage. The wet year of 2017 was characterized by an abundance of diatoms, while cyanobacteria, dinoflagellates, and cryptophytes were more abundant in 2018. This assemblage shift corresponded with shifts in increased ammonium and biomass, and upstream *X2* shift in 2018.

The higher flow rates in 2017 likely selected for diatoms through estuarine circulation in Suisun Bay and Marsh (Cloern, 1983). While less dense taxa are transported seaward during high flow, denser diatoms sink and are transported back upstream via the landward flowing bottom current, which can trap diatom assemblages within Suisun Bay. Despite this potential effect of circulation on the assemblage structure, the overall biomass was low in Suisun Bay and Marsh. In 2018, the phytoplankton communities in Suisun Marsh and Suisun Bay had high biomass and were composed of diatoms and cryptophytes, both of which are rich in PUFAs (Brett and Müller-Navarra 1997). The high salinity during the non-action year may have driven the growth of these large high-quality food sources but the higher

algal biomass and lower zooplankton concentrations in 2018 may indicate lower quality food sources. The large diatoms observed in Suisun Bay and Marsh are well-suited as prey items for herbivorous zooplankton in Suisun Bay and Marsh. A recent single-taxa bloom of the diatom *Aulacoseira granulata* in 2017 did not stimulate production of the copepod *Pseudodiaptomus forbesi* (Jungbluth et al. 2020), whereas a more diverse phytoplankton assemblage may support a wide range of secondary consumers despite much lower biomass.

Although biomass was lower during the Fall *X2* action year, higher phytoplankton biomass negatively correlated with a seaward daily *X2* (Figure 7), possibly due to the transport from upstream assemblages. The daily *X2* did not correlate with the phytoplankton diversity (Table 2), as shifts in the assemblage would lag behind changing flow regimes.

In pelagic food webs, high diversity in the primary consumers promotes high functional diversity in higher trophic levels (D'Alelio et al. 2016). The high phytoplankton diversity within the Lower Sacramento River, coupled with the environmental variability in the region may support a diverse zooplankton assemblage and enhance the overall food web for Delta Smelt in the region and in downstream reaches.

Harmful Algal Blooms

No harmful algal blooms were observed over the course of the study, however *Microcystis spp*. flakes were common in both years. The *Microcystis spp.* colonies were broken up and occurred at relatively low abundance compared with observations upstream in the San Joaquin River (Lehman et al. 2020). *Microcystis spp*. was much more prevalent during the dry year (2018), especially in the Lower Sacramento River. Since *Microcystis spp*. thrives in warm, low-velocity freshwater in the Delta (Mioni et al. 2011) the Fall *X2* action selected against the conditions that promote *Microcystis spp.* blooms. Most *Microcystis spp.* blooms in the Delta originate in the San Joaquin River (Lehman et al. 2017), so

evaluating the growth and transport of those blooms in the Southern Delta under both high flow rates and low export rates will help to assess the impacts of *X2* actions on HAB events.

Although the *Microcystis* observed in Suisun Bay and Marsh was not in bloom conditions, the colonies can continue to produce toxins up to a salinity of 4 ppt (Black et al. 2011). The toxic impact of the observed *Microcystis spp.* cannot be determined without measurement of microcystins. The degraded cyanobacterial colonies may augment the phytoplankton biomass and provide a food source to zooplankton, some of which can consume decomposed *Microcystis* (Hanazato and Yasuno 1987).

There were many other potentially toxic taxa observed over the study, including cyanobacteria, diatoms, and dinoflagellates. These taxa were occasionally common but were not observed to bloom, and therefore were unlikely to produce harmful concentrations of toxins. Similarly, the lack of bloom formation and the relatively high dissolved oxygen concentrations demonstrate a low risk of eutrophication from phytoplankton blooms.

Management Implications

In 2018, the *X2* action was not implemented and the phytoplankton communities in the relatively high-salinity Suisun Bay and Marsh regions had higher biomass but less diversity than in 2017. Despite generally higher biomass in 2018, less nutritious taxa comprised a larger proportion of the assemblage in Suisun Bay and Suisun Marsh and zooplankton abundance was lower (Hassrick et al. 2021).

While the nutritious quality of food in Suisun Bay and Marsh was improved during the Fall X2 action year of 2017, the direct cause driving reduced biomass is unclear. In 2017, there was greater zooplankton abundance, which may have drawn down phytoplankton biomass (Hassrick et al., 2021). The *P. amurensis* population was similar in Fall 2017 to Fall 2018 in Suisun Bay and Marsh (Arena and Wells 2018; Watkins and Wells 2019), so were unlikely to have a driven the lower phytoplankton biomass in the action year. Finally, seaward transport due to higher flow rates may have inhibited phytoplankton biomass during the action. In 2018, less nutritious cyanobacteria made up a larger

proportion of the phytoplankton assemblage throughout the study region, but high-quality diatoms and cryptophytes remained abundant in Suisun Bay and Marsh. Analysis of zooplankton and benthic gut contents and measurement of primary productivity can clarify the causes of the biomass differences and the effects of community structure.

The Delta has been a high nutrient-low chlorophyll system since the onset of the pelagic organism decline. Although the phytoplankton biomass in Suisun Bay and Marsh was low during the action year, the improved Delta Smelt prey field observed during concurrent studies suggest that the impact on the overall food web is minimal. The higher flow rates inhibit formation of toxic *Microcystis* blooms, and the improved habitat availability provides a larger area over which Delta Smelt can utilize the available food. The causes of the low chlorophyll-*a* concentrations observed during the X2 Action warrant further study to establish the direct effects of increased flow on the Delta phytoplankton community.

Acknowledgements

This work was conducted as part of the Directed Outflow Project (DOP) under the Interagency Ecological Program (IEP) annual work plan. Early reviews of related DOP study plans were supported by the IEP Flow Alteration Project Work Team and the Collaborative Adaptive Management Team (special thanks to Larry Brown [USGS]), and USFWS, DWR, CDFW, and USBR. Permitting for this work was facilitated through CDFW, USWFS and IEP. This study was supported by the contribution of multiple IEP agency field sampling activities of fish and zooplankton (CDFW, USFWS, DOP [USBR]), as well as informed by DWR DAYFLOW. Funding and contractual support was provided by USBR, DWR, State Water Contractors (special thanks to Jennifer Pierre) and State and Federal Contractors Water Agency (special thanks to Laura Valoppi). We acknowledge the support of many people from the Delta science community. Contributors from ICF include Colin Brennan, Rob Miller, Athena Maguire, Andrew Winston, Ramona Zeno, Jake Sousa, Angelina Ravani, Tim Carrara, Katherine Maniscalco, Donna Maniscalco, Eric Chapman and Stephanie Owens. Thanks to Erwin Van Nieuwenhuyse (USBR) and Tiffany Brown (DWR) for their

insights while reviewing this manuscript. We thank Catherine Johnston and Lara Mitchell (USFWS) on timely guidance for site selection, coordination, and data; and Tom Philippi (National Park Service) for sampling and GRTS advice. We thank Randy Dahlgren and Xien Wang (U.C. Davis) for analysis of and support with nutrient data. Any use of trade, product, or firm names is for descriptive purposes only and does not imply endorsement by the U.S. Bureau of Reclamation or the U.S. Government. The views expressed are those of the authors and do not represent the official opinion of the U.S. Bureau of Reclamation.

References

Acuña, S., D.F. Deng, P. Lehman, and S. Teh. 2012. Sublethal dietary effects of Microcystis on Sacramento splittail, Pogonichthys macrolepidotus. *Aquat Toxicol* 110-111: 1-8.

Alpine, A.E., and J.E. Cloern. 1992. Trophic interactions and direct physical effects control phytoplankton biomass and production in an estuary. *Limnology and oceanography* 37: 946-955.

Arar, E.J., and G.B. Collins. 1992. In vitro determination of chlorophyll a and pheophytin a in marine and freshwater phytoplankton by fluorescence. *Methods for the Determination of Chemical Substances in Marine and Estuarine Environmental Samples. Cincinnati, EPA/600/R-92/121*: 445.

Arena, B., and B. Wells. 2018. Benthic Monitoring, 2017. *IEP Newsletter* 33: 6-13.

Ball, M.D., and J.F. Arthur. 1979. Planktonic chlorophyll dynamics in the northern San Francisco Bay and Delta. *San Francisco Bay: The Urbanized Estuary. Pacific Division, American Association for the Advancement of Science, San Francisco, California,*: 265-285.

Barrera, J., R. Cantilli, I. Davis, E.H. Dettmann, J. Fisher, T. Gardner, G. Gibson, D. Hart, J.S. Latimer, and P.S. Libby. 2001. Nutrient criteria technical guidance manual: estuarine and coastal marine waters.

Baumsteiger, J., R.E. Schroeter, T. O'Rear, J.D. Cook, and P.B. Moyle. 2017. Long-term surveys show invasive overbite clams (Potamocorbula amurensis) are spatially limited in Suisun Marsh, California. *San Francisco Estuary and Watershed Science* 15.

Baxter, R., L.R. Brown, G. Castillo, L. Conrad, S.D. Culberson, M.P. Dekar, M. Dekar, F. Feyrer, T. Hunt, K. Jones, J. Kirsch, A. Mueller-Solger, M. Nobriga, S.B. Slater, T. Sommer, K. Souza, G. Erickson, S. Fong, K. Gehrts, L. Grimaldo, and B. Herbold. 2015. An updated conceptual model of Delta Smelt biology: our evolving understanding of an estuarine fish: Interagency Ecological Program, California Department of Water Resources.

Bellinger, E.G., and D.C. Sigee. 2015. *Freshwater algae: identification, enumeration and use as bioindicators*: John Wiley & Sons.

Bever, A.J., M.L. MacWilliams, B. Herbold, L.R. Brown, and F.V. Feyrer. 2016. Linking Hydrodynamic Complexity to Delta Smelt (Hypomesus transpacificus) Distribution in the San Francisco Estuary, USA. *San Francisco Estuary and Watershed Science* 14.

Black, K., M. Yilmaz, and E.J. Phlips. 2011. Growth and toxin production by Microcystis aeruginosa PCC 7806 (Kutzing) Lemmerman at elevated salt concentrations. *Journal of Environmental Protection* 2: 669.

Brett, M., and D.C. Müller-Navarra. 1997. The role of highly unsaturated fatty acids in aquatic foodweb processes. *Freshwater Biology* 38: 483-499.

Brown, L., W. Kimmerer, J.L. Conrad, S. Lesmeister, and A. Mueller–Solger. 2016. Food Webs of the Delta, Suisun Bay, and Suisun Marsh: An Update on Current Understanding and Possibilities for Management. *San Francisco Estuary and Watershed Science* 14.

Brown, L.R., R. Baxter, G. Castillo, L. Conrad, S. Culberson, G. Erickson, F. Feyrer, S. Fong, K. Gehrts, L. Grimaldo, B. Herbold, J. Kirsch, A. Mueller-Solger, S.B. Slater, T. Sommer, K. Souza, and E. Van Nieuwenhuyse. 2014. Synthesis of studies in the fall low-salinity zone of the San Francisco Estuary, September–December 2011. In US Geological Survey Scientific Investigations Report, 136: US Geological Survey.

Carlton, J.T., J.K. Tompson, L.E. Schemel, and F.H. Nichols. 1990. Remarkable invasion of San Francisco Bay (California, USA), by the Asian clam Potamocorbula amurensis. I. Introduction and dispersal. *Marine Ecology Progress Series* 66: 81-94.

CDEC. 2020. Chronological Reconstructed Sacramento and San Joaquin Valley Water Year Hydrologic Classification Indices. https://cdec.water.ca.gov/reportapp/javareports?name=WSIHIST. Accessed 12/10/2020

Chow-Fraser, P., and C. Wong. 1985. Herbivorous feeding of three large freshwater calanoid copepods, Limnocalanus macrurus Sars, Senecella calanoides Juday and Epischura lacustris Forbes. *Internationale Vereinigung für theoretische und angewandte Limnologie: Verhandlungen* 22: 3195-3198.

Cloern, J. 2007. Habitat connectivity and ecosystem productivity: Implications from a simple model. *The American Naturalist* 169: E21-E33.

Cloern, J., and R. Dufford. 2005. Phytoplankton community ecology: principles applied in San Francisco Bay. *Marine Ecology Progress Series* 285: 11-28.

Cloern, J.E., A.E. Alpine, B.E. Cole, R.L. Wong, J.F. Arthur, and M.D. Ball. 1983. River discharge controls phytoplankton dynamics in the northern San Francisco Bay estuary. *Estuarine, Coastal and Shelf Science* 16: 415-429.

Cohen, A.N., and J.T. Carlton. 1998. Accelerating invasion rate in a highly invaded estuary. *Science* 279: 555-558.

D'Alelio, D., S. Libralato, T. Wyatt, and M.R. d'Alcalà. 2016. Ecological-network models link diversity, structure and function in the plankton food-web. *Scientific Reports* 6: 1-13.

Dahm, C.N., A.E. Parker, A.E. Adelson, M.A. Christman, and B.A. Bergamaschi. 2016. Nutrient Dynamics of the Delta: Effects on Primary Producers. *San Francisco Estuary and Watershed Science* 14.

Downing, B.D., B.A. Bergamaschi, C. Kendall, T.E. Kraus, K.J. Dennis, J.A. Carter, and T.S. Von Dessonneck. 2016. Using continuous underway isotope measurements to map water residence time in hydrodynamically complex tidal environments. *Environmental science & technology* 50: 13387-13396.

Dugdale, R.C., F.P. Wilkerson, V.E. Hogue, and A. Marchi. 2007. The role of ammonium and nitrate in spring bloom development in San Francisco Bay. *Estuarine, Coastal and Shelf Science* 73: 17-29.

Feyrer, F., S.B. Slater, D.E. Portz, D. Odom, T. Morgan-King, and L.R. Brown. 2017. Pelagic nekton abundance and distribution in the northern Sacramento–San Joaquin Delta, California. *Transactions of the American Fisheries Society* 146: 128-135.

Ger, K.A., S. Naus-Wiezer, L. De Meester, and M. Lürling. 2018. Zooplankton grazing selectivity regulates herbivory and dominance of toxic phytoplankton over multiple prey generations. *Limnology and Oceanography* 64: 1214-1227.

Glibert, P.M., R.C. Dugdale, F. Wilkerson, A.E. Parker, J. Alexander, E. Antell, S. Blaser, A. Johnson, J. Lee, T. Lee, S. Murasko, and S. Strong. 2014. Major – but rare – spring blooms in 2014 in San

Francisco Bay Delta, California, a result of the long-term drought, increased residence time, and altered nutrient loads and forms. *Journal of Experimental Marine Biology and Ecology* 460: 8-18.

Glibert, P.M., D. Fullerton, J.M. Burkholder, J.C. Cornwell, and T.M. Kana. 2011. Ecological stoichiometry, biogeochemical cycling, invasive species, and aquatic food webs: San Francisco Estuary and comparative systems. *Reviews in Fisheries Science* 19: 358-417.

Glibert, P.M., F.P. Wilkerson, R.C. Dugdale, J.A. Raven, C.L. Dupont, P.R. Leavitt, A.E. Parker, J.M. Burkholder, and T.M. Kana. 2016. Pluses and minuses of ammonium and nitrate uptake and assimilation by phytoplankton and implications for productivity and community composition, with emphasis on nitrogen-enriched conditions. *Limnology and Oceanography* 61: 165-197.

Hallegraeff, G. 2003. Harmful algal blooms: a global overview. *Manual on harmful marine microalgae* 33: 1-22.

Hammock, B.G., S.P. Moose, S.S. Solis, E. Goharian, and S.J. Teh. 2019. Hydrodynamic Modeling Coupled with Long-term Field Data Provide Evidence for Suppression of Phytoplankton by Invasive Clams and Freshwater Exports in the San Francisco Estuary. *Environ Manage* 63: 703-717.

Hanazato, T., and M. Yasuno. 1987. Evaluation of Microcystis as food for zooplankton in a eutrophic lake. *Hydrobiologia* 144: 251-259.

Hassrick, J.L., A.G. Smith, C.Y. Lee, D.M. Cox, A.K. Kalmbach, and A. Schultz. 2021. How an estuarine prey field changes with managed freshwater outflow in an increasingly arid climate. Pages xx-xx in Schultz A.A. and N. Bertrand, editors. Directed Outflow Project Technical Report 2. U.S. Bureau of Reclamation, Bay-Delta Office, Mid-Pacific Region, Sacramento, CA. February 2021, xxx pp.

Hobbs, J., P.B. Moyle, N. Fangue, and R.E. Connon. 2017. Is extinction inevitable for Delta Smelt and Longfin Smelt? An opinion and recommendations for recovery. *San Francisco Estuary and Watershed Science* 15.

Ibelings, B.W., and K.E. Havens. 2008. Cyanobacterial toxins: a qualitative meta–analysis of concentrations, dosage and effects in freshwater, estuarine and marine biota. In *Cyanobacterial harmful algal blooms: state of the science and research needs*, 675-732: Springer.

Ibelings, B.W., L.R. Mur, and A.E. Walsby. 1991. Diurnal changes in buoyancy and vertical distribution in populations of Microcystis in two shallow lakes. *Journal of Plankton Research* 13: 419-436.

Jassby, A.D. 2008. Phytoplankton in the Upper San Francisco Estuary: Recent Biomass Trends, Their Causes, and Their Trophic Significance. *San Francisco Estuary and Watershed Science* 6.

Jassby, A.D., J. Cloern, and A. Mueller-Solger. 2003. Phytoplankton fuels Delta food web. *California Agriculture* 57: 104-109.

Jassby, A.D., W. Kimmerer, S.G. Monismith, C. Armor, J.E. Cloern, T.M. Powell, J.R. Schubel, and T.J. Vendlinski. 1995. Isohaline position as a habitat indicator for estuarine populations. *Ecological Applications* 5: 272-289.

Jungbluth, M., C. Lee, C. Patel, T. Ignoffo, B. Bergamaschi, and W. Kimmerer. 2020. Production of the Copepod Pseudodiaptomus forbesi Is Not Enhanced by Ingestion of the Diatom Aulacoseira granulata During a Bloom. *Estuaries and Coasts*: 1-17.

Kendall, C., M. Young, S. Silva, T. Kraus, S. Peek, and M. Guerin. 2015. Tracing nutrient and organic matter sources and biogeochemical processes in the Sacramento River and Northern Delta: proof of concept using stable isotope data. *US Geological Survey*.

Kimmerer, W. 2002. Physical, biological, and management responses to variable freshwater flow into the San Francisco Estuary. *Estuaries* 25: 1275-1290.

Lehman, P., T. Kurobe, and S. Teh. 2020. Impact of extreme wet and dry years on the persistence of Microcystis harmful algal blooms in San Francisco Estuary. *Quaternary International*.

Lehman, P.W. 1996. Changes in chlorophyll a concentration and phytoplankton community composition with water-year type in the upper San Francisco Bay Estuary. .

Lehman, P.W. 2004. The influence of climate on mechanistic pathways that affect lower food web production in Northern San Francisco Bay estuary. *Estuaries* 27: 311-324.

Lehman, P.W., G. Boyer, C. Hall, S. Waller, and K. Gehrts. 2005. Distribution and toxicity of a new colonial Microcystis aeruginosa bloom in the San Francisco Bay Estuary, California. *Hydrobiologia* 541: 87-99.

Lehman, P.W., T. Kurobe, S. Lesmeister, D. Baxa, A. Tung, and S.J. Teh. 2017. Impacts of the 2014 severe drought on the Microcystis bloom in San Francisco Estuary. *Harmful Algae* 63: 94-108.

Lenth, R., H. Singmann, J. Love, P. Buerkner, and M. Herve. 2020. emmeans: Estimated Marginal Means, aka Least-Squares Means (Version 1.5.3).

Liu, Q., F. Chai, R. Dugdale, Y. Chao, H. Xue, S. Rao, F. Wilkerson, J. Farrara, H. Zhang, and Z. Wang. 2018. San Francisco Bay nutrients and plankton dynamics as simulated by a coupled hydrodynamic-ecosystem model. *Continental Shelf Research* 161: 29-48.

Lund, J., C. Kipling, and E. Le Cren. 1958. The inverted microscope method of estimating algal numbers and the statistical basis of estimations by counting. *Hydrobiologia* 11: 143-170.

Luoma, S.N., C.N. Dahm, M. Healey, and J.N. Moore. 2015. Water and the Sacramento-San Joaquin Delta: Complex, Chaotic, or Simply Cantankerous? *San Francisco Estuary and Watershed Science* 13.

Merz, J.E., P.S. Bergman, J.L. Simonis, D. Delaney, J. Pierson, and P. Anders. 2016. Long-Term Seasonal Trends in the Prey Community of Delta Smelt (Hypomesus transpacificus) Within the Sacramento-San Joaquin Delta, California. *Estuaries and Coasts* 39: 1526-1536.

Miller, W.J., B.F.J. Manly, D.D. Murphy, D. Fullerton, and R.R. Ramey. 2012. An Investigation of Factors Affecting the Decline of Delta Smelt (Hypomesus transpacificus) in the Sacramento-San Joaquin Estuary. *Reviews in Fisheries Science* 20: 1-19.

Mioni, C., R. Kudela, D. Baxa, M. Sullivan, K. Hayashi, T. Smythe, and C. White. 2011. Harmful cyanobacteria blooms and their toxins in Clear Lake and the Sacramento-San Joaquin Delta (California), ed. C.V.R.W.Q.C. Board.

Moestrup, O. 2009. IOC-UNESCO taxonomic reference list of harmful micro algae. *http://www. marinespecies. org/HAB*.

Montgomery, G., J.R. Durand, and P.B. Moyle. 2015. Zooplankton biomass and chlorophyll-a trends in the North Delta Arc: two consecutive drought years. . *IEP Newsletter* 28: 14-21.

Muylaert, K., K. Sabbe, and W. Vyverman. 2009. Changes in phytoplankton diversity and community composition along the salinity gradient of the Schelde estuary (Belgium/The Netherlands). *Estuarine, Coastal and Shelf Science* 82: 335-340.

Namikoshi, M., K.L. Rtinehart, and R. Sakai. 1992. Identification of 12 Hepatotoxins from a Homer Lake Bloom of the Cyanobacteria Microcystis aeruginoaa , Microcystis viridis , and Microcystis wesenbergii: Nine New Microcystins. *Journal of Organic Chemistry* 57: 866-872.

NMFS. 2009. Biological opinion and conference opinion on the long-term operations of the Central Valley Project and State Water Project: NMFS Southwest Region, Long Beach, California.

National Marine Fisheries Service. 2019. Biological Opinion on Long-Term Operation of the Central Valley Project and the State Water Project. U.S. Department of Commerce, 900 pp.

Novick, E., R. Holleman, T. Jabusch, J. Sun, P. Trowbridge, D. Senn, M. Guerin, C. Kendall, M. Young, and S. Peek. 2015. Characterizing and quantifying nutrient sources, sinks and transformations in the Delta: synthesis, modeling, and recommendations for monitoring. Richmond, CA: San Francisco Estuary Institute.

Oksanen, J., F. Blanchet, M. Friendly, R. Kindt, P. Legendre, D. McGlinn, P. Minchin, R. O'Hara, G. Simpson, and P. Solymos. 2020. vegan: Community Ecology Package. R package version 2.5-7. 2020.

Parchaso, F., and J.K. Thompson. 2002. Influence of hydrologic processes on reproduction of the introduced bivalve Potamocorbula amurensis in northern San Francisco Bay, California. *Pacific Science* 56: 329-345.

Ptacnik, R., T. Andersen, and T. Tamminen. 2010. Performance of the Redfield Ratio and a Family of Nutrient Limitation Indicators as Thresholds for Phytoplankton N vs. P Limitation. *Ecosystems* 13: 1201-1214.

R Core Team. 2020. R: A language and environment for statistical computing. R Foundation for Statistical Computing, Vienna, Austria. Vienna, Austria: R Foundation for Statistical Computing.

Sobota, D.J., J.A. Harrison, and R.A. Dahlgren. 2009. Influences of climate, hydrology, and land use on input and export of nitrogen in California watersheds. *Biogeochemistry* 94: 43-62.

Sommer, T., C. Armor, R. Baxter, R. Breuer, L. Brown, M. Chotkowski, S. Culberson, F. Feyrer, M. Gingras, B. Herbold, W. Kimmerer, A. Mueller-Solger, M. Nobriga, and K. Souza. 2007. The Collapse of Pelagic Fishes in the Upper San Francisco Estuary: El Colapso de los Peces Pelagicos en La Cabecera Del Estuario San Francisco. *Fisheries* 32: 270-277.

Starcevich, L., G. DiDonato, T. McDonald, and J. Mitchell. 2016. A GRTS user's manual for the SDrawNPS package: a graphical user interface for generalized random tessellation stratified (GRTS) sampling and estimation. *Natural Resource Report NPS/PWRO/NRR–2016/1233. National Park Service, Fort Collins, CO*.

Stevens Jr, D.L., and A.R. Olsen. 2004. Spatially balanced sampling of natural resources. *Journal of the American statistical Association* 99: 262-278.

Thomson, J.R., W. Kimmerer, L. Brown, K.N. Newman, R. Mac Nally, W.A. Bennett, F. Feyrer, and E. Fleishman. 2010. Bayesian change point analysis of abundance trends for pelagic fishes in the upper San Francisco Estuary. *Ecological Applications* 20: 1431-1448.

Tomas, C.R. 1997. *Identifying marine phytoplankton*. Academic Press. New York City, NY.

Turner, R., N. Rabalais, D. Justic', and Q. Dortch. 2003. Global patterns of dissolved N, P and Si in large rivers. *Biogeochemistry* 64: 297–317.

USBR. 2019. Effects analysis for the Delta Smelt Fall Habitat Action in 2019. Appendix in: Delta Smelt Fall Habitat Action in 2019 environmental assessment.

US Environmental Protection Agency. 2012. National Coastal Condition Report IV: EPA-842-R-10-003. U.S. Environmental Protection Agency, Office of Water and Office of Research and Development, Washington, D.C., USA.

USFWS. 2008. Biological Opinion on the Effects of Long Term Coordinated Operations of the Central Valley (CVP) and State Water Project (SWP) on Delta Smelt and Its Designated Critical Habitat. U.S. Department of the Interior.

USFWS. 2019. Biological Opinion for the Reinitiation of Consultation on the Coordinated Operations of the Central Valley and State Water Project. U.S. Department of the Interior.

Watkins, B., and B. Wells. 2019. Benthic Monitoring, 2018. *IEP Newsletter* 37: 23-30.

Wehr, J.D., R.G. Sheath, and J.P. Kociolek. 2015. *Freshwater algae of North America: ecology and classification*: Elsevier.

Wilkerson, F., and R. Dugdale. 2016. The ammonium paradox of an urban high-nutrient low-growth estuary. In *Aquatic microbial ecology and biogeochemistry: a dual perspective*, 117-126: Springer.

Tables

Table 1. Mean and standard deviation of water quality parameters over each study season and region.

Year	Strata	Salinity	Temperature	Turbidity	DO
2017	Cache Slough	0.083 (0.030)	17.6 (2.94)	4.206 (7.798)	8.333 (1.102)
	Sacramento River Shipping Channel	0.25 (0.133)	18.1 (2.74)	13.41 (13.35)	8.596 (0.4808)
	Lower Sacramento River	0.073 (0.029)	16.4 (2.98)	1.388 (1.193)	8.822 (0.4016)
	Suisun Bay	4.65 (3.6)	17.9 (2.47)	14.52 (10.11)	8.649 (0.3755)
	Suisun Marsh	5.34 (2.54)	20.1 (2.67)	26.96 (19.75)	7.868 (0.5413)
2018	Cache Slough	1.47 (3.73)	17.2 (2.46)	1.72 (1.008)	8.498 (0.6436)
	Sacramento River Shipping Channel	0.272 (0.162)	16.8 (3.37)	6.96 (7.815)	8.794 (0.4877)
	Lower Sacramento River	1.19 (1.35)	17.1 (2.38)	3.214 (3.149)	8.545 (0.4244)
	Suisun Bay	11.6 (3.78)	16.5 (2.39)	2.373 (3.179)	8.302 (0.3112)
	Suisun Marsh	9.45 (3.09)	16.4 (2.57)	7.391 (7.788)	7.953 (0.8804)

Table 2. Model summary for biomass and diversity linear models.

Response Variable	Predictor	Estimate	95% Confidence Interval	P Value
Biomass	Sacramento River Shipping Channel	2.06	1.296 — 2.824	<0.001
	Lower Sacramento River	1.14	0.469 — 1.811	0.001
	Suisun Bay	0.9	0.157 — 1.643	0.019
	Suisun Marsh	2.41	1.28 — 3.54	<0.001
	Year	2.87	1.82 — 3.92	<0.001
	Habitat	-0.437	-0.946 — 0.072	0.094
	Salinity	0.118	0.036 — 0.1999	0.005
	NH4	-0.079	-0.106 — -0.053	<0.001
	X2	-0.165	-0.291 — -0.039	0.011
Shannon Diversity	Sacramento River Shipping Channel	0.0552	-0.198 — 0.308	0.669
	Lower Sacramento River	0.635	0.379 — 0.891	<0.001
	Suisun Bay	0.226	-0.013 — 0.465	0.066
	Suisun Marsh	-0.038	-0.339 — 0.263	0.804
	Chlorophyll-*a*	-0.028	-0.058 — 0.002	0.073
	X2	-0.033	-0.049 — -0.017	<0.001

Table 3. Phytoplankon taxa observed in 2017 and 2018. Includes taxa that were observed at 5 or more sites.

Taxa	Group	Mean taxa abundance	Standard Deviation	Number of observances	Potentially toxic algae
Cryptomonas	Cryptophyte	1,451.90	12328.9	74	No
Rhodomonas	Cryptophyte	4,747.40	19914	94	No
Anabaena	Cyanobacteria	148.6	789.6	20	Yes
Aphanizomenon	Cyanobacteria	5,876.00	68266.1	35	Yes
Geitlerinema	Cyanobacteria	626	4666.3	22	Yes
Leptolyngbya	Cyanobacteria	681.2	4092.8	17	No
Oscillatoria	Cyanobacteria	7,919.70	80451.3	42	Yes
Phormidium	Cyanobacteria	4,915.20	28390.5	71	Yes
Planktothrix	Cyanobacteria	321	3259	7	Yes
Pseudanabaena	Cyanobacteria	99.7	824.6	8	No
Achnanthes	Diatom	10.1	79.1	7	No
Adlafia	Diatom	9.4	56.9	19	No
Amphora	Diatom	22	97.3	31	Yes
Asterionella	Diatom	12.7	135.7	5	No
Aulacoseira	Diatom	844.7	3874.8	105	No
Chaetoceros	Diatom	1,515.30	5505.4	135	No
Cocconeis	Diatom	1,395.40	4507.9	183	No
Coscinodiscus	Diatom	199.4	428.1	142	No
Craticula	Diatom	1	7.6	5	No
Cyclotella	Diatom	282.3	640.5	158	No
Cymbella	Diatom	5.1	40.1	10	No
Diatoma	Diatom	26	94.5	44	No
Diploneis	Diatom	5.6	31.6	13	No
Encyonema	Diatom	1.9	13.6	9	No
Entomoneis	Diatom	88.5	250.4	78	No
Epithemia	Diatom	8.2	38.8	20	No
Eunotia	Diatom	197.9	1482.6	16	No
Fragilaria	Diatom	332.9	698.9	168	No
Fragilariopsis	Diatom	9.4	89.6	13	No
Gomphoneis	Diatom	27.1	106.1	45	No
Gomphonema	Diatom	3.5	21.6	10	No
Gyrosigma	Diatom	957.5	2284	197	No
Leptocylindrus	Diatom	1,367.90	11490.4	66	No
Melosira	Diatom	1,763.30	6408.2	113	No
Navicula	Diatom	639.6	1893.4	183	No
Nitzschia	Diatom	2,227.40	20950.5	171	Yes
Paralia	Diatom	1,322.80	17656	19	No
Pinnularia	Diatom	5.4	36.4	11	No
Pleurosigma	Diatom	25.3	92.5	38	No

Rhoicosphenia	Diatom	2.1	19.4	5	No
Rhopalodia	Diatom	3.3	18.4	11	No
Skeletonema	Diatom	71.2	316.8	23	No
Surirella	Diatom	7.9	39.4	21	No
Synedra	Diatom	4.3	29.1	11	No
Thalassionema	Diatom	9.8	112.7	7	No
Thalassiosira	Diatom	471.6	5594.9	77	No
Tryblionella	Diatom	72.9	1066.5	21	No
Ceratium	Dinoflagellate	1.4	15.6	3	No
Dinoflagellate_unid	Dinoflagellate	1.5	17	4	Unknown
Gonyaulax	Dinoflagellate	2	18.8	5	Yes
Gymnodinium	Dinoflagellate	1	8.9	4	Yes
Gyrodinium	Dinoflagellate	3.2	19	9	Yes
Peridinium	Dinoflagellate	7.6	41.4	19	Yes
Prorocentrum	Dinoflagellate	63.3	290.8	53	Yes
Closterium	Green algae	1.4	11.7	5	No
Monoraphidium	Green algae	28.4	105.9	43	No
Pyramimonas	Green algae	1.9	15.5	5	No
Scenedesmus	Green algae	15.2	74.1	14	No
Chrysococcus	Other	91.3	914.3	9	No
Dinobryon	Other	6.6	67.8	7	No
Euglena	Other	139.6	692.5	97	No
Monomorphina	Other	1.5	12.7	5	No
Strombidium	Other	892.6	12569	75	No

Figures

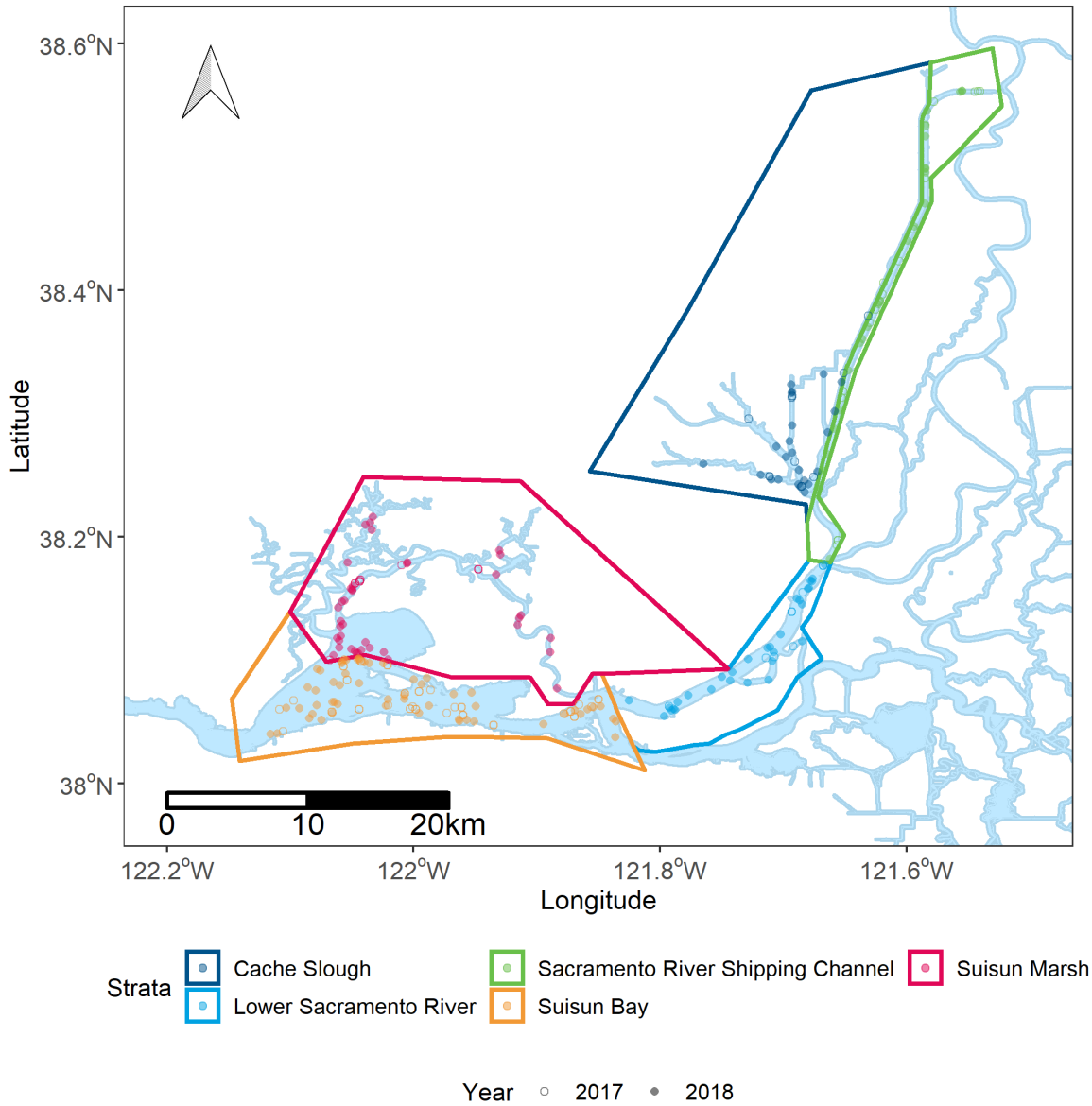

Figure 1. Map of regions and locations sampled in the Delta during fall of 2017 and 2018.

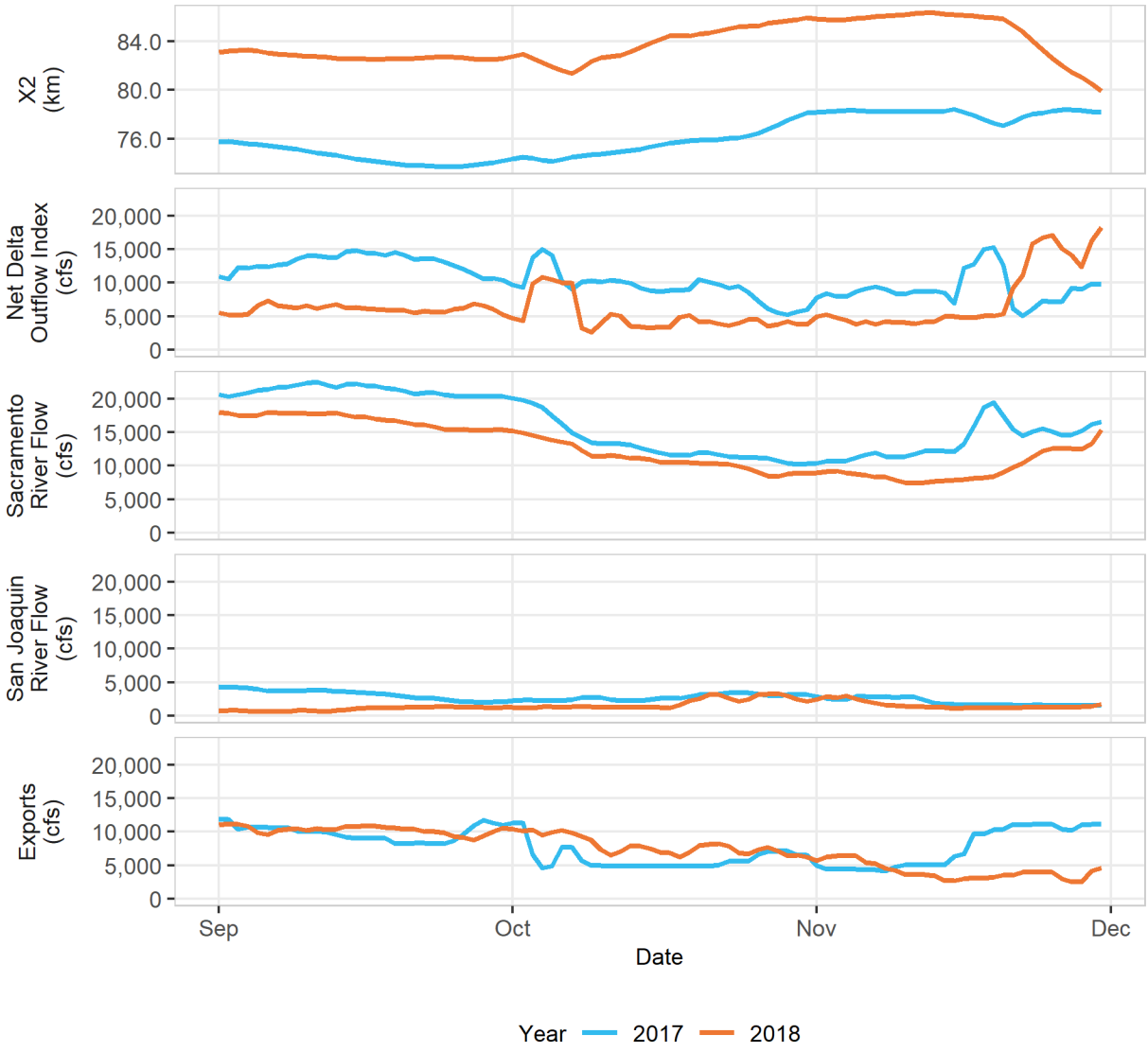

Figure 2. Outflow and X2 in the fall of 2017 and 2018. Measurements from DWR dayflow data.

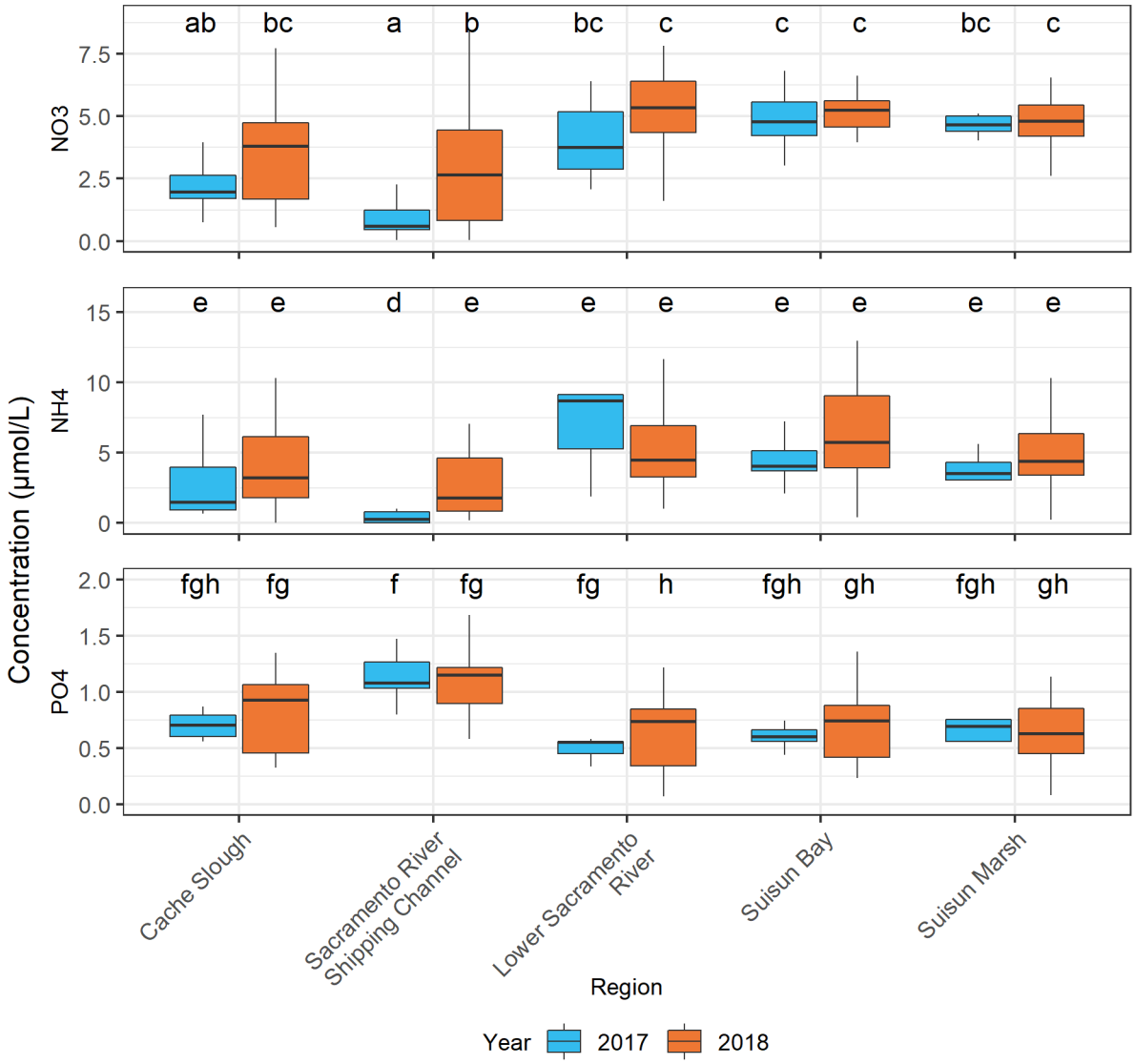

Figure 3. Nutrient concentrations between seasons and study regions in the Delta. Shared letters denote no significant difference observed between regions and years. Outliers are omitted from this plot.

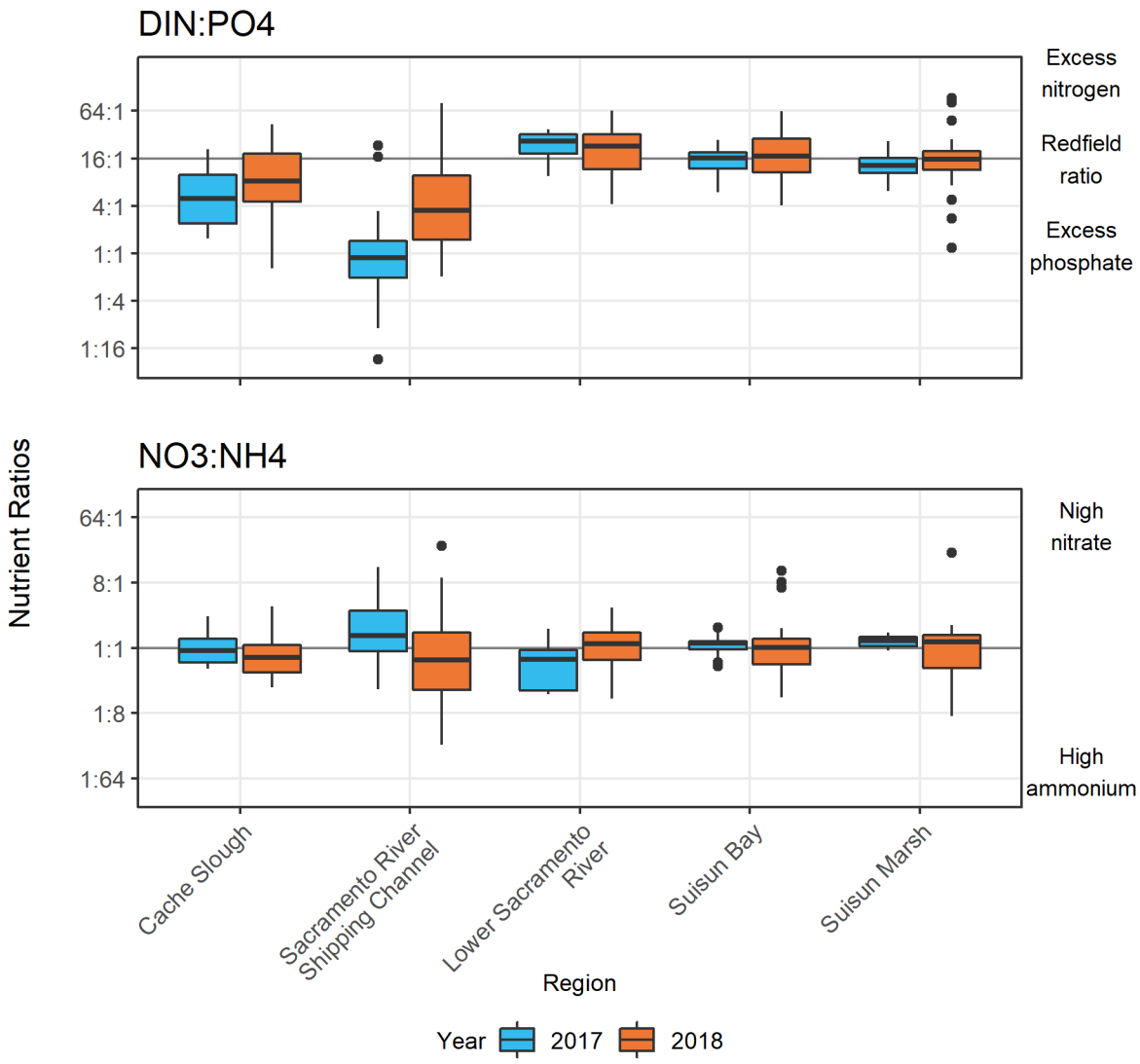

Figure 4. Ratios of dissolved nutrients between years and regions of the Delta, with Dissolved Inorganic Nitrogen to Phosphate (top) and Nitrate to Ammonium (bottom). The dashed line represents the 16:1 Redfield ratio of 16 nitrogen : 1 phosphate.

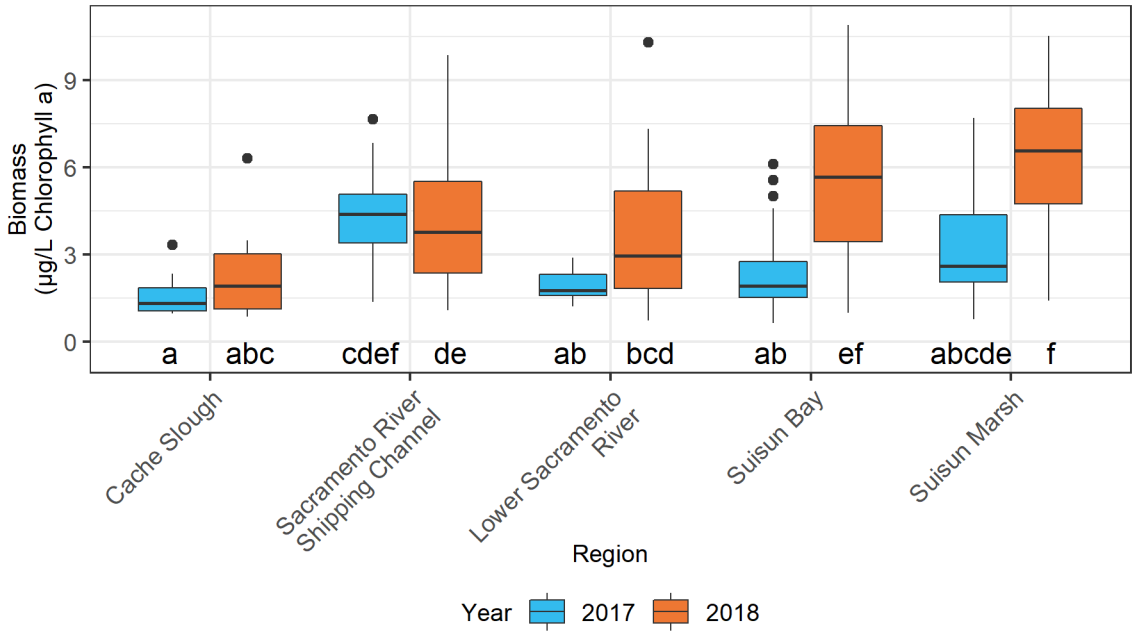

Figure 5. Chlorophyll concentrations between years and regions of the Delta. Shared letters denote no significant difference observed between regions independent of year or years.

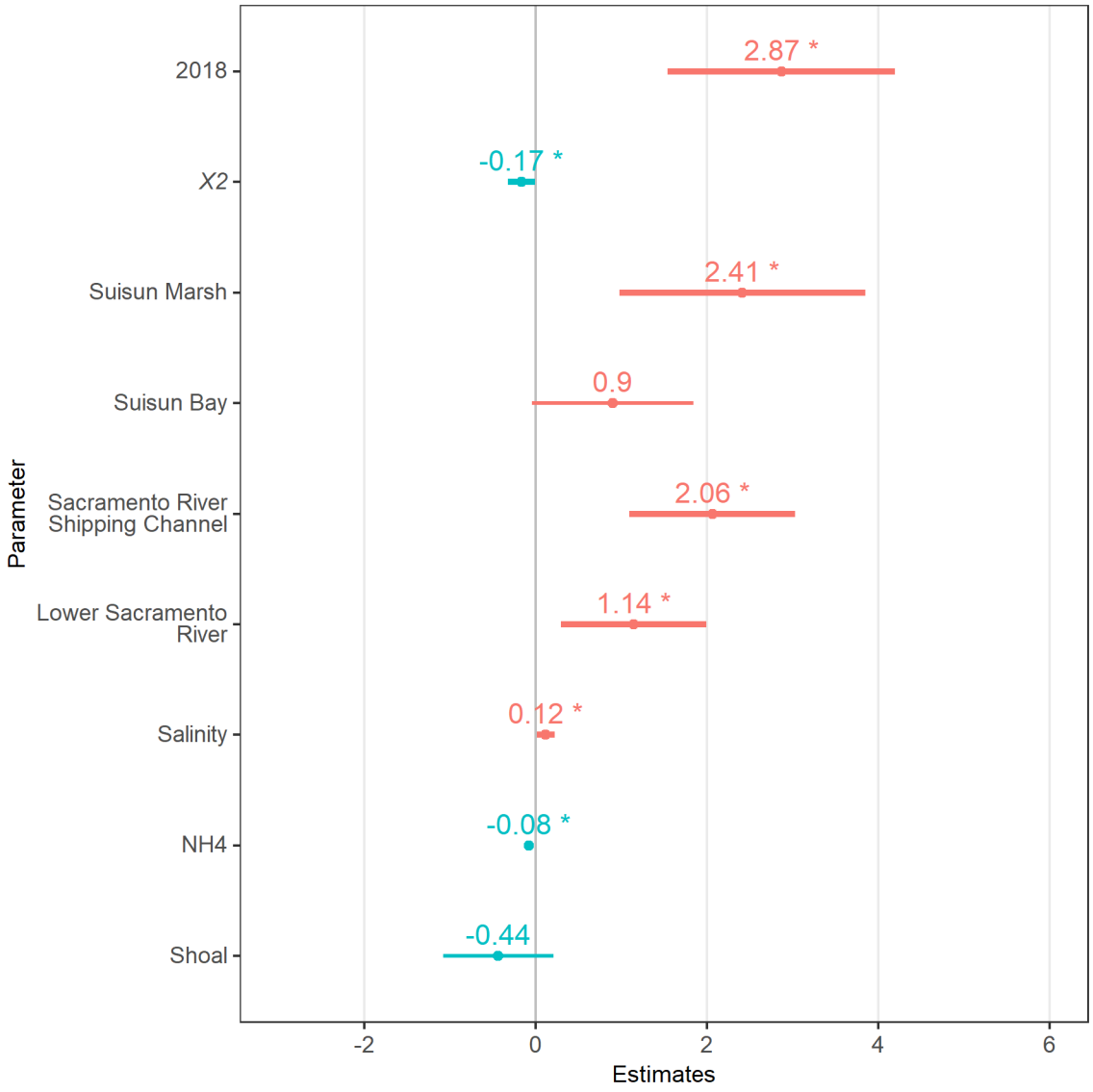

Figure 6. Explanatory used variables to model chlorophyll concentration, with estimated effects size and 95% confidence intervals. Parameters marked with an asterisk are significant. Negative correlations are in blue, positive in red.

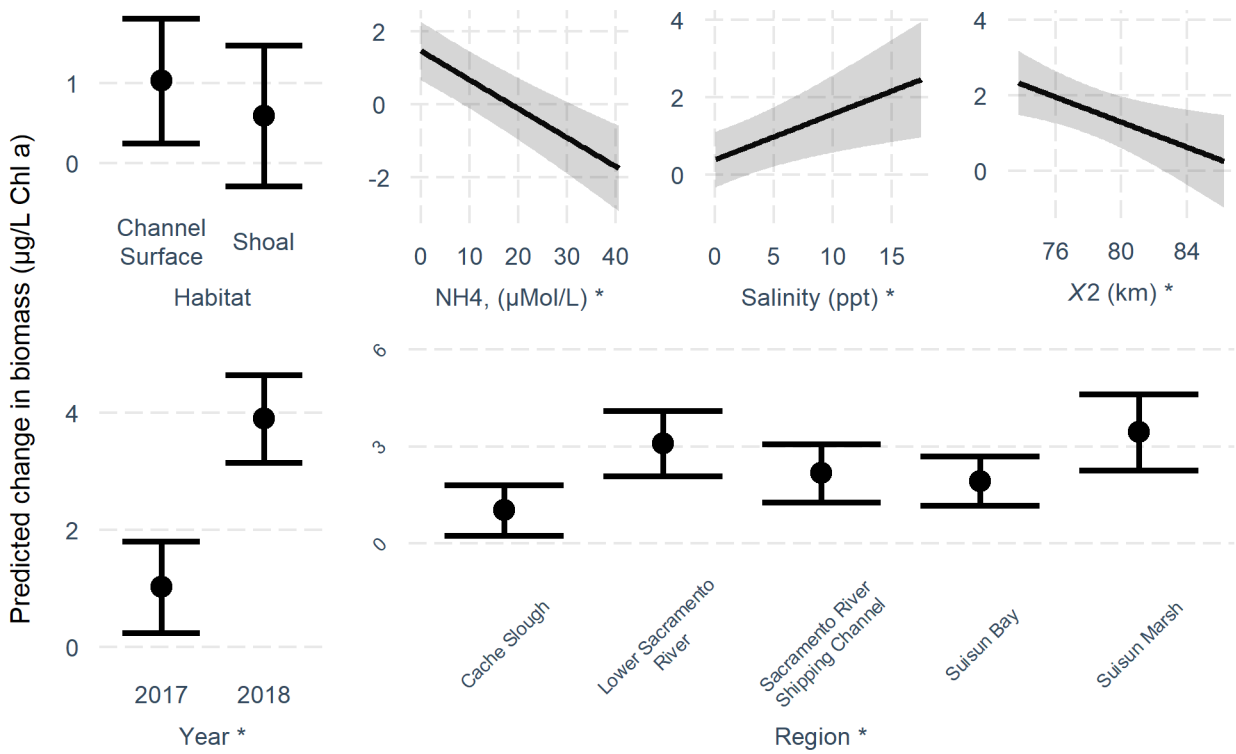

*Figure 7. The predicted effects of selected parameters on phytoplankton biomass as determined by generalized linear modeling. For each plot, all other predictors are set to the mean. Error bars and confidence bands (shaded) indicate the 95% confidence intervals. * indicates significant (P<0.05)*

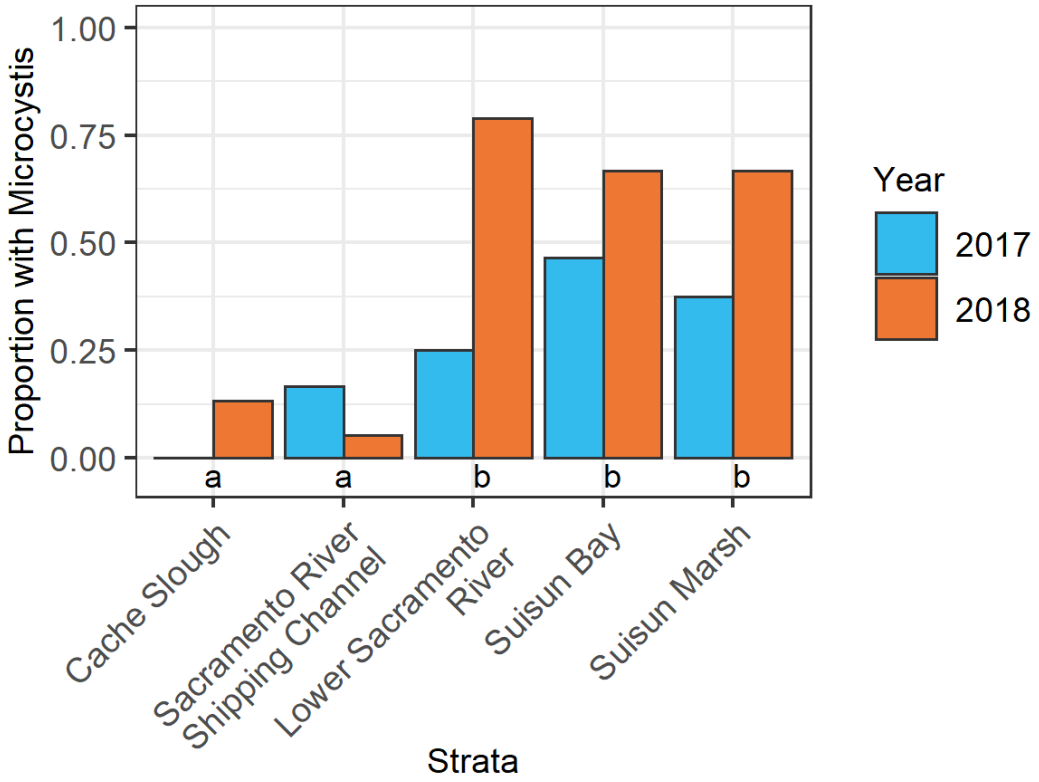

Figure 8. Proportion of sites with colonial Microcystis observed in each region and year. Regions with shared letters are not significantly distinct from each other.

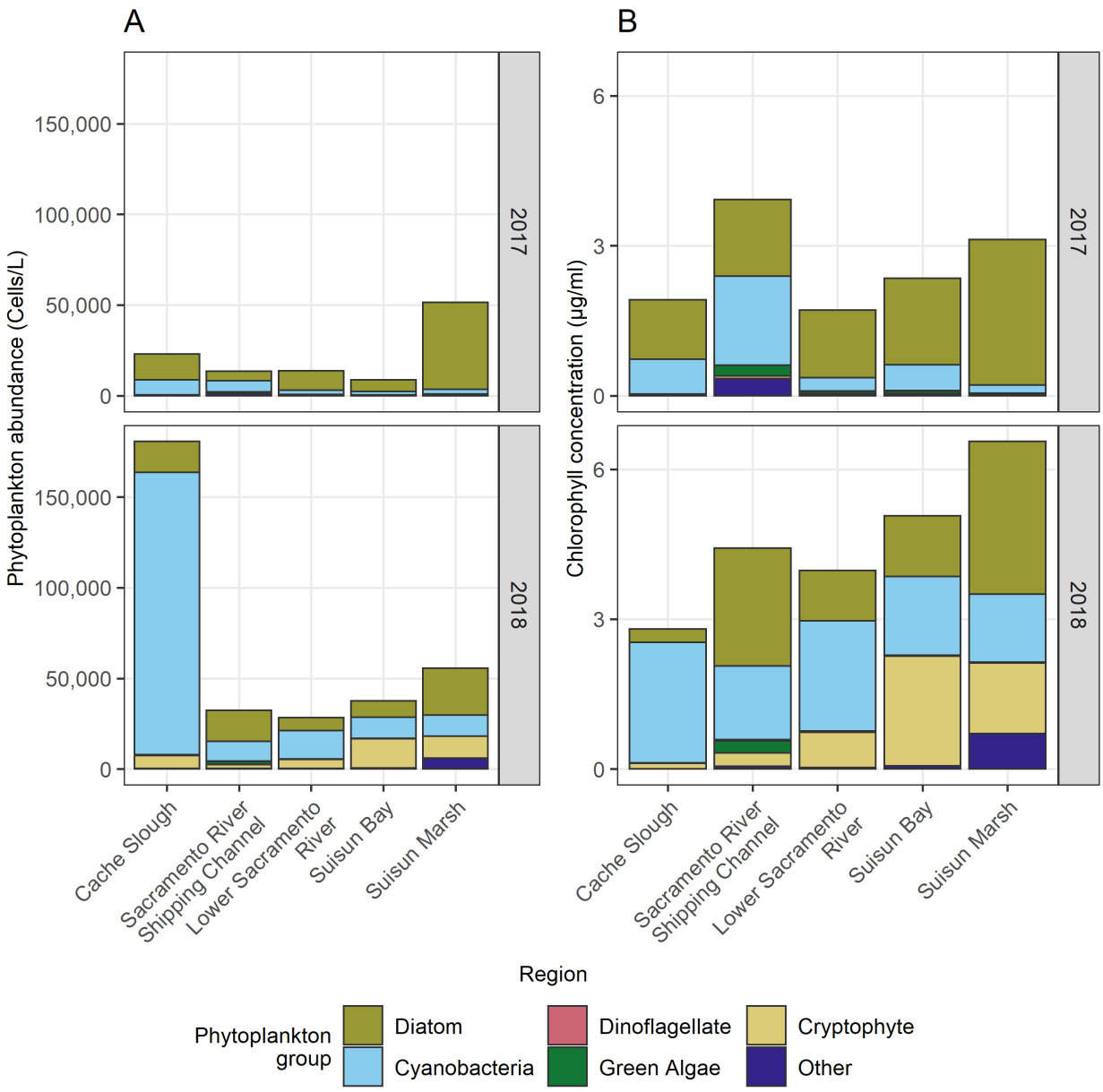

Figure 9. Mean abundance of each phytoplankton group by year and region as (A) proportion of the total phytoplankton abundance and (B) scaled to mean chlorophyll-a to highlight the respective contribution of each group to the phytoplankton biomass.

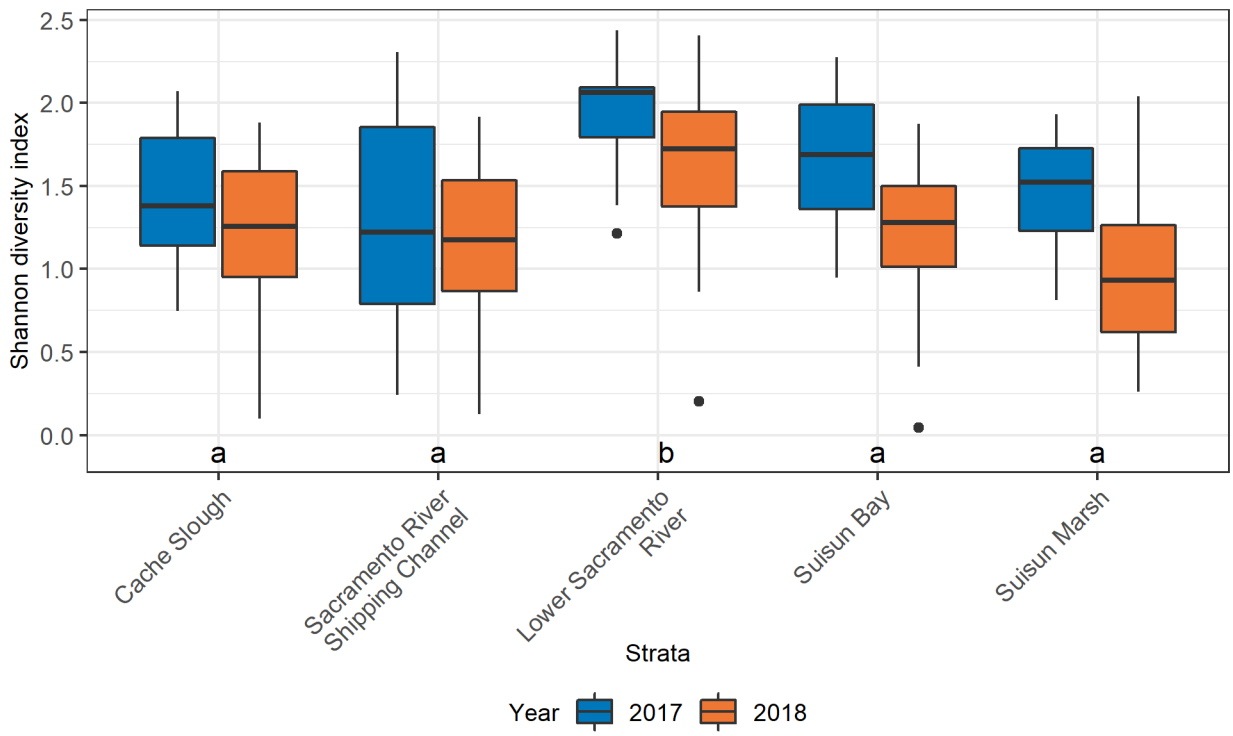

Figure 10. Shannon's index of diversity for phytoplankton samples by region and year. Shared letters denote no significant difference observed between regions.

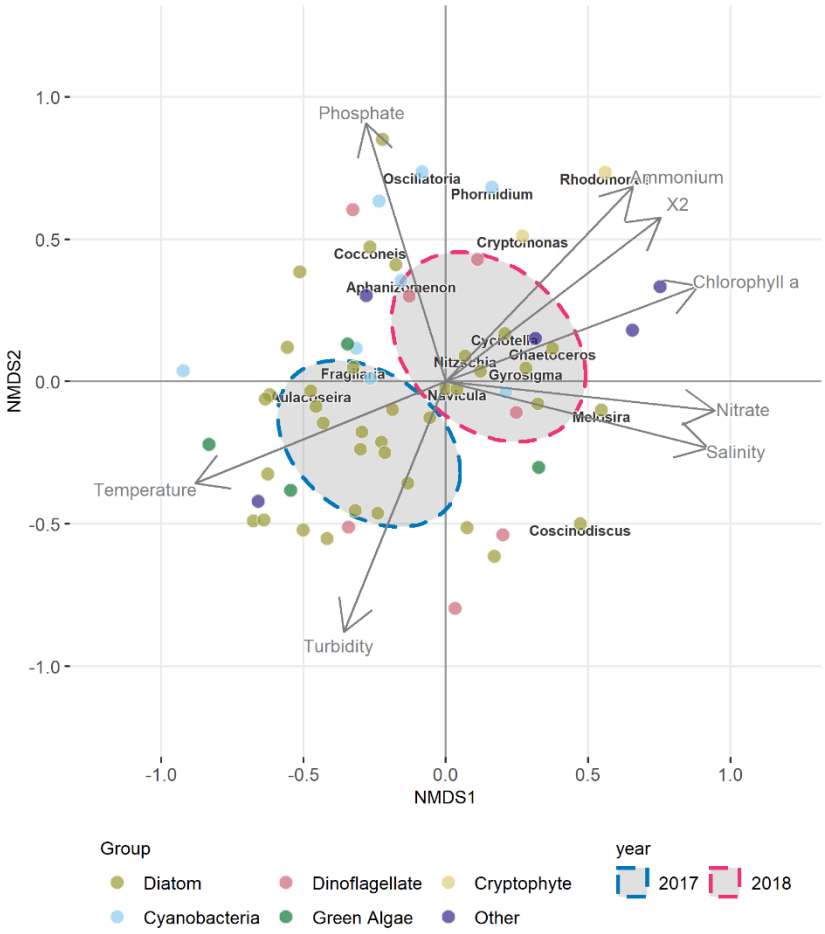

Figure 11. NMDS ordination of phytoplankton assemblages versus selected environmental variables and year. Labels represent the most ubiquitous genera present at the most sample sites; all other genera are represented by the colored points. Shaded ellipses indicate the 95% confidence interval of each year.

Figure 12. NMDS ordination of phytoplankton assemblages versus environmental variables and region. . Labels represent the most ubiquitous genera present at the most sample sites; all other genera are represented by the colored points. Shaded ellipses indicate the 95% confidence interval of each year.

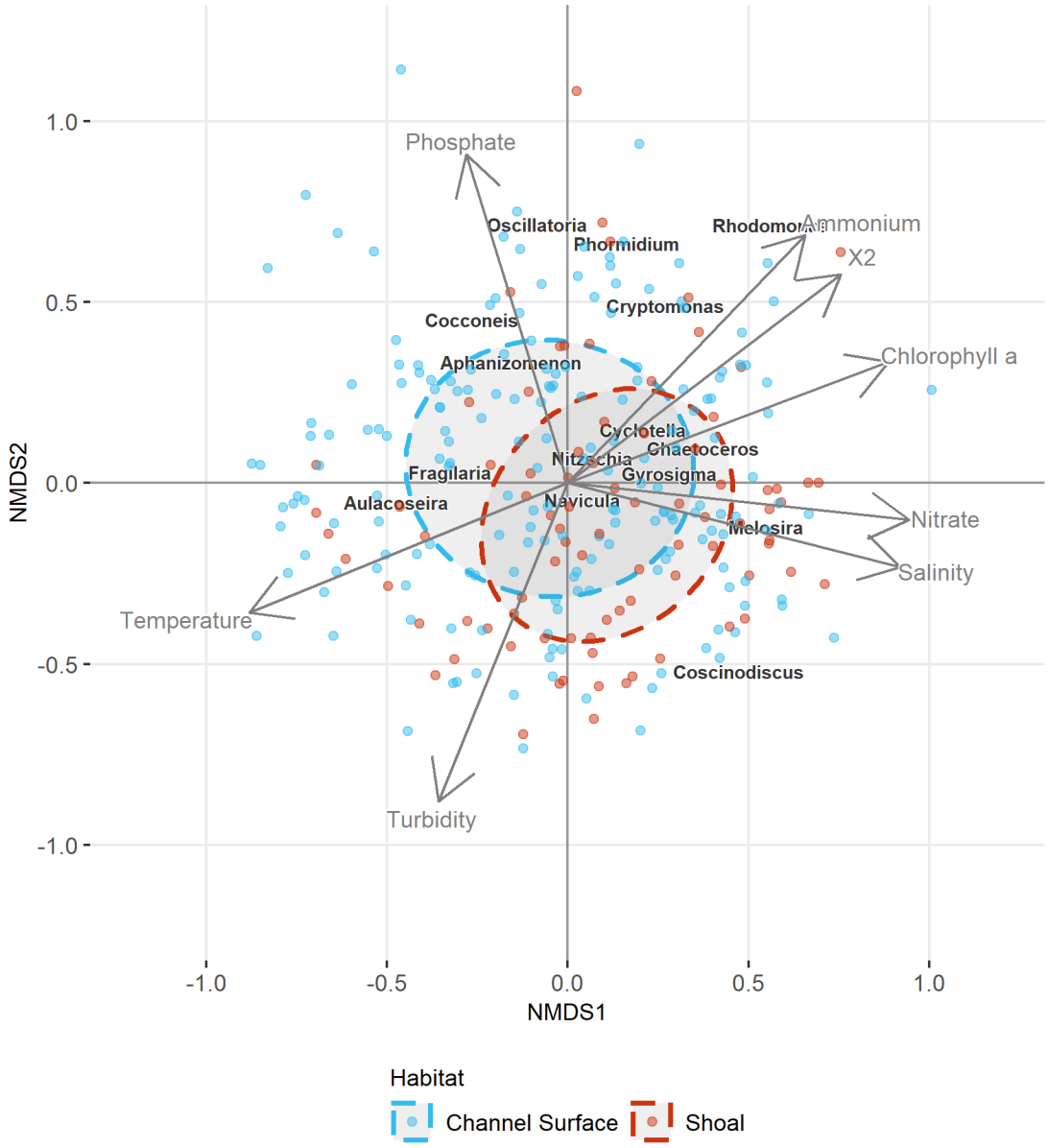

Figure 13. NMDS ordination of phytoplankton assemblages versus selected environmental variables and habitat. Individual sites are represented by dots and the taxa names represent the ten most abundant phytoplankton genera and the ten most ubiquitous genera present at the most sample sites. Shaded ellipses indicate the 95% confidence interval of each habitat.